Mining the RATS archive for compact blue stars

A thesis submitted for the degree of
Doctor of Philosophy

by

Onur ŞATIR, M.Sc., B.Sc.

Armagh Observatory
Armagh, Northern Ireland

&

School of Mathematics and Physics

Department of Astrophysics
The Queen's University of Belfast
Belfast, Northern Ireland

December, 2016

“Let me tell you something you already know.
The world ain’t all sunshine and rainbows.

It’s a very mean and nasty place, and I don’t care how tough you are,
it will beat you to your knees and keep you there permanently,
if you let it.

You, me, or nobody is gonna hit as hard as life.

But it ain’t about how hard ya hit.
It’s about how hard you can get it and keep moving forward.
How much you can take and keep moving forward.

That’s how winning is done!”

Rocky Balboa

“You should bring something into the world
that wasn’t in the world before.

It doesn’t matter what that is. It doesn’t
matter if it’s a table or a film or
gardening—everyone should create.

You should do something,
then sit back and say,
‘I did that.’”

Ricky Gervais

I kept moving forward, and did this!

Onur ŞATIR

To everyone who made me the one who I am,
with their love, hate, presence, absence,
motivation, discouragement,
time, money, trust,
patience...

Acknowledgements

I always loved to read acknowledegments, whether it is from a book, a paper or a thesis, but especially from a thesis. So, now it is my turn to write it and boy, it is overwhelmingly hard to squeeze the amount of appreciation, gratefulness, and all the nostalgia of the last years into a few digit worth of words, in a page or so! For what it's worth, here we go!

The first and the biggest thank you goes to no one else than my supervisor Gavin Ramsay, who has gone far and beyond the call of duty from time to time, to push me forward, keep me in the game, and simply was there all the time. Although we had very different approaches to the problems, in the end, it was this differences that kept me going as he was all for "*quick action with reasonable quality results*" at first and improvements later, and I was a notorious perfectionist who was after "*the perfect results with no regards to the time I spend*". If nothing, he saved me from this awful intellectual illness called perfectionism.

"*Şirin Baba*", Turkish for "*Papa Smurf*", as Tuğça and I secretly called him, was the fatherly figure for me, who always tried his best, and more, to help in any aspect of the observatory life, with all his powers, before his retirement this summer; the former director of Armagh Observatory Mark Bailey deserves the warmest thanks and a hug (no, it is not inappropriate at all, we Turks hug a lot!).

Chapter 4 is a result of the work I had the privilege to do together with Simon Jeffery, who generously shared his expertise on hot subdwarfs and spectral analysis with me through our countless discussions mostly initiated me knocking his office door out of the blue or catching him on his coffee break. I thank him for not turning his back once.

I thank Stefano Bagnulo for his help on the use of ESO proposal system for the data used in Chapter 4, that reduced the time I would spend at least a few magnitudes and made the process totally frustration free.

There were dark periods of time during my project that I was stuck in the jungle of research with twining poison ivy all over me holding me down, from which I was rescued by a band of science knights, Gerry Doyle, Apostolos "*Tolis*" Christou, Jorick Vink, Mark Bailey and Gavin Ramsay, by regular meetings where they would deal with all the problems of mine and take me to the open fields of the research where I can continue my research journey. I am very grateful for all the help and time they gave me.

Although I am very grateful for his spot on constructive comments and suggestions during the revision process that improved the quality of the thesis immensely, I will not thank my internal examiner David Asher, as he has insinuated that I should not when he wrote "*... I also didn't include the examiners (who were very nice actually) considering the thesis as something*

*presented *to* the examiners.*" in an e-mail to which he kindly attached the acknowledgement he wrote in his thesis for me to benefit from while writing this. In this context, I should not thank my external examiner Danny Steeghs neither, even though the discussion we had during the viva voce and his report later have enhanced the content and the character of the thesis extensively.

There was another person without whom not only this project but all the other work has been done at the Observatory would pretty much not exist as today astronomy heavily depends on computers and information technology. He is the superstar IT guy of the Observatory Martin Murphy, who retired on May 2015, and was the kindest and least grumpy IT guy I have ever known! Actually, he was never grumpy when I need help, and he said "*Onur is one of the guys here who knows his way around computers.*" while introducing me to his successor Greg Milligan, who has been creating his own legend although he found himself in an "*IT guy's hell*" during the reforms at the Observatory. I also thank him very much for not once making me wish that Martin had not left.

The lady who helped me with all my paperwork and non-sense administrative needs while I was in Armagh or abroad, Observatory Director's PA and Observatory Group Secretary Aileen McKee is someone whom absence in my professional life will be hugely felt!

All the students and post-docs, recent or former, full-time or temporary, who came and go during my residency in Armagh Observatory have helped one or other way, in one or other aspect of the studentship, scientifically or socially, a bit or hugely, deserves a warm thank you!

The Armstrong Family, Jill, Edward, Will, Maddie and Henry, and also furry members Selwyn, Skippy and Tiny (who passed away recently), deserves a big and warm thank you, and lots of hugs! They were much more than our landlords, they were our family in Armagh. Should we have not found the flat they were letting, our life in Armagh would not be as pleasant and comfortable as it was!

The warmest and most personal thank you is to my (now ex-) wife H. Tuğça ŞENER, with whom I shared not only my life in Armagh but also complete package of being a PhD student, as she was a fellow student here at the Observatory. I owe her a huge thank you from the bottom of my heart for being the best colleague that I could trade ideas and discuss any question stuck in my mind regardless the time of the day, for being the life support while I was navigating through the hurricane called PhD studentship, but mostly being the main reason for me to go to Armagh in the first place!

This last part will be in Turkish if you'll excuse me, as I'd like to thank my family who do not speak English.

Sevgili ailem, canım annem ve babam, biricik kardeşim Vildan ve sevgili damat Levent... Beni her hâlükârda, maddi ve manevi desteklediniz; en ihtiyacım olan günlerde desteğinizi sonuna kadar gösterdiniz; diğer zamanlarda da, yardıma her an hazır olduğunuza dair verdiğiniz güven ile attım adımlarımı hayatta. Hayallerimin peşinden koşmama ve yıllarımı bilimadamı olmak için harcamama can-ı gönülden yardım ettiniz. Şuraya yazacağım hiç bir kelime, cümle size olan minnetimi anlatmaya yetmez. İyi ki varsınız!

Onur ŞATIR
December 2016, Arhavi

Created with LaTeX

Abstract

In the age of big surveys where torrents of data accumulate with a speed ever increasing, astronomers need to utilise data science and data mining techniques more and more to find their "*needles*" in these enormous "*haystacks*". In this study, I set out to find the "*needles*" that we are interested in, compact blue objects, in our "*haystack*", RATS (**RA**pid **T**emporal **S**urvey). Here, the word "*compact*" is used in the manner both "*very dense*" and "*very close*" as the binaries in discussion have very short periods, therefore very tight orbits, and are composed of very dense objects. Discovering, identifying and studying compact blue objects (especially Ultra-Compact Binaries - UCBs), will help theoreticians to address some of the key outstanding questions in stellar evolution models, such as the common-envelope phase, which occurs in close binaries, and other last steps of the binary evolution. Although the overall model of stellar evolution is reasonably understood, there are still many uncertainties and questions which remain.

This study is initiated to exploit the RATS dataset, which has light-curves and colour information of more than 3 million stars (Ramsay and Hakala, 2005). Although the main motivation of the RATS project was to discover rare AM CVn systems, possible progenitors of type Ia supernovae, which are very short-period (less than $\sim$65 minutes) double degenerate binary systems with helium dominated spectra (Solheim, 2010), one can find all kinds of objects with a wide range of characteristics in the dataset.

I have searched for compact blue objects in the data through their colour. This search has yielded 2826 blue objects, containing 384 UCB candidates. We obtained spectra for 17 of these objects using GTC (Grand Telescopio Canarias). The spectral identification resulted in 3 extremely He-rich O-type subdwarfs (He-sdO), 3 B-type subdwarfs (sdB) and 2 B-type (sub)dwarfs, 2 sdOs, 2 H-atmosphere (DA) white dwarfs, 2 QSOs and 3 possible subdwarf and cool dwarf binary systems. As the extremely He-rich sdOs are as rare as AM CVns, we obtained high resolution UVES spectra of two of them (*i.e.* `RATJ1754+0137` and `RATJ1759+0119`) and analysed these objects in detail. Finally, I have identified blue variable objects in the RATS archive, and revealed their nature using their colours, light-curves and spectra.

Contents

List of Tables

List of Figures

Chapter 1

Introduction

The first interests in blue objects have been shown back at the beginning of the 20th century. Indeed, it was around this period in time when stars were being to classified based on their colours which are directly related to their temperature. Fueled by these studies, surveys have been initiated to explore the skies in different colours. For example, in their paper titled as "*A Search for Faint Blue Stars*", Humason and Zwicky (1947) wrote:

> *As part of the work of the 18-inch Schmidt telescope at Palomar, a survey of the sky in different colors has been conducted during the past few years. Large areas of the sky were photographed in the infrared, red, yellow, blue, and near ultraviolet parts of the spectrum with the intention of selecting different types of interesting stars from the relative intensities in various parts of their spectra.*

With the understanding of the importance of the faint —compact—blue stars, many search parties organised, and the number of known such objects have rocketed. Well populated compact object samples have brought better understanding of the final steps of stellar evolution. However, there are still questions to be answered as there are samples of certain types of compact blue objects that do not have statistically significant number of members (*e.g.* AM CVns, He-rich subdwarfs), or samples suffer from discoveries biased towards the higher Galactic latitudes as we only recently started to have surveys concentrate on the Galactic plane (*e.g.* RATS, UVES, IPHAS, OmegaWhite).

In the following sections I first give a basic introduction to stellar evolution and the role of the stellar colours in astrophysics to set the scene before going to answer the basic questions –why, what, how– about this study and give a summary of the RATS project.

1.1 A Glance to the Stellar Evolution

For a star, life starts as a collapsing gas and dust cloud with a radius of $\sim$ 30pc. This collapse is not homogeneous, as some parts of the cloud collapse faster then others, clumps occur. While the clumps get denser, and thus hotter, their gravitational potential energy is radiated as heat. These rotating hot gas spheres that radiate heat are called "*protostars*" (Prialnik, 2010). When the protostar reaches the high enough density and temperature (10^7K) to fuse hydrogen into helium in the core, due to the gravitational contraction, and the star starts its life on the *Main Sequence* which is the band on the spectral type (or $T_{\rm eff}$, colour) vs the absolute magnitude (or brightness) plane, the Hertzsprung-Russell (HR) Diagram (see Figure 1.1 and the discussion in the next section), on where the core-hydrogen burning stars with different masses reside. For the protostars with mass less than 0.08 $M_\odot$, this never happens, and they carry on their lives as "*brown dwarfs*". At this point, the star is in a hydrostatic equilibrium state where the energy produced by the fusion holds the gravitational force, thus the contraction of the outer layers stops.

The mass of stars directly effects the time spent on the main sequence. Low mass red dwarfs stay on the main sequence for hundreds of billions of years by burning their hydrogen in the core, while high mass supergiants evolve faster within a few million years. A solar-like intermediate-mass star spends roughly 10 billion years, the $\sim$ 90% of its life, on the main sequence as a core-hydrogen burning "*normal*" star. During this time, helium core contracts due to increasing helium mass. When the helium mass in the core increases enough to the point that gravitation wins over the gas pressure, the classical Boltzman distribution leaves its role to the quantum effects, and Pauli exclusion principle determines the distribution of the free electrons. Pauli exclusion principle states that two identical fermion (*e.g.* electron, neutron) can not share the same quantum state. Thus the electrons are forced to go higher energy states and the matter becomes degenerate. Electron degeneracy pressure prevents the matter at the core to contract further. Around the helium core, there is hydrogen shell adding helium to the core through the hydrogen burning. The outer hydrogen layer expands and cools due to the rising temperature below, hence, star follows the *Red Giant Branch* (RGB) on the HR diagram and becomes a red-giant.

At the point where hydrogen is burned at the shell around the core, the H-burning is more luminous than it was during the H-core burning, as the H-shell is heated by the contracting core. This causes the H-envelope to expand and cool, thus the star to move to the upper-right of HR diagram. Meanwhile, H-burning keeps contributing to the helium mass of the core, therefore the core contracts further. When the He-core-mass reaches $0.45 - 0.5 M_\odot$ the temperature is around 10^8 K which results the core being able to fuse He into C and O. At this point the RGB phase finishes and the Horizontal Branch (HB) phase starts.

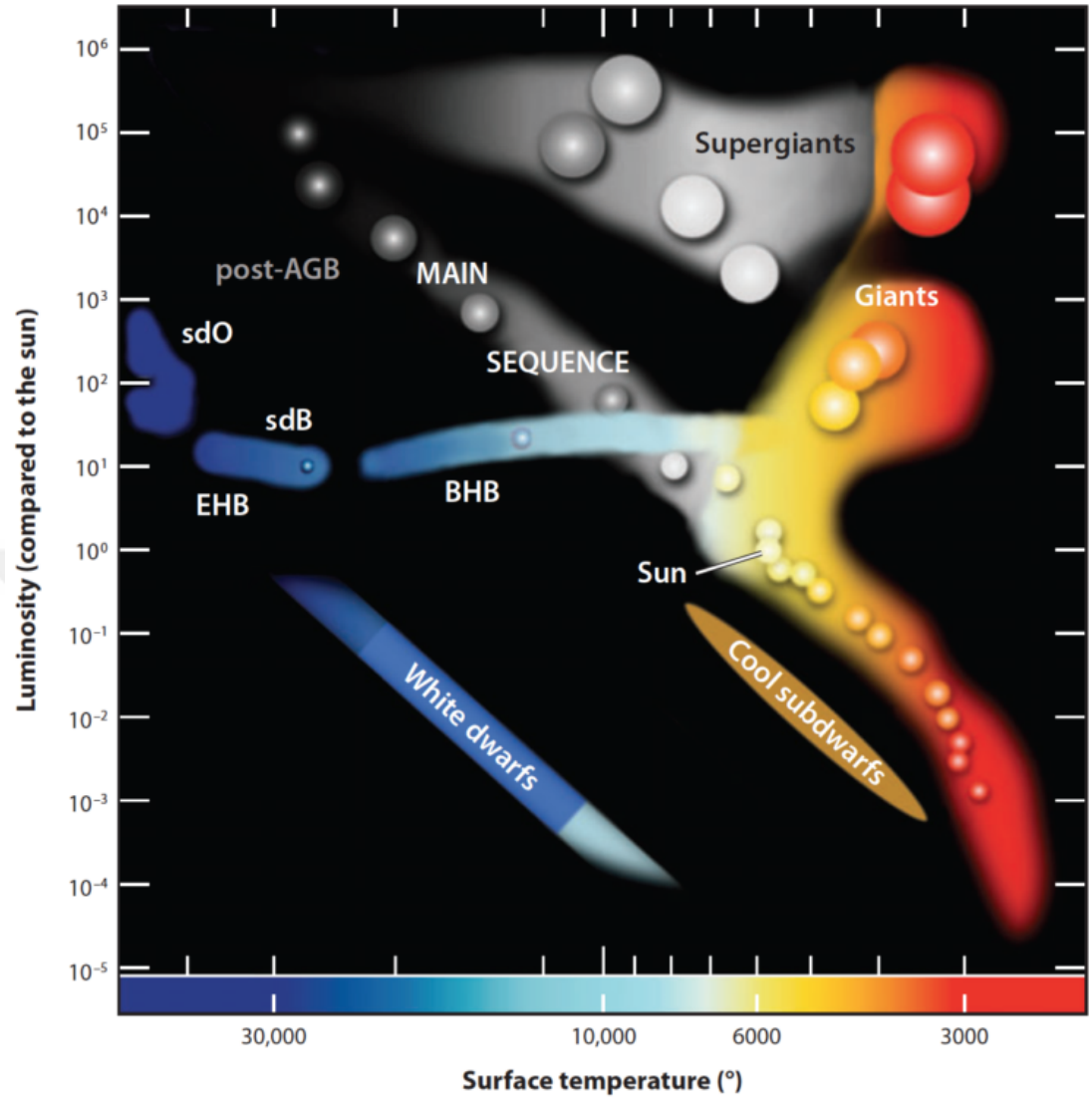

Figure 1.1: Hertzsprung-Russell Diagram. EHB, BHB, AGB, sdO and sdB stands for Extreme/Extended Horizontal Branch, Blue Horizontal Branch, Asymptotic Giant Branch, O-type subdwarf and B-type subdwarf, respectively. Courtesy of ESO, with modifications by S. Geier and K.S. de Boer

During the HB phase, helium is consumed by the triple–α process, which proceeds as following

$$^{4}_{2}He + {}^{4}_{2}He \rightarrow {}^{8}_{4}Be$$
$$^{8}_{4}Be + {}^{4}_{2}He \rightarrow {}^{12}_{6}C$$

Although $^{8}_{4}$Be is very unstable, He fusion is faster than $^{8}_{4}$Be decay, therefore there is always enough $^{8}_{4}$Be to convert into $^{12}_{6}$C.

There are also some ${}^{12}_{6}$C converted into ${}^{16}_{8}$O with one more α capture:

$$ {}^{12}_{6}C + {}^{4}_{2}He \rightarrow {}^{16}_{8}O $$

As the star is in a stable burning phase, the brightness stays roughly constant while the temperature rises, hence the name "*horizontal branch*". At the end of the the HB, He is exhausted in the core. Now, for the star, it is time to go to the Asymptotic Giant Branch (AGB), except for the Extreme Horizontal Branch (EHB) stars which I discuss their evolution in detail in §1.4.2.

When the CO core starts shrinking, the upper shells expand and hydrogen burning in the shell die away. At this stage the CO core becomes degenerate. When the envelope expands and cools, convection goes down to the H shell and when He burning reaches the H burnt out shell, H starts burning again. This phase is called as "*double shell burning*". At this stage the He-burning bottom shell has several thermal pulses due to its instability. Now the star is on the thermally-pulsing asymptotic giant branch.

During these pulses the star loses $\sim 10^{-4}$M$_{\odot}$, and reaches very close to the end of its life. The initial mass is the main parameter defining the fate of a star. Stars with initial masses smaller than ~ 8M$_{\odot}$ die as a white-dwarf (WD)—they rip apart the red giant envelope, so the core cools eventually (see §1.4.1). Stars with initial masses greater than ~ 8M$_{\odot}$ die as supernovae. The survivor of this explosion is either a neutron star or a black hole, again depending on the mass. Besides the mass of a star, metallicity is the other parameter that has an important influence on stellar evolution. Chemical composition of a star is described by

$$ X + Y + Z = 1 $$

where X, Y and Z refers to H, He and metal abundances respectively. Increasing the Z value decreases the luminosity and temperature of a star, and positionally shifting it to a lower right position on the main sequence. Differing values of Z therefore cause the main sequence to become a strip rather than a line on the HR diagram. Among two stars of the same mass, a metal poor star lives longer because the CNO cycle becomes more efficient with increasing metallicity on the main sequence, and the metal poor stars are dominated by proton-proton cycle. Thus the metallicity of a star has a significant role in determining the lifetime and evolution of a star. Additionally, the outer convective layer thickness is proportional with Z.

1.2 The building blocks of the colour-selection: Magnitude, Colour and HR Diagram

In astronomy, the flux, which is the power per unit area, of an celestial object is usually measured by collecting light with a telescope, sending it through a filter allowing only light with specific wavelength, and then determining the power. The process of the calibration of the detector via standard stars, and correction for the absorption in the atmosphere, which gives the flux in the filter band, is known as photometry.

Usually the photometric results are given in terms of magnitudes, which is given by

$$m = -2.5log[Flux/F_0]$$

where F_0 is standard zeroth-magnitude flux for the chosen filter. Since for different scientific goals different filter sets can be useful, there are more than 200 photometric filter systems introduced by different groups. A comprehensive list of all the photometric systems has been published by Moro and Munari (2000) and also presented in detail on their website[1].

The ratio of the fluxes of an object measured at two wavelengths is defined as colour index of that object, as it tells in which wavelength range (colour) the object is brighter. Since the logarithm of a ratio is the difference in the logarithms, these flux ratios are defined by subtracting the magnitudes in different filter bands.

Circa 1910, E. Hertzsprung and H.N. Russell introduced the Hertzsprung-Russell diagram, which is the diagram that shows the spectral types of stars with known distances (through parallaxes) against their brightness, and it was a huge step forward for understanding stellar evolution. Other than this original HR diagram, there are two more main types of Hertzsprung-Russell diagram.

For theoreticians making computer models to study evolution of stars, it is easiest to think in terms of luminosity and radius relative to the Sun. Since the brightness and spectral type are really a measure of luminosity and surface temperature, it is convenient to do a quick conversion using a relation true for all stars, $L = R^2T^4$, where L, R and T are luminosity, radius and temperature in solar units. Therefore, theoreticians' favourite type of HR diagram is a luminosity-temperature diagram, but in logarithmic scale as stellar luminosities and temperatures differ by such large amounts.

The most commonly used type of HR diagram is the one that compares properties of stars which can be observed directly, such as the apparent colour and relative brightness of stars in a cluster. Cluster colour-magnitude diagrams are extremely useful for comparing stars that

[1] `http://ulisse.pd.astro.it/Astro/ADPS/`

were probably formed almost at the same time, but differ in mass, therefore are in different evolutionary states. While colour-magnitude diagrams of young galactic open clusters and old globular clusters teach us about the evolution of high-mass stars and low-mass metal-poor stars, respectively, colour-magnitude diagrams constructed by wide-field observations of the field stars, are used selection and identification of different type of objects within the big data.

1.3 Why are we interested in these compact blue objects?

"*Compact blue objects*" is a term that concerns classes of objects such as white dwarfs, subdwarfs, and their many subclasses including single objects and exotic compact binary systems. There are different reasons to be interested in different types of compact blue objects, as they help to answer different questions. My main interest lies in the ultra compact binaries, especially AM CVn systems.

When binary stars with periods less than hour were discovered at the end of the 1960's, it was understood that both components of these binaries are compact objects - otherwise it is impossible to fit normal stars into such small orbits (Paczyński, 1967; Paczynski and Sienkiewicz, 1981). Compact objects are stellar remnants - stars that are at the last stages of the stellar evolution. Towards the end of their life, stars become a white dwarf if they have a core mass less than 1.44 $M_\odot$ (Chandrasekhar limit), a neutron star if their core mass is between 1.44 and $\sim$2.5 $M_\odot$ or a black-hole if the core mass is greater than $\sim$2.5 $M_\odot$. While the core mass is the main factor that determines the resulting object, the evolution scenario and the time-scale also depends on whether the star is isolated or in a binary system.

Although the big picture of the stellar evolution is understood, there are many open questions about the formation of exotic systems harboring compact objects. A larger sample of interacting ultra-compact binaries is important to understand further the details of the evolution of these systems, specially the common-envelope phase.

The most scientifically interesting objects between these for us are the AM CVn systems, a subgroup of Cataclysmic Variables (CVs) which consist of double hydrogen-deficient degenerate objects (or a degenerate and a semi-degenerate) with a period less than $\sim 65^{min}$. The scientific driver behind our effort is to have a homogeneous sample of AM CVn systems of which only 50 of them are known (Table 1.1 on page 21). AM CVn systems are expected to be the most powerful known gravitational sources to be observed by the proposed gravitational wave space observatories such as eLISA[2]. The foreground radiation that those observatories will encounter, which will be much stronger than any diffuse extragalactic background, will be formed by the high number of sources like ultra-compact binaries within the Galaxy that will

[2] `http://www.elisa-ngo.org/`

not be individually detected (Farmer and Phinney, 2003). Determining the population density of these systems is important to calculate this foreground radiation. Having an unbiased and significantly populated sample of these systems will allow us to test the models which predict their number in the Galaxy as a function of orbital period (Nelemans et al., 2001a).

Besides, most of the known AM CVns are at the longer period end of the scale ($P > 40^{min}$). To find out is it only because the searches are biased, or is it that the nature of these systems impose longer periods, we need to perform a systematic and detailed search for them.

1.4 What types of objects are these compact blue objects?

While searching for AM CVn systems, we anticipate finding several other types of compact blue objects as well, including white dwarfs, white dwarf binaries (apart from AM CVns, other cataclysmic variables (CV's) and non-interacting double white dwarf binaries), hot subdwarfs (He-rich/poor sdBs, sdOs), and stellar pulsators (e.g. SX Phe and δ Scuti stars). These objects are discussed below.

1.4.1 White Dwarfs

White Dwarfs are very common in the universe as they are the final product of the evolution of stars with a large range of mass from $0.07M_{\odot}$ to about $9M_{\odot}$. The fate of over 97% of the stars formed in the Galaxy is to become a white dwarf at the end of their life (Fontaine et al., 2001). They are compact objects with planetary sizes and typical mass around $0.5M_{\odot}$. Thus, high densities, high surface gravities and low luminosities are their characteristic features.

After stars with the suitable masses leave the main sequence, they pass the red-giant and horizontal branch phases and finally eject most of their outer layer during the AGB state. The left-over is basically an extremely hot and dense object, with carbon and oxygen core, a thin layer of neutral or ionized helium, and –if present–a very thin hydrogen atmosphere (Fig.1.2), that ionises the surrounding planetary nebula (Fig. 1.3). The central star is very hot and luminous after the ejection of the outer layers with a temperature greater than 30,000K and luminosity up to $100{,}000L_{\odot}$ but it quickly fades a few order of magnitudes within a century or so, and becomes a WD with a surface temperature of about 10^4K.

The mass is the main factor that determines the end product of evolution of a star. Progenitor stars of white dwarfs whose mass is lower than $0.5M_{\odot}$ never become hot enough to burn helium at the core. Theoretically they can burn all the hydrogen, and finish their evolution as He-WDs but this takes longer than the age of the universe. However, mass loss in binary systems (Benvenuto and De Vito, 2005) or due to a large planetary companion might produce

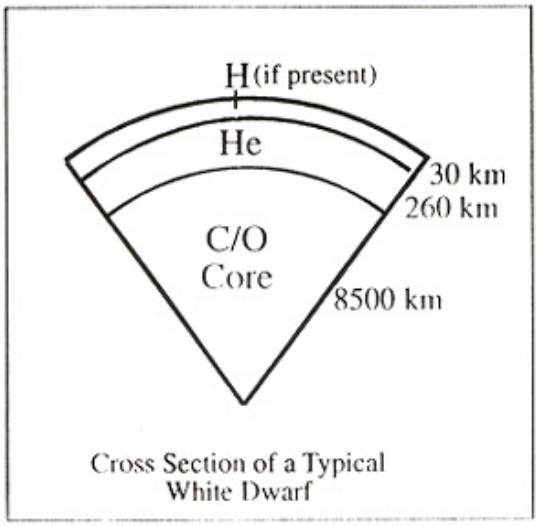

Figure 1.2: Cross-section of a typical white dwarf. Image credit: `http://universe-review.ca/I08-25-whitedwarf.jpg`

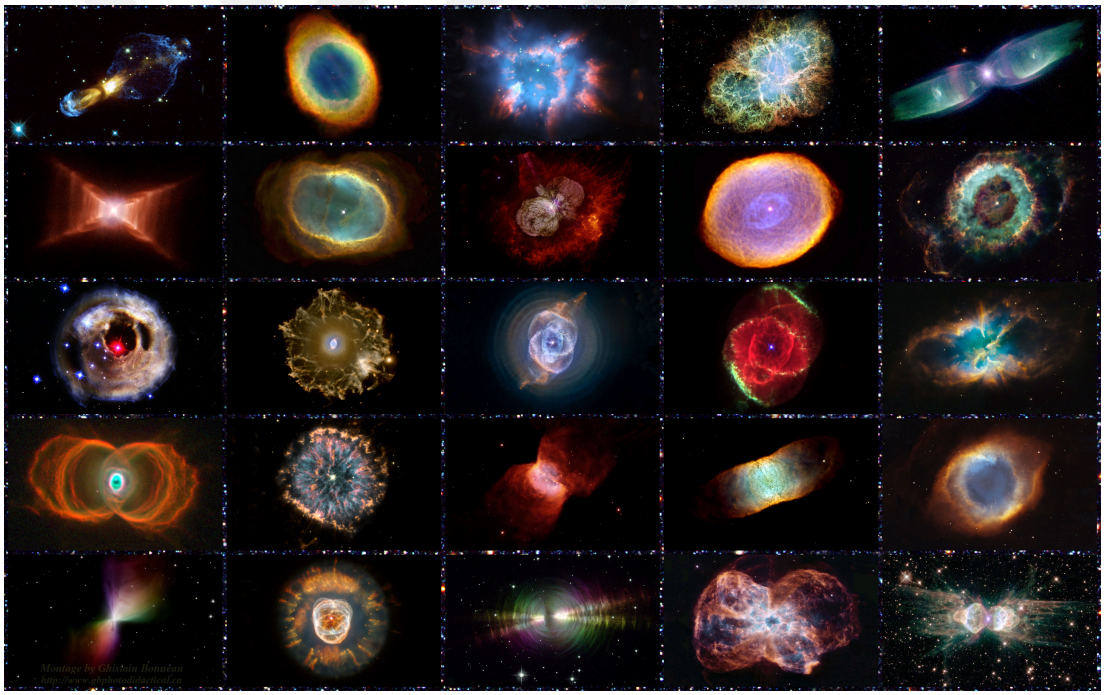

Figure 1.3: A selection of planetary nebulae photographed by the Hubble Space Telescope. Note the central stars, which are white dwarfs. Credit: NASA/ESA

a He-WD from these low mass stars (Nelemans and Tauris, 1998).

Red dwarfs with masses between $0.5M_{\odot}$ and $\sim 8M_{\odot}$ are the typical WD progenitors. They are capable to burn helium into carbon and oxygen. The C-O core is encircled by inner He-burning and outer H-burning shells, and after they expel most of their outer material as

a planetary nebula, the remaining is the central star of a planetary nebula.

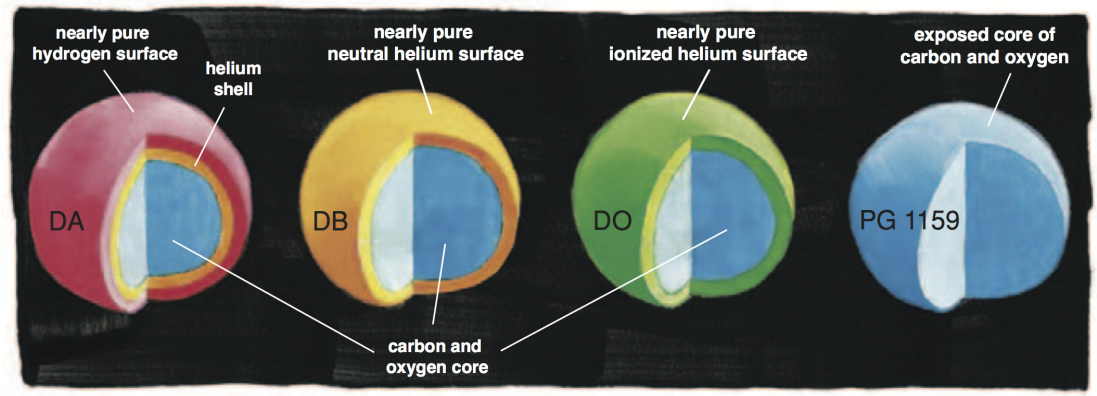

Figure 1.4: Types of white dwarfs is determined by the element at their most outer layer. Due to high gravitational potential, the heavier an element, the deeper it goes; thus the layers of elements are very homogeneous. *The image adapted from Kawaler and Dahlstrom (2000).*

At the core of red dwarfs more massive than $\sim 8 M_{\odot}$, carbon is fused to neon and magnesium, and in case the mass is more then $\sim 10 M_{\odot}$, neon is fused to iron. Most of the time, these stars do not stay as WDs due to the core collapse, and explode. The result is either a neutron star or a black hole, depending on how massive the star is. Nevertheless, if the mass is between 8-$10 M_{\odot}$, the core temperature is not sufficient to fuse neon; there are not any more reactions after carbon fused to neon and magnesium, thus, these objects become an oxygen-neon-magnesium WD.

1.4.2 Hot Subdwarfs

After stars leave the main sequence, they pass the red giant (RGB) and horizontal branch (HB) phase. At this point, ordinary stars (see §1.1) follow the asymptotic giant branch (AGB), then produce a planetary nebula and become a white dwarf. The story for hot subdwarfs (sdBs, sdOs) changes at this part of the stellar evolution story. As the hydrogen-rich outer layer of hot subdwarfs, which covers the helium-burning core, is very thin (less than $0.02 M_{\odot}$ or $\sim 4\%$ of the total mass of the star (Saffer et al., 1994)), the hydrogen shell burning, the process which leads the star to the asymptotic giant branch, cannot take place. Consequently, the star continues its journey on the horizontal branch by getting hotter and slightly dimmer, and reaches the very blue end, the extreme horizontal branch (EHB) (Heber, 2009).

Before going further, I need to mention that hot subdwarfs and subdwarfs are totally different types of objects. Although they share the name, subdwarfs (the cool ones) are very different than their hot cousins. Their nature is very similar to the *ordinary* core-hydrogen-burning main sequence stars, with slightly higher metallicities. As a subdwarf is less luminous than a main sequence star (a dwarf) with the same temperature, they reside just below the main sequence

stars on the HR diagram, hence the prefix "*sub-*".

B-type hot subdwarfs (a.k.a Subluminous B stars) are very common amongst the hot objects and usually outnumber the other types of objects (*e.g*. QSOs and white dwarfs) in blue object surveys and, can be found in many stellar environments. The Far-UV excess seen in elliptical galaxies can be successfully explained if a substantial population of sdB stars is always present in old stellar environments (Podsiadlowski et al., 2008). A large fraction (40-70%) are found in close binaries with orbital periods between 0.05d and 30d (Maxted et al., 2001). Also a significant fraction pulsate, which allows high precision asteroseismology.

The biggest challenge for the formation scenarios of the hot subdwarfs is to answer how they lose most of the material at the atmosphere and end up with a very thin hydrogen-rich layer. There are several formation channels proposed, for single and binary system origins:

i. Mergers of He-WD and a post-sdB or two He-WDs,

ii. Stable Roche lobe overflow to a more massive secondary,

iii. Common-envelope ejection in a close binary.

Except the merger channel, these formation channels generally lead to H-rich sdBs. While it is thought that the hydrogen deficient He-sdO stars are formed through mergers, also the sdB stars may be the progenitors of He-sdOs (Justham et al., 2010).

The vast majority of sdB stars have helium-deficient surfaces. A minority ($\sim 10\%$) show a surface helium abundance in the range of 10% to 99% by number. Since hot subdwarfs have radiative envelopes and a high surface gravity ($\log g \gtrsim 4.1$), radiative levitation and gravitational settling combine to make helium sink below the more opaque hydrogen-rich surface (Heber, 1986). A clue to understanding the helium-rich subdwarfs (He-sds) is that they lie at lower gravities and higher temperatures than helium-poor subdwarfs, essentially on the track of a star evolving onto the low-mass helium main sequence (Figure 1.5). The hypothesis is that roughly 10% of He-sds (1% of sdBs) represent proto-EHB stars. The rationale to support this hypothesis is that EHB stars are believed to form from red-giant cores stripped following a close binary interaction, or following the merger of two white dwarfs. In the case of the stripped core, a thin hydrogen-envelope may remain; it may be polluted by helium following flash-driven convection if helium ignition is late (Miller Bertolami et al., 2008). In a WD merger, the surface of the post-ignition product will be dominated by helium (Zhang and Jeffery, 2012). In either case, the abundances of other elements (carbon, nitrogen, *etc*.) depend on prior history, the physics of helium ignition, and the mixing. In both cases, helium ignition is off-center implying that the "*zero-age*" star is a shell-burning star above the classical zero-age horizontal branch. As helium-burning shifts inwards, the star contracts on a timescale $\sim 10^5$yrs to arrive

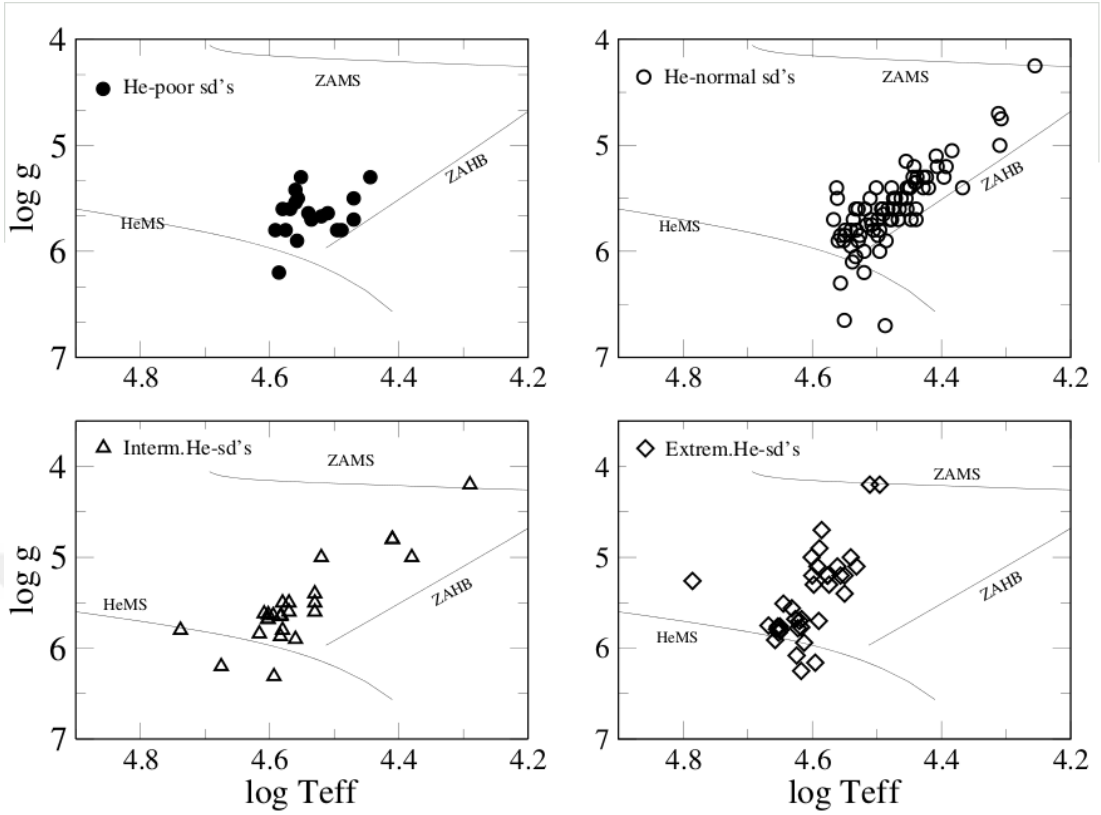

Figure 1.5: Surface gravities and temperatures of helium-poor, helium-normal, intermediate-helium and extreme-helium sdBs (and sdOs). The horizontal-branch and hydrogen and helium main sequences are indicated in each panel. Courtesy: Simon Jeffery

on the EHB when He-burning reaches the center. With decreasing luminosity, and providing $T_{\rm eff} < 40000$K, the radiative diffusion timescale drops from $> 10^6$yrs to $\sim 10^5$yrs, enabling a switch from a surface chemistry determined by nuclear history to one dominated by specific elemental opacities and radiative equilibrium.

Hot subdwarfs are not included in the MK-spectral classification system as they are "*peculiar*" stars. Green et al. (1986) established a system for these "*peculiar*" stars based on `H/He` and `HeI/HeII` line strengths ratios, in a different fashion than MK-system. Drilling (1996) suggested that the system of Green et al. (1986) suffers from large differences in physical characteristics of adjacent classes and an MK-like system is needed. After many revisions and refinements, Drilling et al. (2013) defined *the MK-like spectral classification system for hot subdwarfs* which mainly groups the objects according to their *helium strength*.

This system suggest to group the spectra according to the helium strength first, and than to the MK-type. Following this pattern, and selecting one object as a standard of the class, they produced diagrams that showing these standards ordered in a way that Balmer line strengths change smoothly between the classes (Figure 1.6 –1.9, for He-weak, He-normal, He-strong C

and He-strong, respectively).

In the classification system, the depths of the Hγ (4340Å), HeI 4471Å and HeII 4541Å lines are used as guidelines to determine the Helium class, which shown as an integer between 0 (He-weak) and 40 (He-strong) and is *roughly* calculated by:

$$\begin{aligned} &20\,\frac{HeI\lambda4471+HeII\lambda4541}{H\gamma-0.83HeII\lambda4541} && \text{for } 0 \leq \text{He-class } \leq 20 \\ &40-20\,\frac{H\gamma-0.83HeII\lambda4541}{HeI\lambda4471+HeII\lambda4541} && \text{for } 21 \leq \text{He-class } \leq 40 \end{aligned} \tag{1.1}$$

where $HeI\lambda4471$, $HeII\lambda4541$ and $H\gamma$ represents the depths of respective lines. The four helium classes are defined as following:

i. *He-weak*: only H lines, occasionally HeI or HeII (not both), and very weak metallic lines.

ii. *He-normal*: H lines are dominant, both HeI and HeII and/or metallic lines are present.

iii. *He-strong C*: He lines are dominant and C lines are present.

iv. *He-strong*: He lines are dominant, C lines are very weak or absent.

When Drilling et al. (2013) grouped the spectra based on the spectral type, the luminosity class and helium class, they saw that the spectra form 3 linear relations on the (spectral class) –$T_{\rm eff}$ plane as follows:

$$T_{\rm eff}[K] = \begin{cases} 74900-4030s\pm1700 & \text{for O9–B3, He-class 0–28, L-class V–VIII} \\ 63200-2520s\pm1600 & \text{for O7–B1, He-class 35–40, L-class V–VIII} \\ 28700-841s\ \ \pm1900 & \text{for B2.5–B8, He-class 0–11, L-class I–IV} \end{cases} \tag{1.2}$$

where s equals to spectral subclass index for sdOs and spectral subclass index plus 10 for sdBs (e.g. 1 for sdO1, 3 for sdO3, 12 for sdB2, 15 for sdB5).

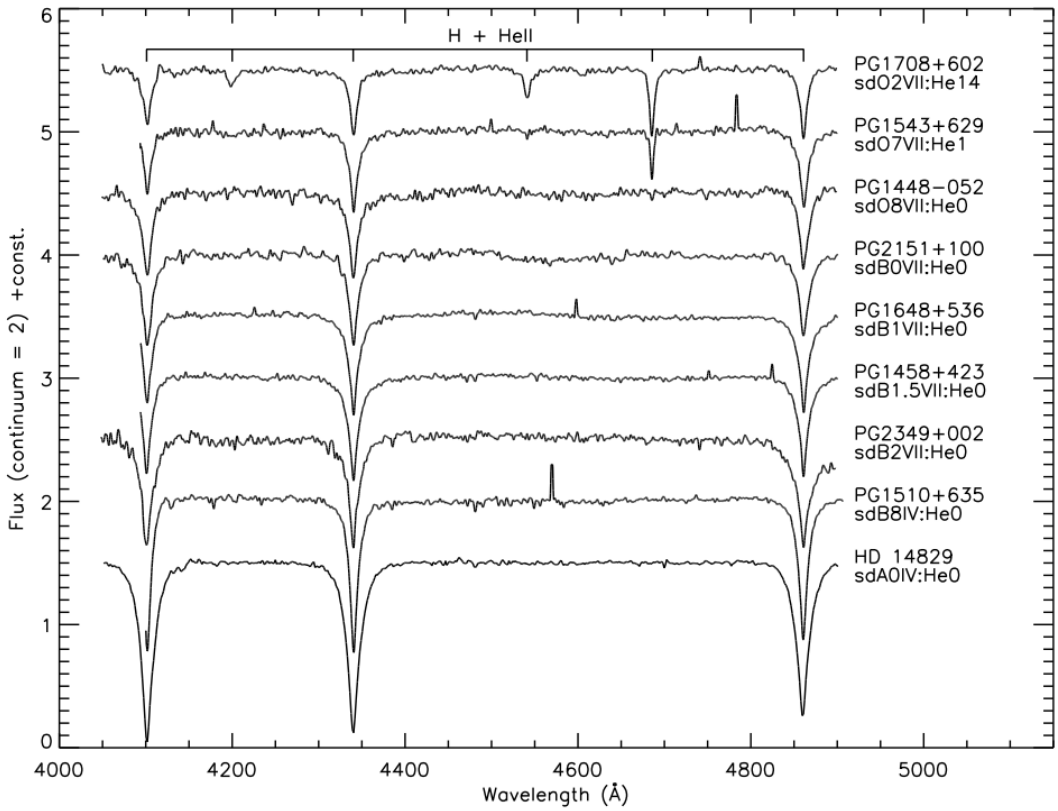

Figure 1.6: The standard spectra of the He-weak class of the system of Drilling et al. (2013), from top to bottom, decreasing order of the Balmer line strength (Fig.2 of Drilling et al. (2013)).

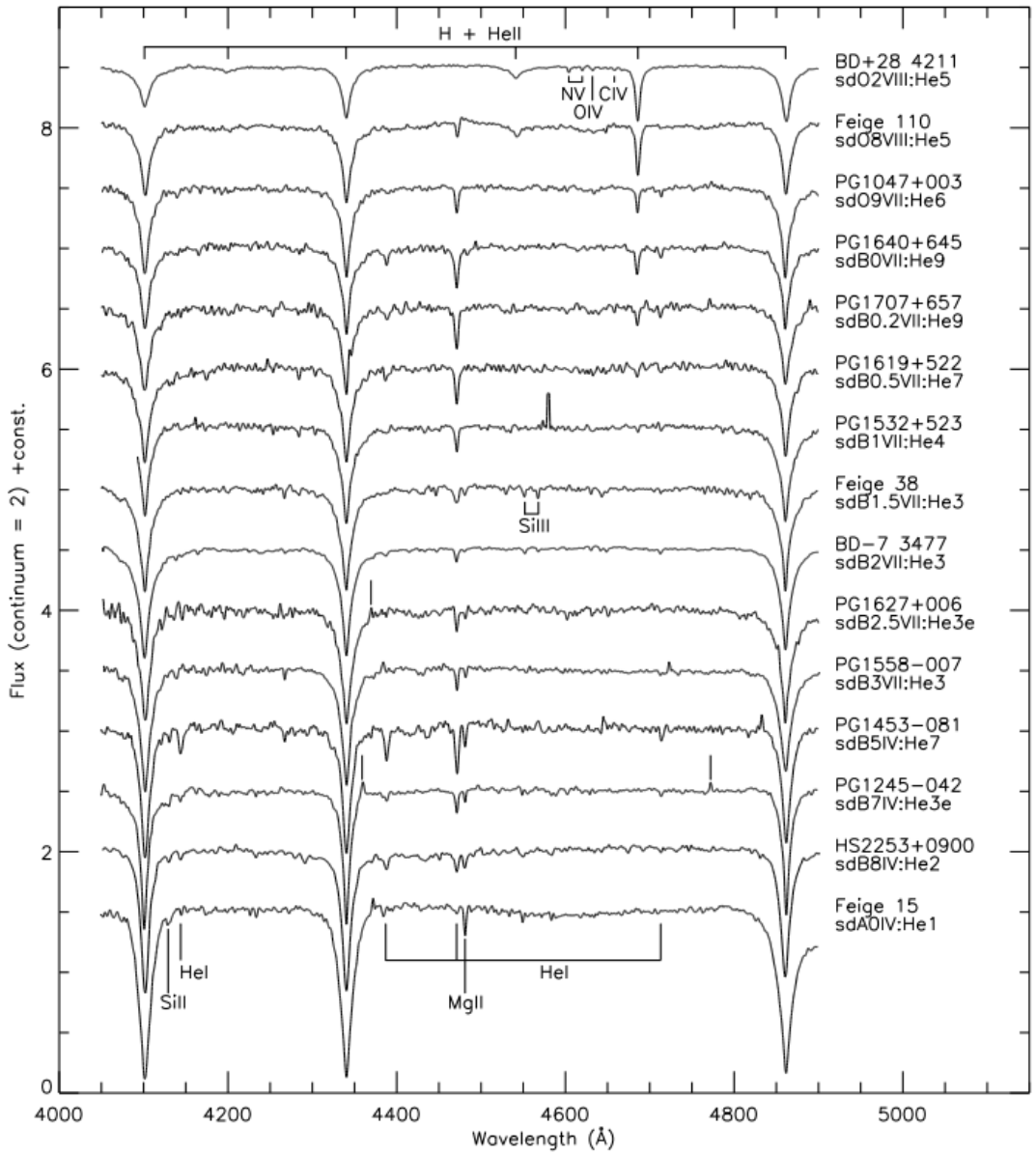

Figure 1.7: The standard spectra of the He-normal class of the system of Drilling et al. (2013), from top to bottom, decreasing order of the Balmer line strength (Fig.1 of Drilling et al. (2013)).

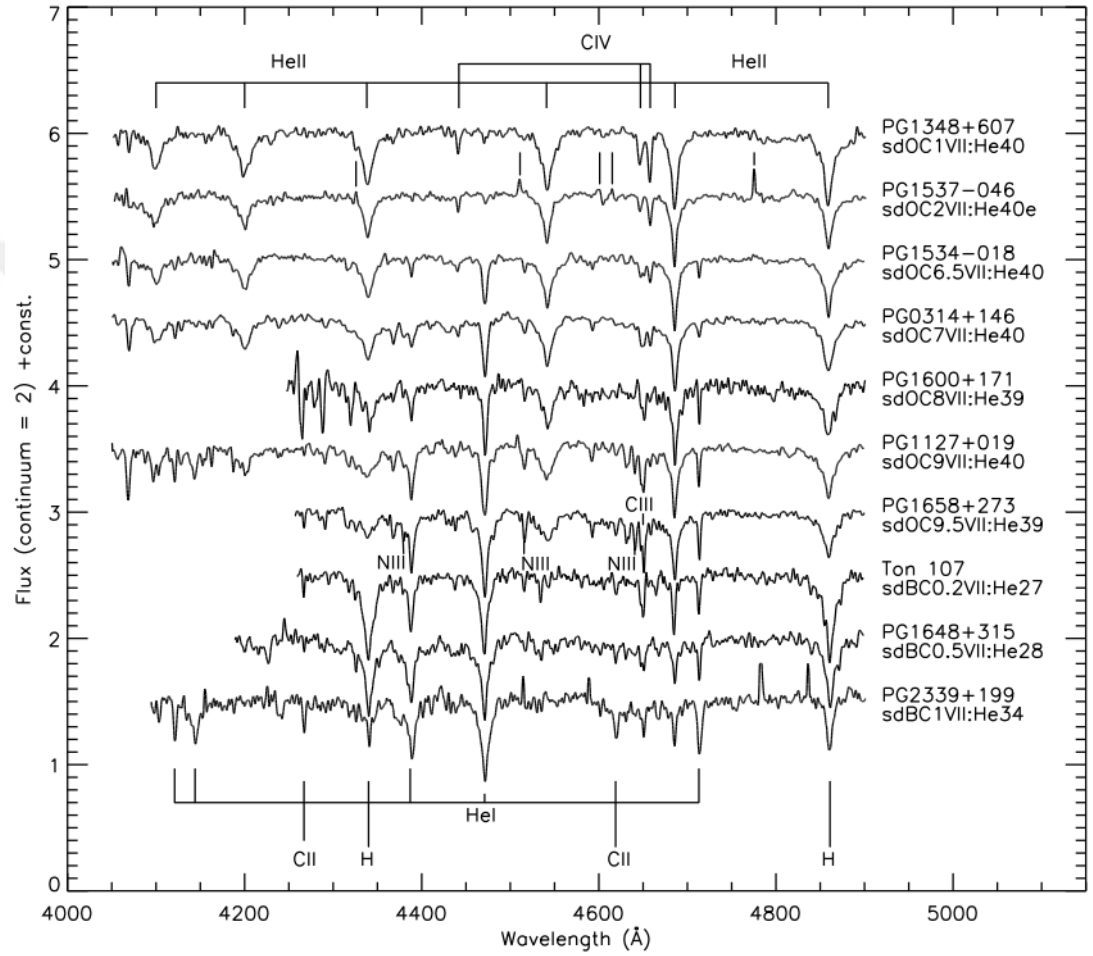

Figure 1.8: The standard spectra of the He-strong C class of the system of Drilling et al. (2013), from top to bottom, decreasing order of the Balmer line strength (Fig.3 of Drilling et al. (2013)).

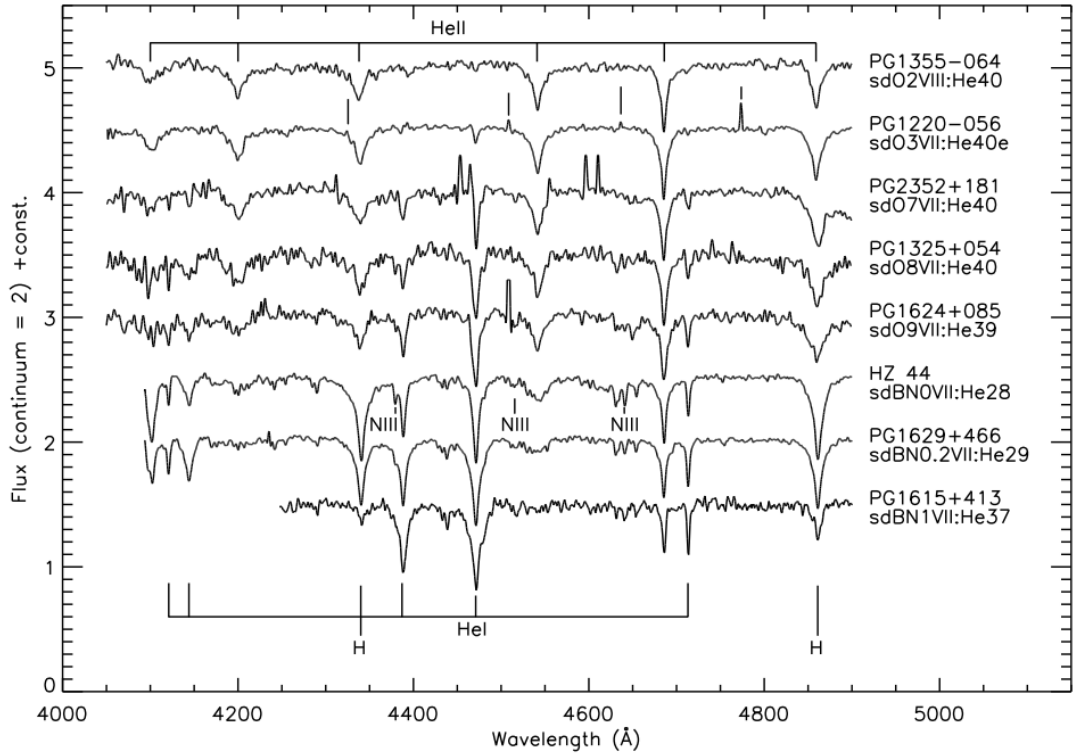

Figure 1.9: The standard spectra of the He-strong class of the system of Drilling et al. (2013), from top to bottom, decreasing order of the Balmer line strength (Fig.4 of Drilling et al. (2013)).

1.4.3 Stellar Pulsators

Stellar pulsators are stars whose radius changes because of instabilities beneath their surface. These instabilities are caused by ionisation of an abundant element at a critical depth in the star (Cox, 1980). While the pulsations could be constant in every direction (*i.e*. radial pulsators), it is also possible to be anisotropic (*i.e*. non-radial pulsators). In the RATS data there are a few types of stellar pulsators, namely δ Scuti stars, SX Phe stars, roAp stars (rapidly oscillating peculiar A type stars), pulsating white dwarfs (*i.e*. hydrogen-rich DAV or ZZ Cet stars, helium-rich DBV or V777 Her stars, carbon-rich DQ pulsators), sdB stars. I give more details on these objects where I identify the nature of blue variable object I have found in the RATS archive, in §5.3.

1.4.4 Cataclysmic Variables

Cataclysmic variables (CVs) consist of an accreting white dwarf and a mass transferring companion star (donor) which can be a main sequence star or a white dwarf (as in AM CVns). Some

of these systems exhibit irregular outbursts which increase the brightness significantly and typically last for several weeks. Outbursts are caused by ignition of the transferring *-usually hydrogen-rich-* matter which forms a disk in most cases and is heated up where it falls onto the white dwarf. If the white dwarf accretes enough matter so that it reaches the Chandrasekhar limit, it can produce a Type Ia supernova explosion and be destroyed completely.

Apart from irregular outbursts, they also show periodic modulations in their light-curves, with periods related to their orbital periods. As these systems have a hydrogen dominated companion unlike AM CVns, their orbital periods *-and periods of modulations on brightness-* have a minimum limit of $\sim 80^{min}$ (Gänsicke et al., 2009), althought there are some sub-period minimum CVs (e.g. Augusteijin et al., 1996; Littlefield et al., 2013). For a detailed review, I refer the reader to Warner (2003).

1.4.5 AM CVn systems

AM CVn systems, a sub-class of Cataclysmic Variables (CVs), are very short-period ($5^{min} <$ P $< 65^{min}$), hydrogen deficient, *-mostly-* double degenerate binary systems. These systems may also be composed of one degenerate and one semi-degenerate helium star. Their helium dominated spectra almost never have any trace of hydrogen (Solheim, 2010). These binaries, before becoming an AM CVn system, pass through one or two common-envelope phases in their evolution, and then, as proposed by Kraft et al. (1962), gradually get closer to each other because of the angular momentum loss due to gravitational radiation. As they get closer, at some point, the Roche lobe of the less massive star gets as small as the volume of the star and the massive one (accretor) starts to accrete helium from the less massive hydrogen-deficient star (donor). From that moment on, those systems are known as AM CVn systems. After some point, the mass transfer begins to dominate the evolution of the system, rather than the gravitational wave radiation, and the orbit stops shrinking. In the course of time, while mass transfer decreases, the period increases. The transferred mass commonly (systems with P $> 10^{min}$) creates a disk around the accretor. Systems with period less than 10 minutes do not develop a disc, as the Roche lobe of the accretor is not big enough, and transferring material hits the accreting white dwarf's surface directly. This hot point on the disc or on the accretor is the reason behind variations in the optical light or X-ray, respectively. As mass transfer decreases to a very low level and period becomes very long (longer than $\sim 40^{min}$), the disk shrinks and the primary star becomes visible; the system does not show variations in brightness any more. After this point, the system lives the last part of its life while the mas transfer rate is decreasing and the period is getting longer. There are two ways that the AM CVn system could end its journey. If the primary star passes the Chandrasekhar Limit due to the mass it has accreted, it explodes and produces a Type Ia supernova (SNIa). Otherwise, transfer stops at the point that the Roche lobe of the secondary star is not filled anymore due to the increased

distance between the stars, and leaves us a planetary mass object orbiting a helium-rich white dwarf (Solheim, 2010).

The prototype of the class, AM CVn itself, was first catalogued by Malmquist (1936) in the "*Investigations on the Stars in High Galactic Latitudes*". Humason and Zwicky (1947) noted it as "*decidedly blue*" and named it HZ29 (star number 29 in the HZ catalogue) in their catalogue of faint blue stars. Greenstein and Matthews (1957) realised that HZ29 was an atypical example and had "*the most peculiar spectrum observed*" amongst the others in the HZ catalogue (Figure 1.10). They stated that its spectrum differed substantially from the normal helium-rich white dwarfs. In HZ29's spectra, HeI lines were "*very shallow and so diffuse as to appear almost double*", instead of "*strong, easily visible and relatively deep*". Even though they suspected binarity as the reason of almost double lines, they concluded that the reason was rotation of the single star.

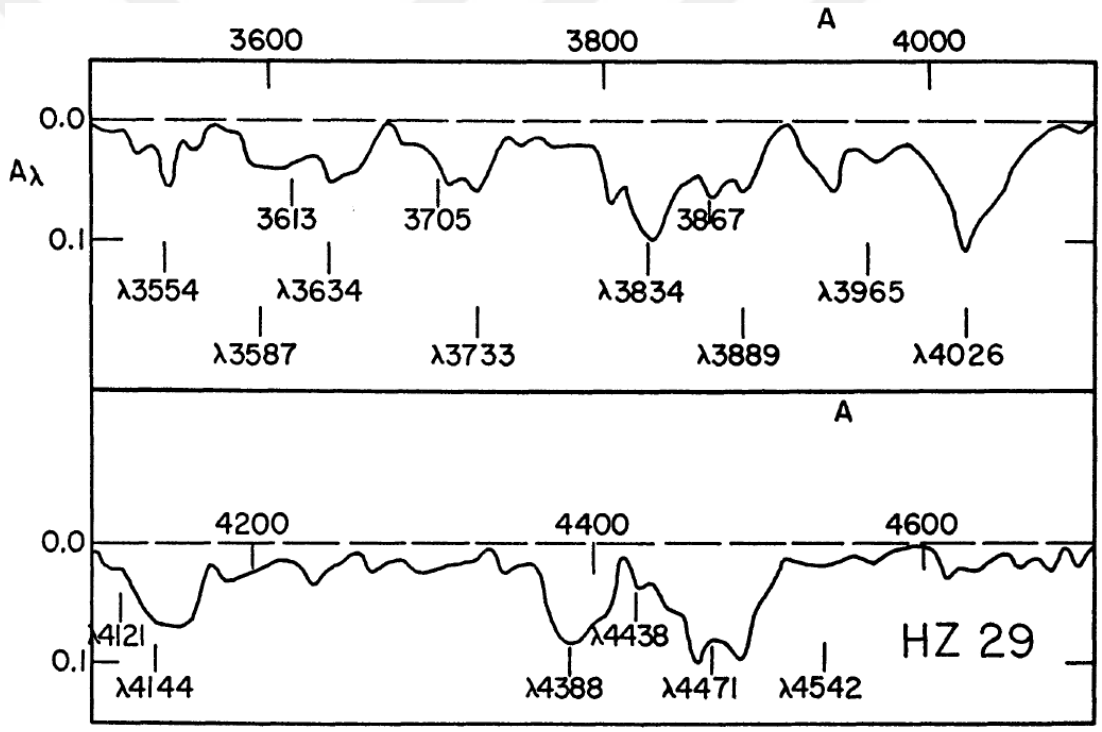

Figure 1.10: Helium dominated spectrum of HZ 29 (AM CVn itself) (Greenstein and Matthews, 1957).

The peculiarities of HZ29's spectrum were even interpreted as a spectrum of a QSO (Quasi-stellar object, Quasar) instead of a white dwarf (Burbidge et al., 1967). Smak (1967) was the first to assign HZ 29 as a binary star, with a period of 18 minutes. Shortly after, Paczyński (1967) realised that HZ29 might be the first example of a close pair of white dwarfs which were entirely hypothetical systems until then. He suggested that if HZ29 is a double white dwarf system, "*this system could be most easily used to check the existence of gravitational*

radiation". In 1968, the star was designated as AM CVn (Kukarkin et al., 1968). Although widely accepted, the binary nature of AM CVn was not proved definitively until Nelemans et al. (2001a) folded its time-resolved spectra on a 1028.73s period and saw clear "*S-wave*" in HeI lines at 4143Å, 4387Å and 4471Å.

After AM CVn, a number of systems have been discovered in the same manner —extremely blue objects with short periodic variations in their brightness and no trace of hydrogen in their spectra (e.g. GP Com, CR Boo, V803, CP Eri and HP Lib). After their spectra were investigated, the real nature of some objects that initially thought to be supernovae turned out to be AM CVn systems with outbursts. For example, KL Dra, designated SN 1998di previously, found by Schwartz (1998) as a 16.8 magnitude source which had not been there in a 19 magnitude limited image taken 11 days ago. Wide HeI lines and a modulation in its light-curve on a period of 25.03^{min} (Wood et al., 2002) revealed it as an AM CVn. The spectra of V406 Hya which was found and designates as SN2003aw by Wood-Vasey et al. (2003), that are consisted of blue continuum with broad and weak neutral helium lines (Chornock and Filippenko, 2003), and fast photometry (Woudt and Warner, 2003), showing a 2041 sec period, revealed its AM CVn nature.

The sources found in the SDSS (Sloan Digital Sky Survey)[3] data made a huge contribution to the number of known AM CVn systems. Since 1967, 13 AM CVns were found until 2005; after 2005 until today, more than that have been found in the SDSS data. A list of known AM CVn systems are presented in Table 1.1.

[3] `http://www.sdss3.org/`

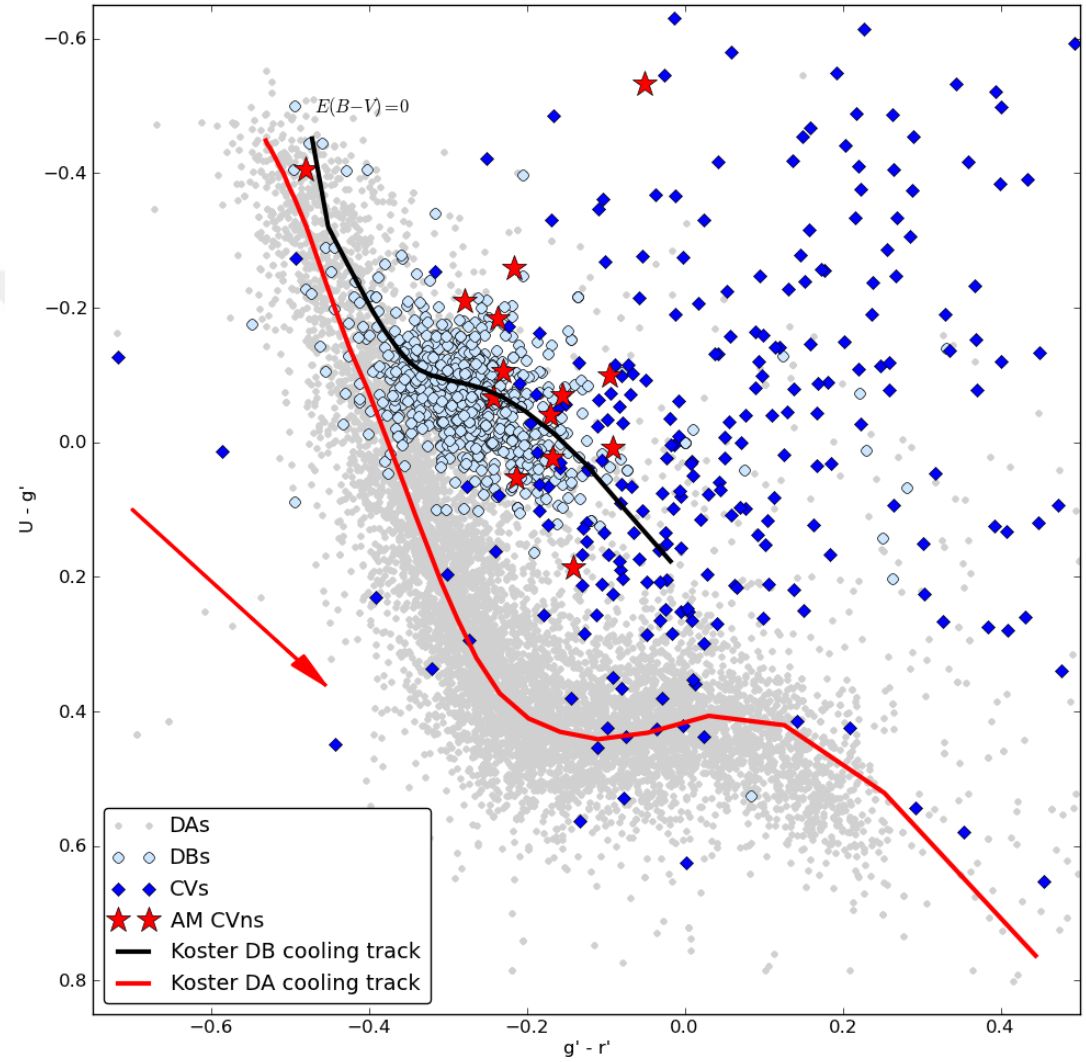

Figure 1.11: A group of AM CVns on the colour-colour diagram, with DAs, DBs, CVs, and Koster WD cooling tracks.

Table 1.1: Known AM CVn systems.

#	Name	Alternative name	Ra	Dec	Period (min)	Magnitude	Outburst?	References
1	HM Cnc	RX J0806.3+1527	08:06:22.84	+15:27:31.5	5.4	21.1	AiHS	1
2	V407 Vul	RX J1914.4+2456	19:14:26.09	+24:56:44.6	9.5	>19.7	AiHS	2
3	ES Cet	KUV 01584-0939	02:00:52.17	-09:24:31.7	10.3	17.1	AiHS	3
4	AM CVn	HZ 29	12:34:54.60	+37:37:44.1	17.1	14.02	AiHS	4
5	SDSSJ1908+3940	KIC004547333	19:08:17.07	+39:40:36.4	18.2	16.1g	AiHS	5
6	HP Lib	EC 15330-1403	15:35:53.08	-14:13:12.2	18.4	13.59^{K215}	AiHS	6
7	CXOGBS J175107.6-294037		17:51:07.60	-29:40:37.0	22.9	17.6	AiHS	37
8	$PTF1J1919+4815^{Eh}$	PTFS1119aq	19:19:05.19	+48:15:06.2	22.5	20.16g	✓	7
9	CR Boo	PG 1346+082	13:48:55.22	+07:57:35.8	24.5	14.5	✓	8, 9
10	KL Dra	SN1998di	19:24:38.28	+59:41:46.7	25.0	16.8-20	✓	10
11	V803 Cen	AE1	13:23:44.54	-41:44:29.5	26.6	14.0	✓	6, 11
12	PTF1J0719+4858	PTF09hpk	07:19:12.13	+48:58:34.0	26.8	15.8-19.4g	✓	12
13	$SDSSJ0926+3624^{E}$		09:26:38.71	+36:24:02.4	28.3	19.0g	✓	13, 14
14	CP Eri		03:10:32.76	-09:45:05.3	28.7	16.5-19.7	✓	15
15	PTF1J0943+1029	PTFS1109h	09:43:29.59	+10:29:57.6	30.4	20.69g	✓	16
16	CSS010550+190317		01:05:50.10	+19:03:17.2	31.6	19.6g	✓	17
17	V406 Hya	SN2003aw	09:05:54.79	-05:36:08.6	33.8	15-20.5	✓	4
18	PTF1J0435+0029	PTF11avm	04:35:17.73	+00:29:40.7	34.3	21.12g	✓	16
19	SDSSJ1730+5545		17:30:47.59	+55:45:18.5	35.2	20.14g	✗	18, 19
20	SDSSJ1240-0159		12:40:58.03	-01:59:19.2	37.4	$18.0 - 19.7^{K217}$	✓	20
21	SDSSJ0129+3842		01:29:40.06	+38:42:10.5	37.6	19.8	✓	13, 21
22	SDSSJ1721+2733		17:21:02.48	+27:33:01.2	38.1	20.1	✓	22
23	SDSSJ1525+3600	ASASSN-15of	15:25:09.58	+36:00:54.6	44.3	19.8g	✓	22, 21
24	SDSSJ0804+1616		08:04:49.49	+16:16:24.8	44.5	18.2g	✗	23
25	SDSSJ1411+4812		14:11:18.31	+48:12:57.6	46.0	19.4g	✗	13
26	GP Com	G 61-29	13:05:42.43	+18:01:04.0	46.5	15.94	✗	24, 25
27	CSS121123:045020-093113		04:50:19.82	-09:31:12.8	47.3	20.5	✓	26
28	SDSSJ0902+3819		09:02:21.36	+38:19:41.9	48.3	20.2g	✓	22
29	$Gaia14aae^{E}$		16:11:33.97	+63:08:31.8	49.7	18.0g	✓	27
30	SDSSJ1208+3550		12:08:41.96	+35:50:25.2	52.6	18.8g	✗	28, 21
31	SDSSJ1642+1934		16:42:28.08	+19:34:10.1	54.2	20.3	✗	22, 21
32	SDSSJ1552+3201		15:52:52.48	+32:01:50.9	56.3	20.2g	✗	6
33	V396 Hya	CE 315	13:12:46.93	-23:21:31.3	65.1	17.6	✗	29
34	ASASSN-14cc		21:39:48.24	-59:59:32.4	$22.5^{sh?}$	19.0-20.0	✓	30
35	ASASSN-15kf		15:38:38.24	-30:35:49.7	27.7^{sh}	19.4	✓	31
36	2QZ J1427-01	SDSSJ1427-0123	14:27:01.70	-01:23:10.0	36.6^{sh}	15-20.3	✓	32
37	ASASSN-14mv		07:13:27.28	+20:55:53.4	40.8^{sh}	17.3^{K218}	✓	17
38	ASASSN-14ei		02:55:33.39	-47:50:42.0	43.0^{sh}	18	✓	33
39	SDSSJ1137+4054		11:37:32.32	+40:54:58.3	59.6?	19.00g	✗	19
40	ASASSN-14fv		23:29:55.13	+44:56:14.4		20.5	✓	34
41	CRTSJ0744+3254		07:44:19.70	+32:54:48.0		20.60g	✓	35
42	CRTSJ0844-0128		08:44:13.60	-01:28:07.0		20.00g	✓	35
43	PTF1J0857+0729	PTF11aab	08:57:24.27	+07:29:46.7		21.83g	✓	16
44	PTF1J1523+1845	PTF10noc	15:23:10.71	+18:45:58.2		23.27g	✓	16
45	PTF1J1632+3511	PTF11dkq	16:32:39.39	+35:11:07.3		22.99g	✓	16
46	PTF1J2219+3135	PTFS1122aw	22:19:10.09	+31:35:23.1		20.38g	✓	16
47	SDSSJ1043+5632	PTFS1210s	10:43:25.08	+56:32:58.1		20.28g	✓	18
48	SDSSJ1319+5915		13:19:54.47	+59:15:14.8		19.1g	✗	36
49	SDSSJ1505+0659		15:05:51.58	+06:59:48.7		19.11g	✗	19
50	SDSSJ2047+0008		20:47:39.40	+00:08:40.3		17.5-24g	✗	28

^{E} : Eclipsing, ^{Eh}: Eclipsing (hot spot), $^{K2\#}$: Falls in K2 #, ^{sh}: Superhump, AiHS: Always in high state

1: Roelofs et al. (2010), 2: Steeghs et al. (2006), 3: Espaillat et al. (2005), 4: Roelofs et al. (2006), 5: Kupfer et al. (2015)
6: Roelofs et al. (2007b), 7: Levitan et al. (2014), 8: Patterson et al. (1997), 9: Kato et al. (2000), 10: Wood et al. (2002)
11: Patterson et al. (2000), 12: Levitan et al. (2011), 13: Anderson et al. (2005), 14: Copperwheat et al. (2011), 15: Groot et al. (2001)
16: Levitan et al. (2013), 17: Motsoaledi (2015), 18: Carter et al. (2013), 19: Carter et al. (2014), 20: Roelofs et al. (2005)
21: Kupfer et al. (2013), 22: Rau et al. (2010), 23: Roelofs et al. (2009), 24: Nather et al. (1981), 25: Marsh (1998)
26: Woudt et al. (2013), 27: Campbell et al. (2015), 28: Anderson et al. (2008), 29: Ruiz et al. (2001), 30: Kato et al. (2015)
31: Kato et al. (2016), 32: Woudt et al. (2005), 33: Prieto et al. (2014), 34: Wagner et al. (2014), 35: Breedt et al. (2014)
36: Kepler et al. (2015), 37 Wevers et al. (2016)

1.5 How do we find these compact blue objects?

Wide field photometric surveys are often used to search for all kinds of celestial objects. There are a number of surveys observing different parts of the sky, with different cadence (the time between exposures), filters, methods, and sensitivities according to the questions they serve to answer. When it comes to compact blue objects, a survey should have high sensitivity as these objects are intrinsically faint. Although there are dedicated surveys (*e.g*. Supernova Legacy Survey, Faint Sky Variability Survey), general surveys like SDSS can also be used to search for compact objects. To find systems with very short periods (less than one hour) like AM CVn systems, one needs a deep survey with high cadence. The RATS project has been initiated to satisfy this need.

The details of the search for these compact objects in the survey data is discussed in §2.

1.5.1 RATS: RApid Temporal Survey

The RATS project was started with the motivation of exploring the space density of AM CVn systems. For this purpose, a strategy of taking short exposures ($\sim$30 seconds) of a field for approximately two hours with 2 meter class telescopes was followed. While no filter was used for time-series, complementary colour information was taken through several filters for each field. Considering its high cadence (3 min.) and depth in magnitude ($g' = 23$), the RATS project was a whole new window on the variable sky. The survey ran for $\sim$7 years and captured data from $\sim$25 square degrees of sky near to the Galactic plane, and a further $\sim$15 square degrees away from the Galactic plane (Ramsay and Hakala, 2005; Barclay et al., 2011).

1.5.2 How does the RATS strategy compare to previous surveys?

There are similar surveys, some are deeper than that adopted for the RATS strategy, some have higher cadence; but none of them have both of these specifications at once. For example, while the SuperWASP project has a really high cadence of 1 minute (only in some fields and epochs), its sensitivity doesn't go to fainter than $\sim$15 mag. Detailed information about other surveys and their features can be seen in Table 1.2.

Table 1.2: Overview of recent high-cadence synoptic surveys. Taken from Macfarlane et al. (2015).

Survey	Field location (deg)	Total sky coverage (deg^2)	Depth (V mag)	Variability sensitivity (min)
OmegaWhite[a]	$\|b\| \leq 10$	400	21.5	>6
RATS[b]	$\|b\| \leq 30$	46	22.5	>5
RATS-Kepler[c]	$6 \leq \|b\| \leq 21$	49	22.5	>5
FSVS[d]	$\|b\| \geq 20$	23	24.0	>24
DLS[e]	$\|b\| < 10$	21	25.5	>15
Kepler[f]	$15 \leq \|b\| \leq 25$	116	20.0	>1 or > 30
SuperWASP[g]	All sky	All sky	15.0	>10

[a]Macfarlane et al. (2015), [b](Ramsay and Hakala, 2005), [c]Ramsay et al. (2014)
[d]Faint Sky Variability Survey (Groot et al., 2003), [e]Deep Lens Survey (Becker et al., 2004)
[f]Borucki et al. (2010), [g]Wide Angle Search for Planets (Pollacco et al., 2006)

1.5.3 The current status of the RATS project

After 10 observation runs in 7 years, ∼40 square degree of the sky, of which ∼25 square degrees near the Galactic plane and a further ∼15 square degrees away from the plane in a total of 151 fields, have been observed. Details can be seen in the Table 1.3.

Table 1.3: Summary of observation epochs.

Run ID	Epoch ID	Dates	# of fields	Square degree	Galactic latitudes	# of stars	Filters
1	INT1	2003 Nov 28-30	12	3.4	$> \|16^o\|$	45572	WBVi′
2	INT2	2005 May 28-31	14	4.0	*	234029	WBVi′
11	ESO1	2005 Jun 03-07	20	6.2	**	750109	WBVI
3	INT3	2007 Jun 12-20	26	7.5	$< \|15^o\|$	1223803	WUg′r′
4	INT4	2007 Oct 13-20	29	8.3	$< \|10^o\|$	678025	WUg′r′
5	INT5	2008 Nov 03-09	9	2.6	$< \|10^o\|$	112788	WUg′r′
6	INT6	2009 Oct 09-13	20	5.7	$< \|11^o\|$	383960	WUg′r′
7	INT7	2009 Dec 08-12	11	3.2	***	153991	WUg′r′
12	ESO2	2010 Mar 18-24	15	4.7	****	531135	WUBV
8	INT8	2010 Jun 16-20	13	3.7	$5^o < b < 17^o$	369463	WUg′r′

*: 3 fields $< |10^o|$ and 11 fields $> |22^o|$ ***: 1 field $\sim 25^o$ and 19 fields $< |10^o|$
: 4 fields $< |10^o|$ and 16 fields $> |16^o|$ **: 2 fields $> |20^o|$ and 13 fields $< |10^o|$

The data obtained in the first five years of the RATS project have been investigated via short-term flux variability with a method developed by Barclay et al. (2011). The method makes use of two different algorithms, namely analysis of variance (AoV) and the Lomb-Scargle periodogram (LS) (Lomb, 1976; Scargle, 1982), and `VARTOOLS` suite of software (Press et al., 1992; Hartman et al., 2008). Using this method, $1.2x10^5$ objects out of $3x10^6$ (4.1%) have been

assigned as periodic variable. 66 of these variable sources showed periodic modulations less than 40 minutes, which is the upper limit for any known AM CVn system to vary in optical light (see first paragraph of §1.4.5 and Table 1.1), while having colours consistent with the known AM CVn systems. A number of these candidates have been observed spectroscopically to verify their status. Although no AM CVn systems have been confirmed by follow-up spectroscopic observations, some A-type stars with short periods (20-35 min) and a pulsating white dwarf with a hot companion have been identified (see Barclay et al. (2011) for further details).

1.6 Thesis Outline

The next chapter is "*Identifying classes of objects through colour selection*", where I introduce the method I developed to find the compact blue objects in the RATS archive, and give further details about the refinement of the selected sample. Afterwards I present the spectral follow-up observations of the blue sources that have been selected, that is carried out using the 10.4 meter GTC (Grand Telescopio Canarias), and the identification of the sources we have observed. Chapter 4, "*Detailed analysis of UVES spectra of two He-rich subdwarfs*", focuses on the high resolution spectra of two He-rich subdwarf I identified in using GTC spectra. In Chapter 5, I identify the blue objects that show short-term periodic flux variations using the light curves in the RATS archive, and unravel their nature using all the information I could put my hands on. Chapter 6 is where I summarise all my efforts and findings, draw conclusions, and envisage the work to be done in the future.

Chapter 2

Identifying classes of objects through colour selection

The primary objective of my study is to find interacting ultra compact binaries (UCBs) in the fields covered by the RATS project. Previous studies using the RATS data were focused on identifying UCBs via photometric variability first, and then selecting those which were found to be variable which had colours similar to known UCBs. However, photometric variability analysis has a number of limitations. If an object varies with an amplitude which is smaller than the survey is sensitive to, or it does not vary in brightness at the time of observation, or it does not vary in optical light at all (*e.g.* non-interacting double white dwarf binaries, AM CVn systems with orbital period longer than 40^{min}), then it will not be identified through photometric variability analysis. As a complementary approach, I have developed an alternative selection method to identify the most astrophysically interesting systems - a method that selects candidate UCBs through their colours. As a followup I also look at the variability of stars in the later RATS fields which had not previously been studied. (§5).

Similar colour-selection procedures have been used for decades to select certain types of objects from surveys. When the targets are AM CVn systems, Cataclysmic Variables and other white dwarf binary systems, sources which are intrinsically blue are identified and selected. Applying basic colour-cuts to data in the light of previous studies and the expectations of the colour of classes of object, is a sensible approach for surveys like SDSS which are away from the Galactic plane. For instance, Roelofs et al. (2009); Carter et al. (2013), used a fairly tight and well defined limits to select their candidates from SDSS.

However, when it is a survey aiming for the Galactic plane, it is not as straightforward as a simple colour-cut to whole data, as the extinction becomes an issue. Since RATS data mainly come from galactic latitude $-15^o < |b| < 15^o$, but also from higher latitudes as well, there is a

big difference between individual fields line of sight extinction (see in Fig. 2.1).

Verbeek et al. (2012) have tackled this problem by doing the colour selection field-by-field to select objects for their "*UV-excess object catalogue*" from UVEX survey which covers galactic plane. Inspired by their work, I have developed a method to select blue objects in our archive by a field-by-field colour-selection. The details of my method and the results are discussed in this chapter.

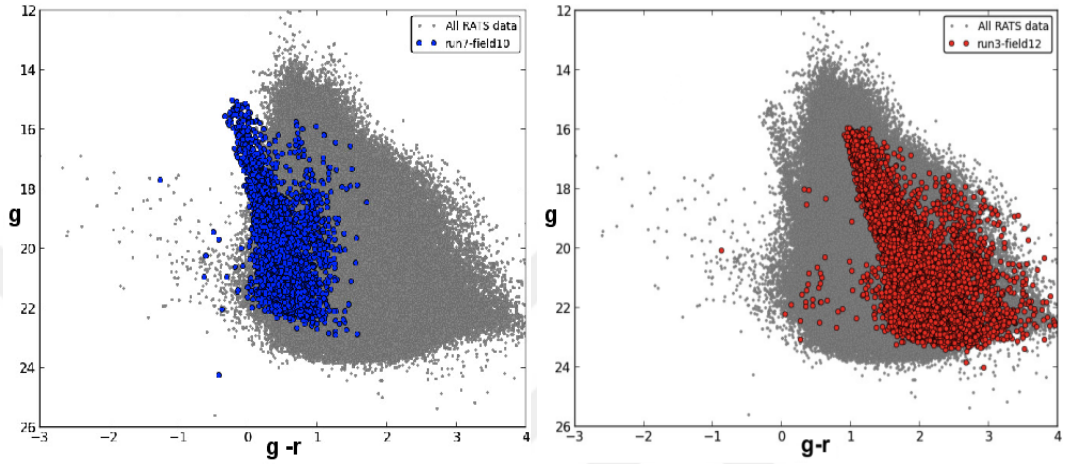

Figure 2.1: The colours of all sources in the RATS database are shown in grey in the $g' - r'$ *vs* g' colour-magnitude diagram with a low-extinction field (left-hand side, blue, Run7-Field10) and a high-extinction field (right-hand side, red, Run3-Field12) over-plotted.

2.1 Colour selection

The colour selection method I have developed, selects objects according to their relative position in the colour-magnitude or colour-colour space for every field. There are number of factors that affect the selection results — the plane that the code works on (i.e. colour-colour or colour-magnitude), the colour (i.e. $g' - r'$ or $U - g'$), the magnitude system (i.e. AB or Vega), the binning method, bins per field, σ cut and so on. After several tests, using different types of known compact blue objects in the data, for some factors I found the optimum values (e.g. 15 magnitude bins per field, 3σ cuts), and for the others, combined the results from a few different choices as I explain below.

As can be seen in Table 1.3, several filter sets were used during the project —Harris BV and Sloan i' for INT1 and INT2; Bessel BVI for ESO1, Bessel UBV for the second ESO observations; RGO U and Sloan $g'r'$ for the rest of the INT observations (Figure 2.2). As the highest number of objects observed using the same filters are observed during INT3 to INT8, I have used only those epochs for the colour selection.

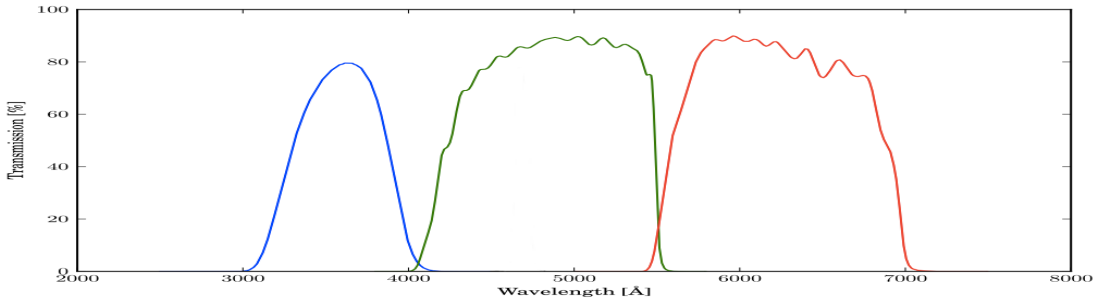

(a) Filters used during the INT3 to INT8 runs. The blue, green and red curves are the RGO U, the Sloan g' and r' filters, respectively. Adapted from Fig.2.5 of Barclay (2010)

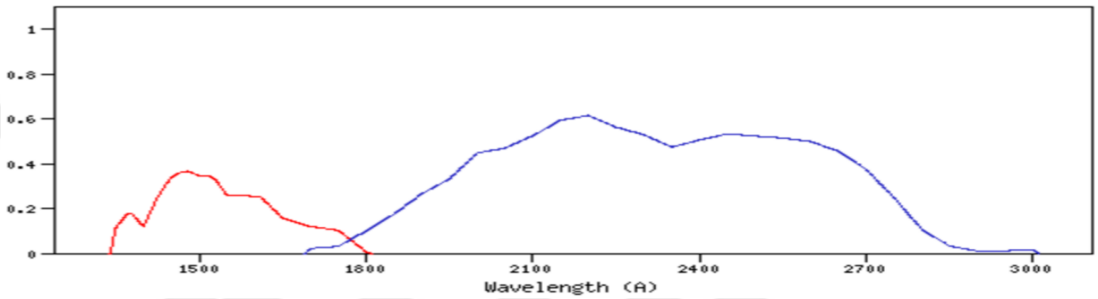

(b) GALEX filters. The red and blue curves are the FUV, far ultra-violet, and the NUV, near ultra-violet filters (2.3.1). Image credit: http://svo2.cab.inta-csic.es/svo/theory/fps3/

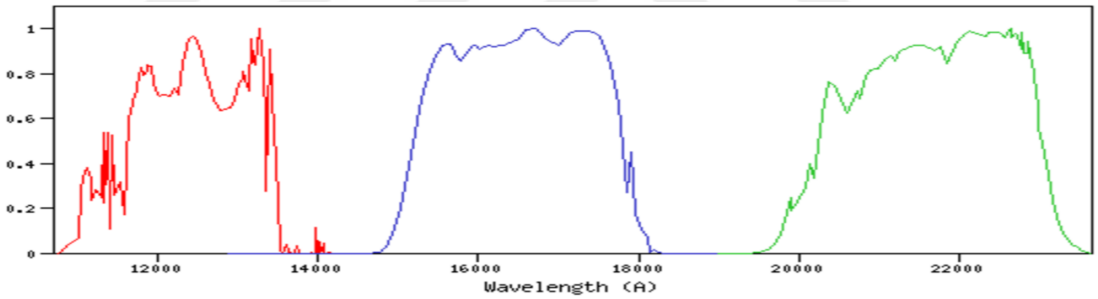

(c) 2MASS filters. The red, blue and green curves are the J, H and the K filters, respectively (2.3.2). Image credit: http://svo2.cab.inta-csic.es/svo/theory/fps3/

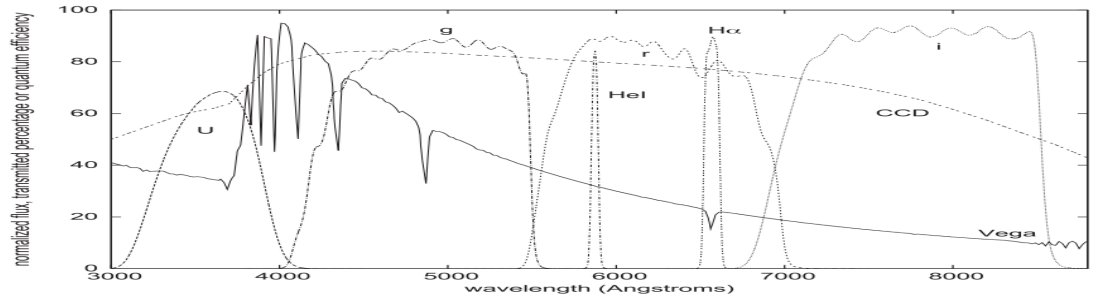

(d) Filter efficiency curves of the U, g, r, HeI 5875, H and i- band filters used in the UVEX survey and IPHAS (dashed and dashdotted curves), overplotted on to the spectrum of Vega (solid curve), together with the CCD-efficiency curve (dashed). Taken from Groot et al. (2009)[Fig.2]

Figure 2.2: Filter efficiency curves of the filters used by the surveys mentioned or of which data is used in this study.

The magnitude information is calculated in the Vega system, and also converted to the AB system to make it possible to compare to SDSS. One can think that the magnitude system should not make any difference in the color selection results. However, as the conversion is not perfect (see CASU webpage[1]) and introduces different errors to the magnitudes in different filters, there are small differences in these approaches. Using the Vega magnitudes, the selection has been done in three different planes — two colour-magnitude planes (i.e. $g' - r'$ *vs* g', and $U - g'$ *vs* g') and a colour-colour plane (i.e. $g' - r'$ *vs* $U - g'$). The selection in each plane has its own advantages, and allows different types of objects to be picked up as well as various further studies to be carried out. Since blue objects are located in different regions in the colour-colour and colour-magnitude planes, the exact algorithim which was used differed. The selection procedure for the colour-magnitude planes (i.e. $g' - r'$ *vs* g' and $U - g'$ *vs* g') basically follows these steps for a given field (see Fig.2.4 and Fig.2.5):

1. Order the sample in g' magnitude and divide the sample into bins;
2. For each and every bin in the field:
   (i) Calculate the standard deviation (σ) of the colours.
   (ii) Assign an object as "*blue*" if
      (a) it is on the blue side of the 3σ cut at the blue side, and
      (b) its distance to the 3σ cut is bigger than 3 times its photometric error.

The method for selecting blue objects from the colour-magnitude plane was inspired by the method selecting the UV-Excess catalogue from the UVEX survey (Verbeek et al. (2012)) although this did not employ the binning method. For specifying the bins two different methods were explored: bins of equal depth in magnitude space, and bins with equal numbers of objects in each bin (Fig. 2.3). I found that, whilst the former method yields good results in the fainter part of the plane, as the number of objects per bin is higher in that region, the latter is a better method to pick up blue objects in the brighter region of the plane. To reduce the effect of outliers on the selection, rather than using the mean, the median was used as the measure of central tendency while the standard deviation was calculated.

[1] `http://www.ast.cam.ac.uk/~wfcsur/technical/photom/colours/`

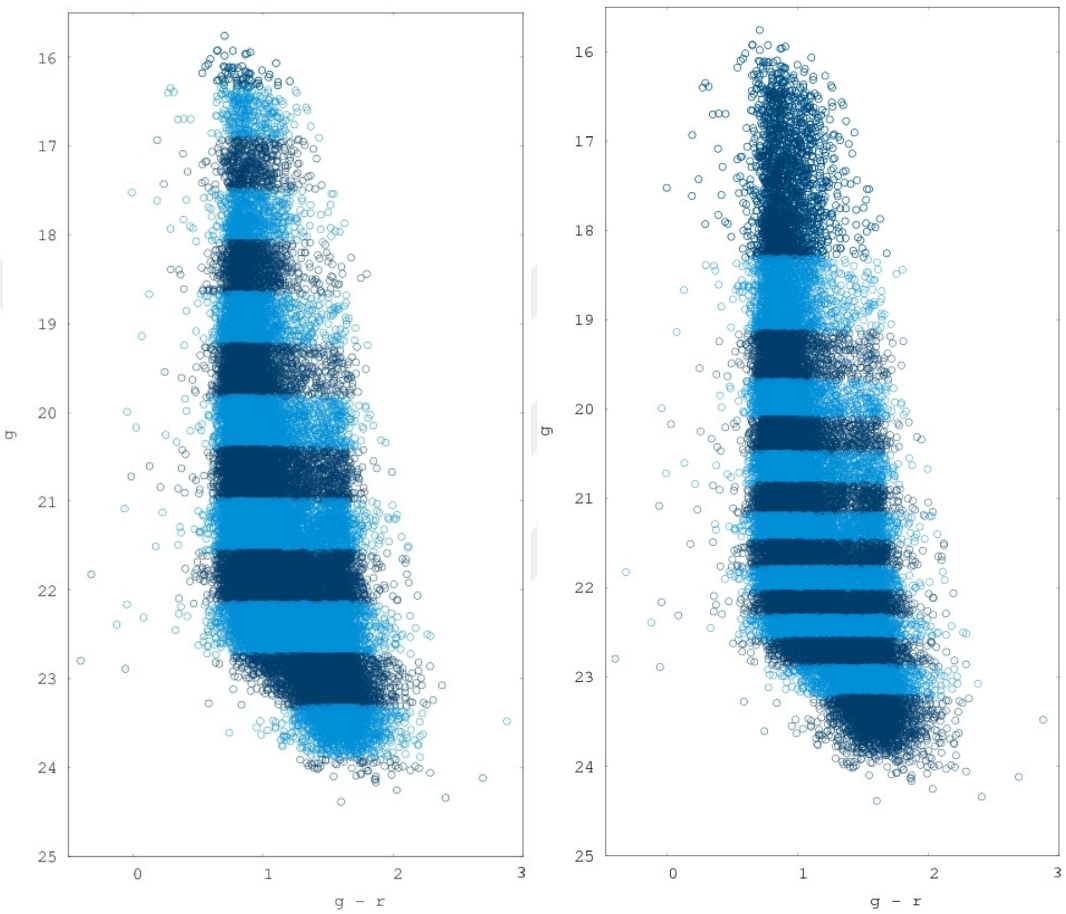

Figure 2.3: Two different binning methods, with 15 bins for each method, is presented using the colour-magnitude diagram of Run3-Field8. On the left-hand side, bins have an equal magnitude depth, and on the right-hand side, bins consist of equal number of stars. While the first method performs well at selecting blue objects at fainter regimes, the second method is more effective in bright regimes.

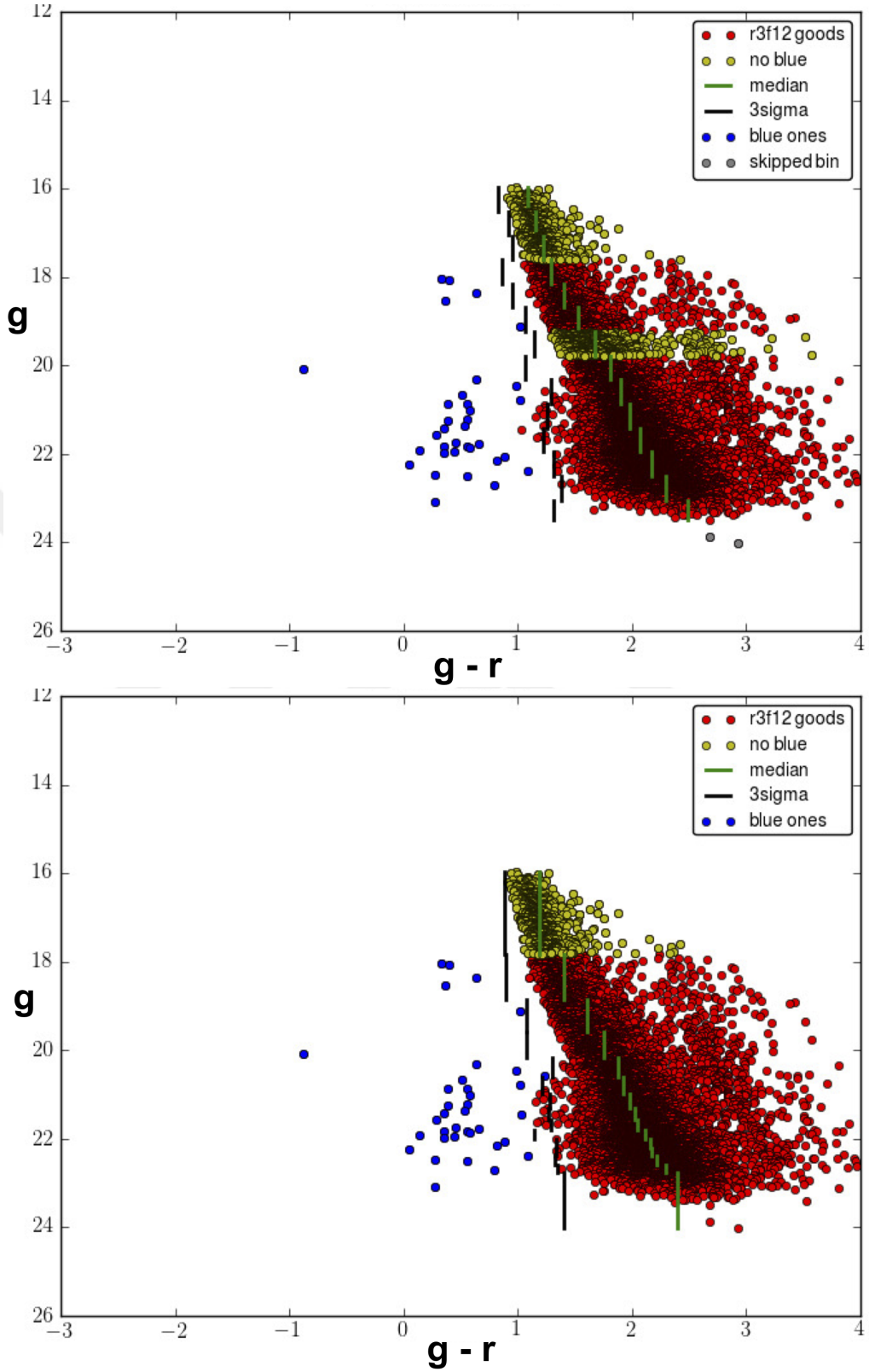

Figure 2.4: Colour selection for Run3-Field12 on the $g' - r'$ *vs* g' colour-magnitude plane. While on the top panel, binning method 1 is used, in the bottom panel, binning method 2 is used, which are "*equal magnitude width*" and "*equal numbers of stars*" bins respectively.

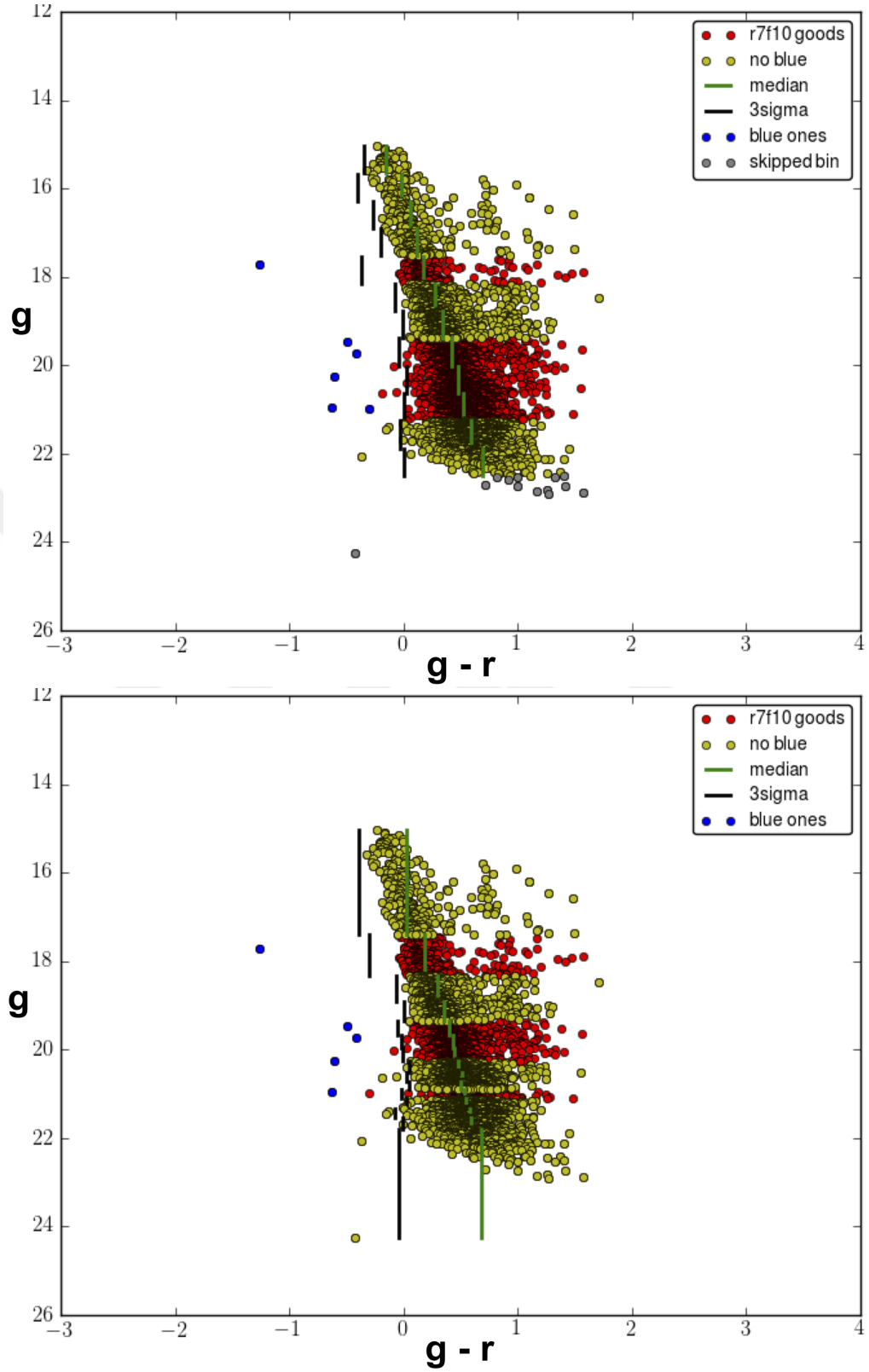

Figure 2.5: Colour selection for Run7-Field10 on the $g' - r'$ *vs* g' colour-magnitude plane. While on the top panel, binning method 1 is used, on the bottom panel, binning method 2 is used, which are "*equal magnitude width*" and "*equal numbers of stars*" bins respectively.

On the other hand, objects spread differently on the colour-colour plane (i.e. $g' - r'$ vs. $U - g'$). Thus, the selection based on colour-colour- diagram needs a different approach than the selection based on colour-magnitude diagram. If the goal is to pick blue objects up from a few fields, the solution is very simple: manual selection. As one can see in Fig.2.6, blue objects naturally gather at the blue corner (bluer side of both colours) of the colour-colour diagram, and -*most of the time*- very distinctively away from the main locus.

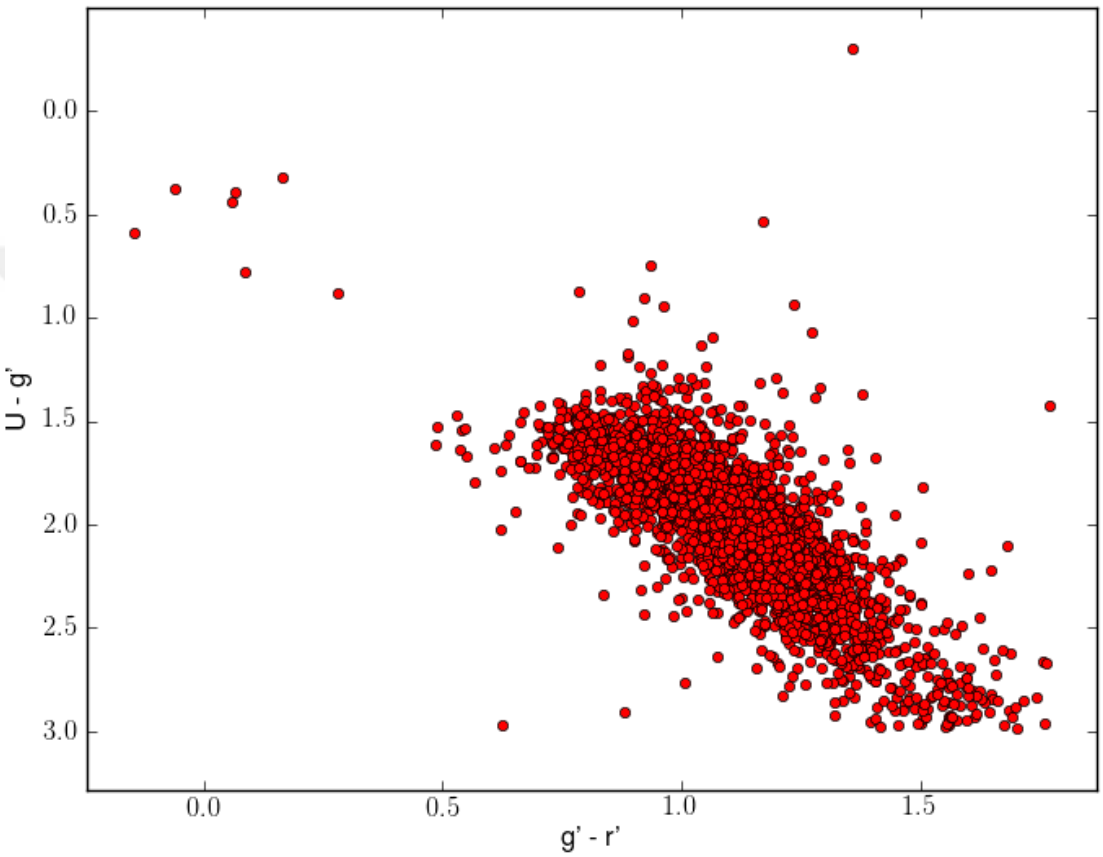

Figure 2.6: The location of sources in Run4-Field17 in the $g' - r'$ *vs* $U - g'$ colour-colour diagram. Blue objects are located in the upper left corner of the diagram.

However, when data from many different fields exist, or the objects are not well separated from the main locus, the selection process needs to be automated using statistical methods. Hence, I have developed a method to tackle this problem. Using this method, the selection was done by taking the following steps for a given field (step 1 is illustrated in Figures 2.7 and 2.8,and steps 2-6 in Figure 2.9):

1. Exclude the "*purple*" objects (see next paragraph) from the sample by fitting a line to the data, and clipping iteratively by 3σ.

2. Calculate the standard deviation (σ) for the $g' - r'$ axis.

3. Assign an object as "*blue in*" $g' - r'$ if
   (a) it is on the blue side of the 3σ cut at the blue side, and
   (b) its distance to the 3σ cut is bigger than 3 times its photometric error.
4. Calculate the standard deviation (σ) for the $U - g'$ axis.
5. Assign an object as "*blue in*" $U - g'$ if
   (a) it is on the blue side of the 3σ cut at the blue side, and
   (b) its distance to the 3σ cut is bigger than 3 times its photometric error.
6. Assign an object as "*blue*" if it is assigned as blue in both step 3 and 5.

The objects that are blue in $U - g'$ colour while red in $g' - r'$ colour are labeled as "*purple*" by Verbeek et al. (2012), not because they are physically but metaphorically purple, as they are blue and red at the same time. They do not form an astrophysical group. These objects could be several kinds of objects including X-ray sources, TTauri stars, Mira stars, carbon stars, emission-line stars, IR sources, radio sources, and galaxies (Verbeek et al., 2012). As this study does not aim to specifically study purple objects, I do not define a definite colour region for them. I only initially put them aside while calculating 3σ cuts to remove their influence, in order to be able to select the blue objects in both colours. As one can see in Figure 2.9, the purple objects pull the 3σ cut towards themselves, in $U - g'$ colour, causing the blue objects to be left out by the selection.

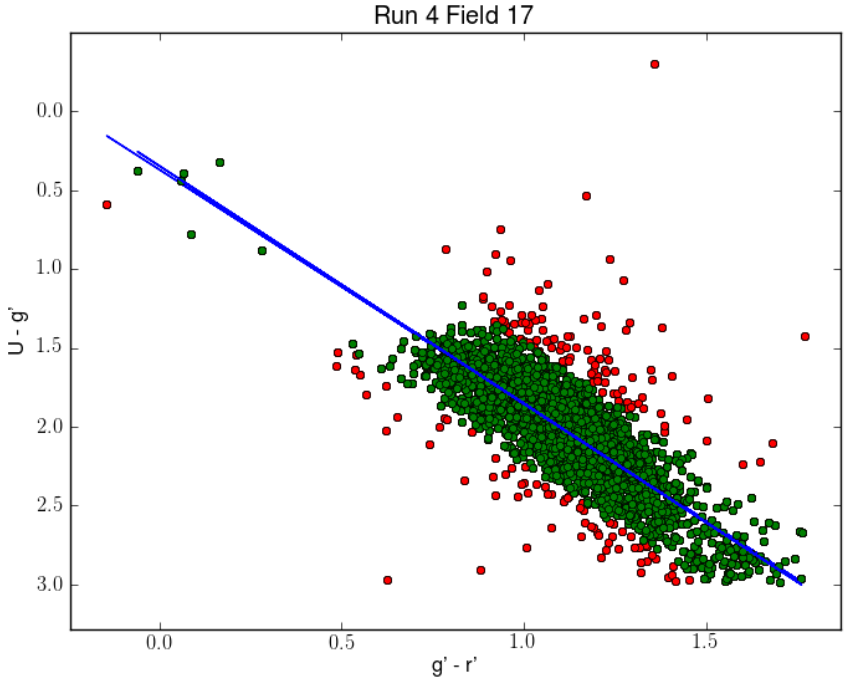

Figure 2.7: **Excluding purple objects - stage 1:** A linear function (blue line) is fitted to the data in such an iterative way that after each fitting, data points left from previous 3σ clipping (green dots) are clipped off again, if they are further than 3σ to the new fit (red dots). Iteration finishes when the slope of the fit (m) does not change significantly ($dm \leqslant 0.01$). In this particular field, only 2 iterations were made, as the slope of the third fit is less than 1% different than of the second, and the third fit is not plotted.

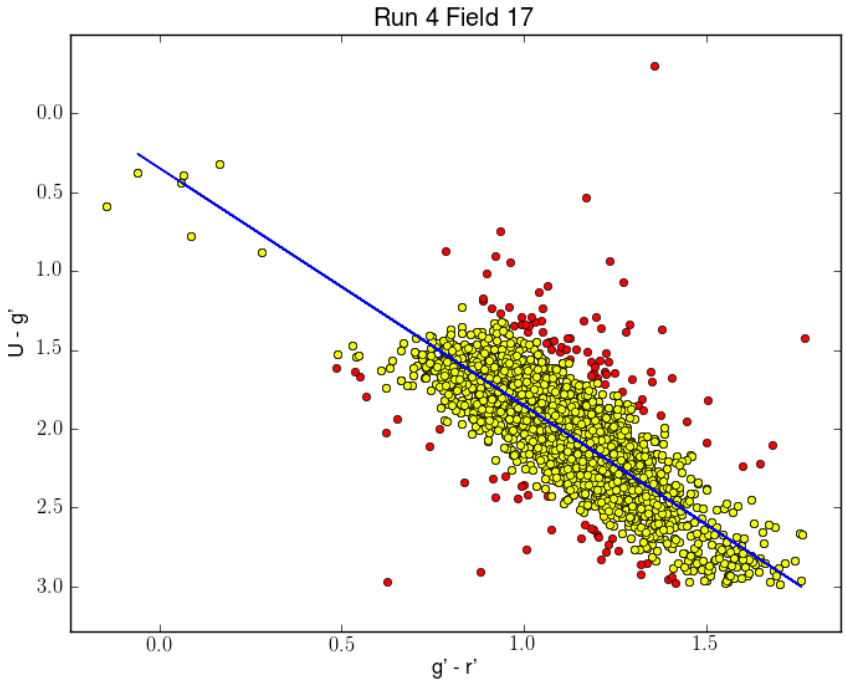

Figure 2.8: **Excluding purple objects - stage 2:** Once the best fit is calculated, the whole data is clipped according to 3σ around the best fit, so that the data is ready for the blue selection steps. The yellow dots are in 3σ, so, used for the next steps.

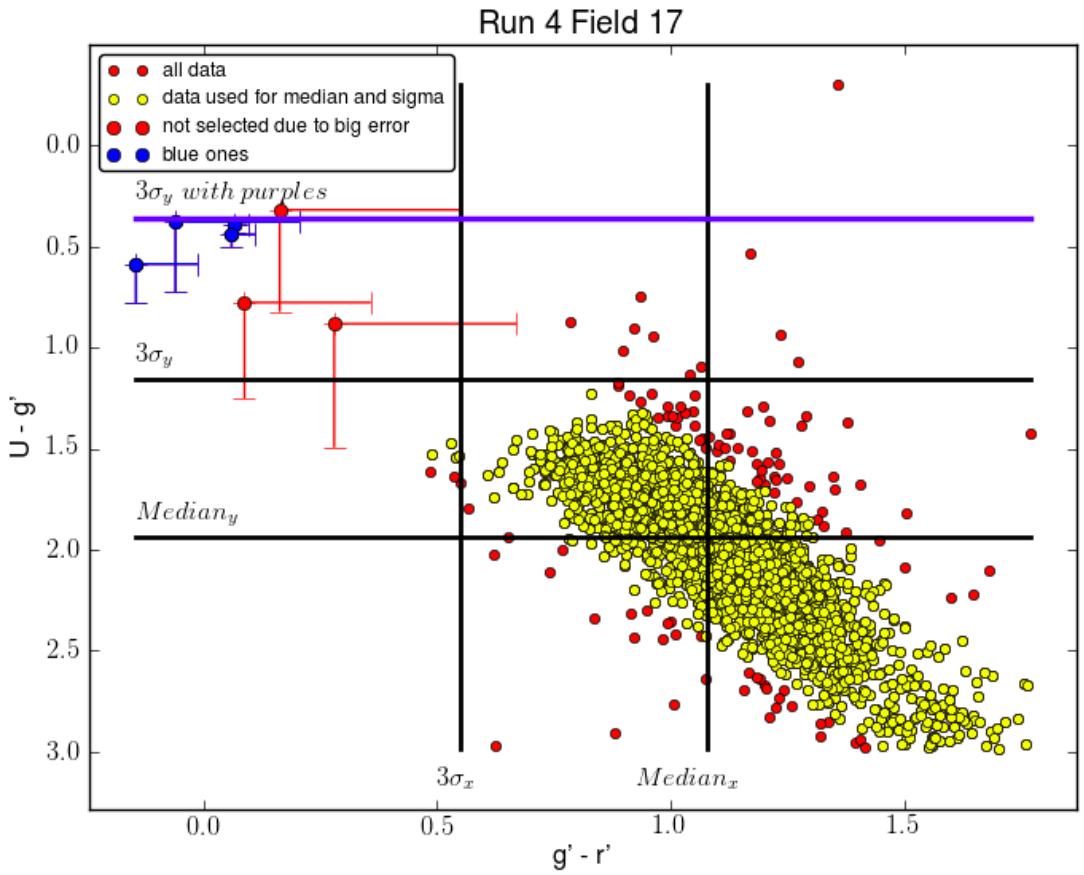

Figure 2.9: After the dataset has been cleaned of purple objects, it is then used for selection as explained in §2.1. Blue dots are the objects assigned as blue, since they are at the blue side of both 3σ-cuts and 3 times of their own photometric error away from the cuts (errors shown are triple). Without excluding purple objects, 3σ-cut for the $U - g'$ axis would be lie at much bluer colours, as shown by purple line, and the code would not pick any objects in this field.

The purple objects are not the only sources causing this effect; blue objects themselves do so as well. As the blue objects are present at the extreme part of the colour-colour plane, 3σ-cuts in both axes are pulled towards the blue objects. The process for cleaning purple objects solves this problem too. This effect can be seen in Figure 2.10.

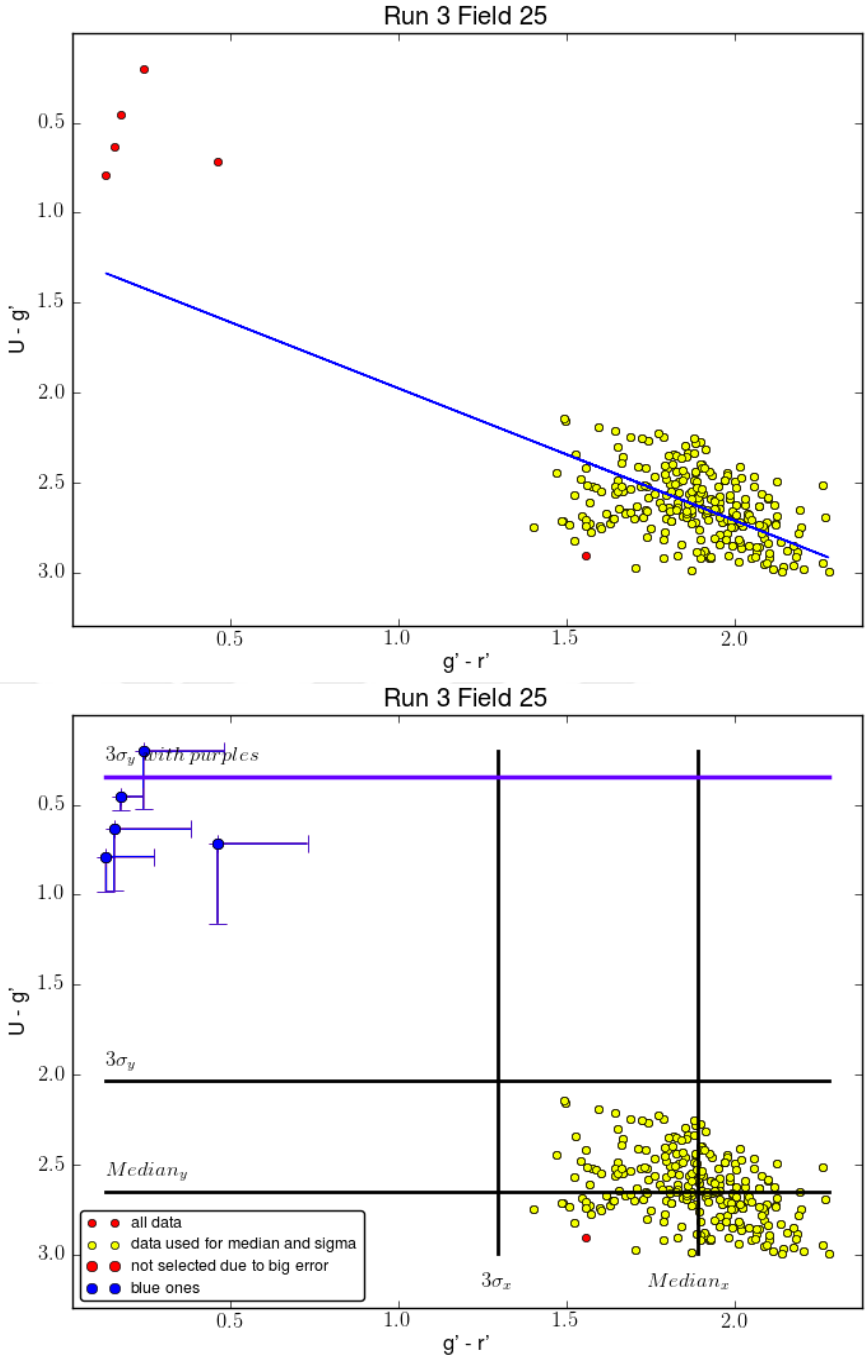

Figure 2.10: ***Top panel:*** The process that cleans the data from the purple objects, as explained in Fig.2.8, has excluded significantly blue objects in this case. The yellow points will be used for the next step. ***Bottom panel:*** Blue objects pull the 3σ-cuts towards themselves as well as purple objects. As can be seen, in this specific case, there are not any purple objects to pull 3σ-cut in y-axis. But the 3σ-cut (purple line) is still very high and excludes significantly blue objects (upper-left corner - blue dots with error-bars with triple errors). Ironically, the blue objects themselves cause this to happen. The same process, which excludes purple objects, keeps these blue objects out of the data in this case, while σ is being calculated, so that the code is able to catch the blue objects.

Since there are three planes (i.e. $g' - r'$ *vs* g', $U - g'$ *vs* g', and $g' - r'$ *vs* $U - g'$), two magnitude systems (i.e. AB and Vega), and two binning methods (only for colour-magnitude planes, i.e. equal number of objects, and equal magnitude width), I had ten blue samples at the end (see Table 2.1). The selection procedures were done using Python[2] scripts written by myself, which are fairly fast; it does not take longer than 5 minutes for them to run for a particular combination of these parameters (e.g. $g' - r'$ *vs* g' & AB & binning method 1). Hence, less than an hour for all ten combinations. The results from all ten samples have been combined as the last step of the colour selection. While some of the objects are present in all ten samples, others are in only a few or just one sample. I added this information to the data table as an indicator of the degree of blueness (*PUF* (picked up from) column in Table 2.3).

Table 2.1: Results of the colour selection. Selection has been done in three planes, using magnitudes from two systems and two binning methods (only for the colour-magnitude planes) – there are therefore ten samples of blue objects. As some objects does not have all three (`Ugr`) magnitude information, input numbers vary from plane to plane. Binning method 1 creates bins with "*equal magnitude width*", while the method 2 creates bins with "*equal numbers of objects*".

Plane	Input	Mag. Sys.	Binning	Blue Objects	%
(g-r) vs g	1,334,882	AB	1	2759	0.207
			2	2792	0.209
		Vega	1	2618	0.196
			2	2646	0.198
(U-g) vs g	411,231	AB	1	651	0.158
			2	725	0.176
		Vega	1	640	0.156
			2	724	0.176
(g-r) vs (U-g)	411,223	AB	-	615	0.150
		Vega	-	623	0.152
Total	**2,173,272**			**3,767**	**0.173**

2.2 Sample verification

There are some objects that have colours which are clearly erroneous in the RATS database (see Figure 2.11). As there are a number of reasons for spurious colours, the images in two to four different filters for every object should be checked by eye. The big numbers of objects make it extremely time consuming. To make the manual inspection easier, I wrote a script

[2] www.python.org

(§A.2) that uses the "*Activation Action*" feature of TOPCAT[3], which allows users to use their own scripts, and the "*command line options*" of DS9[4]. The script opens images for the object in all available filters with DS9, zoomed and panned to the object with a circle around it (Figure 2.12), when one clicks any object in a TOPCAT table or a plot (Figure 2.12).

A relatively large number of false positives (∼25%) were found in the blue sample, due to being very close to the bad columns or the edge of the CCD, as well as very surprising coincidences like occultations by an air-plane or an artificial satellite. Because the auto-guider was not used (for technical reasons related to interference between the readout of the CCD and the auto-guider) during the observations, sources are not at the exactly same position on the CCD. If an object partially coincides with a bad column or goes out of the CCD, it appears to be dimmer in one of the filters than the others, hence the very blue (or very red) colour information. A few examples can be seen in Figure 2.11.

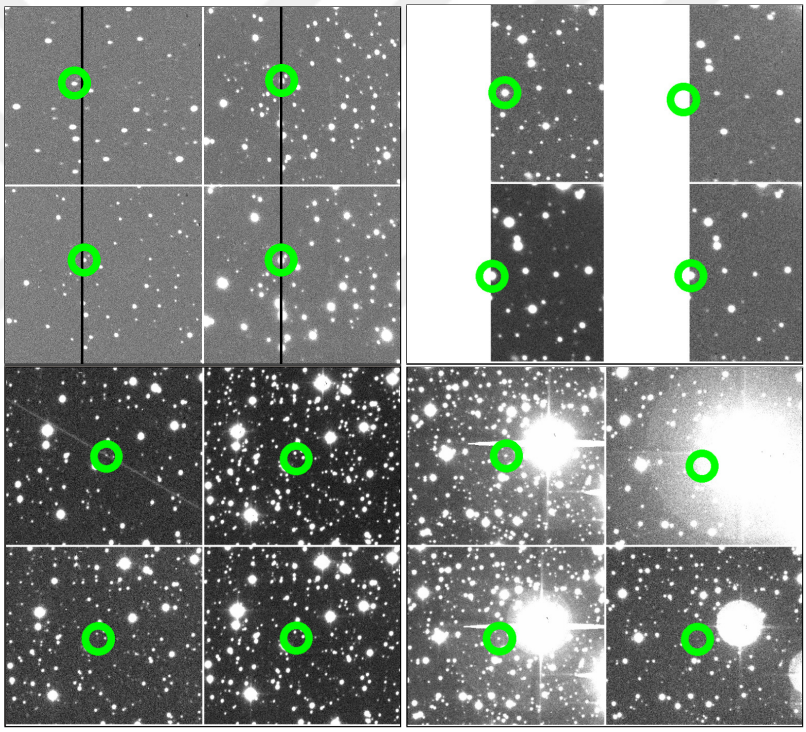

Figure 2.11: Some examples where colour information was contaminated. Top left panel: bad columns on the CCD. Top right panel: An object is very close to the edge of the CCD. Bottom left panel: artificial satellite occultation. Bottom right panel: An object is very close to a saturated star.

At this stage there are 2826 objects remaining in the blue sample, as 941 objects have been identified as having spurious colours. We expect that the blue sample contains a range of hot objects: single white dwarfs, white dwarf binaries with variety of companions (*i.e.*

[3] `http://www.star.bris.ac.uk/\simmbt/topcat/`
[4] `http://hea-www.harvard.edu/RD/ds9/ref/command.html`

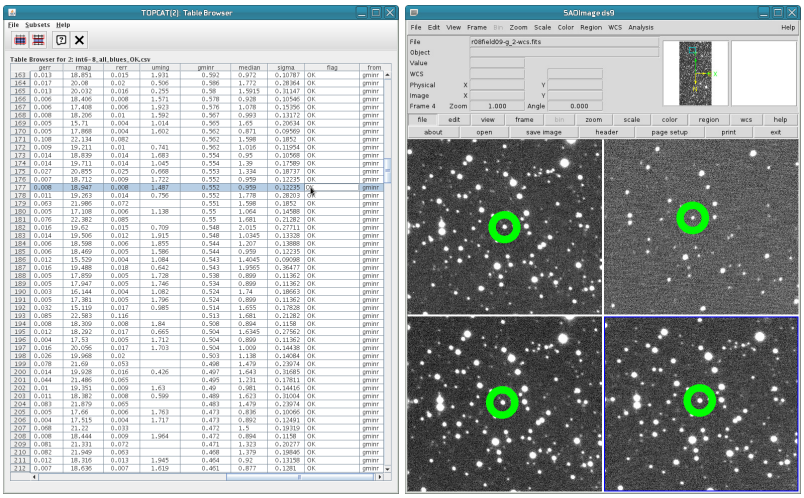

Figure 2.12: Example of manual verification of source colours. Left panel: TOPCAT table window. Right panel: DS9 window which shows all images in different filters for an object clicked in the TOPCAT table.

main-sequence stars, brown dwarfs, white dwarfs, sub-dwarfs), QSOs, main sequence stars and so on. To classify the nature of these objects, one can cross-match the blue sample with the different databases and catalogues, and also do further colour selections using colours in other parts of the spectrum, *e.g.* infra-red and ultra-violet. In the next section, I give details of these identification efforts.

2.3 Additional multi-wavelength information and He-rich object selection

In the previous sections, I identified 2826 out of more than 2 million sources as having significantly blue colours. This sample of blue sources is expected to contain a range of of objects, our main aim is to find UCBs, especially AM CVns. With this objective in mind, I have proceeded by cross-matching the blue sample with several infra-red and ultra-violet databases to use other wavelength magnitudes for further colour-cuts. These colour-cuts allowed me to separate some of the QSOs and sub-dwarfs from the blue sample (Carter et al., 2013). For this purpose, I made use of the X-Match service of CDS[5] and "*Multi-cone Search*" feature of TOPCAT. Afterwards, I used the colours of the known DA and DB white dwarfs (Eisenstein et al., 2006) in the $g' - r'$ *vs* $U - g'$ colour-colour diagram to select a smaller He-rich object candidates sample, which includes AM CVns.

[5] `http://cds.u-strasbg.fr/`

2.3.1 Ultra-violet

As UCBs are bright in UV colours, the first cross-match to be executed was for UV magnitudes with the all sky UV survey GALEX[6]. Although GALEX is named as "*all-sky-*" it does not cover most of the Galactic plane as it is stated on the mission website: "*Areas within 20 degrees of the Galactic plane have patchy coverage due to detector safety limits on the total UV sky brightness in the instrument field of view*". Out of 2826 blue objects, only 1177 were in the observed patches. Within these 1177, the cross-match with 2 arcsec radius yielded 589 (∼50%) UV counterparts. Using NUV (Near Ultra Violet 1692.52Å–3006.67Å) magnitudes from GALEX, and colour-cuts defined by Carter et al. (2013) (Eq.2.1 and Eq.2.2) as shown in Figure 2.13, some of the subdwarfs and other objects have been excluded from the AM CVn candidates sample.

$$NUV - U > 4.34(g' - r') + 0.5 \tag{2.1}$$

$$NUV - U < 6.76(r' - i') + 1.85 \tag{2.2}$$

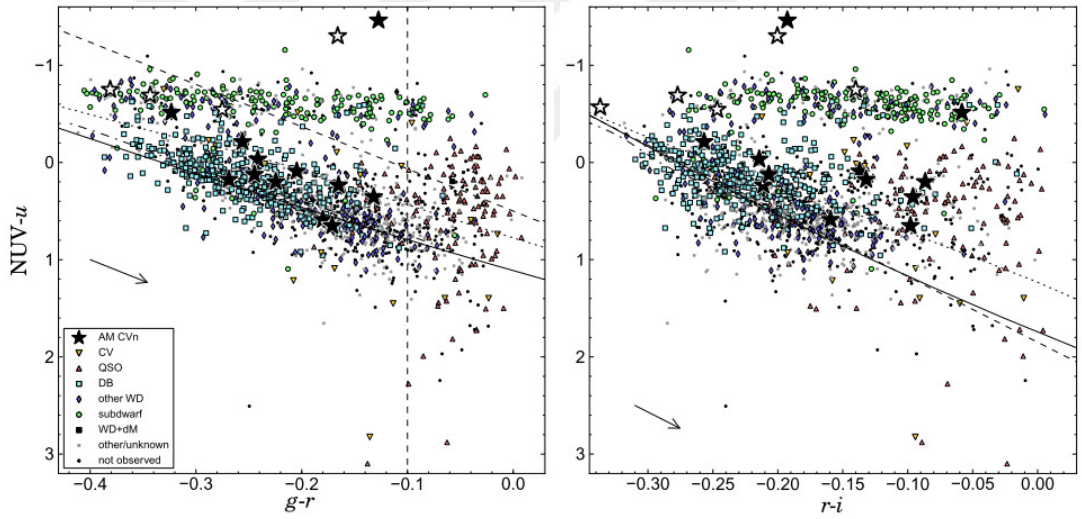

Figure 2.13: As an example of colour selection using GALEX data, the $NUV - u'$ *vs* $g' - r'$ and $NUV - u'$ *vs* $r' - i'$ colour-colour diagrams and colour-cuts (dashed lines) are shown from Carter et al. (2013) (Fig.12). The colour-cuts are defined by Eq.2.1 (left panel) and Eq.2.2 (right panel). Colours of the knownAMCVn binaries (black stars), their sample of candidates from SDSS DR7 combining GALEXNUVdetections are represented by the symbols shown on the legend. The open stars represent, from top to bottom, CR Boo, PTF1 J2219, ES Cet, HM Cnc (right-hand panel only) and PTF1 J0857. The solid line shows the blackbody cooling track, the dotted and dotdashed lines represent the DA and DB white dwarf cooling tracks, and the arrows represent reddening vectors for an extinction of A(g)=0.2.

[6] `http://galex.stsci.edu/GR6/`

2.3.2 Infra-red

The blue sample has been cross-matched with UKIDSS[7], WISE[8] and 2MASS[9], aiming to find infra-red counterparts of the blue objects. UKIDSS, WISE and 2MASS cross-matches returned 50 ($\sim$ 1.34%), 523 ($\sim$ 13.88%) and 797 ($\sim$ 21.16%) objects within 2 arcseconds, respectively. The main reason for the low match rates are the depths of surveys in magnitude, but the sky coverage around the Galactic plane is also at the play as it was with the GALEX. I used a rather big circle for the search due to the low match rate, but considering the good astrometric precision of RATS and the other surveys, 2 arcseconds is the biggest I could go without the chance of alignment of unrelated objects gets significant. As most objects had 2MASS counterparts, I proceed with 2MASS.

Having J, H and K broadband infra-red magnitudes from 2MASS, allowed me to apply further colour-cuts. On the $H-K$ *vs* $J-H$ colour-colour plane, QSOs tend to gather distinctively away from white dwarfs as one can see in Figure 2.14 on the next page. A rough colour-cut such as

$$(J-H) \geqslant 1-(H-K) \tag{2.3}$$

excludes a number of QSOs from the sample. As the colour-cut is very rough, it might exclude some WDs and, although very unlikely, AM CVn systems as well, while keeping some QSOs in. Thus, this colour-cut makes it difficult to determine the completeness of our AM CVn candidate sample, but reduces the number of the candidates further by 97 ($\sim$2.58%).

2.3.3 Helium-rich object selection

The resulting blue sample includes hot objects from several luminosity classes (e.g. main sequence stars, sub-dwarfs, white dwarfs). As we are interested in finding ultra compact objects, particularly the helium-rich ones, I have done further selections.

On the $g'-r'$ *vs* $U-g'$ colour-colour plane, helium-rich compact objects (e.g. DB white dwarfs and AM CVn systems) can be distinguished from hydrogen-rich compact objects (e.g. DA white dwarfs). Using colours of the known AM CVn systems and white dwarf cooling tracks, and taking the reddening into account as well, I selected a smaller sample of DB white dwarf candidates (see Figure 2.15 on page 43).

Barclay (2010) put a colour limit of 0.5 in $g'-r'$ to his sample of AM CVn candidates.

[7] http://www.ukidss.org/
[8] http://wise.ssl.berkeley.edu/
[9] http://www.ipac.caltech.edu/2mass/

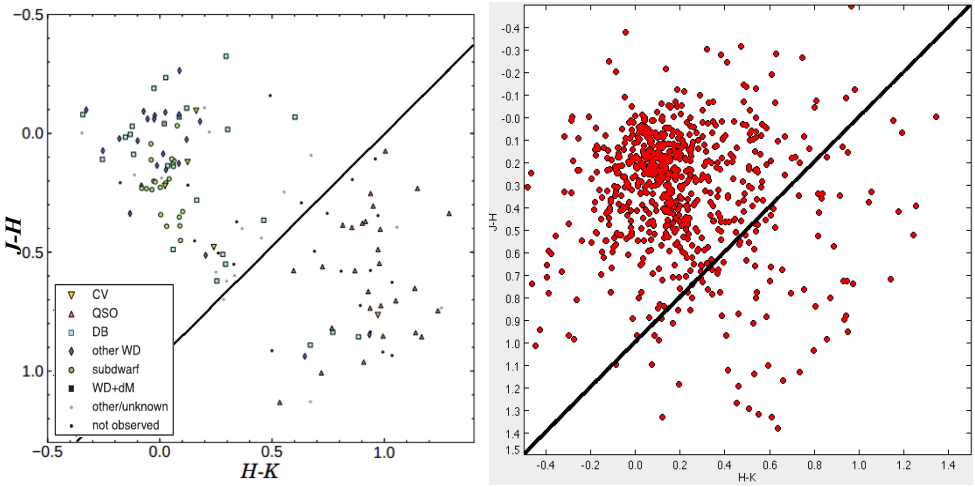

Figure 2.14: ***(a):*** $J-H$ *vs* $H-K$ colour-colour diagram adopted from Fig.13 of Carter et al. (2013). As DB white dwarfs are mainly gathered in the upper-left part of the graph (blue in both colours), a rough colour-cut as $(J-H) \geqslant 1-(H-K)$ excludes all QSOs and some other objects, and some DB white dwarfs too as it is rough. ***(b):*** $J-H$ *vs* $H-K$ colour-colour diagram of the blue sample. Colour-cut found on the left hand side is applied.

He calculated this limit considering that our data has not been de-reddened and all the known AM CVn systems have colours bluer than $g'-r' = -0.1$ (Roelofs et al., 2009). He calculated an optical extinction A_V=1.66 using the average hydrogen column density to the edge of the Galaxy (N_H) in the RATS fields close to the Galactic plane ($|b| < 5^o$), given by Kalberla et al. (2005) as $3.7 \times 10^{21} cm^{-2}$, and the relation found by Guver and Ozel (2009), $N_H = (2.21 \pm 0.09) \times 10^{21} A_v$. The reddening was $E(B-V) = 0.54$ from $A_V = 3.10 \times E(B-V)$ (Fitzpatrick, 1999), which is equal to $E(g'-r') = 0.6$. Thus, the reddest AM CVn which could be found in the RATS data would have a colour index of $g'-r' = 0.5$.

Since the slope of the reddening vector, which I have calculated using Koster WD cooling tracks, equals to proportion of the reddening in two colours, $E(U-g')$ is calculated as 0.802. Using calculated $E(U-g')$ and the colour of the reddest known AM CVn in $U-g'$ colour, I estimated the $U-g'$ colour-cut as $U-g' = 0.9$. As the last step, a parallel line to the reddening vector has been drawn in a way that would keep all the known AM CVn systems and the most of the DB white dwarfs in, while keeping as many as possible DA white dwarfs out. Finally, objects that meet these criteria are selected as DB white dwarf candidates, which naturally includes AM CVn systems as well. This reduced the number of objects to 384 (Figure 2.15 on the next page, Table 2.4 on page 46).

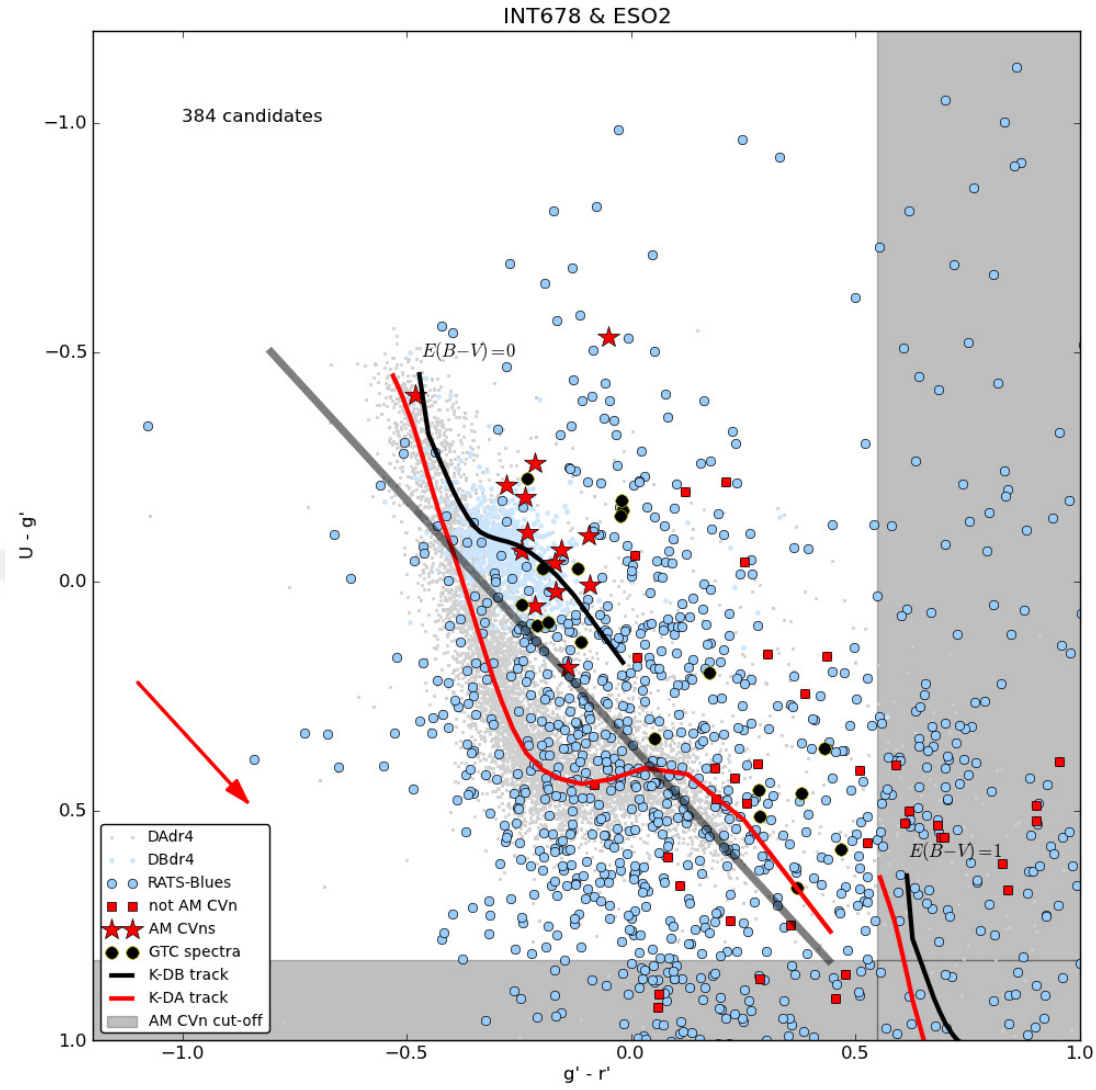

Figure 2.15: The graph shows our blue sample (light blue filled circles), DA (light grey dots) and DB (light blue dots) white dwarfs from SDSS DR4 (Eisenstein et al., 2006), known AM CVn systems (red stars), Koster cooling tracks of DA (red curve) and DB white dwarfs (black curve) for different reddenings (Verbeek et al., 2012), reddening vector (red arrow), the objects where we have GranTeCan spectra (black filled circles), and the objects that are not AM CVn (red squares) (see §2.3). The grey shaded areas are colour-cuts determined by using the colour of the reddest known AM CVn and the maximum reddening in our survey. The objects above the grey line, which is parallel to the reddening vector and placed in a way that would not exclude the known AM CVn systems, are our DB white dwarf candidates.

2.3.4 SIMBAD and other catalogues

Before determining the colour-cuts and selections outlined above, a series of cross-matches have been carried out with SIMBAD[10] and numerous catalogues from Vizier[11] to see if any of

[10] `http://simbad.u-strasbg.fr/simbad/`

our objects are already identified.

Twenty-one objects are found in the SIMBAD database. Six of these objects are excluded from the sample as it turned out that they are not AM CVn systems. Fifteen of them are still in the sample, of which eight are variable objects, with no further identification, from the RATS database (Barclay et al., 2011), published before by our group; five are cluster stars; and two are white dwarf candidates from SDSS. For details, see Table 2.2 on the next page.

Lots of other surveys and catalogues for blue objects from Vizier have been cross-matched with the blue sample with no significant results - some return a negligible number of matches or the same ones with SIMBAD while others return no match at all.

2.4 Summary

With the goal of finding interacting ultra compact binaries, I have identified blue objects from the RATS dataset. Out of $\sim$2.2 million objects, 3767 objects have been identified as having significantly blue colours. As our data is not dereddened, I could not use the tight and global colour limits as Carter et al. (2013) defined to select their sample from deredenned SDSS data. Therefore my colour selection method was inspired by field-by-field method of Verbeek et al. (2012).

After the automatic selection, a manual quality check showed that 941 of the selected objects have colours which have been contaminated by various effects. This suggests that any future data sample should correctly flag the photometric properties in each filter. The number of blue sources therefore decreased to 2826 (Table 2.3). This blue sample, which contains a range of different type of hot objects, has been cross-matched with several surveys to find their IR and UV counterparts with the aim of differentiating these different type of objects. Using IR and UV colours gathered from 2MASS and GALEX, a fraction of these objects that are probably QSOs, sub-dwarfs, main sequence stars etc., and most probably not AM CVn systems, have been excluded from the white dwarf candidates sample.

Afterwards, several databases and catalogues have been cross-matched with the UCB candidate list, with the intention to find out if any of them is a known object. It turned out that 21 of them are present in the SIMBAD database. Six of them were clearly not AM CVn sources: one RR Lyr star, one long period variable, one QSO, one Landolt standard star, and two possible QSO (see §2.3.2); they are therefore excluded from the list.

The main target for our project, AM CVn binaries, are He-rich, and therefore additional colour cuts have been made using H-rich (DA) and He-rich (DB) white dwarf cooling tracks,

[11] `http://vizier.u-strasbg.fr/viz-bin/VizieR`

Table 2.2: List of the objects from the blue sample, found within the SIMBAD database. The stars in the lower six rows are excluded from the blue sample as they are not an AM CVn system. The reason for exclusion is stated below those objects. The fourth column is the seperation in arcseconds. The last two columns are taken from SIMBAD directly. The type column has *inCl, V*, Candidate WD*, EmObj, Star, QSO, X and RR Lyr, which notes cluster star, variable star, white dwarf candidate star, emission object, regular star, Quasi Steallar Object, X-ray source and RR Lyr type of variable star, respectively.

ID	g'	$g'-r'$	d (arcsec)	SIMBAD ID	type
RATJ212845.57+475225.5	15.484	0.499	0.300	Cl* NGC 7092 PLAT 1025	*inCl
RATJ212902.46+481030.8	16.021	0.477	0.100	Cl* NGC 7092 PLAT 1237	*inCl
RATJ213007.54+474905.8	15.820	0.534	0.302	Cl* NGC 7092 PLAT 2219	*inCl
RATJ213020.42+480012.5	15.614	0.487	0.501	Cl* NGC 7092 PLAT 2454	*inCl
RATJ213022.75+480733.5	15.712	0.483	0.361	Cl* NGC 7092 PLAT 2502	*inCl
RATJ043210.39+403334.0	20.502	0.243	0.152	RAT J043210.40+403333.9	V*
RATJ180002.54+003408.4	19.275	0.564	0.000	RAT J180002.54+003408.4	V*
RATJ180250.62+004352.8	18.668	0.458	0.000	RAT J180250.62+004352.8	V*
RATJ182141.24+082228.2	19.416	0.370	0.100	RAT J182141.24+082228.3	V*
RATJ205902.97+453736.1	18.430	0.186	0.465	RAT J205902.93+453735.9	V*
RATJ234746.84+562852.2	21.178	0.248	0.259	RAT J234746.82+562852.0	V*
RATJ234906.89+562440.2	18.032	0.494	0.200	RAT J234906.89+562440.4	V*
RATJ235242.09+563153.3	19.822	-0.028	0.193	RAT J235242.07+563153.2	V*
RATJ013950.00+542159.8	17.843	0.060	0.252	SDSS J013949.98+542159.6	Candidate WD*
RATJ015039.81+562507.9	16.452	0.202	0.220	SDSS J015039.82+562507.7	Candidate WD*
RATJ035824.00+522312.9	21.421	0.783	0.549	IPHAS J035823.95+522312.6	EmObj
↳ *Excluded based on 2MASS colour-cut - see §2.3.2*					
RATJ204219.95+514213.7	17.760	0.344	0.553	Lan 98	Star
↳ *Main Sequence star - see Table1 of Lanning and Lépine (2006)*					
RATJ180415.98+010132.4	17.963	0.776	0.198	QSO B1801+010	QSO
↳ *Excluded based on GALEX and 2MASS colour-cuts - see §2.3.1 and 2.3.2*					
RATJ000156.56+554726.3	18.775	0.273	0.100	RX J0001.9+5547	X
↳ *Excluded based on 2MASS colour-cut - see §2.3.2*					
RATJ182000.88+082509.4	15.379	0.376	0.313	USNO-A2.0 0975-11206579	V*
↳ *Kolesnikova et al. (2008)*					
RATJ180308.44+012359.1	14.630	0.378	0.250	V* V950 Oph	RRLyr
↳ *Haussler et al. (2006)*					

colours of known AM CVns on $g'-r'$ *vs* $U-g'$ colour-colour plane, and the reddening (§2.3.3). This final sample contains 384 objects (Table 2.4). Given the difficulty in classifying compact sources using only broad band colour information, spectroscopic information is required to identify their nature. In the next chapter, I outline the spectroscopic follow-up program and the observations of the most likely AM CVn candidates from this sample.

Table 2.3: A short sample of the selected blue object list of 2826 objects. The whole list can be requested from me. Object IDs are in the format of "*RATJ[ra][dec]*", and magnitudes are in AB system. Last column, *PUF* (Picked Up From), shows that in how many combinations of magnitude system, plane and binning method (ten in total, for the details see the last paragraph of §2.1) the object is selected.

ID	g'	$g'-r'$	PUF
RATJ000014.77+533452.9	20.885	−0.131	3
RATJ000016.22+555911.0	18.075	0.19	4
RATJ000031.05+554435.6	21.67	−0.991	4
RATJ000041.42+533237.5	19.178	0.265	2
⋮	⋮	⋮	⋮

Table 2.4: The full list of the selected UCB candidate list of 384 objects. Electronic version of the list can be found on-line. Object IDs are in the format of "*RATJ[ra][dec]*", and magnitudes are in AB system. The column *PUF* (Picked Up From), shows that in how many combinations of magnitude system, plane and binning method (ten in total, for the details see the last paragraph of the §2.1) the object is selected.

No.	ID	g'	$g'-r'$	PUF
1	RATJ000227.27+531831.3	20.216	0.256	2
2	RATJ000241.04+505209.0	20.133	0.511	4
3	RATJ000420.44+512009.4	17.886	−0.368	10
4	RATJ000530.63+514332.8	19.397	0.326	4
5	RATJ000548.13+515718.2	20.602	0.165	8
6	RATJ000619.20+521948.6	20.880	0.137	5
7	RATJ000638.33+514053.5	20.909	−0.124	6
8	RATJ000707.13+520430.3	20.611	0.129	8
9	RATJ000727.71+521208.8	20.854	0.181	7
10	RATJ011012.65+552107.1	19.674	−0.166	10
11	RATJ012452.49+545026.8	22.187	0.164	2
12	RATJ012554.79+540611.9	20.104	0.021	10
13	RATJ012720.91+543228.0	18.652	0.065	10
14	RATJ013939.06+542448.8	20.829	−0.124	10
15	RATJ014018.96+563931.4	20.732	0.138	10
16	RATJ014107.48+544754.9	21.134	−0.054	2
17	RATJ014134.93+541655.6	22.607	0.012	1
18	RATJ014142.68+535338.0	19.857	0.490	4
19	RATJ014156.07+544905.6	20.530	0.507	1
20	RATJ014159.59+551014.9	20.730	0.368	2
21	RATJ014201.48+535914.0	19.561	−0.231	10
22	RATJ014244.06+540820.3	20.513	0.316	4
23	RATJ014249.34+563638.6	21.425	−0.212	6
24	RATJ014255.52+541245.6	20.240	0.467	2
25	RATJ014301.40+535055.7	20.890	0.367	1
26	RATJ014313.32+541105.3	20.531	0.284	3
27	RATJ014326.57+535119.4	20.326	0.324	2
28	RATJ014721.46+560604.7	20.338	0.504	2
29	RATJ014740.28+560726.7	16.787	0.029	8
30	RATJ014745.12+560942.9	18.043	−0.397	10

Continued on next page...

Table 2.4 – continued from previous page

No.	ID	g'	$g'-r'$	PUF
31	RATJ014828.67+561155.9	21.161	0.029	2
32	RATJ022739.84+545241.1	20.347	−0.236	10
33	RATJ023025.46+550615.2	20.384	0.543	1
34	RATJ023054.97+545528.3	21.217	−0.097	7
35	RATJ023100.56+550625.7	22.022	−0.105	1
36	RATJ025355.41+500056.1	19.816	0.091	10
37	RATJ025535.22+494144.2	19.204	−0.053	10
38	RATJ025537.44+493557.3	19.839	−0.058	10
39	RATJ025540.88+493939.8	20.615	−0.139	10
40	RATJ033355.35+523224.3	21.012	0.296	6
41	RATJ042943.28+415516.0	22.797	0.193	2
42	RATJ043116.49+404119.5	20.303	0.150	10
43	RATJ043201.62+403211.1	21.743	0.041	8
44	RATJ045600.02+343027.8	22.152	0.409	4
45	RATJ050236.42+453532.8	20.544	0.509	7
46	RATJ050308.99+360750.0	20.397	0.186	10
47	RATJ050455.13+361302.6	21.539	0.258	8
48	RATJ050827.42+435441.1	19.092	0.374	7
49	RATJ052826.14+213158.7	20.006	0.478	4
50	RATJ062749.68+141904.4	21.463	−0.102	8
51	RATJ062838.45+144617.1	20.851	0.267	5
52	RATJ065510.41+104824.8	18.359	0.526	4
53	RATJ065510.93+104712.5	18.515	0.482	2
54	RATJ065512.68+104732.8	20.750	0.498	2
55	RATJ065514.50+104821.0	19.531	0.497	4
56	RATJ065519.79+104626.5	19.899	0.395	4
57	RATJ065520.24+103049.0	19.840	0.548	4
58	RATJ065522.50+105016.4	20.036	0.501	2
59	RATJ065539.71+105041.3	18.979	−0.131	10
60	RATJ065601.91+102913.6	18.865	0.509	4
61	RATJ065947.33+074539.9	19.922	0.240	1
62	RATJ070015.65+074741.4	19.728	0.525	2
63	RATJ070032.49+080222.8	19.250	−0.242	10
64	RATJ070038.25+074722.6	18.849	−0.015	8
65	RATJ070839.63-561108.4		−0.088	2
66	RATJ070849.79-560515.9		−0.131	2
67	RATJ071001.54-560851.7		−0.192	2
68	RATJ071019.88-562519.0		−0.133	2
69	RATJ071035.18-562854.1		−0.029	2
70	RATJ071101.97-560646.8		0.134	2
71	RATJ071105.73-562602.3		−0.173	2
72	RATJ071140.09-560100.4		−0.116	2
73	RATJ071159.18-561940.9		−0.008	2
74	RATJ075129.60-282427.0		−0.110	2
75	RATJ075159.57-284021.7		0.102	2
76	RATJ075206.08-283648.5		0.017	2
77	RATJ075257.25-282849.6		0.100	2
78	RATJ075324.31-284246.9		−0.270	2
79	RATJ075336.42-281318.9		0.091	2
80	RATJ080354.29-270602.2		−0.399	2
81	RATJ080444.87-271840.6		0.159	2
82	RATJ080534.15-271948.5		0.135	2

Continued on next page...

Table 2.4 – continued from previous page

No.	ID	g'	$g'-r'$	PUF
83	RATJ080542.96-270256.2		−0.054	2
84	RATJ080615.89-284228.3		0.000	2
85	RATJ080629.14-283017.1		0.059	2
86	RATJ080753.91-282721.8		0.067	2
87	RATJ080825.04-284428.7		0.024	2
88	RATJ080829.92-284431.2		0.118	2
89	RATJ080833.32-283505.1		0.000	2
90	RATJ080843.43-284201.5		0.072	2
91	RATJ095229.63-405135.1		0.097	2
92	RATJ095245.31-382248.6		−0.060	2
93	RATJ095249.14-380752.0		0.173	2
94	RATJ095254.27-382706.8		0.062	2
95	RATJ095305.42-402607.2		0.094	2
96	RATJ095305.96-382533.8		0.076	2
97	RATJ095323.71-402559.5		0.029	2
98	RATJ095338.52-383307.8		0.247	2
99	RATJ095346.79-403442.2		0.018	2
100	RATJ095348.75-383608.5		0.252	2
101	RATJ095350.88-404715.2		0.284	2
102	RATJ095353.49-383215.4		−0.040	2
103	RATJ095418.76-382443.8		0.226	2
104	RATJ095425.32-382804.2		0.264	2
105	RATJ095427.07-380502.3		0.238	2
106	RATJ095434.28-383612.0		0.276	2
107	RATJ095450.31-403050.8		0.211	2
108	RATJ095501.59-381231.3		0.177	2
109	RATJ095819.88-393326.6		0.081	2
110	RATJ095832.59-394139.9		−0.151	2
111	RATJ095832.83-393422.5		−0.299	2
112	RATJ095837.09-392808.1		−0.085	2
113	RATJ095838.76-394718.1		0.056	2
114	RATJ095908.39-395420.3		0.034	2
115	RATJ095921.76-392627.6		0.219	2
116	RATJ095924.56-393843.7		0.044	2
117	RATJ095932.90-393242.8		0.108	2
118	RATJ095941.17-394502.7		−0.137	2
119	RATJ100004.12-395730.4		0.113	2
120	RATJ100004.40-394345.6		−0.167	2
121	RATJ100015.81-394646.8		0.023	2
122	RATJ100031.05-393351.3		−0.027	20
123	RATJ100046.91-394644.7		0.103	2
124	RATJ100048.43-394931.4		−0.034	2
125	RATJ100054.75-393751.4		0.051	2
126	RATJ100058.75-392622.6		0.046	2
127	RATJ100304.83-393926.4		−0.073	2
128	RATJ100343.60-395030.5		−0.158	2
129	RATJ100351.08-392114.2		0.205	2
130	RATJ100420.39-392617.8		0.119	2
131	RATJ100423.73-392319.3		−0.085	2
132	RATJ100435.38-394452.5		0.179	2
133	RATJ100442.13-392945.2		0.074	2
134	RATJ100447.40-393656.8		0.202	2

Continued on next page...

Table 2.4 – continued from previous page

No.	ID	g'	$g'-r'$	PUF
135	RATJ100457.73-393031.5		0.218	2
136	RATJ100504.38-393810.1		0.176	2
137	RATJ100528.08-394553.0		0.004	2
138	RATJ100532.12-394936.8		−0.066	2
139	RATJ100541.46-392231.5		0.095	2
140	RATJ100542.63-394513.6		−0.032	2
141	RATJ100550.00-393648.9		−0.509	2
142	RATJ120722.92-574440.2		0.130	2
143	RATJ120742.23-573441.2		−0.129	2
144	RATJ120743.99-571948.3		−0.278	2
145	RATJ120746.45-573418.8		0.207	2
146	RATJ120800.70-571656.4		0.330	2
147	RATJ120831.94-571958.7		0.080	2
148	RATJ120836.33-574311.9		0.282	2
149	RATJ120911.85-572809.2		0.051	2
150	RATJ120957.10-572418.7		0.271	2
151	RATJ120957.81-571719.4		−0.231	2
152	RATJ121011.79-574016.8		0.094	2
153	RATJ132319.26-413117.1		0.198	2
154	RATJ132320.02-414116.5		0.234	2
155	RATJ132336.72-413120.0		0.266	2
156	RATJ134756.87-574734.9		0.241	2
157	RATJ134847.46-573814.3		0.070	2
158	RATJ134904.94-573226.2		−0.068	2
159	RATJ134905.05-572327.8		−0.010	2
160	RATJ135003.20-575014.9		0.208	2
161	RATJ135034.84-573839.8		0.165	2
162	RATJ135114.39-574958.4		0.404	2
163	RATJ140749.36-574414.2		0.421	2
164	RATJ140811.62-574300.0		0.361	2
165	RATJ141130.23-574055.0		0.474	2
166	RATJ155020.63-484711.8		0.111	2
167	RATJ155108.90-482456.3		0.362	2
168	RATJ155115.66-482232.1		0.006	2
169	RATJ155145.08-483325.9		0.052	2
170	RATJ155157.78-484519.1		0.306	2
171	RATJ155203.00-484345.2		0.292	2
172	RATJ155211.91-484930.7		0.067	2
173	RATJ155225.59-483316.0		0.084	2
174	RATJ155355.17-482735.8		0.189	1
175	RATJ175348.73+014412.4	20.478	0.311	8
176	RATJ175431.29+013753.2	17.409	−0.018	10
177	RATJ175436.44+013339.1	19.060	0.053	10
178	RATJ175453.96+012924.2	20.965	−0.040	10
179	RATJ175457.13+013458.9	20.775	0.471	2
180	RATJ175508.82+013623.4	21.361	0.303	1
181	RATJ175512.41+015915.3	21.935	−0.070	6
182	RATJ175526.97+013207.3	18.343	0.379	10
183	RATJ175738.28+013816.7	18.702	0.368	10
184	RATJ175756.35+014156.9	20.310	−0.140	10
185	RATJ175808.39+012740.4	19.942	0.047	10
186	RATJ175846.52+015358.0	20.685	0.077	10

Continued on next page...

Table 2.4 – continued from previous page

No.	ID	g'	$g'-r'$	PUF
187	RATJ175902.17+020858.6	19.551	0.072	10
188	RATJ175914.97+011906.4	16.854	−0.112	10
189	RATJ175917.81+020221.0	19.009	−0.029	10
190	RATJ175917.90+022516.5	18.592	0.175	10
191	RATJ175918.00+013149.8	20.639	−0.192	9
192	RATJ175921.75+022208.6	18.917	−0.015	10
193	RATJ175923.37+014409.3	19.635	0.424	8
194	RATJ175925.79+022222.1	20.232	0.194	3
195	RATJ175931.32+014401.4	21.278	0.003	6
196	RATJ175947.90+014459.2	19.351	0.491	7
197	RATJ175957.71+022144.8	19.738	0.521	4
198	RATJ180005.91+002654.7	19.189	0.231	10
199	RATJ180013.31+003824.6	19.294	0.308	10
200	RATJ180016.36+014508.9	18.095	0.247	10
201	RATJ180022.01+020007.3	18.679	−0.233	10
202	RATJ180025.28+012127.4	18.315	−0.025	10
203	RATJ180032.66+013007.2	21.540	0.268	4
204	RATJ180035.92+020046.6	19.752	0.137	4
205	RATJ180036.57+022358.0	17.558	−0.120	10
206	RATJ180043.35+011859.6	21.536	0.128	1
207	RATJ180044.00+005040.4	20.185	−0.020	10
208	RATJ180054.43+003232.0	16.115	−0.021	10
209	RATJ180102.93+003707.6	21.839	0.340	2
210	RATJ180247.10+022057.1	19.905	0.160	3
211	RATJ180253.11+021520.3	17.159	0.216	4
212	RATJ180307.08+022147.0	20.007	0.160	4
213	RATJ180310.04+004255.2	20.831	0.081	8
214	RATJ180324.64+013853.1	18.085	−0.245	10
215	RATJ180344.24+020251.2	19.756	−0.066	3
216	RATJ180344.53+023315.4	20.884	0.232	2
217	RATJ180404.52+022720.2	19.695	−0.010	4
218	RATJ180427.32+010039.1	18.774	0.466	10
219	RATJ180429.69+011434.4	20.108	0.501	3
220	RATJ180438.61+022226.8	18.683	−0.198	9
221	RATJ180441.91+013832.9	17.263	0.287	9
222	RATJ181743.74+072708.8	18.822	0.360	10
223	RATJ181743.75+072708.7	18.874	0.435	5
224	RATJ181746.01+072117.8	18.098	0.431	10
225	RATJ181748.40+064638.5	21.824	−0.047	2
226	RATJ181752.11+074008.6	18.032	−0.211	10
227	RATJ181754.82+074548.9	20.779	0.234	7
228	RATJ181807.04+073348.0	20.462	0.012	9
229	RATJ181819.01+063253.0	20.457	−0.054	8
230	RATJ181820.92+062624.5	21.658	0.371	2
231	RATJ181847.36+062115.4	21.319	−0.055	6
232	RATJ181847.48+063113.5	20.783	−0.125	7
233	RATJ181931.29+053751.0	18.026	−0.105	10
234	RATJ181952.31+082444.2	20.155	−0.179	10
235	RATJ181958.34+075511.4	19.045	−0.186	10
236	RATJ182020.83+075449.6	20.993	0.007	2
237	RATJ182040.64+082702.7	19.412	−0.141	10
238	RATJ182042.96+080254.7	18.675	0.386	8

Continued on next page...

Table 2.4 – continued from previous page

No.	ID	g'	$g'-r'$	PUF
239	RATJ182126.34+083014.8	18.926	−0.251	10
240	RATJ182234.14+060440.5	19.286	−0.138	10
241	RATJ182251.53+083359.3	21.146	−0.303	8
242	RATJ182256.00+081536.6	18.756	−0.030	10
243	RATJ182309.97+055400.3	19.203	−0.012	10
244	RATJ182318.33+082437.5	17.382	−0.187	10
245	RATJ182318.39+080850.0	20.088	−0.019	10
246	RATJ182319.73+054011.3	19.079	0.423	4
247	RATJ182332.90+054011.2	20.014	0.448	3
248	RATJ182346.94+055044.7	19.058	0.508	4
249	RATJ183350.57+282156.0	18.695	0.282	4
250	RATJ183506.53+284609.5	19.415	0.265	3
251	RATJ183518.68+281329.6	18.824	0.302	4
252	RATJ183857.96+280444.0	19.743	0.038	2
253	RATJ183930.26+280220.4	19.546	0.138	3
254	RATJ184034.04+281116.0	18.856	0.432	4
255	RATJ184044.49+274501.4	19.767	−0.413	8
256	RATJ184207.58+001854.6	21.027	0.463	6
257	RATJ184209.26+001953.7	20.923	0.243	6
258	RATJ184253.13-000810.7	19.147	0.175	8
259	RATJ184326.30+305003.1	20.894	−0.432	5
260	RATJ192655.76+222611.0	21.182	0.214	6
261	RATJ192819.91+360344.2	20.775	0.355	2
262	RATJ192836.64+355032.9	20.147	−0.072	6
263	RATJ192837.82+354422.2	19.475	0.105	7
264	RATJ192847.67+360028.2	20.671	0.266	2
265	RATJ192857.59+360243.4	18.684	0.156	6
266	RATJ192941.13+361442.8	18.698	0.154	6
267	RATJ192943.35+184654.6	20.937	0.465	4
268	RATJ192949.96+361121.3	19.571	0.211	4
269	RATJ193011.43+355238.2	20.029	0.113	4
270	RATJ193041.27+360702.5	20.600	−0.024	4
271	RATJ193103.06+191309.8	18.511	0.252	10
272	RATJ193659.36+193416.9	22.209	0.516	4
273	RATJ193937.90+223326.7	21.867	0.456	4
274	RATJ193950.61+224230.0	20.869	0.241	6
275	RATJ194009.33+224630.5	20.880	0.437	6
276	RATJ194010.52+224228.0	18.381	0.528	10
277	RATJ194029.31+225907.0	21.221	0.438	5
278	RATJ194044.29+194420.9	20.863	0.183	8
279	RATJ194055.81+190841.9	19.147	0.379	10
280	RATJ194126.56+195910.4	19.201	0.043	10
281	RATJ194142.10+185012.8	21.242	0.186	6
282	RATJ194147.81+200239.3	21.026	0.535	8
283	RATJ194223.69+191729.0	20.984	−0.141	8
284	RATJ194245.67+185806.1	20.523	0.389	6
285	RATJ194823.47+441646.0	18.704	0.205	10
286	RATJ194845.08+441448.7	21.518	−0.288	7
287	RATJ195004.40+442623.4	22.009	−0.077	2
288	RATJ195019.62+442602.2	20.516	0.231	3
289	RATJ195024.76+441653.7	18.134	0.230	10
290	RATJ195025.09+443608.3	21.220	0.250	1

Continued on next page...

Table 2.4 – continued from previous page

No.	ID	g'	$g'-r'$	PUF
291	RATJ195055.04+441247.9	19.129	0.025	10
292	RATJ195541.63+441751.3	18.515	−0.013	10
293	RATJ195638.60+444526.9	20.122	0.547	4
294	RATJ195651.48+441538.7	20.102	0.541	4
295	RATJ195821.71+444853.2	19.572	−0.009	10
296	RATJ195842.08+451552.9	18.980	0.119	10
297	RATJ200434.12+445323.3	19.109	−0.278	10
298	RATJ200521.67+444740.8	18.917	0.456	8
299	RATJ200553.65+494655.1	20.287	−0.334	10
300	RATJ200559.31+494938.8	19.044	−0.505	10
301	RATJ200632.13+481900.5	20.709	−0.166	10
302	RATJ200655.92+493050.7	19.800	0.151	8
303	RATJ200723.01+493931.5	20.633	0.449	2
304	RATJ200732.15+481714.5	21.129	0.217	5
305	RATJ200735.10+493851.9	20.990	0.084	1
306	RATJ200735.53+493233.9	20.957	0.167	1
307	RATJ200744.42+484706.7	21.584	−0.004	3
308	RATJ200745.01+501723.5	20.244	0.520	4
309	RATJ200834.25+482013.2	20.145	−0.064	10
310	RATJ202936.21+271545.7	19.685	0.277	10
311	RATJ203020.52+271846.4	21.641	0.269	3
312	RATJ203100.16+272735.8	21.249	0.362	1
313	RATJ203121.57+273416.8	19.296	−0.302	10
314	RATJ203133.64+273432.6	20.072	0.170	10
315	RATJ203935.02+512642.8	20.091	−0.243	10
316	RATJ204024.40+513059.4	15.646	0.206	8
317	RATJ204051.61+514245.0	20.959	0.040	6
318	RATJ204219.95+514213.7	17.747	0.189	10
319	RATJ205815.54+452819.9	21.151	−0.438	8
320	RATJ205941.05+443036.3	21.186	0.395	4
321	RATJ210001.05+443301.4	21.657	0.122	5
322	RATJ210038.59+445540.2	21.786	0.159	6
323	RATJ210046.12+442208.6	21.352	0.294	5
324	RATJ210146.64+451134.9	21.143	0.101	6
325	RATJ210148.74+452101.1	22.059	−0.719	8
326	RATJ210212.75+443109.6	19.969	−0.144	10
327	RATJ210216.16+463724.1	18.460	0.261	10
328	RATJ210406.63+464500.1	21.034	0.306	6
329	RATJ210448.35+462439.4	20.863	−0.291	8
330	RATJ210448.41+462438.5	20.752	−0.305	9
331	RATJ210558.29+463434.6	19.463	0.339	8
332	RATJ210617.19+440909.0	21.348	0.190	6
333	RATJ210810.76+443022.5	20.018	−0.068	10
334	RATJ210812.71+442420.1	19.843	−0.225	10
335	RATJ210911.15+494856.2	20.920	0.304	6
336	RATJ211023.45+491516.3	21.551	0.447	4
337	RATJ212757.35+474616.6	20.564	0.527	4
338	RATJ212804.21+475915.9	20.022	−0.002	10
339	RATJ212833.23+475704.9	19.771	0.441	8
340	RATJ212844.28+475946.4	19.815	0.527	8
341	RATJ212906.29+481137.0	18.889	0.256	10
342	RATJ212906.93+475541.9	20.712	0.230	8

Continued on next page...

Table 2.4 – continued from previous page

No.	ID	g'	$g'-r'$	PUF
343	RATJ212923.03+475140.6	21.679	0.113	7
344	RATJ213024.13+475523.7	20.796	0.095	9
345	RATJ215713.99+541245.8	21.580	0.216	4
346	RATJ220852.93+551054.6	21.220	−0.065	7
347	RATJ221023.62+551616.6	19.766	0.206	10
348	RATJ222242.73+442719.7	21.535	0.030	2
349	RATJ222400.60+443615.0	20.546	0.062	10
350	RATJ222401.08+441237.5	20.452	0.474	4
351	RATJ222417.30+444010.1	20.920	0.118	5
352	RATJ231414.07+541800.7	21.142	−0.352	10
353	RATJ231441.59+543455.7	20.308	0.401	4
354	RATJ231444.49+544043.3	20.698	0.407	1
355	RATJ231446.40+542748.7	19.720	−0.157	10
356	RATJ231557.68+541810.6	21.198	−0.084	8
357	RATJ231625.64+542549.1	19.953	0.352	5
358	RATJ231711.82+544303.1	19.569	0.518	4
359	RATJ232848.09+494515.6	20.431	−0.096	4
360	RATJ232934.74+500533.4	18.907	0.257	4
361	RATJ233847.13+570018.8	19.949	0.527	4
362	RATJ234001.46+565734.8	20.902	−0.009	7
363	RATJ234020.50+570624.4	21.090	0.176	6
364	RATJ234525.77+562919.7	21.039	0.158	4
365	RATJ234532.54+542004.6	21.543	−0.059	6
366	RATJ234556.67+562254.0	21.521	0.037	5
367	RATJ234742.54+564158.0	19.446	0.105	10
368	RATJ234753.31+543630.1	21.536	0.486	1
369	RATJ234806.09+562401.3	21.154	−0.022	7
370	RATJ234815.15+561853.8	20.591	0.525	2
371	RATJ234828.02+562238.5	18.905	0.061	10
372	RATJ235016.20+562437.1	18.333	0.088	10
373	RATJ235146.05+561234.6	21.025	−0.177	9
374	RATJ235148.75+561316.1	20.559	−0.298	10
375	RATJ235148.79+563125.5	20.400	−0.059	10
376	RATJ235322.48+562025.6	19.400	−0.098	10
377	RATJ235603.47+560856.0	20.365	−0.123	10
378	RATJ235643.21+561237.5	20.392	−0.265	10
379	RATJ235650.64+560422.1	21.895	−0.060	5
380	RATJ235703.25+562153.5	22.895	−0.424	7
381	RATJ235704.91+561858.1	21.658	−0.039	3
382	RATJ235815.66+555404.6	21.440	−0.135	2
383	RATJ235822.27+561430.0	20.632	0.271	4
384	RATJ235927.81+554719.6	21.899	−0.097	1

Chapter 3

Spectral follow-up of blue sources

In §2, I outlined a method to identify sources from the RATS archive which were *significantly blue*, and in particular, sources which had colours consistent with that of known AM CVn binaries. This strategy specifically set out to identify potentially interesting sources by applying colour selection cuts. However, source identifcation by means of variability is discussed in §5. The colour selection revealed 2826 "*blue*" sources out of which 384 are AM CVn candidates. Since a range of astrophysical sources can have colours similar to AM CVn binaries, spectroscopic follow-up observations are essential to reveal their nature. For instance, although the colours of AM CVn binaries and DA white dwarfs in the $(g' - r')$ *vs* $(U - g')$ plane are very similar, the latter show hydrogen absorption lines, whilst DB white dwarfs show helium absorption lines. On the other hand, AM CVn binaries show helium lines in the form of absorption or emission depending on their accretion state. AM CVns in a "*high state*" show shallow absorption lines. They can be distinguished from DBs by the lower equivalent widths of their absorption lines, in particular by the low ratio of (`HeI` 4713Å + `HeII` 4686Å) to `HeI` 4471Å (Roelofs et al., 2004).

The RATS project had a spectroscopic follow-up program which consisted of observations made using the Isaac Newton Telescope (INT) and the William Herschel Telescope (WHT) on the island of La Palma, and the Gemini South telescope in Chile. Target selection for these observations were done by prioritising the sources which showed short period flux variations. This follow-up programme has identified various sources including one EC 14026 type pulsating subdwarf and a few dozens of SX Phe and δ Scuti variables (Ramsay et al., 2006, 2011), one pulsating white dwarf with a hotter companion and eight variable A-type main sequence stars (Barclay et al., 2011).

Unlike the previous spectroscopic work done using RATS data, here, the targets for the spectroscopic follow-up have been selected in a systematic way through their colours. We

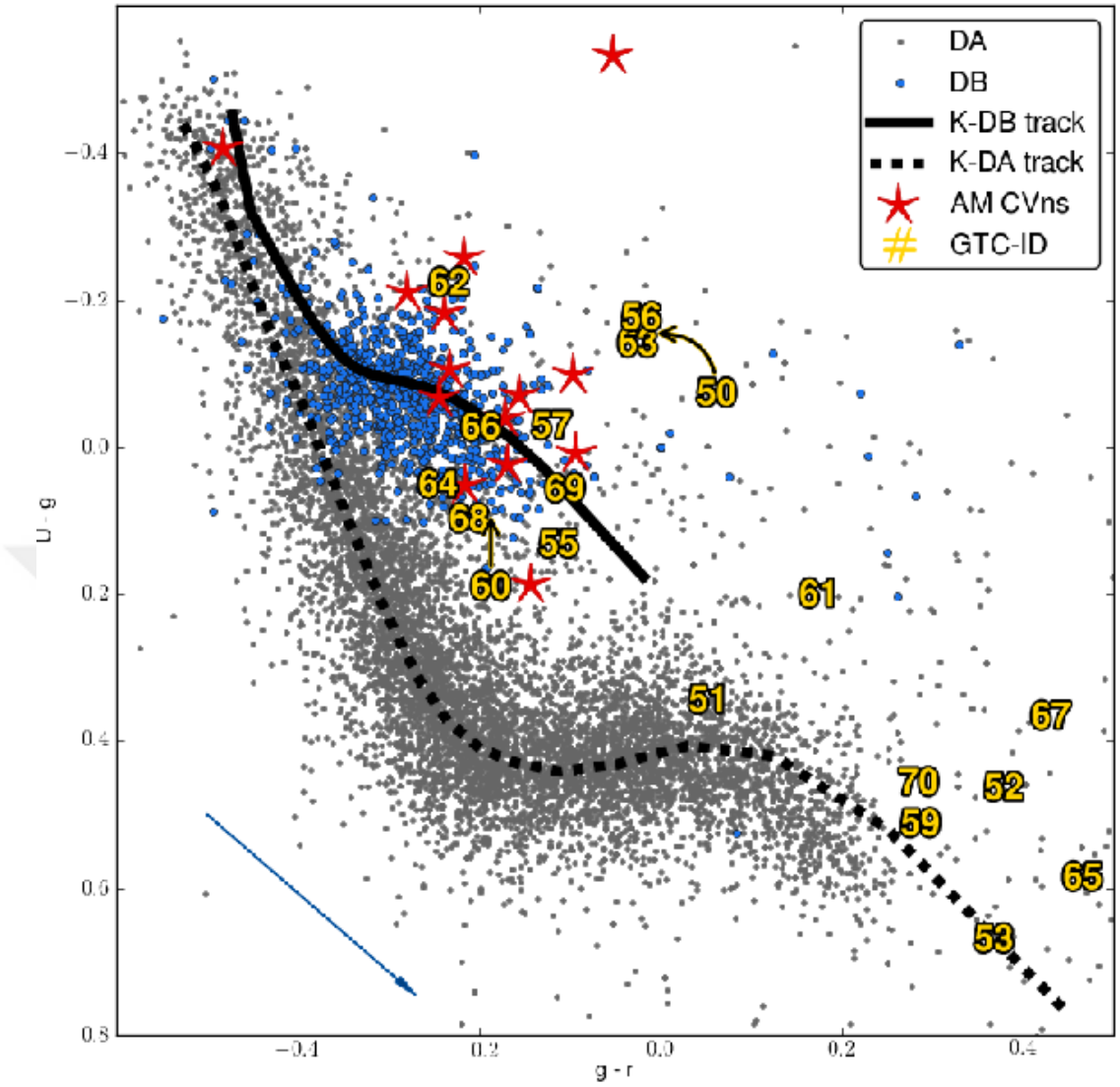

Figure 3.1: Objects (yellow numbers) that we obtained GTC spectra are shown in the $(g' - r')$ *vs* $(U - g')$ colour-colour diagram. The numbers correspond to the last two digits of the GTC-IDs in Table 3.1. In the background, DA (grey dots) and DB (blue dots) white dwarfs from SDSS DR4 (Eisenstein et al., 2006) are shown, together with Koster cooling tracks (solid line for DBs, dashed line for DAs) and known AM CVns (red stars). The blue arrow shows the direction of the reddening and its size represents a colour excess of $E(B-V) = 0.2$. While all other magnitudes are dereddened (SDSS photometry), RATS magnitudes (yellow numbers) are not.

ranked our He-rich object candidates (384 objects with colours similar to that of known AM CVn systems) according to several criteria (*e.g.* right ascension, brightness, colour, "*PUF*" (see Table2.4)) and then selected a smaller sample for a target list. As the observations would be made in service mode and therefore could be made on any date and time, we have selected targets with a range in RA. We also selected rather bright targets since the time we had was

through a poor weather programme. Also the source variability was not taken into account. Considering all these issues, I can say the target selection for the spectral observations within the UCB candidates list was rather randomised, and not biased towards any period or amplitude range.

We obtained spectra for 17 objects[1] from the list (see Figure 3.1 for their colours in the $(g' - r')$ *vs* $(U - g')$ plane), through a poor weather condition programme on the GTC (Grand Telescopio Canarias) using OSIRIS (Optical System for Imaging and low Resolution Integrated Spectroscopy). As the name of the program implies, the conditions were not optimal since thin clouds and/or poor seeing were present. Even so, the spectra have a high enough signal-to-noise to reveal the nature of the most of the observed objects (Table 3.1).

GTC, is a 10.4 metre telescope on the Roque de los Muchachos Observatory on the island of La Palma, in the Canary Islands in Spain. Since 2009, it is the world's largest single-aperture optical telescope. `OSIRIS`[2], is a multiple purpose instrument for imaging, and long slit and multiple object spectroscopy with low-resolution. It is sensitive in the wavelength range from 3650Å to 10500Å and has a field of view of 7.8 x 8.5 arcmin (7.8 x 7.8 arcmin unvignetted), and 7.5 x 6.0 arcmin, for direct imaging and multi-object spectroscopy, respectively. Its spectral resolution varies between R=360 and R=1122 depending on the grism and slit width. We used the R1000B grism with 1.0" slit, giving a spectral resolution of $R \sim 653$ at 5455Å and a wavelength range of 3630Å – 7500Å.

[1] We obtained additional two spectra but they have very low signal-to-noise ratio, and no useful information could be extracted.

[2] `http://www.gtc.iac.es/instruments/osiris/`

Table 3.1: The sources for which we obtained optical spectra using the GTC. ID column is in RATJ[hhmmss.s][±ddmmss.ss] format, where [hhmmss.ss] is RA and [±ddmmss.s] is Dec. For brevity, I use a short version (RATJ[hhmm][±ddmm]) in the text to refer to the objects. *GTC ID* is the Observation Block name. The magnitudes are in AB system. The last column indicates the classifications that we assigned: `He-sdO` for helium-rich subdwarf O, `sdB` and `sdO` for B- and O-type subdwarfs, `(s)dB` for subdwarf or main sequence (dwarf) B star, `DA` for DA white dwarf, `QSO` for Quasi-stellar Object, `sd+CoolMS?` for a—possible—binary consisting of a hot subdwarf and a late-type main sequence star.

ID	GTC ID	Obs. Date	Exposure	g'	$U-g'$	$g'-r'$	Type
RAT J175431.29+013753.2	OB0050	20130514	3 x 600 sec	17.41	−0.15	−0.02	He-sdO
RAT J175914.97+011906.4	OB0055	20130514	2 x 600 sec	16.85	0.13	−0.11	He-sdO
RAT J180054.43+003232.0	OB0056	20130514	2 x 600 sec	16.12	−0.18	−0.02	He-sdO
RAT J175526.97+013207.3	OB0052	20130514	2 x 1200 sec	18.34	0.46	0.38	sdB
RAT J180036.57+022358.0	OB0057	20130514	2 x 600 sec	17.56	−0.03	−0.12	sdB
RAT J181931.29+053751.0	OB0069	20130701	2 x 400 sec	18.03	0.06	−0.11	sdB
RAT J180441.91+013832.9	OB0059	20130517	3 x 300 sec	17.26	0.51	0.29	(s)dB
RAT J181752.11+074008.6	OB0068	20130520	2 x 400 sec	18.03	0.10	−0.21	(s)dB
RAT J182318.33+082437.5	OB0060	20130520	3 x 300 sec	17.38	0.09	−0.19	sdO
RAT J180438.61+022226.8	OB0066	20130620	2 x 500 sec	18.68	−0.03	−0.20	sdO
RAT J175436.44+013339.1	OB0051	20130514	2 x 900 sec	19.06	0.34	0.05	DA
RAT J180324.64+013853.1	OB0064	20130620	2 x 400 sec	18.09	0.05	−0.25	DA
RAT J175738.28+013816.7	OB0053	20130514	2 x 600 sec	18.70	0.67	0.37	QSO
RAT J183350.57+282156.0	OB0070	20130620	2 x 450 sec	18.65	0.46	0.29	QSO
RAT J181746.01+072117.8	OB0067	20130520	2 x 400 sec	18.10	0.37	0.43	sd+CoolMS?
RAT J180025.28+012127.4	OB0063	20130620	2 x 400 sec	18.32	−0.14	−0.03	sd+CoolMS?
RAT J175917.90+022516.5	OB0061	20130605	2 x 400 sec	18.59	0.20	0.18	sd+CoolMS?

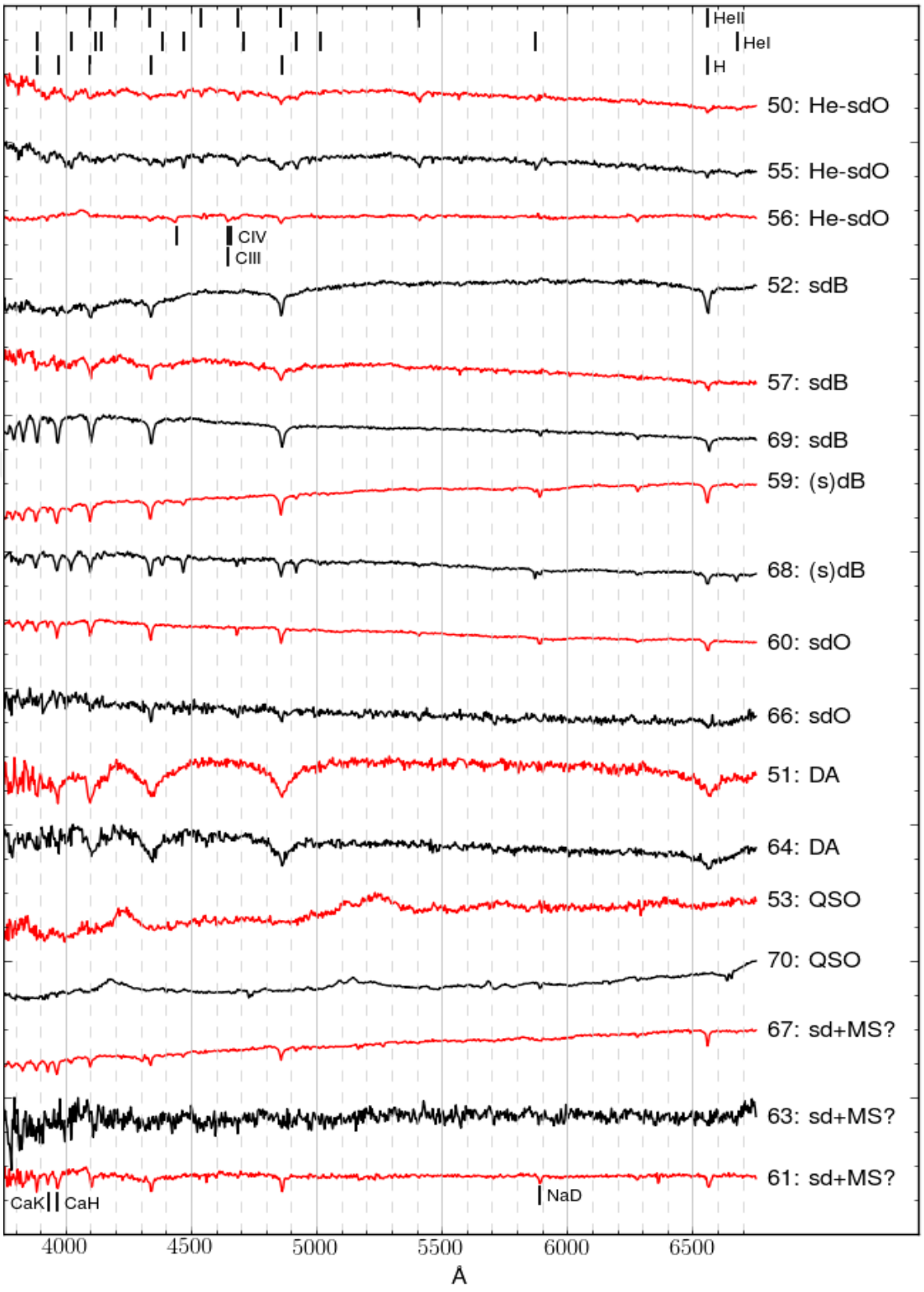

Figure 3.2: Spectra of the objects in Table 3.1 from which numbers and classifications shown on the right hand side are taken. The wavelengths of the most prominent and important lines are marked.

3.1 Reduction of the GTC data

Modern astronomical observations are generally recorded using Charged Coupled Devices (CCDs). The CCDs consist of an array of metal-oxide-semiconductor (MOS) capacitors — pixels of the camera, and necessary electronics to read and output the contents of the MOS's. Basically, these capacitors trap the electrons which are freed via the photoelectric effect, by the photons interacting with them, and then counts them. These "*counts*" are then converted to flux, during the reduction process.

As in every branch of science, the data recorded during an experiment (observation in case of astronomy) should be reduced and/or calibrated. The need for reduction is caused by the fact that the counted electrons do not only consist of electrons that are freed by the photons from the observed object, but also includes the electrons that are freed due to instrumental processes. I made use of FIGARO packages from the STARLINK[3] software suite for the reduction process, which contains a few steps as follows.

3.1.1 Bias subtraction

The analog signal is converted into a digital signal by the analog–to–digital converter (ADC). During this process, the ADC produces a statistical distribution of counts for every pixel, varying around the mean value. This statistical behaviour introduces negative values for some of the zero counts, which requires a "*sign bit*" in the digital data. To avoid this, every CCD has a built-in positive off-set, which is called "*zero level*" or "*bias level*". Therefore, this bias level should be subtracted from every image, in order to determine the errors on the resulting flux measurements properly. The bias level can be estimated using zero exposure-time frames called "*bias frames*" — essentially, a read-out of the unexposed CCD.

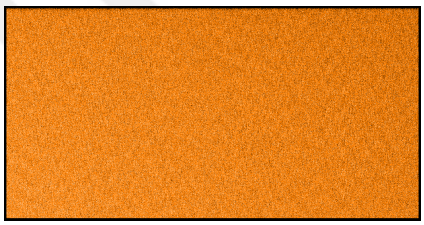

Figure 3.3: A master bias frame produced by taking median average of the bias frames taken at the same run with the science frames.

I have used a number of bias frames taken on the same day with the science frames to produce a master bias (Fig.3.3), and then subtracted it from all the flat, standard and science frames.

[3] `http://starlink.jach.hawaii.edu/starlink`

3.1.2 Dark current subtraction

Dark current is the extra signal caused by the electrons freed by the thermal energy produced by the instrument. It can be minimised by cooling the CCD to very low temperatures. Modern instruments have good cooling systems, usually using liquid nitrogen, hence the dark current is negligible in most cases, including ours, and therefore, we have not obtained dark frames.

3.1.3 Flat-fielding

Each pixel of a CCD responds to light slightly differently. In other words, the number of electrons freed by a photon is not constant over the plane of the CCD. The responses of equally illuminated pixels give information about these slight differences, which allows us to remove these effects. This exposure is called a "*flat-field*". Using the flat-field frames, every science exposure is "*flattened*", basically, by dividing the science exposure by the normalised flat-field.

For photometry, there are two common methods to obtain flat-fields. One is to take multiple exposures of the twilight sky (sky-flat) with the telescope spiraling around a point, then median averaging all exposures to eliminate any counts introduced by the stars in the field. The other is to take an exposure of a homogeneously illuminated surface, which is usually a white flat surface in the dome (dome-flat).

For spectroscopy, on the other hand, although the concept remains the same, there are a few differences. The flat field spectra are usually obtained using a Tungsten lamp located inside the spectrograph, and the flat field frame contains the spectral distribution of the lamp as the light passes through the slit and the grating. In other words, the pixels of the CCD are not illuminated homogeneously, because of the flux that comes from the lamp changes depending on the wavelength. This signature of the lamp must be removed from the flat field frame, before it is applied to the science frames. Therefore, the flat field frame is collapsed along other axis than the dispersion lies, and fitted with a polynomial. This fit is used to remove the spectral signature of the lamp from the flat field frame. Then, finally, this final frame is used to flatten the science images.

However, fitting the 1D spectrum of the flat field with a polynomial is not as straightforward as it sounds, and this process may introduce artificial fluctuations into the data. I have used a number of flat field frames to produce a "*master flat*" (Fig.3.4) to be fitted using a polynomial, and using that fit, flattened the science images. Although I have tried polynomials with several degrees, I could not obtain a good fit to adequately remove the effect. As I

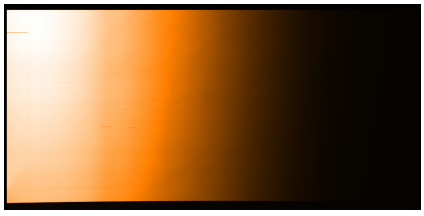

Figure 3.4: A master flat frame produced by taking median average of the flat frames.

had standard star frames, and flux calibration helps to remove this effect to some extend (see Sec.3.1.6), I have omitted the flat-fielding stage.

3.1.4 Extracting a spectrum

The light from the target, background sky and other any nearby objects passes through the slit, and then, dispersed by the grating onto the CCD (Fig.3.5a). While the spectrum of a nearby object could also be a problem, the real complication is caused by the background sky; as its spectrum is embedded in the spectrum of the target. The general practice to estimate the flux distribution of the sky embedded in the target spectrum is to fit two regions of the sky on the both sides of the target spectrum using a polynomial, along "*the spatial axis*", and interpolate it for the region that the object lies (Fig.3.5c). The spatial axis is the one along the length of the slit, whereas the one along the width of the slit is called "*the dispersion axis*".

Before the sky-subtraction, the image is cleaned from cosmic-rays, which are highly energetic charged particles that saturate the pixels they hit (Fig.3.5b).

After the sky-subtraction, a profile of the target spectrum is produced by fitting a Gaussian to every column (*i.e.* pixel group along the spatial axis, Fig.3.5d and 3.5e). Then a polynomial is fitted to the peaks that follow the spectrum along the dispersion axis. The fit is used to follow the spectrum of the object along the dispersion axis. To extract the 1D target spectrum from the sky-subtracted 2D image, a sum of the pixel values along the spatial axis is taken for every point on the polynomial fit along the dispersion axis.

3.1.5 Wavelength calibration

The spectrum extracted by the procedure described in Sec.3.1.4 shows the count distribution as a function of the on the dispersion axis of the CCD. The relation between pixel number and wavelength can be found by using an "*arc frame*" (Fig.3.6), which is a spectrum of an emission line lamp located in the spectrograph. These lamps usually contain a combination of `CuNe`, `CuAr` or `ThAr`, depending on the region of the electromagnetic spectrum in interest. In our case there were two lamps — one `HgAr` and one `Ne`. The wavelengths of the emission lines produced by the lamps are precisely known. Thus, once the relation between the pixels and the laboratory wavelengths is determined, the dispersion axis is converted to wavelength.

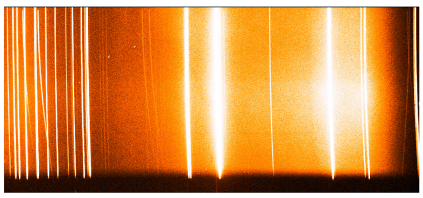

Figure 3.6: An example of an arc frame.

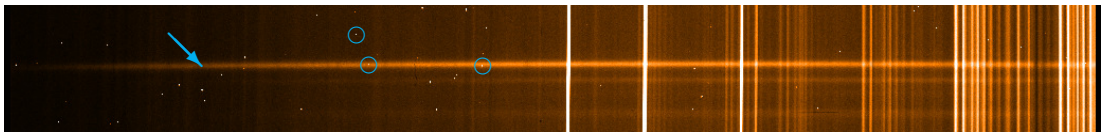

(a) A debiased science frame. The spectrum of the target is pointed by the cyan arrow. Note the cosmic rays (*i.e.* randomly distributed bright dots) marked with cyan circles, sky spectral lines (*i.e.* vertical lines), and spectra of other objects (*i.e.* other horizontal lines).

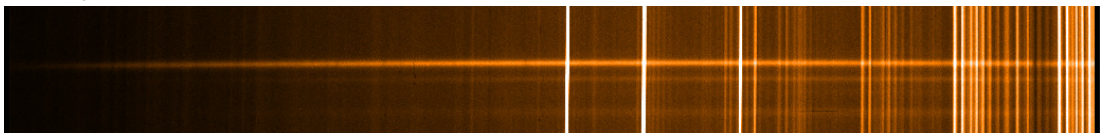

(b) The same science frame after cosmic ray cleaning.

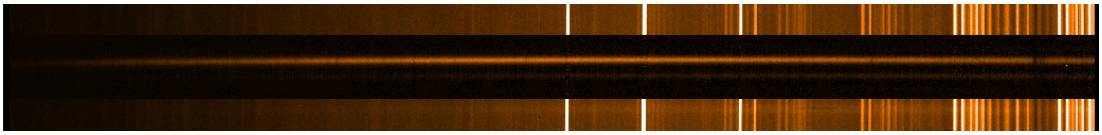

(c) The output of the sky-subtraction process.

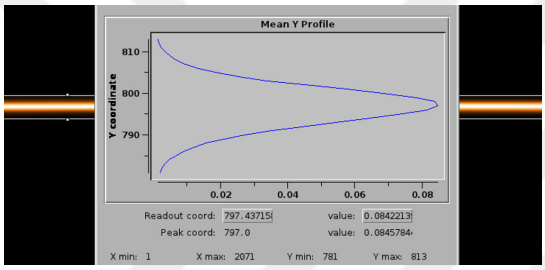

(d) The mean profile of the spectrum along the y-axis.

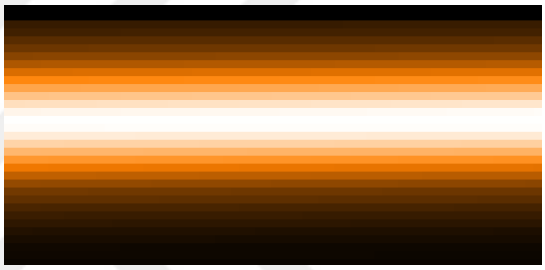

(e) Close-up of the profile

(f) The extracted 1D spectrum of the target.

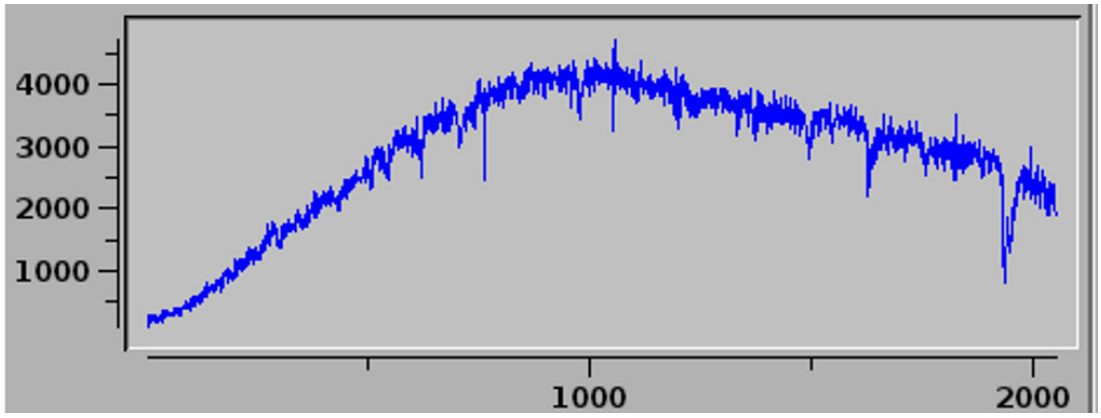

(g) The profile of the reduced 1D spectrum of the target..

Figure 3.5: Steps of the extraction of a spectrum. The image (a) is cleaned from cosmic rays (b), and then sky is subtracted from it (c). Columns of the spectrum are fitted gaussians (d & e) of which the peaks follow the spectrum of the object along the dispersion axis. Finally, using a polynomial fitted to these peaks, the 1D spectrum of the object is extracted (f & g).

3.1.6 Flux calibration

As the dispersion axis has been converted into wavelength from pixels via wavelength calibration, the y-axis of the profile of the 1D spectrum needs to be converted from counts per Å into flux per Å as well. Flux calibration does not only correct the y-axis of the profile, but also removes the instrumental response, which has a varying sensitivity over the CCD with wavelength (see the shape of the continuum in Figure 3.5g).

For the flux calibration, a constant stellar source, whose intrinsic spectrum is well known, is observed. To determine the instrumental response of the CCD, the instrumental spectrum of the standard star is compared to a template spectrum, which is the intrinsic spectrum of the standard star that is free from any instrumental effect. The difference is fitted with a spline, and then the fit is applied to the science spectra.

If the observed spectrum of the standard star is not flat-fielded, the flux calibration removes the effect that flat-fielding corrects, fairly well. Therefore, where the flat-fielding is omitted for any reason, a not-flat-fielded standard spectra can be used for the flux calibration to remove both effects at once, as I did to remove instrumental response and flat-field effect from our spectra.

3.2 Spectral Classification of the GTC spectra

Our targets are selected from an area of the $(g' - r')$ *vs* $(U - g')$ colour-colour diagram where the DB white dwarf cooling sequence track occurs (see §2.3.3). Nevertheless, the same area of the colour-colour diagram hosts other types of blue objects as well. Thus the expected type of sources in the same region include different types of white dwarfs (*e.g.* hydrogen (DA), neutral helium (DB), ionized helium (DO) or carbon (DQ) dominated atmospheres), QSOs, hot subdwarfs, O- or B-type main sequence stars, CVs and AM CVns (for the details see Section1.4). Example spectra for these objects can be seen in Figure 3.7.

An initial analysis of our GTC spectra showed that we have three extremely He-rich hot subdwarfs in our sample ($\sim$ 99% helium on the surface by number) out of 17 spectra, which are rare as only about two dozen with this high He abundances are currently known (see Table 3.3). As these objects are of interest because they can shed light on the questions about their formation (see Sec.1.4.2), we bid for and obtained high-resolution ($R \sim 40000$) spectra of two of them using the ESO VLT (Very Large Telescope), of which a full analysis is presented in §4. I classified the other 14 spectra as hot subdwarfs (He-weak and He-normal), DA white dwarfs, QSOs and possible sd+MS binaries. Details of the classification process of each class and each individual object are discussed in the next sections.

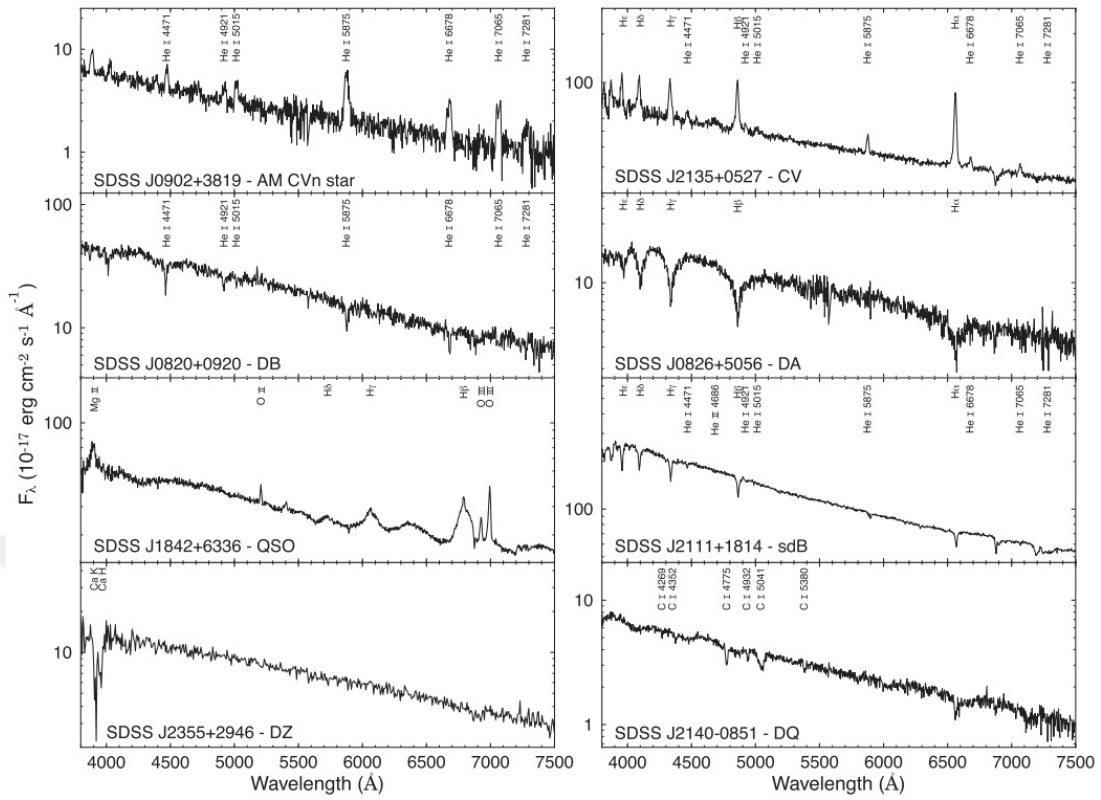

Figure 3.7: Spectra of the different type of sources to be found in a sample of AM CVn binary candidates identified using a colour selection (taken from Carter et al. (2013).)

3.2.1 Hot subdwarfs

Hot subdwarfs are core helium burning stars. They skip the Asymptotic Giant Branch (AGB) and the Planetary Nebulae (PN) phase, as their outer shell is not thick enough to sustain hydrogen burning. After the Red Giant Branch (RGB) phase, they get hotter and slightly less luminous, and become Extreme Horizontal Branch (EHB) stars (for details see Section1.1 and 1.4.2). As they reside below the main sequence stars (MS) on the HR diagram and have spectral types earlier than A, they are called O- and B-type subdwarfs (sdO and sdB stars).

Subdwarf B stars (sdBs) have very thin (less than $\sim 4\%$ of the total mass) and almost pure hydrogen atmospheres, hence the deep Balmer lines in their spectra. These lines are also relatively wide, due to their higher surface gravities ($\log g \gtrsim 4$) compared to the main sequence B stars. Their spectra do not usually show other lines, although a small fraction could have weak `HeI` lines. On the other hand, O-type subdwarfs (sdOs) show the `HeII` 4686Å line, and occasionally other `HeII` lines, in most cases, together with the Balmer lines. Although they are grouped under the same name, sdOs, because they lie around the same region in the HR diagram, the sdO group is not as spectroscopically homogeneous as the sdB group (Moehler

et al., 1990).

Based on the information above and the classification system of Drilling et al. (2013) (for details, see page 12), I have identified 13 objects amongst our spectra as hot subdwarfs of several sub-groups—3 extreme HesdOs (Fig.3.8), 3 sdBs (Fig.3.9), 2 (s)dBs (Fig.3.10), 2 sdOs (Fig.3.11) and 3 sd+CoolMS?s (Fig.3.12). I discuss the details of the classification of the individual objects in the following subsections. This classification system allows one to estimate $T_{\rm eff}$ for an object using the empirical relations between $T_{\rm eff}$ and the spectral class assigned by the classification system. The $T_{\rm eff}$ values found via these relations are given in Table 3.2.

Table 3.2: Spectral classifications and $T_{\rm eff}$ values that are calculated via Equ.1.2 for hot subdwarfs identified through the GTC spectra. The uncertainties of the classifications and $T_{\rm eff}$ are due to low signal-to-noise and/or resolution of the spectra.

ID	Spectral Classification	$T_{\rm eff}$
RAT J1754+0137	sdOC7VII:He40	45500K $\pm$1600K
RAT J1759+0119	sdO8VII:He40 – sdO9VII:He39	38900K $\leqslant T_{\rm eff} \leqslant$ 44600K
RAT J1755+0132	sdB1VII:He0	30500K $\pm$ 1700K
RAT J1819+0537	sdB2VII:He2	26500K $\pm$ 1700K

3.2.1.1 Extreme He-rich Hot Subdwarfs

Three of our objects have extremely He-strong spectra (He-class of $\sim$ 40, which is maximum in the scale) — RAT J1754+0137, RAT J1759+0119 and RAT J1800+0032 (the top, the middle and the bottom panel of Fig.3.8, respectively). All three spectra show very weak Balmer lines, relatively strong HeI and HeII lines, and some C lines (*e.g.* CIV 4647Å-4668Å).

As detailed in page 10, about 10% of hot subdwarfs should have helium-rich surfaces between 10% and 99% (by number of atoms), as well other exotic chemistries. Roughly one tenth of these He-sds (1% of all hot subdwarfs) should have extreme helium abundances, higher than 90% — the number of currently known extreme helium-rich hot subdwarfs are about six dozen (Table 3.3). Our new three extreme He-rich objects, which have $\sim$ 99% helium on their surface, are a significant addition to these rare group of objects. The majority of these extreme and intermediate He-rich subdwarfs were discovered from quasar surveys (*e.g.* Palomar-Green, SDSS) which were strongly biased towards the high Galactic latitudes. In contrast, the three new extreme He-sds are at lower latitudes ($b \sim 12^o$) which may imply that they come from a different Galactic population.

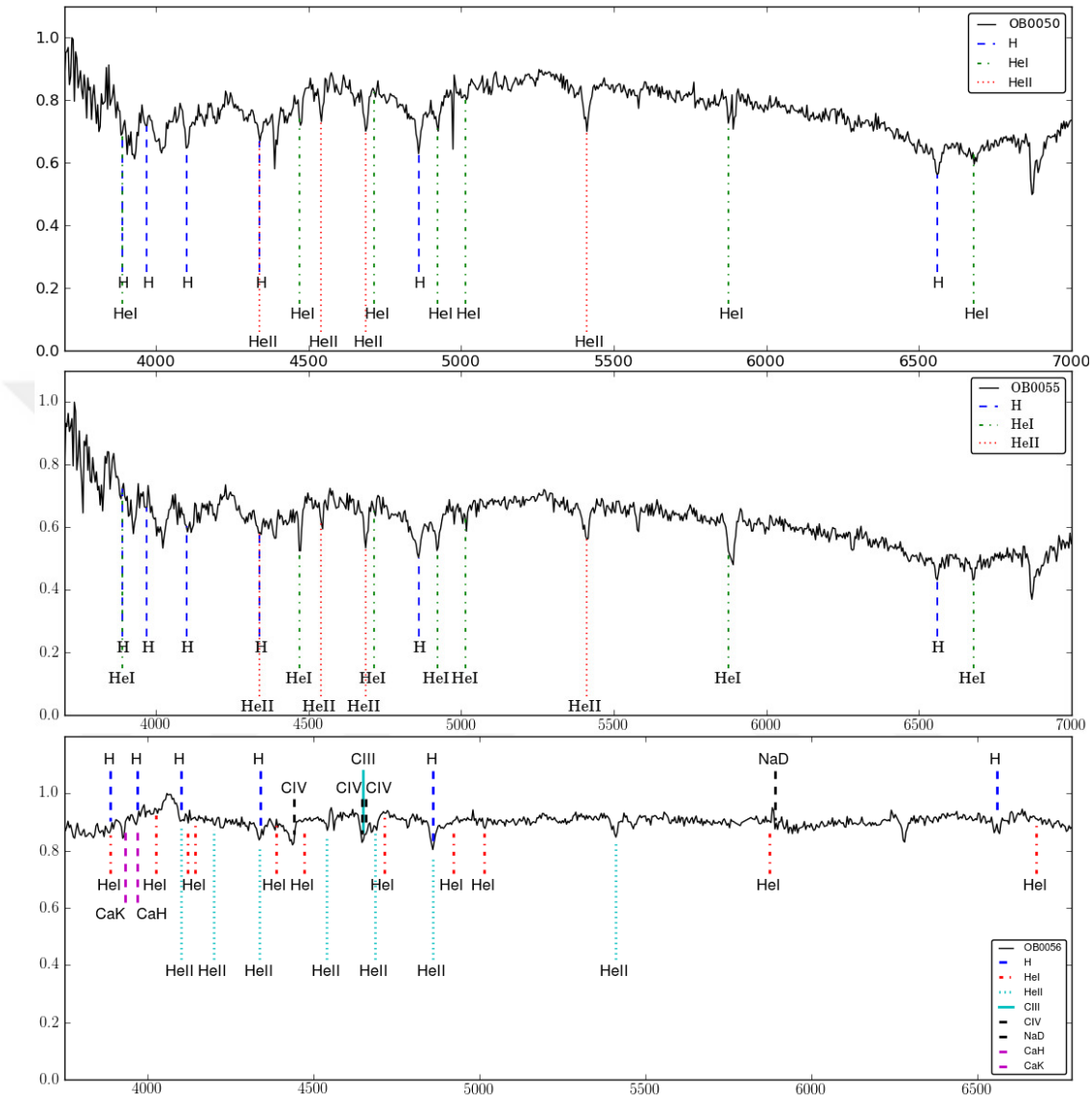

Figure 3.8: The spectra of our extremely He-rich hot subdwarfs where the flux has been normalised to unity at maximum. `RAT J1754+0137` (top panel) is an `sdOC7VII:He40`, `RAT J1759+0119` (middle panel) is an `sdO8VII:He40` or `sdO9VII:He39`. Although it is almost certain that `RAT J1800+0032` (bottom panel) is an extreme He-rich subdwarf, there is some uncertainty in its class due to the relatively low signal-to-noise of its spectrum while the cool lines like `Ca H&K` and `Na D` may imply that it has a cool companion (see Sec.3.2.1.3).

Table 3.3: Extreme helium rich hot subdwarfs that are currently known. The information in the table is gathered by C.S. Jeffery and edited by myself. References to the individual stars are given at the end of the table. "*:*" notes an uncertain value. $T_{\rm eff}$ and $\log g$ values are approximate as they are rounded and their errors are omitted for simplicity. Also the catalogue name of `GALEX J042034.8+012041.0` is shortened as `GALEX J[RA±DEC]` as the RA and Dec values are already presented.

#	Catalogue name	RA	Dec	Galactic		Spectral	$T_{\rm eff}$ ^{ref}	$\log g$ ^{ref}	nHe^{ref}
				Longitude	Latitude	Type^{ref}	$x10000^{o}K$		per cent
1	HE 1251+0159	12:54:08.4	+01:43:24.0	304.5	+64.6	He-sdO[a]	48[5]	6.0[5]	0.91[5]
2	PG 0039+135	00:42:16.6	+13:45:40.6	119.5	−49.1	He-sdO[a]	45[6]	5.0[6]	0.91:[6]
3	PG 0208+015	02:10:54.2	+01:47:47.1	159.6	−55.3		40[6]	5.0[6]	0.91:[6]
4	PG 0838+133	08:41:43.9	+13:04:30.0	213.2	+30.3		44[6]	4.8[6]	0.91:[6]
5	PG 1249+761	12:50:37.8	+75:53:22.0	123.0	+41.2		68[6]	5.8[6]	>0.91[6]
6	PG 1536+690	15:36:50.0	+68:52:18.0	104.3	+41.8		63[6]	5.8[6]	>0.91[6]
7	PG 2158+082	22:00:54.7	+08:28:31.0	067.6	−35.5		67[6]	5.5[6]	>0.91[6]
8	PG 2215+151	22:17:48.3	+15:20:54.0	077.0	−33.5		40[6]	5.0[6]	>0.91[6]
9	PG 2352+181	23:55:17.3	+18:20:15.3	104.7	−42.5		45[6]	5.5[6]	>0.91[6]
10	HE 1511-1103	15:14:17.0	−11:14:13.6	014.6	+52.9	He-sdO[a]	42[5]	5.7[5]	0.93[5]
11	HE 1430-0815	14:33:36.9	−08:28:24.8	000.0	+59.5	He-sdO[a]	61[5]	5.3[5]	0.94[5]
12	GALEX J[RA±DEC]	04:20:34.8	+01:20:41.0	192.2	−32.2	He-sdO[1]	45[1]	5.7[1]	>0.94[1]
13	PG 1325+054	13:28:21.4	+05:08:56.0	326.4	+66.3	He-sdO[a]	41[6]	5.0[6]	>0.91[6]
14	PG 1624+085	16:26:55.0	+08:25:36.0	023.3	+35.9	He-sdO[a]	40[6]	5.3[6]	>0.95[6]
15	PG 1401+289	14:03:17.1	+28:39:29.4	042.6	+74.1		47[6]	5.5[6]	>0.95[6]
16	HE 0342-1702	03:44:58.8	−16:52:42.2	171.7	−29.1	He-sdB[2]	42[5]	5.8[5]	0.96[5]
17	HE 1203-1048	12:05:56.6	−11:05:29.4	267.0	+70.7	He-sdO[a]	45[5]	5.9[5]	0.96[5]
18	HE 1446-1058	14:49:24.5	−11:11:19.0	008.8	+58.0	He-sdO[a]	45[5]	5.8[5]	0.96[5]
19	HE 0952+0227	09:55:34.6	+02:12:47.9	235.9	+41.1		47[5]	5.8[5]	0.96[5]
20	HE 1203-1048	12:05:56.6	−11:05:29.4	267.0	+70.7		45[5]	5.9[5]	0.96[5]
21	HE 1446-1058	14:49:24.5	−11:11:19.0	008.8	+58.0		45[5]	5.8[5]	0.96[5]
22	HE 2347-4130	23:50:19.7	−41:14:01.1	110.7	−20.2	He-sdO[a]	45[5]	5.8[5]	0.96[5]
23	HE 0016-3212	00:18:53.0	−31:56:03.0	114.9	−30.4		42[3]	5.8[3]	0.97[3]
24	HE 0414-5429	04:15:30.2	−54:21:58.7	149.9	+02.5	He-sdO[a]	45[5]	5.8[5]	0.97[5]
25	HE 0451-3706	04:53:32.0	−37:01:43.0	167.1	−04.3	He-sdO[a]	43[3]	6.7[3]	0.97[3]
26	HE 0914-0314	09:17:15.6	−03:53:57.3	227.6	+34.0	He-sdO[a]	45[5]	5.8[5]	0.98[5]
27	HE 0155-3710	01:58:01.4	−36:56:21.9	137.5	−24.0	He-sdO[a]	41[5]	5.8[5]	0.98[5]
28	BPS CS 22955-0024	20:23:50.3	−25:08:28.8	065.9	−07.0	He-sdO[a]	45[5]	5.8[5]	0.98[5]
29	HE 1136-1641	11:38:54.6	−16:58:13.4	240.4	+70.4		45[5]	5.8[5]	0.98[5]
30	HE 0958-1151	10:00:42.6	−12:06:00.0	225.0	+47.3		44[5]	5.5[5]	0.99[5]
31	HE 0016-3212	00:18:53.2	−31:56:01.7	114.9	−30.4	He-sdO[a]	42[5]	5.7[5]	0.99[5]
32	HE 0031-5607	00:34:07.8	−55:51:05.9	120.5	−06.9	He-sdO[a]	41[5]	6.3[5]	0.99[5]
33	LB 3229	01:47:17.5	−51:33:39.2	131.7	−10.4	He-sdO[a]	40[8]	5.2[8]	0.99[8]
34	PG 1127+019	11:30:03.7	+01:37:37.3	262.1	+57.9	sdOD[4]	40[7]	5.0[7]	0.99[7]
35	PG 1415+492	14:17:02.7	+48:57:29.0	091.5	+62.6	sdOD[4]	32[7]	4.2[7]	0.99[7]
36	PG 1544+488	15:46:11.7	+48:38:37.0	077.5	+50.1	sdOD[4]	34[7]	5.1[7]	0.99[7]
37	PG 1554+408	15:55:50.4	+40:38:51.0	064.8	+49.9	sdOD[4]	38[7]	5.2[7]	0.99[7]
38	PG 1615+413	16:17:38.8	+41:12:52.0	065.3	+45.8	sdOD[4]	36[7]	5.2[7]	0.99[7]
39	PG 1658+273	17:00:14.3	+27:12:35.0	048.4	+35.3	sdOD[4]	39[7]	4.9[7]	0.99[7]
40	PG 1715+273	17:17:03.2	+27:16:37.0	049.7	+31.7	sdOD[4]	35[7]	5.0[7]	0.99[7]
41	HS 1844+637	18:43:59.8	+63:46:51.0	093.8	+25.0		36[7]	5.1[7]	0.99[7]
42	PG 2321+214	23:24:27.2	+21:38:52.0	097.4	−36.9	sdOD[4]	40[7]	5.3[7]	0.99[7]
43	BPS CS 22940-0009	20:30:20.2	−59:50:39.4	095.1	+12.0	He-sdB[2]	34[8]	4.7[8]	0.99[8]
44	PG 2258+155	23:00:57.8	+15:48:39.8	087.7	−39.4	sdOD[4]	42[5]	6.1[5]	1.00[5]
45	PG 1632+222	16:34:16.1	+22:11:40.9	040.3	+39.5		39[5]	6.2[5]	1.00[5]
46	HE 0001-2443	00:04:31.0	−24:26:21.1	109.5	−37.2	He-sdB[3]	40[5]	5.9[5]	1.00[5]
47	HZ 1	04:50:13.5	+17:42:06.2	182.2	−16.8		41[5]	5.7[5]	1.00[5]
48	HE 1316-1834	13:19:16.9	−18:49:52.0	342.0	+79.5	He-sdO[a]	43[5]	5.6[5]	1.00[5]
49	SB 21	00:04:30.7	−24:26:18.0	109.5	−37.2	He-sdB[2]	36[8]	5.4[8]	1.00[8]
50	LB 1766	04:59:19.3	−53:52:55.0	154.5	+07.0		36[8]	5.2[8]	1.00[8]
51	BPS CS 29496-0010	23:34:01.8	−28:51:38.0	103.1	−31.0	He-sdB[2]	39[8]	5.6[8]	1.00[8]

[a]Jeffery, C.S. (pri.comm.), [1]Vennes et al. (2011), [2]Beers et al. (1992), [3]Edelmann et al. (2003), [4]Green et al. (1986)
[7]Ahmad and Jeffery (2003), [8]Naslim et al. (2010), [5]Stroeer et al. (2007), [6]Dreizler et al. (1990)

Considering that these are rare and interesting objects, we acquired high resolution spectra for RAT J1754+0137 and RAT J1759+0119, using ESO VLT (Very Large Telescope). We have two groups of spectra for each object separated by roughly 3 weeks (3 spectra per night), to look for evidence for binarity and also to measure their chemical abundances, and thereby, test the models which predict their formation. The detailed analysis of these high-resolution spectra are given in §4; here I present an preliminary analysis of their GTC spectra that allowed us to give the initial classifications and to find approximate $T_{\rm eff}$ values (Table 3.2).

RAT J1754+0137 ***(sdOC7VII:He40)*:** A continuum rising towards the shorter wavelengths indicates that this object is blue and hotter than an A type star. Additionally, the presence of ionized helium (HeII) lines also supports this. Relatively wide Balmer lines, compared to B- or O-type main sequence stars, indicate that this object is a subdwarf rather than a main sequence object.

Observing stronger HeII lines (especially the 4686Å line) than HeI lines indicates that this object is an O-type subdwarf. As radiative atmospheres of sdOs are hotter than atmospheres of sdBs, helium does not sink as it does in sdBs, and thus can get ionised (for more details, see page 12). The He-class of ~ 40 (Equation 1.1 on page 12) means that this sdO is extremely He-rich (more than 99% helium on the surface). Additionally, the CIV lines between 4570Å – 4645Å are identifiable; this puts our objects into the He-strong C category. One can see that the spectrum of our object finds its place close to the sdOC7VII:He40 spectrum in Figure 1.8. The best way to see the resemblance of the two spectra is to check line strength ratio of HeI 4471Å and HeII 4541Å lines. Other HeI, HeII and Balmer lines also supports this classification. Using Equation 1.2 (page 12), one can derive a $T_{\rm eff}$ for this object as below:

- The objects falls into the middle group in the Eq.1.2,
- for O-types, s equals to spectral class index, hence $s = 7$,
- $63200 - 2520s \pm 1600 = 43560 \pm 1600$

RAT J1759+0119 ***(sdO8VII:He40 – sdO9VII:He39)*:** The continuum and the line profiles of the spectrum of RAT J1759+0119 imply it is a hot subdwarf. Although the ratio of the line strength of HeI 4471Å and HeII 4541Å lines puts this object very close to a B-type on the spectral scale, comparison with spectra in Fig.1.9 pulls the indicator towards the O-type. With the He-class of ~ 40 (Eq.1.1), this object too has an extremely helium rich surface. Although it is arguable that very weak carbon lines may present, the signal-to-noise ratio of the spectrum is not high enough to be conclusive. Therefore, the comparison is made with He-strong spectra (Fig.1.9). The spectrum falls between the spectra for class of sdO8VII:He40 and sdO9VII:He39. A spectrum with higher S/N would yield a more accurate classification. In this case, effective temperature is in the range of 38900K $\leqslant T_{\rm eff} \leqslant$ 44600K (Equ.1.2).

RAT J1800+0032: With its relatively strong HeII lines and very weak Balmer lines, the spectra of RAT J1800+0032 most probably belongs to an early-type, hot object. Besides, relatively broad lines suggest that it is not an MS star, rather a hot subdwarf, and the lack of HeI lines while HeII lines present is a clue for an O-type nature. Some carbon lines are also present (*e.g.* CIV 4442Å,4647Å,4658Å and CIII 4650Å). These suggest that it is a C-strong He-rich hot subdwarf. Nevertheless, the signal-to-noise ratio of the spectrum is not high enough to give it a more certain classification.

3.2.1.2 "*Normal*" hot subdwarfs

An examination of our GTC spectra indicated that our target list includes seven more subdwarfs, in addition to the three He-rich subdwarfs. Using the classification scheme by Drilling et al. (2013), I have revealed their He-weak hot subdwarf nature, which implies that they belong to the group that contains 90% of subdwarfs. In other words, they are fairly common amongst the hot blue objects (*e.g.* sdBs and sdOs constitute 40% and 13% of the Palomar-Green survey, respectively (Green et al., 1986)). Amongst these seven He-weak hot subdwarfs, three have very typical B-type spectra, with their relatively strong and wide Balmer lines, and weak (if any) HeI lines (Figure 3.9). While two are just at the border of being a B-type subdwarf or a main sequence star with their relatively narrow Balmer lines, the other two are sdOs with their He-dominated spectra.

RAT J1755+0132 - *sdB1VII:He0*: In the top panel of Figure 3.9 is the spectrum of RATJ1755 +0132. The continuum rising towards the shorter wavelengths implies the blue and hot nature of the object. The strong Balmer lines and the lack of other lines are clear. The Balmer lines are too narrow for a DA white dwarf, while they are too wide for an early type main sequence star. Comparing the spectrum to the spectra in Figure 1.6, I identified RAT J1755+0132 as a sdB1VII:He0, which corresponds to $T_{\rm eff}$ of 30570K $\pm$ 1700K (Eq.1.2).

RAT J1800+0223 - *sdB0VII:He0*: The spectrum of RAT J1800+0223 is presented in the middle panel of Figure 3.9. The lack of lines other than the Balmer lines with profiles that are wide and deep enough for an sdB on the blue spectrum indicate the sdB nature of this object. Although the lines are not very strong, they are wider than that of main sequence stars. Comparison with the spectra in Figure 1.6 dictates its classification as sdB0VII:He0 with a $T_{\rm eff}$ of 34600K $\pm$ 1700K (Eq.1.2).

RAT J1819+0537 - *sdB2VII:He2*: The bottom panel of Figure 3.9 shows the spectrum of RATJ1819 +0537. The Balmer lines are strong and wide, but not as wide as that of WDs.

Additionally, a few HeI lines (*i.e.* 4471Å, 4921Å, 5015Å and 6678Å) are recognisable, although they are very weak. With stronger Balmer lines and a very weak HeI line at 4471Å, RATJ1819 +0537 shows a resemblance with sdB2VII:He0 type of spectra in Figure 1.6, but has a He-class ~ 2 (Eq.1.1). This classification implies a $T_{\rm eff}$ of 26540K $\pm$ 1700K (Eq.1.2).

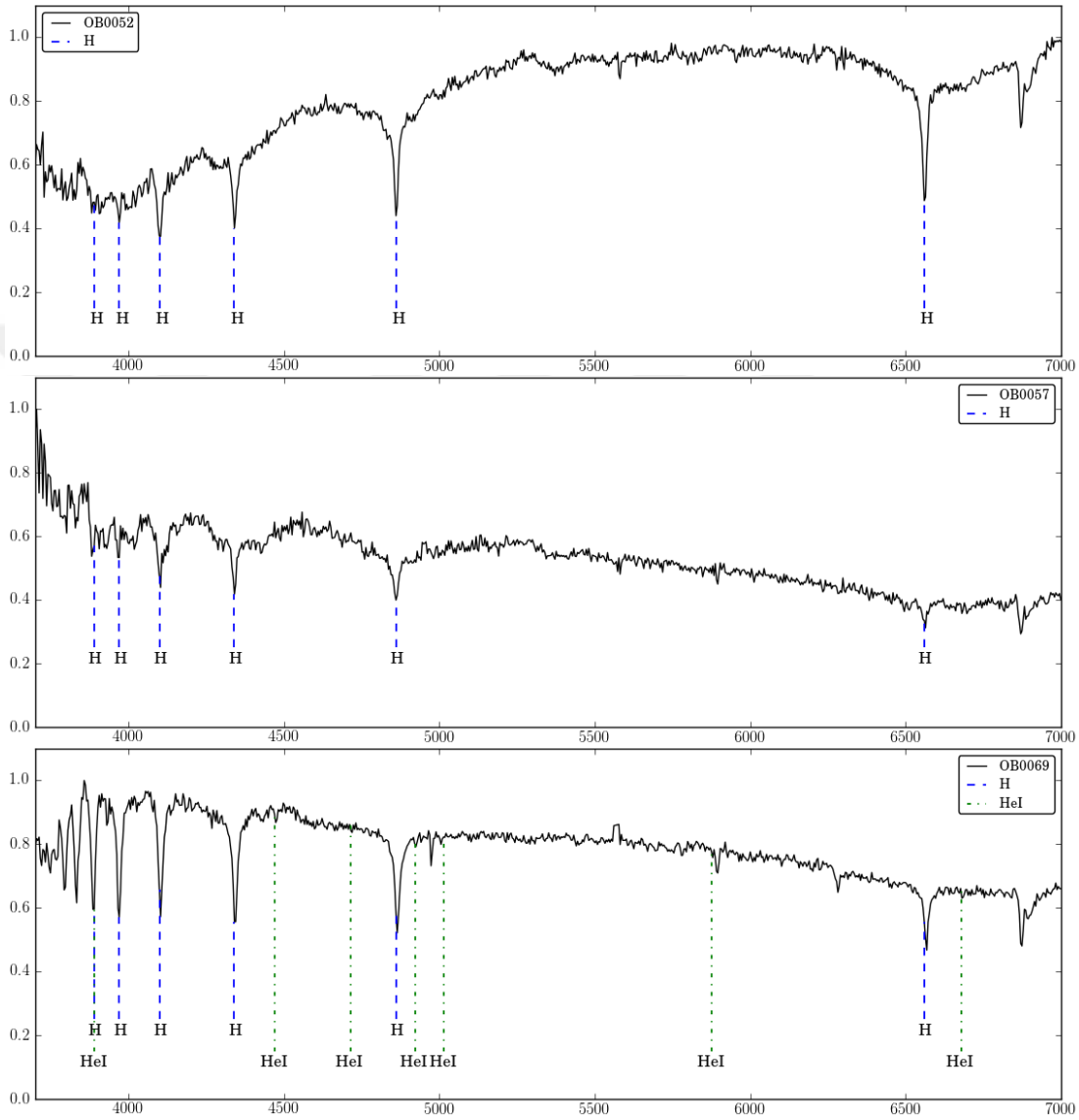

Figure 3.9: The spectra of B-type hot subdwarfs (sdBs) where the flux has been normalised to unity at maximum. *Top:* RAT J1755+0132 is an sdB1VII:He0 with strong Balmer lines with out any other feature. *Middle:* RAT J1800+0223 is an sdB0VII:He0 relatively weaker Balmer lines and no other lines. *Bottom:* RAT J1819+0537 is an sdB2VII:He2 with strong Balmer lines and very weak HeI line at 4471Å.

RAT J1804+0138 and RAT J1817+0740 - *(s)dB*: Spectra of RAT J1804+0138 and RAT J1817+0740 (Figure 3.10) are consistent with that of late B-type objects, considering the strong Balmer lines and the high HeI 4471Å/HeII 4541Å ratio. Since the S/N of the spectrum does not allow us to decide whether the line widths and wings are pointing to a main sequence or subdwarf nature, I have classified these objects as (s)dB — (sub)dwarfB.

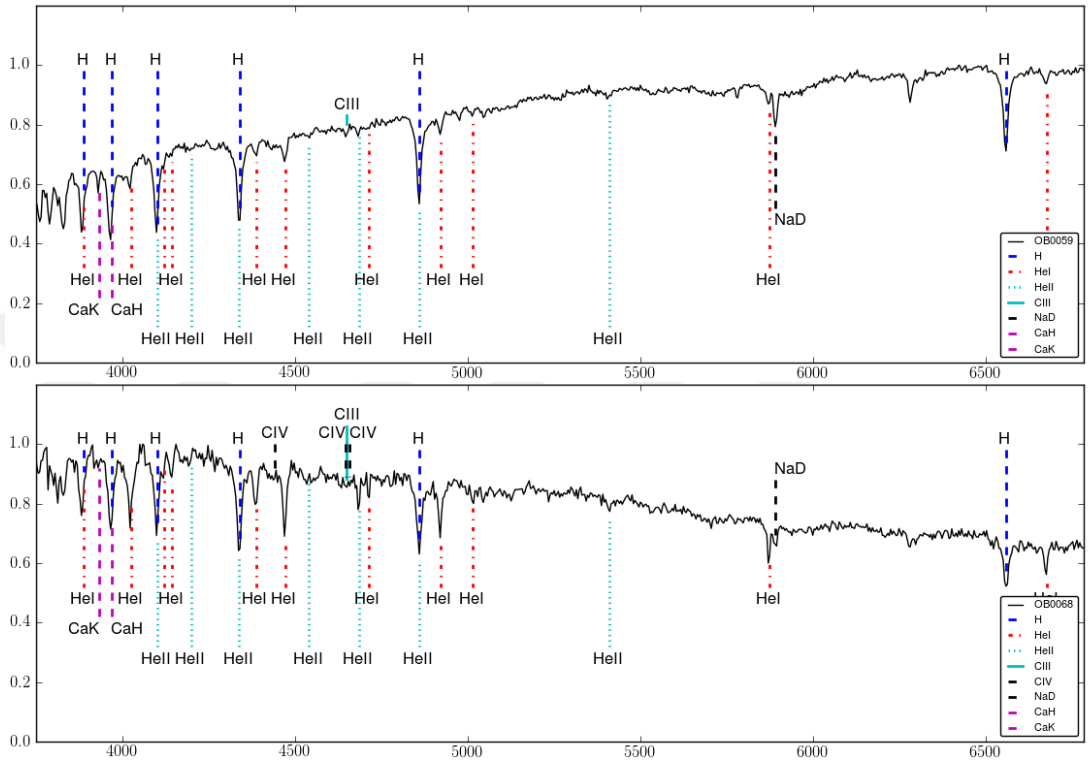

Figure 3.10: The spectra of RAT J1804+0138 and RAT J1817+0740 which are B-type main sequence or subdwarf stars where the flux has been normalised to unity at maximum.

RAT J1823+0824 - *sdO7VII:He1*: The top panel of Figure 3.11 shows the spectrum of RAT J1823+0824. Considering the notable HeII 4686Å line accompanied by another HeII line at 5411Å and Balmer lines with profiles pointing to the subdwarf nature, this object is an sdO. Its spectrum looks very similar to the sdO7VII:He1 spectrum in Figure 1.6, hereby it has a $T_{\rm eff}$ of 46090K $\pm$ 1700K.

RAT J1804+0222 - *sdO8VII:He0*: The low signal-to-noise ratio spectrum of RATJ1804 +0222 on the bottom panel of Figure 3.11 does not show many features. Nonetheless, weak Balmer lines, and weak HeII lines at 4686Å and 5411Å on its blue spectrum, has a good resemblance with sdO8VII:He0 spectrum in Figure 1.6, which indicates an $T_{\rm eff}$ of 42600K $\pm$ 1700K.

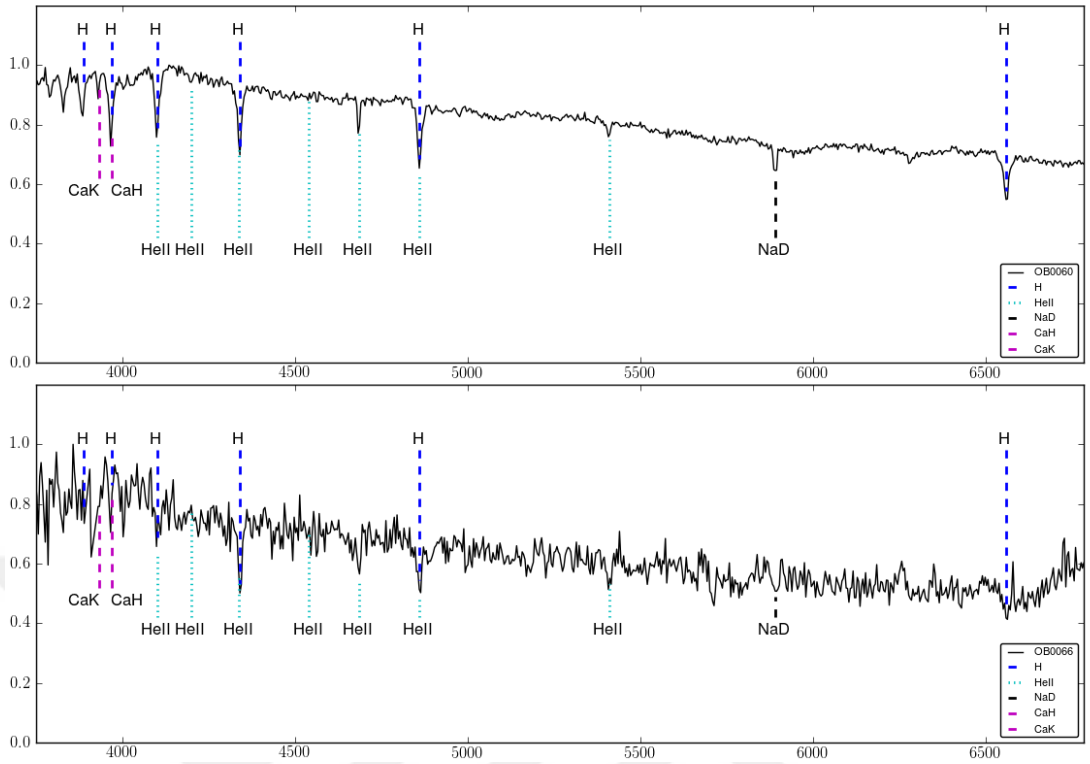

Figure 3.11: The spectra of O-type subdwarfs. While both the x-axes are in wavelength (Å), the y-axes are arbitrary fluxes normalized to 1 at maximum. *Top:* `RAT J1823+0824` is an `sdO7VII:He1` with relatively strong Balmer lines and also `HeII` lines at 4686Å and 5411Å line. *Bottom:* `RAT J1804+0222` is an `sdO8VII:He0` with weak Balmer lines, and weak `HeII` lines at 4686Å and 5411Å.

3.2.1.3 Cool-looking spectra of hot objects

There are three objects (*i.e.* `RAT J1817+0721`, `RAT J1800+0121` and `RAT J1759+0225` – the top, middle and bottom panel of Fig.3.12, respectively) whose spectra show features associated with late type stars (*e.g.* `CaII H&K` lines, `Na D` line *etc.*) alongside the hot features (*e.g.* `HeI`, `HeII` and `C` lines), although they have blue photometric colours that caused them to be picked by the selection method in the first place. Wade et al. (2009) checked GALEX colours of similar objects from Palomar-Green photometric survey that were not included to the final catalogue because of the `CaII H&K` lines in their spectrum, and concluded that some of these objects are binary systems that consists of a late-type star and a hot subdwarf. They argue that while the cool star shapes the continuum, the subdwarf produces the most of the flux in the UV and only adds its signature to the spectrum with lines.

In this case, one expects a rise of the continuum at the wavelengths shorter than $\sim$ 4000Å. But, it is not necessarily the case, as one can see that the spectrum of some objects in the same wavelength range with our spectra do not have such a feature (Fig.3.13). Nevertheless,

there are HeI and HeII lines, some C lines on the spectra which supports the hot nature of these objects and the scenario. To conclude that these objects are sd+coolMS systems, we need UV and IR photometry —to construct an SED (spectral energy distribution) as in Girven et al. (2012)—and spectroscopy of these objects. While RAT J1817+0721 has a GALEX colour of $fuv - nuv = -0.258$, which points to an increase in the energy radiated in the shorter wavelengths and supports the blue and hot nature of the object, the other two objects do not have a counterpart in any UV or IR database.

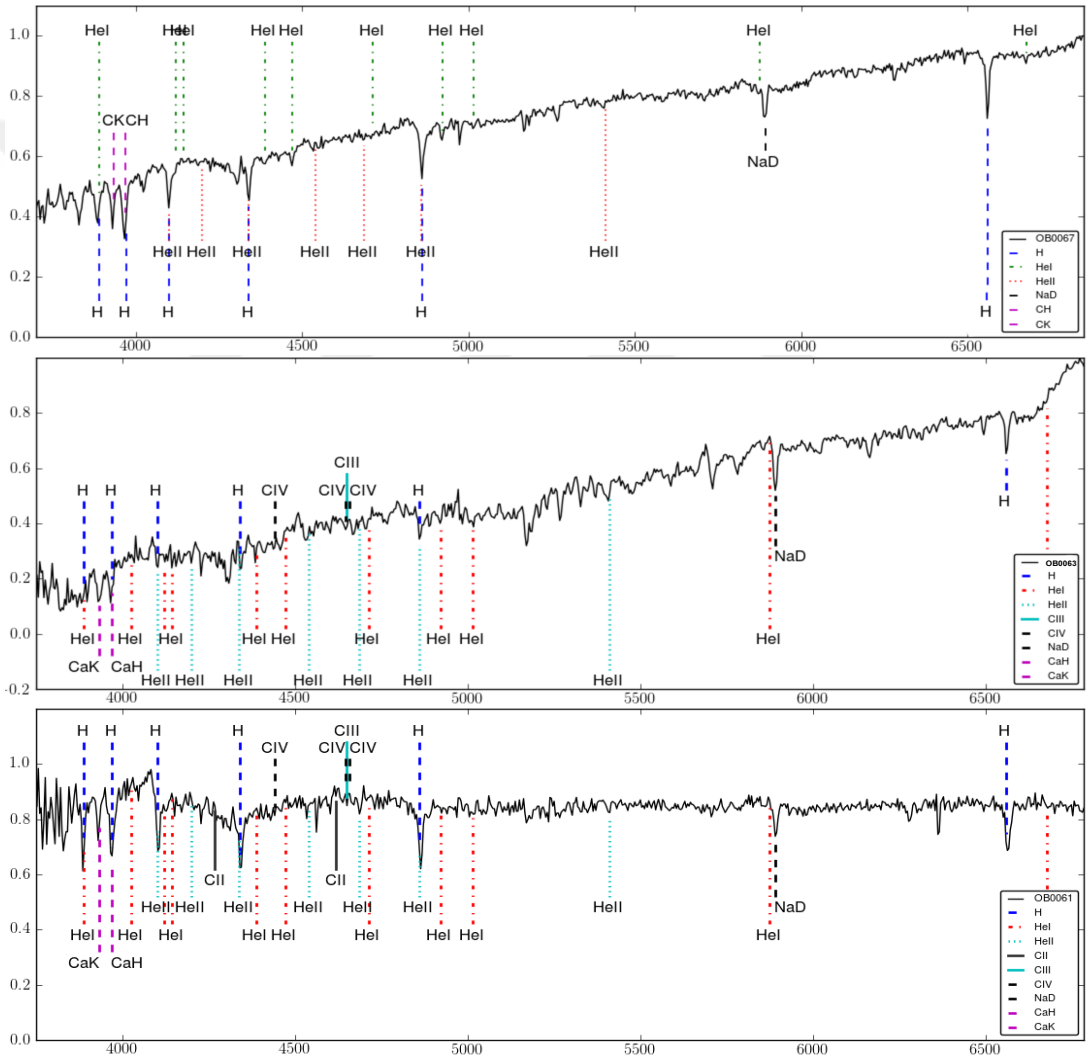

Figure 3.12: Possible sd+CoolMS binaries RAT J1817+0721 (top), RAT J1800+0121 (middle) and RAT J1759+0225 (bottom). With the CaII H&K and Na D lines, they show late-type star nature, while HeI and HeII lines imply a high effective temperature, which may be explained with a "*hot subdwarf–late-type star*" syatem (Wade et al., 2009).

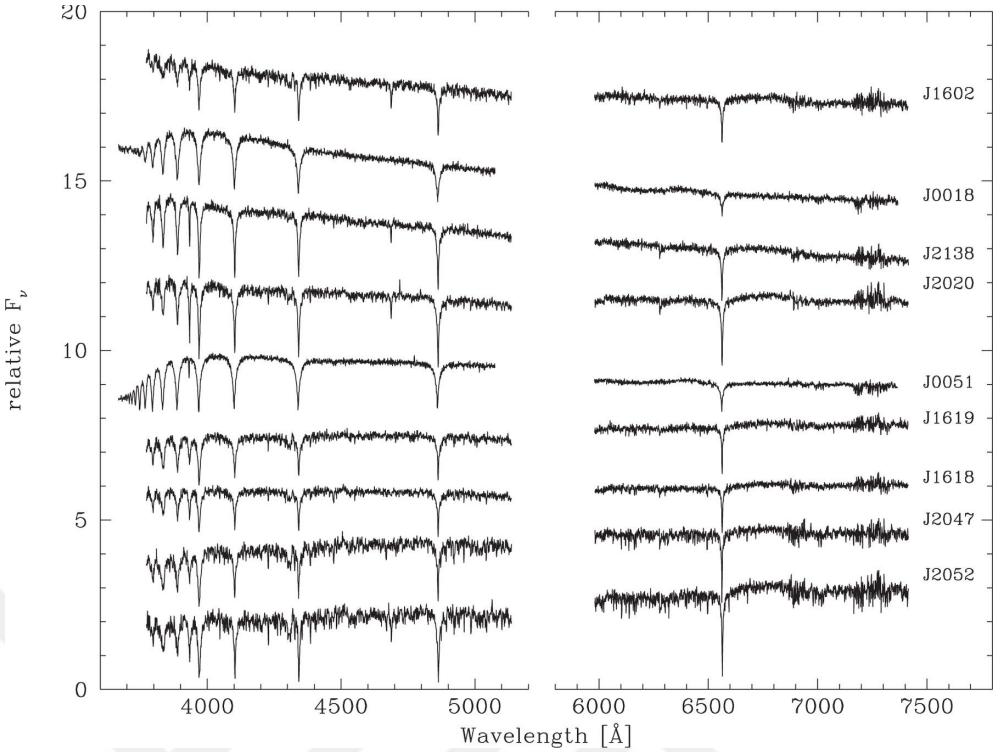

Figure 3.13: WHT spectra of colour-selected sdB+MS candidates by Girven et al. (2012). One can see that the spectrum at the bottom does not show a blue continuum because of contribution of the cool component. All, except J0051 which is probably an A-star, are sdBs.

3.2.2 DA white dwarfs

The optical spectra of DA white dwarfs are identifiable by extremely broadened Balmer lines, and — generally — the lack of other lines due to — almost — pure hydrogen atmosphere with high surface gravity ($\log g \gtrsim 7$). While the majority of DA white dwarfs show only Balmer lines ($\sim$80%), there are groups with spectra in which neutral or ionized helium, or — seldom — metal lines are present. These subgroups are called DAB (HeI), DAO (HeII), DAQ (C) and DAZ (metals). According to their temperature, an index between 0 and 9, calculated by $50400/T_{\rm eff}$ (closest integer or half), is appended to the subgroup name (*e.g.* DA3, DAB1.5, DAZ8 *etc.*) (Sion et al., 1983).

For DA white dwarfs the profiles of the Balmer lines show a smooth transition from the higher temperatures to the lower temperatures (see Fig.1 and Fig.2 of Wesemael et al. (1993)). With the decreasing temperature, line strength first increases, reaches to the peak at $\sim$ 12000K and $\log g \approx 8$, and then keeps weakening to the point that all the lines other then H_α disappear. With a low signal-to-noise spectrum, it is highly possible to misidentify a DA10 as a DC (a white dwarf with a featureless continuum spectrum). On the other hand, the relation between the broadening and the temperature is more straightforward — the shallow and extremely

broadened Balmer lines at the high temperatures, becomes slightly narrower with the decreasing $T_{\rm eff}$ (Wesemael et al., 1993).

There are two DA white dwarfs in our list of 17 objects — RAT J1754+0133 and RAT J1803+0138. Their characteristic spectra (Figure 3.15) are easily distinguishable by wide and deep Balmer lines, and the lack of other lines. Although weak helium or carbon lines may be present, with the relatively low S/N ratio of these spectra, one can not differentiate those lines from the noise. Thus, these two objects are classified as classical DA white dwarfs, without extra notation for neutral or ionised helium (B or O), carbon (Q) or other metals (Z).

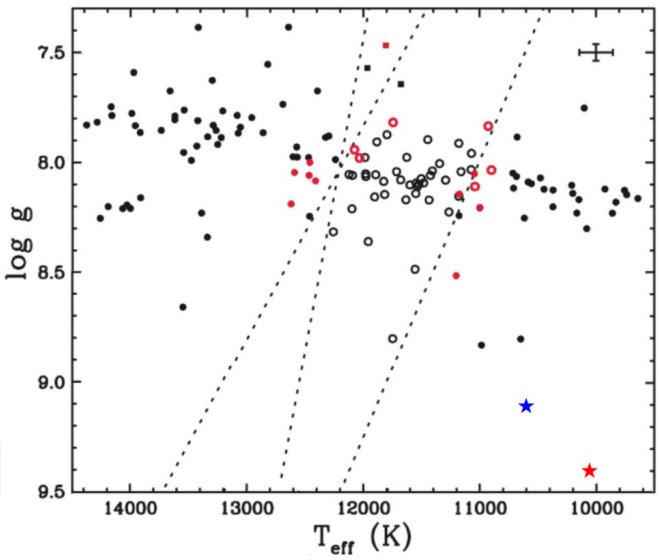

Figure 3.14: The instability strip for DA WDs. Our two DA WDs are shown overplotted with data from Gianninas et al. (2006). The blue star represents RAT J1754+0133 and the red star RAT J1803+0138. Open circles represent DAV (variable DAs, a.k.a ZZ Cet stars), closed circles non-variable DAs. The white dwarfs outlined here do not lie in the instability strip.

Although the spectra we obtained of our sources were primarily for identification and classification purposes, it was also possible to fit the spectra with a grid of model spectra of various effective temperatures and surface gravities. We used the FITSB2 fitting program (Napiwotzki et al., 2004) to fit the Balmer lines of each spectrum with a grid of white dwarf atmospheres[4] (Fig.3.16). The derived values (Table 3.4) indicate that they are very far from the instability strip (Fig.3.14) where the pulsating DA white dwarfs reside on the $T_{\rm eff}$ –log g plane, and of which the borders and the pureness have tried to be established by myriad of studies for decades. Considering the high log g values, these objects seem to be rather massive WDs, but this is fairly consistent with their colours.

For DA white dwarfs, this narrow region in the $T_{\rm eff}$ –log g plane, known as the instability strip, is roughly located in the temperature range 10800–12300K (Bergeron et al., 2003; Mukadam et al., 2004), where the pulsations are driven by the $\kappa-$ and $\gamma-$mechanisms in the hydrogen partial ionization zone. It is determined from observations that the instability strip also has a small dependence on mass (*e.g.* Giovannini et al. (1998)). The theorisation of the purity

[4] A grid of hot white dwarf models was kindly supplied by Detlev Koester. These models range between $T_{\rm eff}$ of 6000–100000K and log g of 5.5–9.5.

of the instability strip for DA white dwarfs by Fontaine et al. (1982) suggested that if a DA white dwarf is in the instability strip, it would have to be pulsating. This meant DA white dwarf pulsations are a phase through which all DA white dwarfs evolve as they cool, as argued by Fontaine et al. (1982) and Greenstein (1982). Thus studying the seismological properties of pulsating DA white dwarfs would provide constraints on the properties of all DA white dwarfs (*e.g.* Daou et al. (1990)). The theoretical models predicts that WD mass and the physical characteristics of the hydrogen envelope determine the position of the blue edge of the instability strip (Winget and Fontaine, 1982). Studying the position of the blue edge by determining $T_{\rm eff}$ and $\log g$ values of DA white dwarfs which is close to this border informs us about the pulsation mechanism and its characteristics. Similarly, studying the other edge of the instability strip would tell about the mechanism that is responsible for stopping pulsations at this point (Tassoul et al., 1990; Gianninas et al., 2005).

Table 3.4: Spectral classification, $T_{\rm eff}$ and $\log g$ values that are derived from the GTC spectra for two DAs. The $T_{\rm eff}$ and $\log g$ values are produced by model atmosphere fitting, while the *Type* is the corresponding spectral class to the calculated $T_{\rm eff}$.

ID	$T_{\rm eff}$	$\log g$	**Type**
RAT J1754+0133	10600 ± 625K	9.1 ± 0.4	DA4.5 / DA5
RAT J1803+0138	10060 ± 1030K	9.4 ± 0.4	DA4.5 / DA5.5

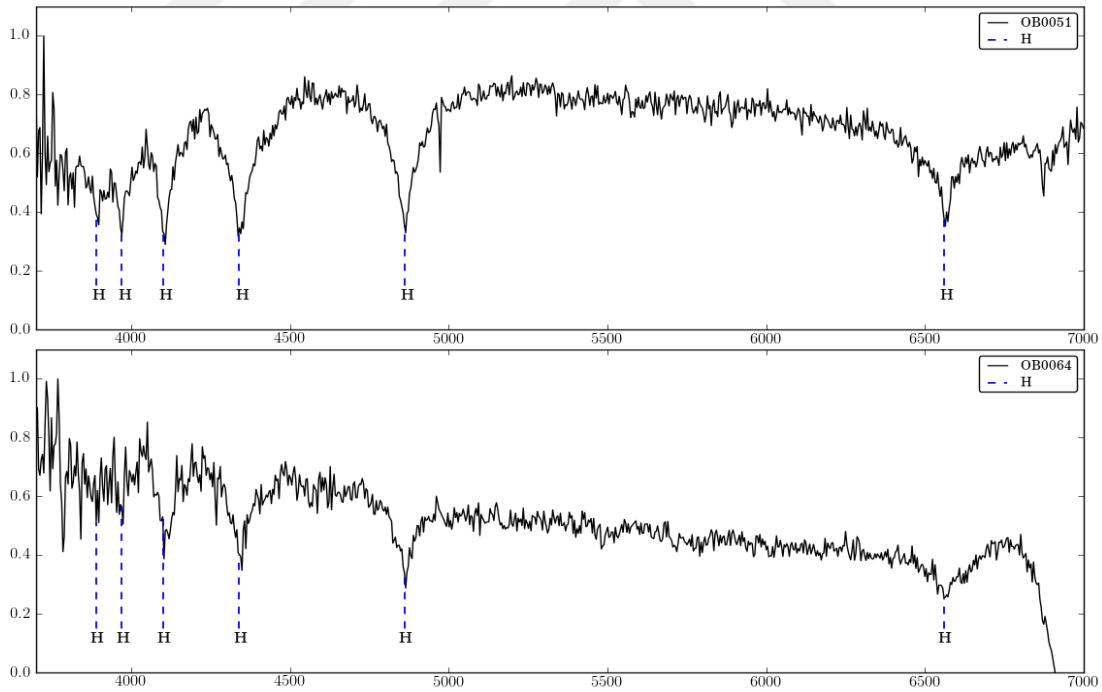

Figure 3.15: The spectra of DA white dwarfs. *Top panel*: `RAT J1754+0133` has a DA4.5 or DA5 classification with $T_{\rm eff}$ of 10600 ± 625K. *Bottom panel*: `RAT J1803+0138` is classified between DA4.5 and DA5.5 with $T_{\rm eff}$ of 10060 ± 1030K.

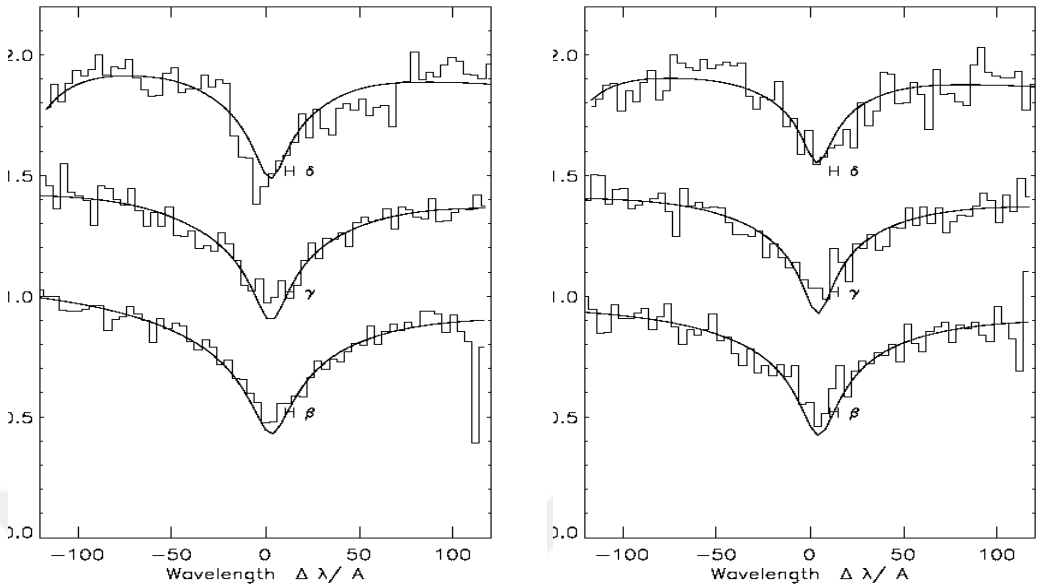

Figure 3.16: The model atmosphere fits to the $H\beta, H\gamma$ and $H\delta$ lines of the spectra of RAT J1754+0133 (the left panel) and RAT J1803+0138 (the right panel). The derived $T_{\rm eff}$ and $\log g$ values are presented in Table 3.4.

3.2.3 QSOs (Quasi-stellar Objects)

Although I applied an infra-red colour cut-off (see Figure 2.14), it was expected that some QSOs may remain in the sample – we identify two of our targets as QSOs. QSO spectra are easily distinguishable by the wide emission bands with very high red-shifts (see the $H_\beta(4860\text{Å})$ at 6800Å in the spectrum of SDSS J1842+6336 in Figure 3.7 on page 64) due to their cosmological distances.

Spectral classification of QSOs is not as straightforward as white dwarfs or subdwarfs. The main reasons for the complicated process are the high redshift and more complicated physical structure of QSOs, and the structural parts very different from each other, contribute to the spectra in very different ways.

I used the median composite spectrum at rest, produced by Vanden Berk et al. (2001) using spectra of QSOs in SDSS database, to determine rough redshift values for our QSOs. I redshifted the composite spectrum and matched the most prominent lines (*e.g.* Si IIIÅ, Mg IIÅ) by eye. The redshift values of $z = 1.74$ and $z = 1.7$ are the best for the spectra of RAT J1757+0138 and RAT J1833+2821, respectively (see Figure 3.17).

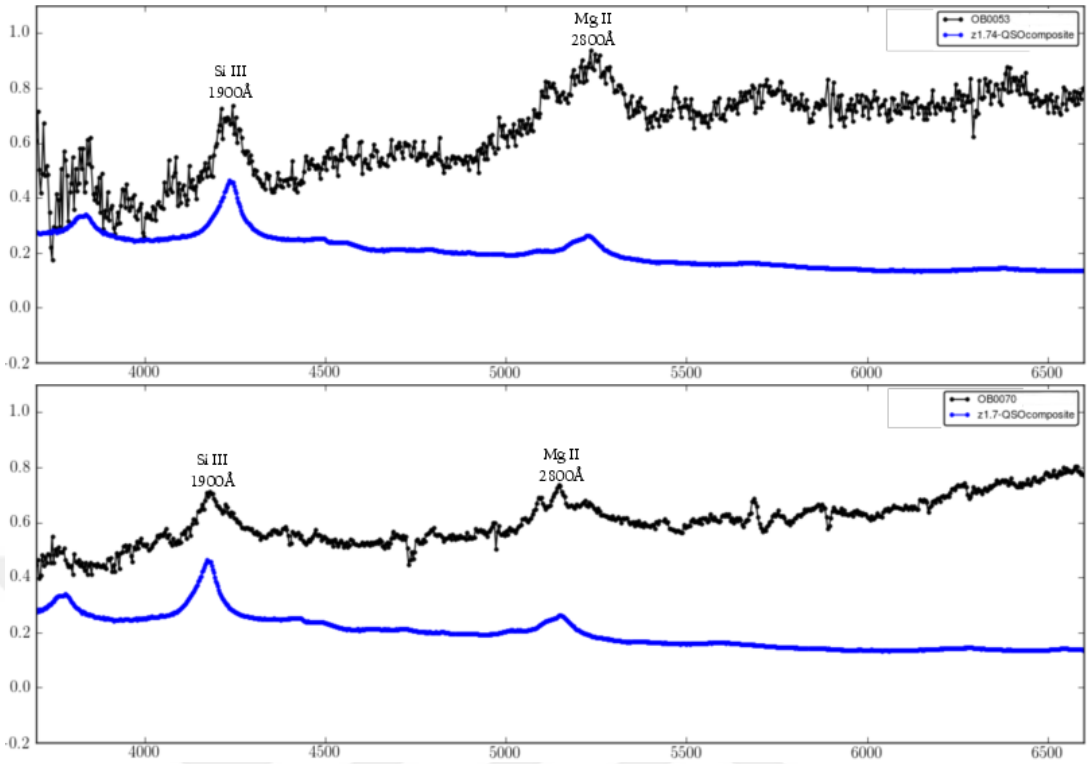

Figure 3.17: The GTC spectra of `RAT J1757+0138` and `RAT J1833+2821` (black line) overplotted with median composite spectrum (Vanden Berk et al., 2001) (blue line) redshifted by $z = 1.74$ and $z = 1.7$, respectively.

3.3 Conclusion

In §2, I outlined a method to identify *significantly blue sources* from the RATS archive. The main focus was on the sources with colours similar to that of known AM CVn binaries. In this chapter, I presented spectroscopic follow-up observations and initial classifications of some of these blue objects (Fig.3.18). The objects in the blue list have been ranked according to several criteria (*e.g.* right ascension, brightness, colour, "*PUF*" (see Table2.4)), and around three dozen of them have been selected to the target list for these spectral follow-up observations using GTC. We obtained 17 spectra with a S/N high enough to provide a spectral classification (Tab.3.1). In addition I determined $T_{\rm eff}$ and $\log g$ values for some of the objects (Tab.3.2 and Tab.3.4).

As the selection for the target list focused on the region in the $(g' - r')$ *vs* $(U - g')$ plane that DB white dwarfs populate (Sec.2.3.3), these objects were expected to be relatively He-rich. Even though I have applied additional colour-cuts (Sec.2.3) to reduce contamination by H-rich objects, having a number of H-rich objects in the selected subset was anticipated. As the result of the classification, we have identified 3 extremely He-rich hot subdwarfs (more then

99% He by number of atoms on the surface, Sec.3.2.1.1) and 2 sdOs (Sec.3.2.1.2) as relatively H-deficient objects. Although we have spectra for only a small fraction of 384 candidates, these results suggest there might be more than 100 objects with He in their spectra and around five dozens extreme He-rich objects in the blue object list, which implies that our selection method is rather fruitful, even though none of the targets are AM CVn systems.

Roelofs et al. (2007c) predict that there should be between 50 and 70 AM CVn systems in the SDSS photometry based on the fact that six AM CVns have been discovered in the

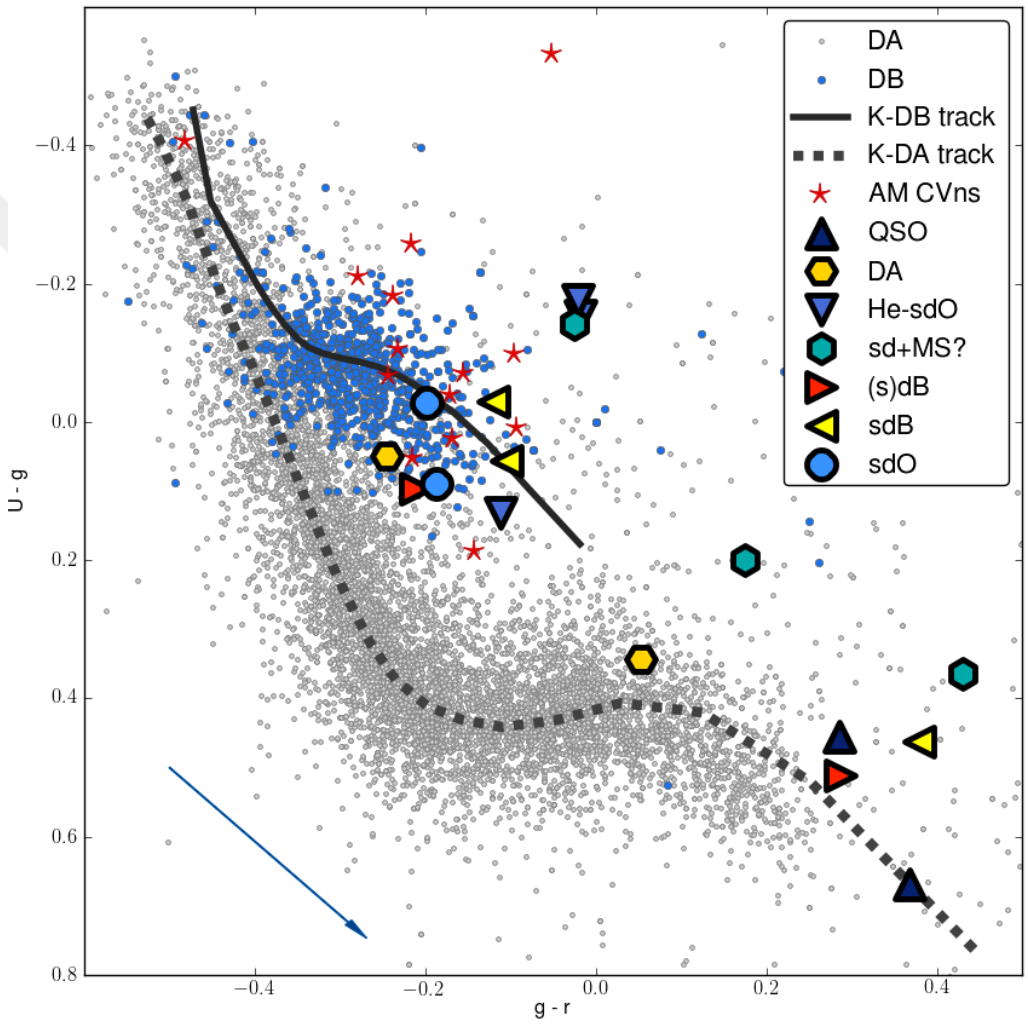

Figure 3.18: Objects that we obtained GTC spectra and classified are plotted on $(g' - r')$ *vs* $(U - g)$ plane. In the background, DA (grey dots) and DB (blue dots) white dwarfs from SDSS DR4 (Eisenstein et al., 2006) are shown, together with Koster cooling tracks (solid line for DBs, dashed line for DAs) and known AM CVns (red stars). The blue arrow shows the direction of the reddening and its size represents a colour excess of $E(B-V) = 0.2$. While all other magnitudes are dereddened (SDSS photometry), RATS magnitudes are not. Also all magnitudes are in AB system.

SDSS at the time of their work, and the models of Nelemans et al. (2001b, 2004). A similar approach for RATS survey of ~ 40 square degrees suggests that we should have roughly 10 AM CVns in our database (Barclay et al., 2011). However, based on their results and Roelofs et al. (2007a), Carter et al. (2013) states that the predictions of Nelemans et al. (2001b, 2004) are over-estimated by about an order of magnitude. As a result, the expected AM CVns in the RATS survey drops to only one or two systems. Therefore, to identify any AM CVn systems in the RATS survey, the spectroscopic survey would need to cover the majority of sources in the AM CVn candidates list.

On the other hand, our survey has identified examples of other type of rare and interesting objects — extreme He-rich hot subdwarfs. The population synthesis for hot subdwarfs predicts that $\sim 1\%$ of all hot subdwarfs must have more than 90% helium on their surfaces. Therefore, there should be much more than ~ 50 currently known extreme He-sds in the Galaxy (Table 3.3). Hence, having discovered three extreme He-sds and the possibility of having ~ 60 more are significant results. Additionally, as most of the known objects are at high Galactic latitudes, while our objects are with Galactic latitudes lower than $\sim 15^o$, we might, quite possibly, enrich the number of extreme He-rich hot subdwarfs from "*the Thick Disc*", not "*the Halo*" like previously known objects.

Having discovered these interesting objects, we have bid for and obtained high resolution spectra from VLT (Very Large Telescope of ESO) for two of them. The detailed analyses of these spectra are presented in §4.

Chapter 4

Detailed analysis of UVES spectra of two He-rich subdwarfs

As outlined in §3, I discovered three helium-rich subdwarf stars through their blue colours and follow-up GTC low resolution optical spectra. There are around 300[1] extreme and intermediate helium-rich subdwarfs currently known. The majority were discovered from quasar surveys (*e.g*. PG (Green et al., 1986), HE (Reimers, 1990), HS (Hagen et al., 1995), SDSS) which were strongly biased toward fields at high Galactic latitudes. In contrast, the three new He-sds are at lower latitudes ($b \sim 12^o$).

I led a successful bid for ESO time to observe two of these three new helium rich stars using the high resolution UVES echelle spectrograph. The goals of this chapter are to measure the chemical abundances of these stars; to search for enhanced heavy metals; to determine whether they are part of a binary system and thereby test models which predict how these objects are formed. I first give details of the observations and the data reduction, then summarise the spectral classification process and outline the stellar parameters which were determined through spectral fitting. The evolutionary states of the two objects are then briefly explored.

4.1 Observation and data reduction

The Ultra-Violet Echelle Spectrograph (UVES) is located at the Nasmyth B focus of the UT2 8m Very Large Telescope (VLT) which is operated by the European Southern Observatory (ESO) in Chile. UVES is an echelle spectrograph covering the wavelength range 3000-5000Å (blue arm) and 4200-11000Å (red arm). The spectral resolution for a 1-arcsec slit is ∼40,000. The blue arm of UVES has a single thinned EEV CCD with 2K×4K pixels. Given that most of

[1] C.S. Jeffery, private communication

the interesting spectral features appear in the blue arm data, the red arm data was not studied. Each arm has two cross disperser gratings working in first spectral order and a typical order separation of 10 arcsec.

To perform a detailed abundance analysis, we require an average signal-to-noise ($\langle S/N \rangle$) of ~ 30 per spectral bin. Using the ESO Exposure Time Calculator[2] we have found that, assuming a B3V star spectrum as a template, we would obtain a spectrum with $\langle S/N \rangle \sim 30$ per spectral bin in a 3600 sec exposure in the blue arm (3600Å-4800Å). To enable cosmic ray removal, we split these into three 1200 sec exposures. To search for evidence of binarity we obtained similar data taken at two epochs separated by 19 days (2014 May 9th and 2014 May 28th) giving six individual spectra each with an exposure of 1315 sec and an average signal-to-noise ratio of ~ 30 per spectral bin (see Table 4.1).

Table 4.1: VLT-UVES observation log

ID	g'	$U-g'$	$g'-r'$	Date	Start Time (UT)
RATJ1754+0137	17.41	-0.15	-0.02	20140509	06:36:46
					06:59:32
					07:22:17
				20140528	05:48:21
					06:11:07
					06:33:52
RATJ1759+0119	16.85	0.13	-0.11	20140509	07:51:03
					08:13:49
					08:36:35
				20140528	07:00:35
					07:23:21
					07:46:06

UVES spectra can be reduced using the ESO pipeline[3] which employs a set of 8 stand-alone recipes for the reduction:

1. `uves_cal_mbias` : Creates a master bias frame.
2. `uves_cal_mdark` : Creates a master dark frame.
3. `uves_cal_predict` : Implements the UVES physical model.
4. `uves_cal_orderpos` : Defines the echelle order positions.
5. `uves_cal_mflat` : Creates a master flat field frame.
6. `uves_cal_wavecal` : Performs the wavelength calibration.

[2] `http://www.eso.org/observing/etc/bin/gen/form?INS.NAME=UVES+INS.MODE=spectro`
[3] `http://www.eso.org/sci/software/cpl/index.html`

7. uves_cal_response : Determines the response function and quantum efficiency.

8. uves_obs_scired : Reduces a science frame.

Alternatively one may employ the uves_obs_redchain recipe to run the full data reduction chain at once. As it allows one to see the result of every step and change parameters accordingly, and allows fine-tuning of the procedures, I have used the recipes one-by-one.

The pipeline has two versions—a more automated GUI version (Reflex) and a more flexible and customisable command-line version (EsoRex), which I have used. A disadvantage of EsoreX is that the user must manually classify and associate the data using the FITS headers, and define the input set-of-frames (SOF) and the appropriate configuration parameters for each recipe run. Each pipeline recipe takes an SOF file as input—an ASCII file listing paths to a set of data file to be used by the recipe, together with their DO category, a label assigned to any data type in order to identify the frames listed in the SOF. There are a list of DO categories associated with FITS header keywords DPR.TYPE (and DPR.CATG) (see Table 4.2). Here is an example SOF I have used for uves_cal_scired recipe:

```
../UVES.2014-05-09T06:59:32.314.fits    SCIENCE_BLUE
./ordertable_blue.fits  ORDER_TABLE_BLUE
./linetable_blue.fits   LINE_TABLE_BLUE
./masterbias_blue.fits  MASTER_BIAS_BLUE
./masterflat_blue.fits  MASTER_FLAT_BLUE
../../UV_MRSP_041130_BLUE437.tfits  MASTER_RESPONSE_BLUE
../../../install/calib/uves-5.4.0/cal/atmoexan.fits EXTCOEFF_TABLE
```

Care needs to be taken when assigning DO categories to the FITS files as the UVES pipeline recipes do not verify in any way the correctness of the classification tags specified by the user in the SOF. For example, in the above SOF, the recipe uves_cal_scired will treat the file ../UVES.2014-05-09T06:59:32.314.fits as SCIENCE_BLUE frame, even if it does not contain this type of data. The recipe also assumes that all frames are associated correctly, in other words all frames come from the same arm, dichroic and bin setting. If an incorrect SOF is used, a recipe may display unclear error messages, or even worse, it would apparently run without any problem and produce reasonable looking, but actually incorrect products. For further details, I refer the reader to the manual of the UVES pipeline.

The resulting spectra of both sources are shown in Figure 4.1. For comparison we also show the lower resolution spectra of each source taken using the GTC and OSIRIS.

Table 4.2: FITS header keywords of ESO data products for the raw data identification. Labels correspond to those keywords as used in `SOF` files for the pipeline.

DPR.TYPE / DPR.CATG	DO category
BIAS	BIAS_BLUE
DARK	DARK_BLUE
PARASITIC	PDARK_BLUE
LAMP,ORDERDEF	ORDER_FLAT_BLUE
LAMP,FLAT	FLAT_BLUE
LAMP,DFLAT	DFLAT_BLUE
LAMP,IFLAT	IFLAT_BLUE
LAMP,SFLAT	SFLAT_BLUE
LAMP,FMTCHK	ARC_LAMP_FORM_BLUE
LAMP,CDALIGN	CD_ALIGN_BLUE
LAMP,WAVE	ARC_LAMP_BLUE
STD	STANDARD_BLUE
OBJECT	SCIENCE_BLUE
SCIENCE	SCIENCE_BLUE

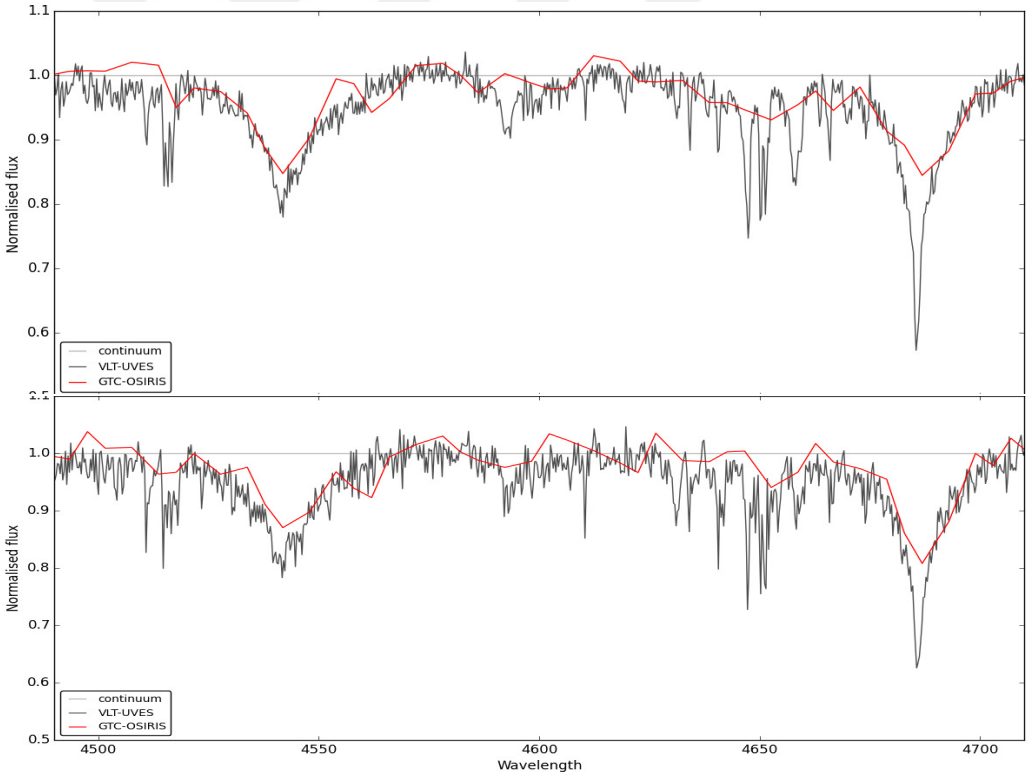

Figure 4.1: The upper panel shows high resolution ($R \sim 40000$) UVES echelle spectra of `RAT J1754+0137` and for comparison much lower resolution ($R \sim 653$) GTC spectra (Chapter 3). The lower panel shows the spectra obtained for `RAT J1759+0119`.

4.2 Radial velocity measurements

Repeated observations of a binary system taken at different epochs could be expected to show Doppler shifts due to changes in the relative radial velocity (RV) of the binary components. I have therefore made a cross-correlation between the individual spectra of both sources using basic routines which are part of the `DIPSO`[4] software package and `SciPy` Python library.

We obtained three consecutive spectra on both nights for both objects. I initially measured the relative radial velocities of the three spectra from one night. The spectrum taken first was used as the template and cross-correlated with all three spectra taken that night, including itself, using `DIPSO` commands. These routines output a cross-correlation function (CCF), which takes RVs in a range around $0 km/s$ and gives a probability of that RV being the relative RV between the two input spectra. Thus, the peak of this function is the most probable result. But conventionally, the result is found by fitting the CCF a curve. Therefore, I have found the relative RVs and their standard errors by fitting the CCF a spline and finding the FWHM (full width at half maximum) of the fit, hence the standard deviation, using `SciPy` python libraries (Figure 4.2). Standard deviations and standard errors are calculated as

$$\begin{aligned} \sigma &= \frac{FWHM}{2.355} \\ \sigma_{\bar{x}} &= \frac{\sigma}{\sqrt{n}} \end{aligned} \tag{4.1}$$

where σ is standard deviation, $FWHM$ is full width at half maximum, $\sigma_{\bar{x}}$ is standard error and n is the number of data points in the part of the CCF that is fitted. Afterwards, the same procedure is applied to the rest of the spectra, and all the results are presented in Table 4.3.

Table 4.3: Relative radial velocities calculated by cross-correlating all three spectra (s1, s2, s3) taken at the same night (a: 1st night, b: 2nd night) with other two and with themselves in both ways, to check the consistency of the technique, for both objects (1: `RAT J1754+0137` and 2: `RAT J1759+0119`).The spectrum on the second column of the table was taken as the template. For instance, the relative radial velocity of second spectrum of the first object taken in the first night (1a-s2) compared to first spectra (1a-s1 - template), is $-1.7 km/s$. All velocities are given in km/s.

		a			b		
		s1	**s2**	**s3**	**s1**	**s2**	**s3**
1	**s1**	0.0 ± 1.5	-1.7 ± 5.7	-0.7 ± 5.0	0.0 ± 1.5	5.9 ± 6.5	1.7 ± 6.8
	s2	1.7 ± 5.7	0.0 ± 1.5	-2.6 ± 5.8	-5.9 ± 6.5	0.0 ± 1.4	1.1 ± 5.1
	s3	0.7 ± 5.0	2.6 ± 5.8	0.0 ± 1.5	-1.7 ± 6.8	-1.1 ± 5.3	0.0 ± 1.5
2	**s1**	0.0 ± 2.2	1.2 ± 5.0	1.0 ± 4.9	0.0 ± 2.2	-0.3 ± 4.7	-0.2 ± 4.7
	s2	-1.2 ± 5.0	0.0 ± 2.3	1.2 ± 5.0	0.3 ± 4.7	0.0 ± 2.1	0.8 ± 4.9
	s3	-1.0 ± 4.9	-1.2 ± 5.0	0.0 ± 2.2	0.2 ± 4.7	-0.8 ± 4.9	0.0 ± 2.1

[4] `http://www.starlink.rl.ac.uk/docs/sun50.htx/sun50.html`

The three spectra for each source were then combined giving one spectrum for each source for each night. The radial velocity of those two spectra were then determined using the same process. As the data were taken at different epochs, heliocentric velocity corrections, which has been taken from the headers of the ESO pipeline output, were applied. The results were within the intrinsic spectral resolution (Table 4.4). Therefore, I could not find any evidence pointing to a binary nature for these two objects. Finally, I have combined the two spectra from each night.

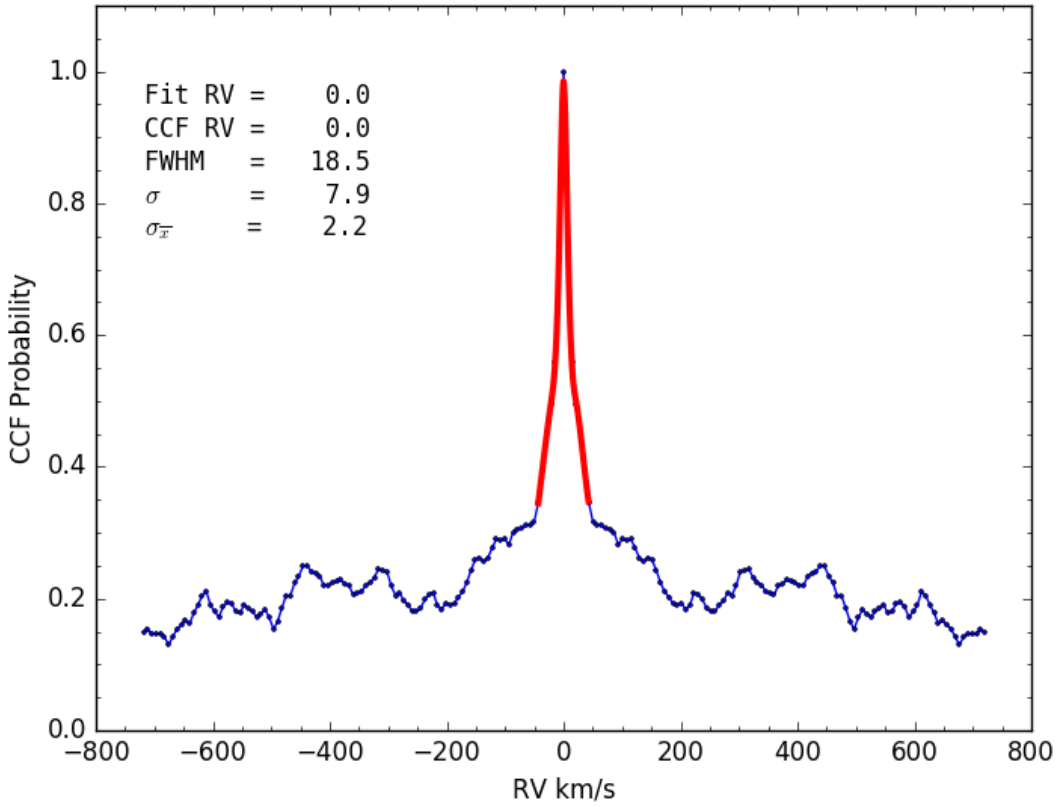

Figure 4.2: The output (blue dotted-line) of the self cross-correlation of 1^{st} spectrum (s1) of the 2^{nd} object (o2: RAT J1759+0119) at the 2^{nd} night (b), "*2b-s1*" as named in Table 4.3, which is fitted with a spline (red line) is presented. "*Fit RV*" and "*CCF RV*" note the RV corresponding to the peak of the fit and the ccf, while σ and $\sigma_{\bar{x}}$ is standard deviation and standard error, respectively.

To increase the S/N further, the spectra were re-binned using several different methods such as taking the mean or median of several data points which may cause a lowering of the spectral resolution if the data is over-binned. If the sampling is close to the expected resolution one needs to preserve the number of data points per Å, a running-mean can be used instead. As the UVES spectra are highly over-sampled (0.03Å/pixel), there was enough

Table 4.4: Absolute (*i.e*. cross-correlated to model, v_a and v_b) and relative (*i.e*. cross-corelated to each other, v_{ba}) radial velocities measured by cross-correlating the combined spectrum from two epochs (a: 1st night, b: 2nd night) for each object with a suitable standard spectra from (Drilling et al., 2013) and with each other are presented. v_{ca}, v_{cb} are velocities that are heliocentric corrections (h_a and h_b) applied. Δv_c is the relative RV between the epochs and calculated by subtracting the difference between h_a and h_b ($h_a - h_b$) from v_{ba}.

Object	v_a	v_b	v_{ba}	h_a	h_b	v_{ca}	v_{cb}	Δv_c
RAT J1754+0137	66.6	58.7	2.0	17.5	10.1	49.1	48.6	−5.4
RAT J1759+0119	44.5	47.2	6.6	17.8	10.5	26.7	36.7	−0.7

room for improvement by resampling. After many experiments using different methods and $\delta\lambda$ values, I have resampled the spectra to $\delta\lambda = 0.3\text{Å}/\text{pixel}$ using `IDL` procedure `resample.pro`[5]. Figure 4.3 and 4.4 show the results of the resampling.

[5] `http://star.arm.ac.uk/$\sim$csj/idl/DIPSO/resample.pro`

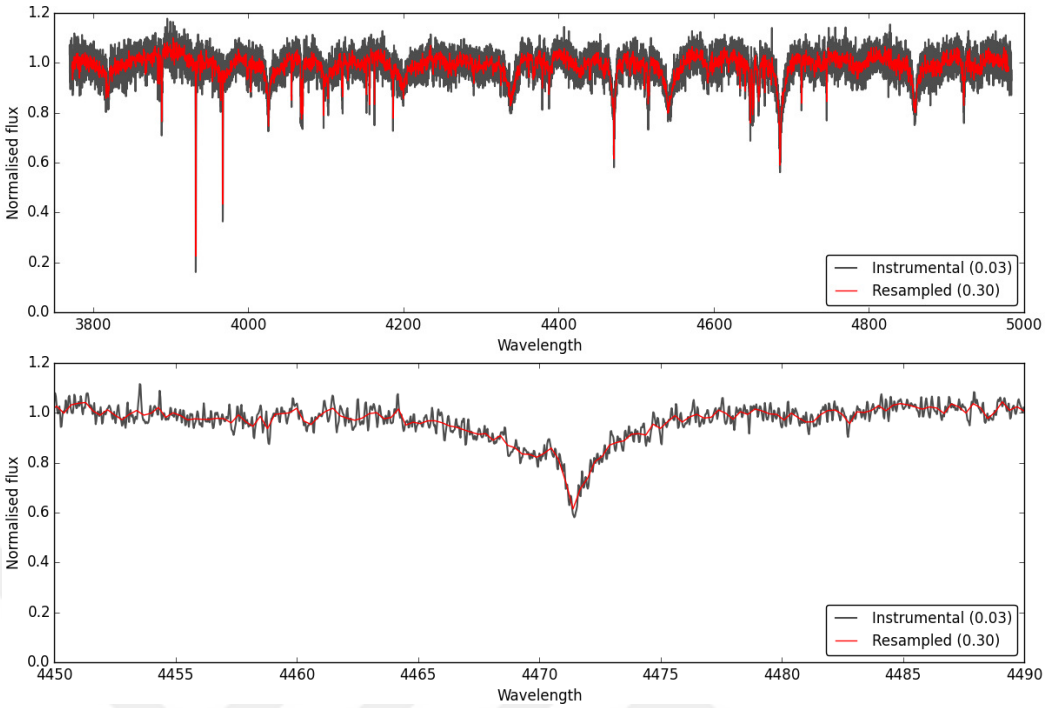

Figure 4.3: The UVES spectrum of RAT J1754+0137 in the top panel where the black line represents the intrinsic spectral resolution of the instrument (0.03Å) and the red line the re-binned spectrum (0.3Å). In the lower panel we show a closer look to the spectrum centered on the HeI 4471Å line.

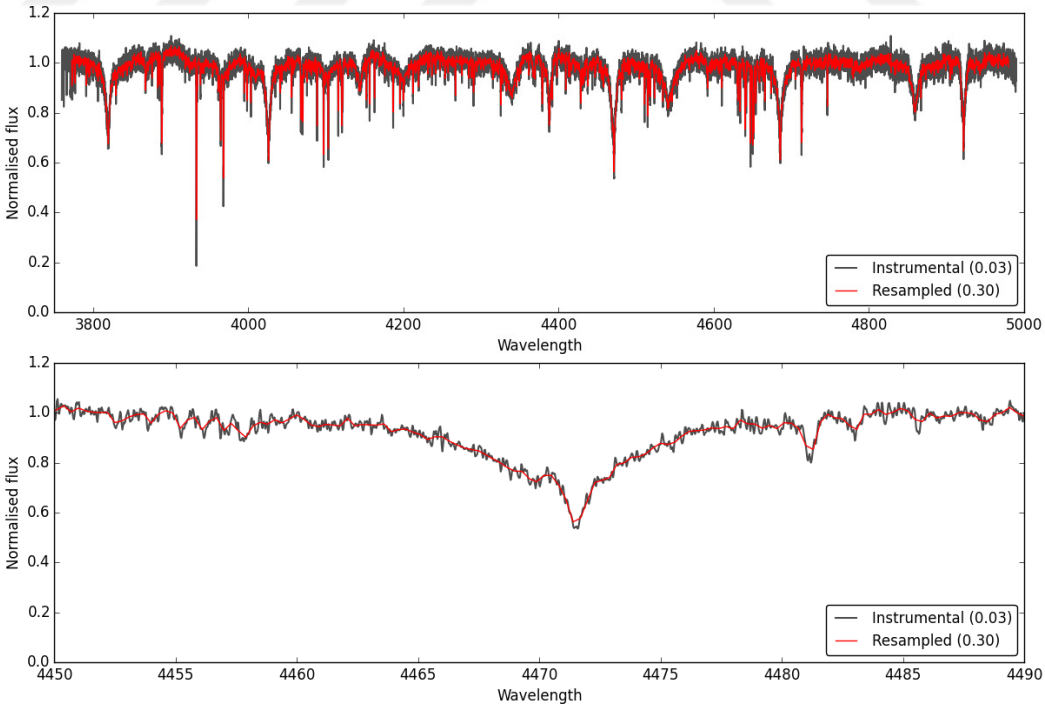

Figure 4.4: Same as Figure 4.3 for RAT J1759+0119.

4.3 Spectral Classification

Since our new UVES data are of much higher quality than the GTC spectra, I have derived the spectral classification of both sources with the new data using the same method and standard spectra (Drilling et al., 2013) that I used in Chapter 3. The method is to compare the spectra, which have been re-sampled to classification resolution (1Å) to the spectra from the Drilling et al. (2013) standard spectra library. The basic criteria entail a comparison of the HeI and HeII line profiles. As one can see in Figure 4.5 for RAT J1754+0137 and 4.6 for RAT J1759+0119, which show standard spectra ordered with increasing $T_{\rm eff}$ from top to bottom, HeI 4471Å and 4713Å lines get shallower while HeII 4541Å and 4686Å lines get deeper. The HeII Pickering lines 4338Å and 4859Å, which coincide with Balmer lines, also follow the trend as long as the H abundances (or He classes) of the standards are similar. Despite the difference in the spectral resolution between the UVES and GTC spectra the results are consistent: RAT J1754+0137 has a spectral class between sdOC7VII:He40 and sdOC8VII:He40 as it has a spectrum which is cooler then subclass of 7 while hotter then 8 (Figure 4.5), while RAT J1759+0119 has a spectral class of sdOC9VII:He40 (Figure 4.6). Based on these spectral classifications, we predict approximate values for $T_{\rm eff}$, $\log g$ and $log(nHe/nH)$ values for our stars using Equation 1.2, as seen in Table 4.5.

Table 4.5: The results of the classification using a manual Drilling classification and spectral fitting as explained in Section 4.4. log(nHe/nH) values given for Drilling classification are the values of standard spectra, and obviously too less for our objects. "*Spectral Type Index*" is calculated using $T_{\rm eff}$ found by spectral fitting, via Equation 1.2.

		RATJ1754+0137	**RATJ1759+0119**
Drilling Classification	**Class**	sdOC7.5VII:He40	sdOC9VII:He40
	$T_{\rm eff}$ **[K]**	44000 ± 1600	40000 ± 1600
	$\log g$ **[cgs]**	5.0	5.0
	log(nHe/nH)	1.3	1.0
Spectral Fitting	**Spectral Type Index**	6.9 ± 1.4	8.5 ± 1.4
	$T_{\rm eff}$ **[K]**	46000 ± 2000	42000 ± 2000
	$\log g$ **[cgs]**	6.2 ± 0.4	5.4 ± 0.4
	log(nHe/nH)	4.0	4.0

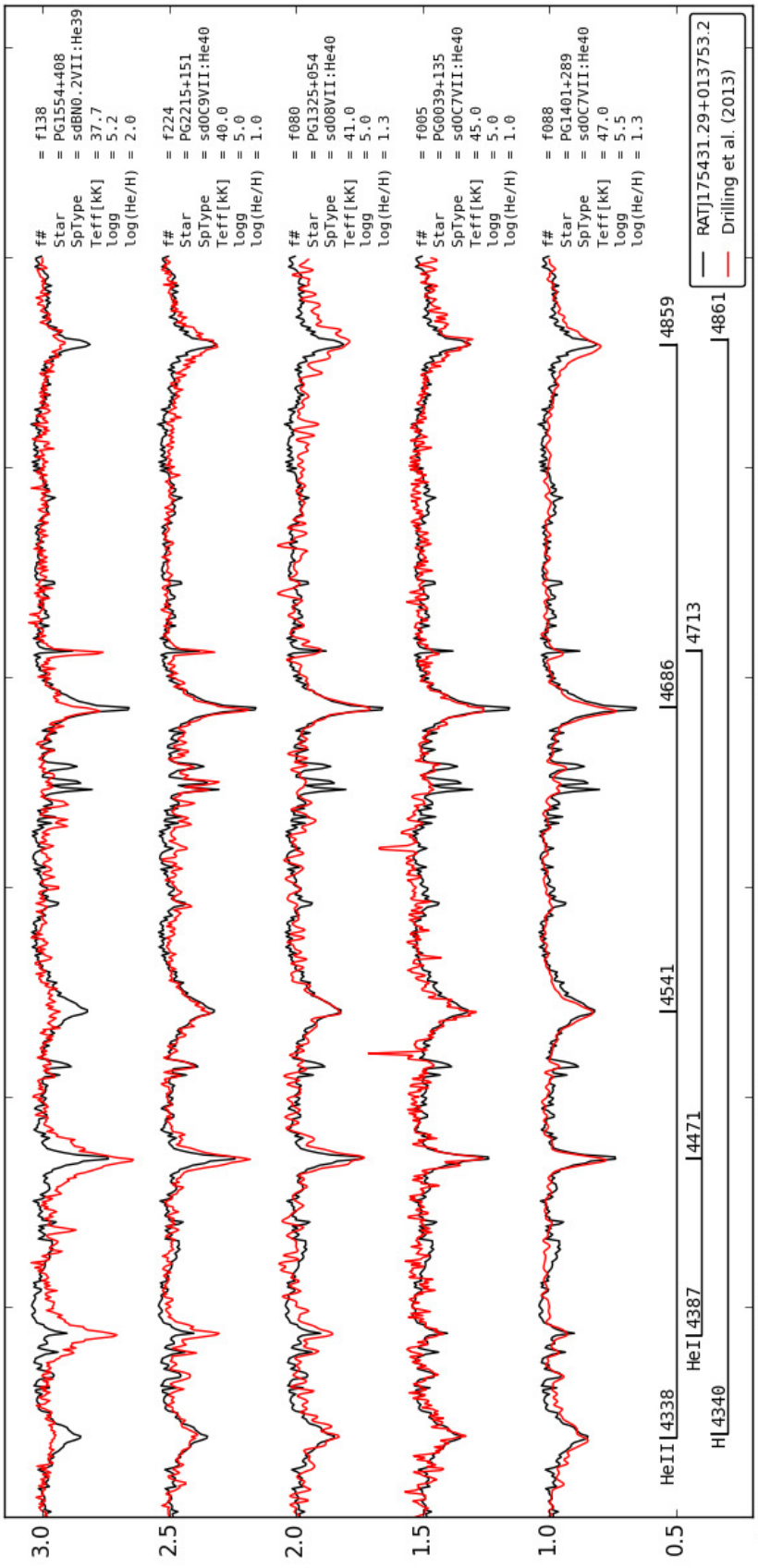

Figure 4.5: The spectrum of RAT J1754+0137 (black) is compared with standard He-rich subdwarf spectra (red) from Drilling et al. (2013), which are in the increasing order in $T_{\rm eff}$ from top to bottom. Note that C features around 4500Å on our spectrum is reproduced by the model spectrum second from the top.

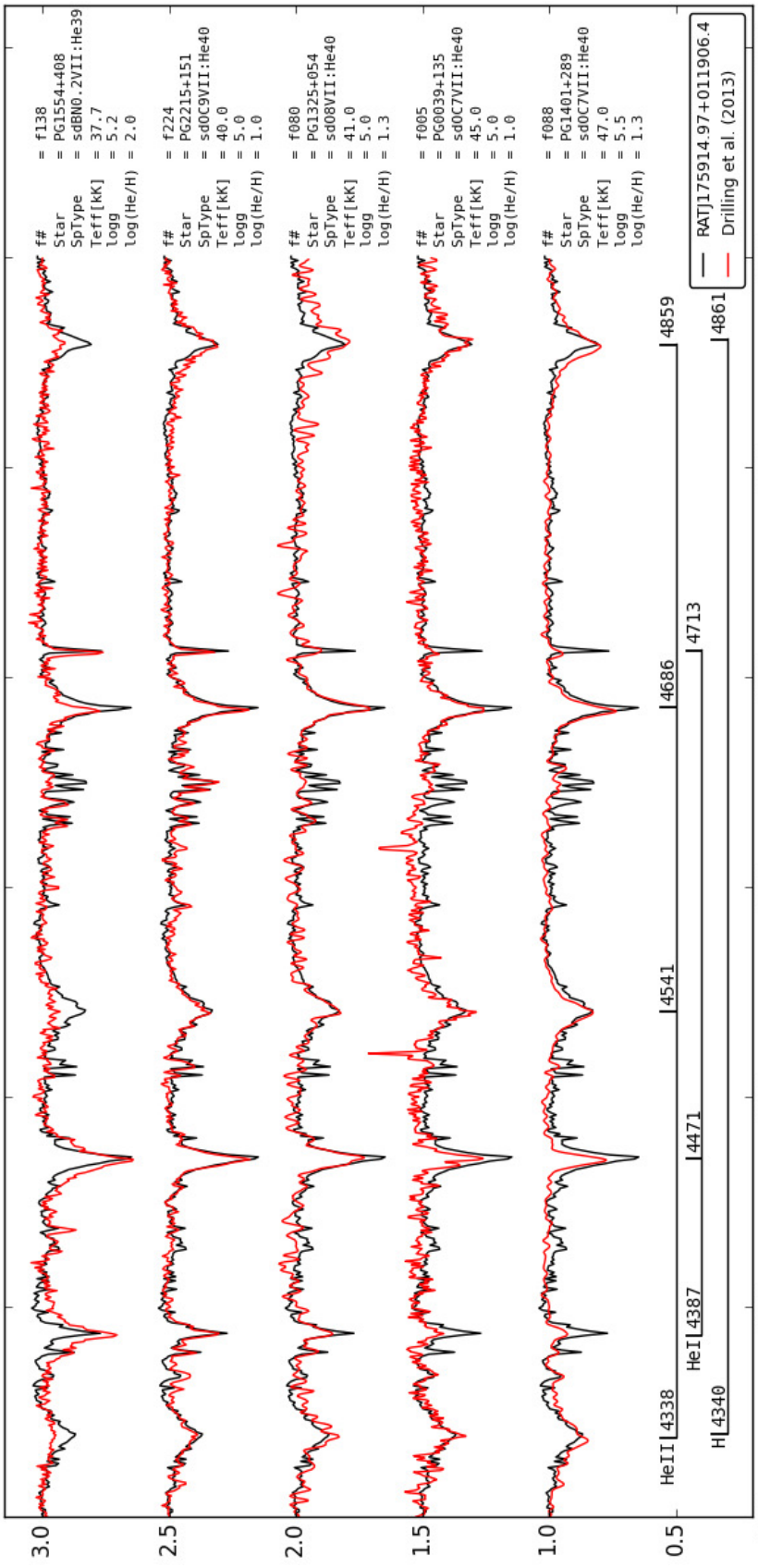

Figure 4.6: The spectrum of RAT J1759+0119 (black) is compared with standard He-rich subdwarf spectra (red) from Drilling et al. (2013), which are in the increasing order in $T_{\rm eff}$ from top to bottom. Note that C features around 4500Å on our spectrum is reproduced by the model spectrum second from the top.

4.4 Spectral Fitting

Manual classification gave approximate values for atmospheric parameters $T_{\rm eff}$ and $\log g$, and chemical compositions of the objects. To measure these parameters with higher precision, we fitted our spectra with synthetic model spectra for helium-rich sdO stars. Model spectra are computed with the formal solution code `SPECTRUM` Jeffery et al. (2001), using model atmospheres calculated with `STERNE` (Behara and Jeffery, 2006). `STERNE` assumes fully-blanketed plane-parallel atmosphere structures in local thermodynamic equilibrium (LTE) with effective temperatures between 10000K and 50000K for a number of different chemical compositions. The fitting procedure is done using spectral-fitting software `SFIT` (Jeffery et al., 2001) which interpolates on a grid of model spectra to find a best-fitting solution for a single or binary star spectrum by χ^2 minimisation.

I choose models for the grid in a way that the initial parameters from manual classification would be covered —$T_{\rm eff} = [36000, 40000, 45000, 50000]$ and $\log g = [3.50, 4.00, 4.50, 5.50]$ for relative abundances by number of hydrogen $(nH) = 0.0001$, of helium $(nHe) = [0.997, 0.990, 0.970]$ and of carbon $(nC) = [0.003, 0.010, 0.030]$. For the procedure, I followed the steps below:

1. All parameters, except *vsini*, are fixed into an initial value that were chosen by manual classification, so *vsini* is solved.
2. Fixing the vsini to the calculated value, $T_{\rm eff}$ and $\log g$ are solved.
3. All parameters apart from the `He` abundance (*ahe*) are fixed, and *ahe* is solved.
4. Once the *ahe* is determined, $T_{\rm eff}$ and $\log g$ are solved by fitting models for the abundance determined.

The first three steps establish approximate initial starting values for temperature and gravity. Once the rotational velocity, abundance and the initial condition for initial ($T_{\rm eff}$,$\log g$) are found, the final fitting for the temperature and the gravity can be done. Using models for the most appropriate `H`, `He` and `C` abundances (0.0001, 0.997 and 0.003 relatively), and this $T_{\rm eff}$-$\log g$ pair as the starting point, I run `SFIT` on the whole spectrum, as well as the different parts of the spectrum, to see the effects of the systematic errors. The comparison of these fits can be seen in Figure 4.7 and 4.9. For all the fittings, I have masked out the parts of the spectra that do not have `H`, `HeI` or `HeII` lines. For this procedure, the spectra are divided into 4 equal parts (335Å) in a way that every consecutive part would overlap 50Å. The results from sub-regions are then compared with the result from the whole spectrum fittings.

In determining the best fit atmospheric parameters and likely uncertainties many criteria have been taken into account such as goodness of the sub-regional and general fits to the

Table 4.6: The lines used for the fitting subregions and the whole spectrum. The wavelengths harbouring multiple lines are showed in boldface.

Line(Å)		Region(Å)				
		3800 4135	4085 4420	4370 4705	4655 4990	3800 4990
HI	**3820**	✓				✓
	3889	✓				✓
	3970	✓				✓
	4100	✓	✓			✓
	4340		✓			✓
	4861				✓	✓
HeI	**3820**	✓				✓
	3889	✓				✓
	4026	✓				✓
	4121	✓	✓			✓
	4389		✓	✓		✓
	4471			✓		✓
	4713				✓	✓
	4921				✓	✓
HeII	**4100**	✓	✓			✓
	4200		✓			✓
	4338		✓			✓
	4541			✓		✓
	4686			✓	✓	✓
	4859				✓	✓

particular lines that are important in the measurement of surface gravity (*i.e.* HeI 4387Å and 4471Å, especially the line wings), or, for the effective temperatures, the ratio between HeI and HeII line depths. Regarding the surface composition, although CIII and CIV lines look good, CII lines are disregarded as they are not considered reliable because of the strong departures from LTE at these effective temperatures (Jeffery and Heber, 1992). Also the H abundance is too low to be detected (threshold is 0.001%) as the HeII Pickering lines that are coinciding with the Balmer lines (*e.g.* H_α 4100Å, H_β 4338Å, H_γ 4859Å) do not show any contribution from the Balmer lines when compared to the Pickering lines that are not coinciding with the Balmer lines (*e.g.* 4200Å, 4541Å, 4686Å).

As can be seen in Table 4.7 and 4.8, the χ^2_ν (reduced χ^2) values for the whole range and for all the individual subregions are very close to each other. While the degrees of freedom, which basically equals the number of fitted parameters subtracted from the number of data points, is not exactly the same in all cases, the reduced χ^2 statistic divides by degrees of freedom to take account of this. After these experiments and checks, considering the close χ^2_ν values, and

the $T_{\rm eff}$ and $\log g$ values coming from the fit to whole spectrum falls very close to the mean of the values from the fit to the subregions, I have concluded that the best solution, although not very statistically robust, is that to simply take the mean of all the results—from subregions and the whole. This basic approach gives $T_{\rm eff} = 46530K \pm 690K$ and $\log g = 6.35 \pm 0.24$ for `RATJ1754+0137` and $T_{\rm eff} = 41200K \pm 700K$ and $\log g = 5.13 \pm 0.14$ for `RATJ1759+0119` (Table 4.5).

Considering the strong departures from LTE in these effective temperatures, a fit was also made by using publicly available non-LTE synthetic spectra of Peter Nemeth[6]. The grid used was composed of models with 100% He, $T_{\rm eff}$ between 35000K and 50000, and $\log g$ between 5.00 and 6.00. As done with the LTE models, the spectra were masked in a way that only H and Helium lines would be left, and divided into 4 sub-ranges (Figure 4.8 and 4.10), and following the same procedures of fitting and averaging the results, best atmospheric parameters are found. The results of these fits can be seen in Table 4.7 and 4.8. One can note that the non-LTE results are very close to the LTE results while a bit hotter and denser. Also, to compare the fits visually, both fits are plotted on the spectra in Figure 4.11.

Table 4.7: Fit results for the `RAT J1754+0137`.

Region(Å)	**LTE**			**Non-LTE**		
	$T_{\rm eff}$	$\log g$	χ^2_ν	$T_{\rm eff}$	$\log g$	χ^2_ν
3800–4135	44453 ± 69	5.722 ± 0.044	2.27	48331 ± 92	5.722 ± 0.014	2.69
4085–4420	45907 ± 229	5.938 ± 0.050	1.75	47023 ± 160	5.388 ± 0.028	3.28
4370–4705	47501 ± 97	7.056 ± 0.030	2.01	49465 ± 194	5.715 ± 0.025	2.85
4655–**4990**	48485 ± 119	6.621 ± 0.028	2.43	49996 ± 149	6.165 ± 0.025	3.02
3800–4990	46326 ± 85	6.419 ± 0.023	2.09	50018 ± 180	6.075 ± 0.027	3.25
Mean	46534	6.351	2.11	48967	5.813	3.02
Std.Deviation	1542	0.534	0.26	1284	0.313	0.25
Std.Error	690	0.239	0.12	574	0.140	0.11

Table 4.8: Fit results for the `RAT J1759+0119`.

Region(Å)	**LTE**			**Non-LTE**		
	$T_{\rm eff}$	$\log g$	χ^2_ν	$T_{\rm eff}$	$\log g$	χ^2_ν
3800–4135	41211 ± 88	5.046 ± 0.022	2.58	44623 ± 36	5.754 ± 0.014	3.72
4085–4420	43838 ± 72	5.678 ± 0.035	2.91	43243 ± 103	5.339 ± 0.031	4.97
4370–4705	40000 ± 81	4.952 ± 0.012	4.20	44943 ± 79	5.656 ± 0.026	4.92
4655–**4990**	40001 ± 80	4.901 ± 0.013	3.40	45043 ± 55	6.050 ± 0.018	3.24
3800–4990	40957 ± 56	5.095 ± 0.012	2.96	45031 ± 65	5.938 ± 0.020	3.85
Mean	41201	5.134	3.21	44577	5.747	4.14
Std.Deviation	1573	0.313	0.63	765	0.275	0.77
Std.Error	703	0.140	0.28	342	0.123	0.34

[6] `http://www.ster.kuleuven.be/~petern/work/sd\_grid/`

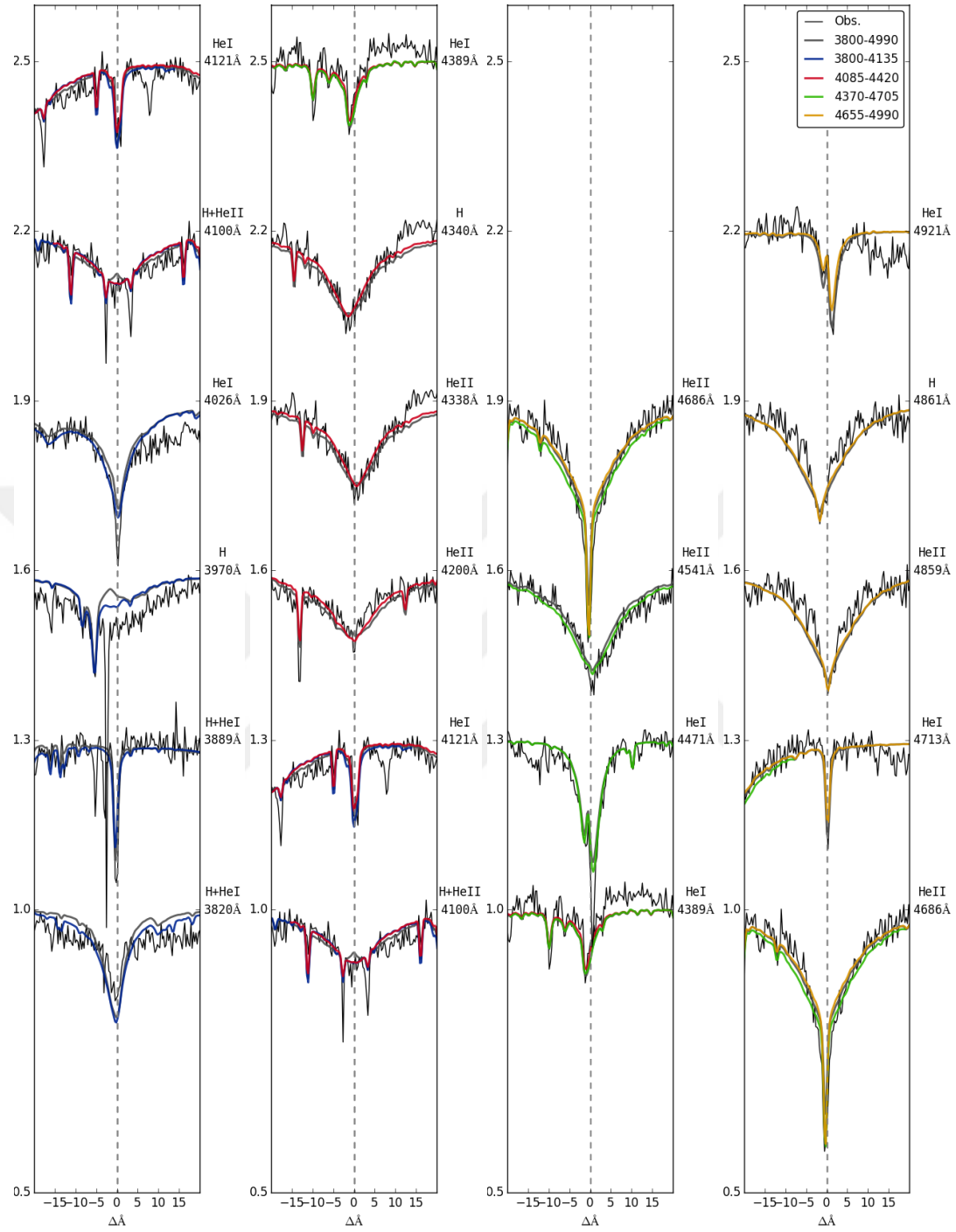

Figure 4.7: Spectrum of RAT J1754+0137 (black) over-plotted with the LTE model fit using whole spectral range (grey) and model fit using only a quarter of the spectrum (blue, red, green, yellow). Physical parameters produced by the general and the subregional fits are given in Table 4.7.

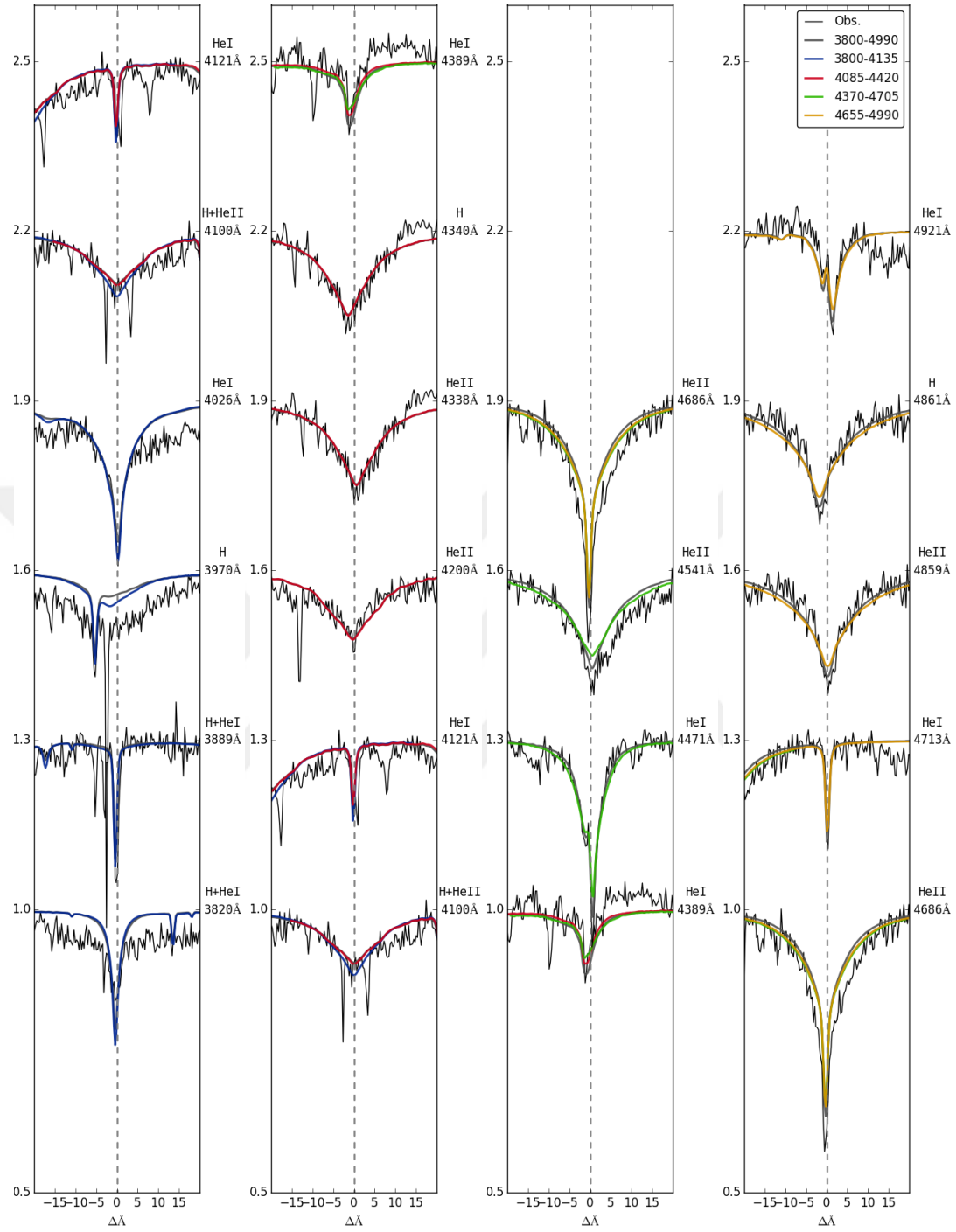

Figure 4.8: Spectrum of RAT J1754+0137 (black) over-plotted with the Non-LTE model fit using whole spectral range (grey) and model fit using only a quarter of the spectrum (blue, red, green, yellow). Physical parameters produced by the general and the subregional fits are given in Table 4.7.

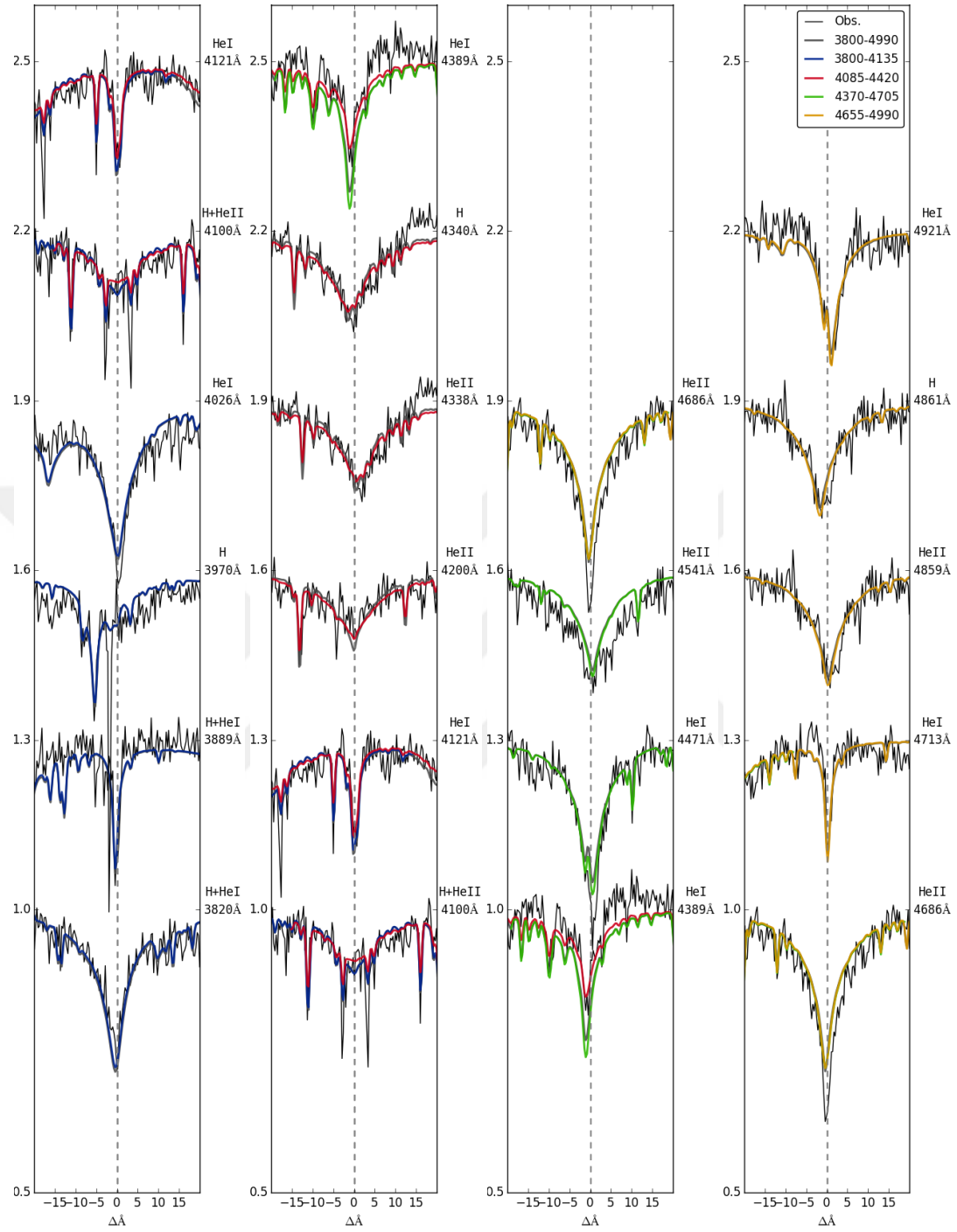

Figure 4.9: Spectrum of `RAT J1759+0119` (black) over-plotted with the LTE model fit using whole spectral range (grey) and model fit using only a quarter of the spectrum (blue, red, green, yellow). Physical parameters produced by the general and the subregional fits are given in Table 4.8.

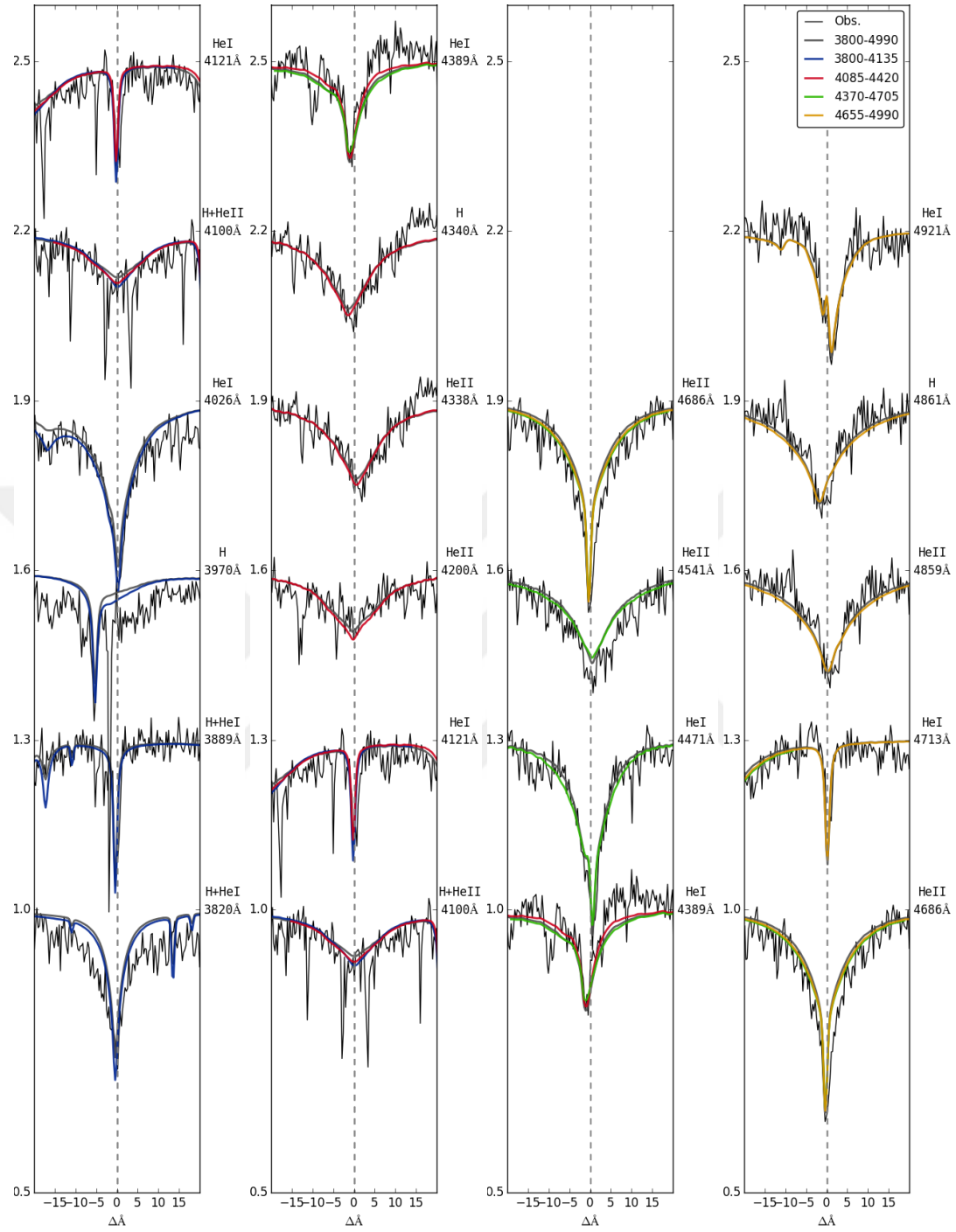

Figure 4.10: Spectrum of `RAT J1759+0119` (black) over-plotted with the Non-LTE model fit using whole spectral range (grey) and model fit using only a quarter of the spectrum (blue, red, green, yellow). Physical parameters produced by the general and the subregional fits are given in Table 4.8.

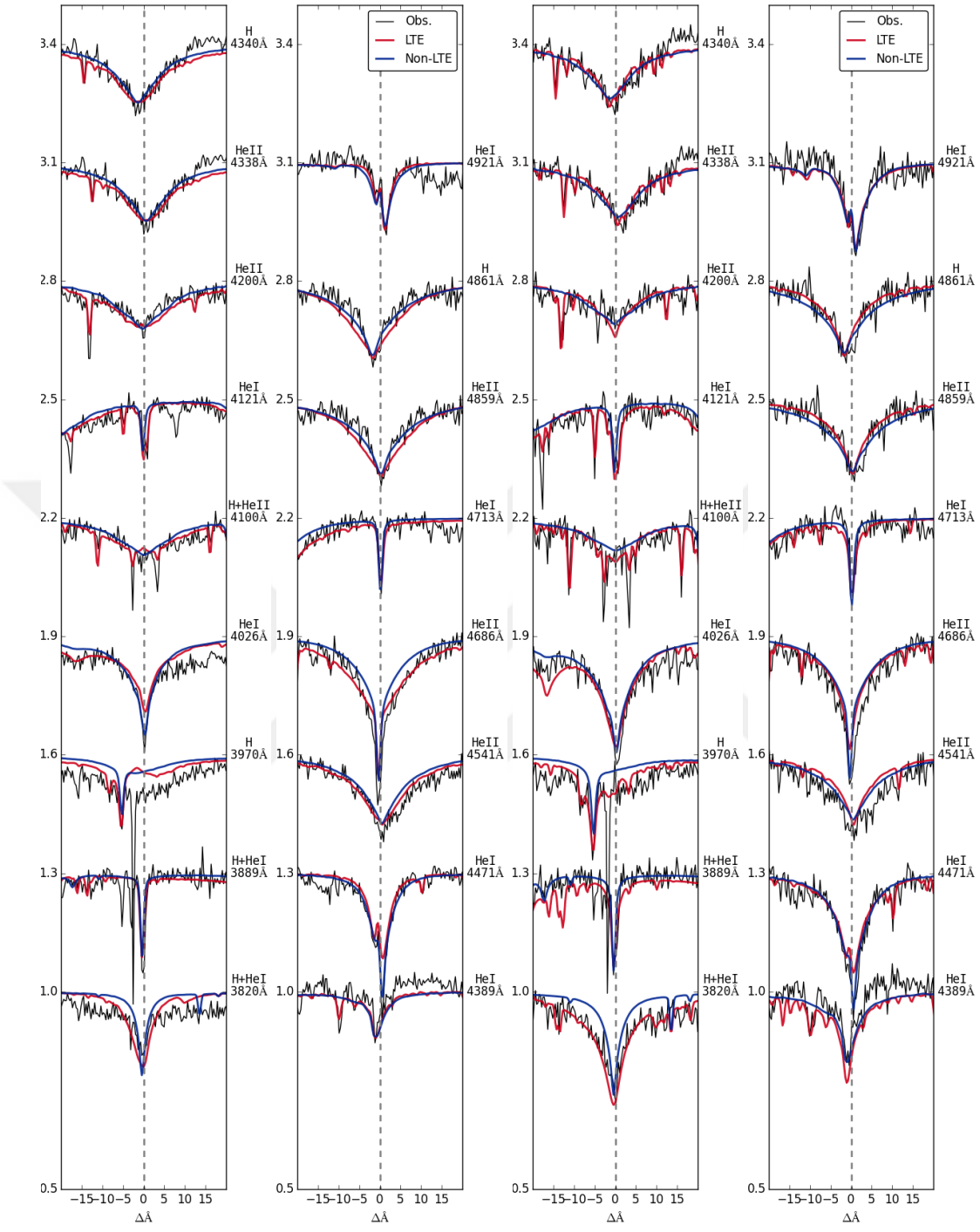

Figure 4.11: The comparison of the LTE and Non-LTE model fits for both objects: `RAT J1754+0137` – two panels on the left hand side and `RAT J1759+0119` – two panels on the right hand side. Spectrum of the object (black) over-plotted with the LTE (red) and Non-LTE (blue) model fit using whole spectral range. Physical parameters produced by the model fits are given in Table 4.7 and 4.8. Only the lines that are used in the fitting are shown. While the x-axis is relative wavelength to the line center in Å, y-axis is the normalised flux, with 0.3 increment for consecutive lines.

4.5 Evolutionary state

The temperature and gravity of hot subdwarfs ($\log T_{\rm eff}$ –$\log g$) contain information about their evolutionary state. As can be seen in Figure 4.12 sdBs and sdOs reside on different places depending on their He abundance and on their evolutionary status.

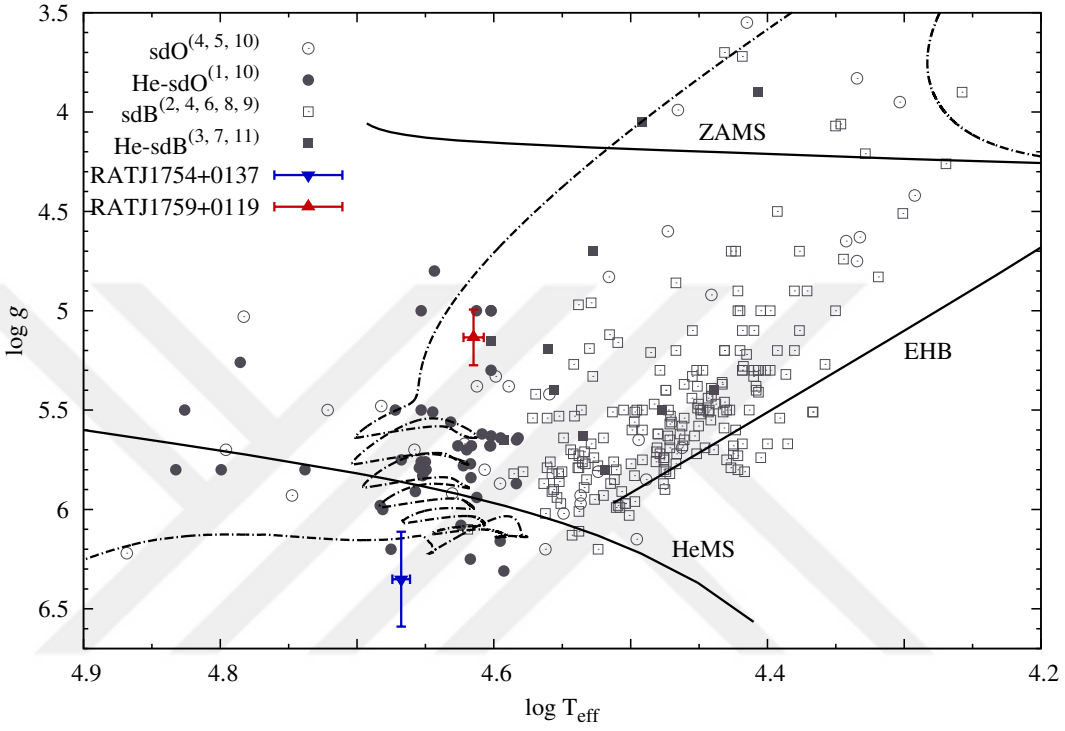

Figure 4.12: Our two He-sdOs are shown on the $\log T_{\rm eff}$-$\log g$ plane, together with ZAMS (Zero Age Main Sequence), HeMS (Helium Main Sequence), EHB (the canonical extended horizontal branch) (solid black lines) and an evolutionary track for a late hot flasher for a sdO of $0.47 M_{\odot}$ core mass (Miller Bertolami et al., 2008) (dash-dotted black line), on top of the He-rich (filled) and -poor (dotted) sdOs (circles) and sdBs (squares) on the $\log g$ –$T_{\rm eff}$ plane. $T_{\rm eff}$ and $\log g$ values for other objects are taken from Dreizler et al. (1990)[1], Moehler et al. (1990)[2], Viton et al. (1991)[3], Saffer et al. (1994)[4], Heber et al. (1996)[5], Moehler et al. (1997)[6], Jeffery (1998)[7], Maxted et al. (2001)[8], Lisker et al. (2004)[9], Stroeer et al. (2007)[10], Naslim et al. (2010)[11].

In Figure 4.12, which shows ZAMS (Zero Age Main Sequence), HeMS (Helium Main Sequence), EHB (Extreme Horizontal Branch) and evolutionary track for an sdO with $0.47 M_{\odot}$ on top of the He-rich and -poor sdOs and sdBs on the $\log g$-$\log T_{\rm eff}$ plane, it can be seen that both of our objects lie together with the other He-rich sdO stars. They are also at the proximity of the evolutionary track for a late hot flasher for a sdO with typical $0.47 M_{\odot}$, although this does not tell much as the evolutionary tracks depend on so many variables (for details see Miller Bertolami et al. (2008)). The main point to take from this track on this plot is that

the most of the He-sdOs are at the region that the track twists around the HeMS (helium main sequence). While RAT J1759+0119 is slightly less luminous than the evolutionary model, RAT J1754+0137 is in good coherence with it, although both have large error-bars.

Neither of the stars are on the HeMS so we can eliminate the core He-burning scenario. Since the binary nature scenario is not completely eliminated, this might also be a factor for their position on the $\log g$-$\log T_{\rm eff}$ diagram.

Although their place on the $\log g$-$\log T_{\rm eff}$ plane give a rough idea, a detailed spectral analysis study is needed to tell more about evolutionary state of our objects.

4.6 Conclusion

In this chapter, I have presented an analysis of the high resolution ($R \sim 40000$) echelle spectra that we obtained using the ESO VLT, of the two of the three extreme helium-rich hot subdwarfs that I have discovered through their RATS colours (§2) and low resolution ($R \sim 653$) GTC optical spectra (Chapter 3).

To search for evidence of binarity I searched for radial velocity shifts in the spectra. I have measured relative radial velocities of individual exposures taken at the same night (Table 4.1), and all the results were consistent with no radial velocity shift (Table 4.3). Then, I measured the relative velocities of mean spectra from two epochs 17 days apart, and the results were consistent with no significant radial velocity shift (Table 4.4). There is therefore no evidence for binarity for either of our two objects.

Afterwards, these two objects were manually classified according to *the Drilling classification system for hot subdwarfs*, using the combined and appropriately binned mean spectra (Table 4.5). Drilling classification predicts $T_{\rm eff}$ and $\log g$ based on the spectral class, and it turned out that those atmospheric parameters, except the $\log g$ of RAT J1754+0137, are in agreement with the parameters that I found by fitting model atmospheres to our spectra via χ^2 minimisation software SFIT, within the error margin. For both objects, the best model was those with 99.7% He, 0.3% C.

Additionally, non-LTE models of Peter Nemeth are also used to calculate the physical properties of these objects. It is seen that the results are consistent with the results of LTE results (Table 4.7 and 4.8).

The results of the spectral fitting (*i.e.* $T_{\rm eff}$, $\log g$) allowed us to compare our new He-sdOs to hot subdwarfs in the literature (Figure 4.12). It can be seen that our He-sdOs are located within the envelope of He-sdOs on the $\log g$-$T_{\rm eff}$ plane, and in agreement with the evolutionary track for a He-sdO with a mass of $0.47 M_{\odot}$, which is a typical value for the class.

Chapter 5

Blue variables detected in the RATS archive

In this Chapter I identify and outline variable stars within the blue sample of stars that I presented in §2. To identify those variable blue objects, I cross-match the blue objects with the variable stars previously identified in the RATS archive (Barclay et al., 2011). The aim is to reveal the nature of these blue variable objects using their colours and, if available, their spectra.

In this Chapter, I briefly summarise how the variable objects are identified within $\sim 3 \times 10^6$ light-curves in the RATS database, then present and discuss the blue variable objects which have been identified, by dividing them into three broad groups (*i.e.* δ Sct stars candidates, compact object candidates, and the others). I finish by giving detailed identifications of the individual objects.

5.1 Variable sources in the RATS

The RATS project produced light curves of $\sim 3 \times 10^6$ stars lasting 2 hours within a cadence of ~ 1 minute in fields covering ~ 40 deg^2, mostly close to the Galactic plane, during 10 epochs over 7 years (§1.5.1). Initially, the data obtained in the first five years (6 epochs) have been analysed to identify the objects with periodic short-term flux variability and the results of this have been published in Barclay (2010), and some of the follow up works in Ramsay et al. (2009); Barclay et al. (2011); Ramsay et al. (2011). The data from the final 4 epochs have been analysed in a similar manner, but with some improvements in the method (*e.g.* different period bins, more liberal or conservative FAP cuts from field-to-field *etc.*), and additional short period variable sources are found. The improved method is also used to reselect variables from the

earlier epochs.

To identify variable objects, a method developed by Barclay et al. (2011) is used. The method makes use of two different statistical tests, namely analysis of variance (AoV) and the Lomb-Scargle periodogram (LS) (Lomb, 1976; Scargle, 1982) via the VARTOOLS suite of software (Press et al., 1992; Hartman et al., 2008).

Some statistical tests are more suitable to identify particular kinds of variability than others. For example, to detect pulsating variables, especially where the pulsation period is shorter than the duration of the light curve, one might obtain optimal results using the Lomb–Scargle (LS) Periodogram. On the other hand, where the aim is to pick eclipsing or contact binaries, the Alarm test (Tamuz et al., 2006) and the Analysis of Variance (AoV) test (Schwarzenberg-Czerny (1989); Schwarzenberg-Czerny (1996); also see Devor (2005) for the implementation used by VARTOOLS) should be the test of choice. If one is searching for flare stars, the χ^2 test could be the preferred choice. For a recent review that discusses performances of different tests for identifying different kinds of variable stars, I refer the reader to Graham et al. (2013).

The VARTOOLS suite of software (Hartman et al., 2008) allows the parametrization of large numbers of light curves in a quick and simple manner using a variety of different statistical tests. Using this suite of software, we apply the LS Periodogram, the Alarm test, the AoV test, and determine the χ^2 and RMS value for each of our light curves.

The Lomb-Scargle periodogram is designed to pick out periodic variables in unevenly sampled data, while the AoV algorithm folds the light curve and identifies the period which minimises the variances of a second-order polynomial in eight phase-bins. Both AoV and LS algorithms produce a periodogram and associated parameters. From the highest peak in the periodogram, the most likely period of a given light curve is determined. Afterwards, two of these parameters are used to pick periodic variables—LS-FAP (the Lomb-Scargle formal false-alarm probability) and AoV-FAP (the analysis of variance formal false-alarm probability), which are the measures of the probability that the highest peak in the periodogram is due to random noise. Once the FAP values and the periods are determined, the variable selection begins — on the *FAP vs Period* planes, the objects that are most likely variable tend to separate from non-variable objects. To compare these different tests, I chose one pulsating object, namely RAT J2059+4537 (Table 5.1), and plotted all the objects in the same field on the g vs RMS, LS-Period vs LS-FAP and AOV-Period vs AOV-FAP planes (Figure 5.1). As can be seen for this object, the best plane to use is the LS-Period vs LS-FAP, although our pulsating DA white dwarf is also well separated from the bulk of the objects on the AOV-Period vs AOV-FAP plane, but would not be selected as variable in the g' vs RMS plane.

As the last step, for each source the peak period determined using AoV is compared to the best period determined using the LS test, and sources that have matching periods and have

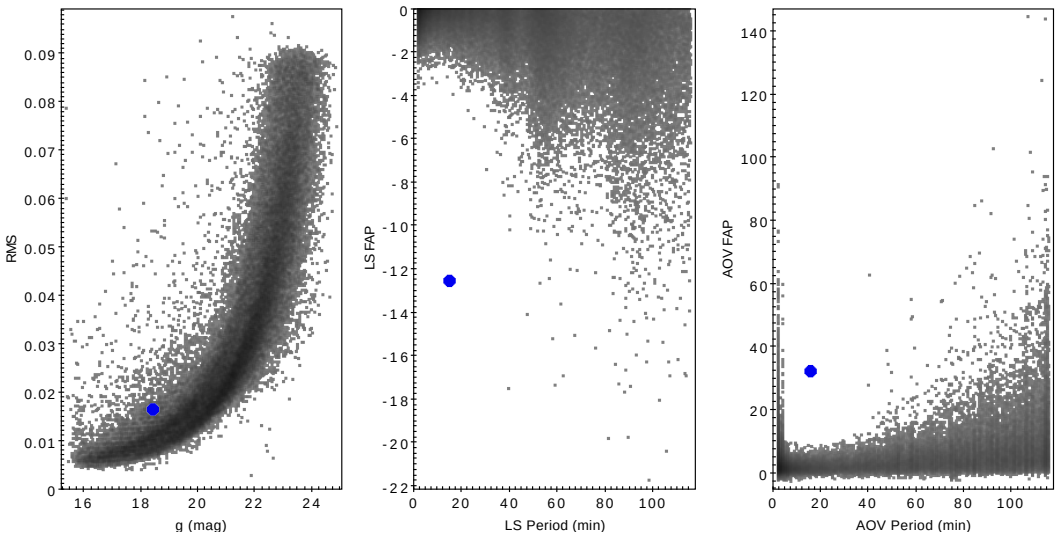

Figure 5.1: Comparison is made of three variability tests. From left to right, the RMS, raw root-mean-square level over all the data points for the given object, is shown as a function of g magnitude; the Lomb-Scargle False Alarm Probability as a function of period of the most prominent peak in the power spectrum; and Analysis of Variance False Alarm Probability as a function of period. The data originate from the same field (INT4-Field9) and the blue filled circle represents the same object (Pulsating WD `RAT J2059+4537` in Table 5.1). The Lomb-Scargle and Analysis of Variance identify the short period variable object.

been classified as candidate variable sources by both `AoV-FAP` and `LS-FAP` are then regarded as "*significantly*" variable sources. With this method, 124334 objects (4.1%) of just over 3×10^6 sources in the data from the first 6 epochs (5 years) of the RATS project are determined as periodic variables (Barclay et al., 2011), and a further 3060 (0.45%) of 679749 sources from 3 later epochs (*i.e*. INT6, INT7 and INT8). There are a number of potential reasons why significantly lower numbers of variable objects selected from the latest epochs comparing to the earlier epochs. One reason is that the recent selection was more conservative, and another reason is that the problems with tracking during the observations in earlier epochs were mostly resolved and it is ensured that sources did not move over the plane of the CCD detector in the recent epochs, which caused systematic trends to be reduced. Therefore the false positive numbers decreased significantly.

5.2 Identifying blue variable stars

In §2, I outlined how blue stars were selected in the RATS archive. Here I identified the variable objects within blue stars by simply cross-matching the two samples, which has yielded 31 significantly blue periodic variable objects. These objects are listed in Table 5.1, while their light-curves are presented in Figure 5.5, 5.8, 5.11 and 5.12.

There are 66 short-period ($P < 40$min) blue periodic variables which have been selected from the first 6 epochs of the RATS archive by Barclay (2010). They were selected by first identifying periodic variables in the RATS archive, and then, from the variable list, selecting the ones with colours compatible with AM CVn systems. A number of those 66 objects are analysed further using follow-up spectral observations (Barclay et al., 2011; Ramsay et al., 2006, 2009).

Contrary to what one may initially expect, not all of the 66 blue short period variables identified by Barclay (2010) have been identified as such in my study —indeed only 5 of them have (Table 5.1). There are a number reasons for why 61 objects have not been selected as blue variables in this study. The main reason is that most of them (48) are not selected as blue objects by my method, which is not surprising as the method of Barclay (2010) was –in comparison– somewhat crude since it did not account for varying extinction from field to field. A further 10 objects are not in the list, simply because they are from two epochs (*i.e.* INT1 and INT2) at which the observations were done using BVi' bands and not $Ug'r'$ bands as the later epochs that are used in the colour selection (see §1.5.1). The last 3 objects were selected as blue but they were not in the updated variable objects list created using an improved version of the method of Barclay (2010). Also 30 of the 48, which are not blue, are not in the updated variable objects list. A Venn-diagram showing this number distribution between the lists is presented in Figure 5.2. The more detailed comparison between Barclay's and my approach is presented in §6.

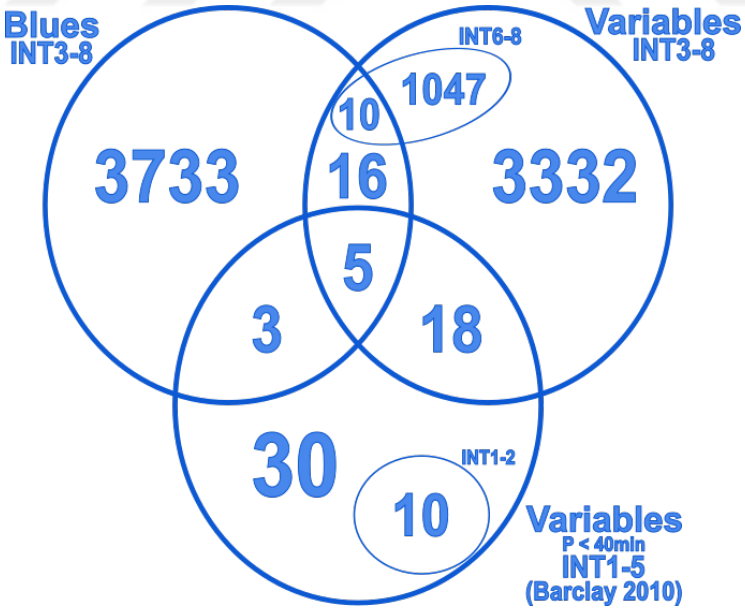

Figure 5.2: A Venn diagram showing the number distribution of the objects between all the blue objects that are selected in §2, variable objects reselected using improved selection algorithm, and the 66 short period variables that have similar colours to AM CVn systems selected by Barclay (2010).

Table 5.1: Blue periodic variables. The catalogue name, (which is in the form of Run-Field-Chip-ID); Right Ascension; Declination; Lomb-Scargle period; Amplitude; g' magnitude; $U-g'$ and $g'-r'$ colours; J magnitude; J−H and H−K colours (taken from 2MASS) and proper motion (taken from Zacharias et al. (2013)). In the last column we indicate our most likely classification.

#	Cat. name	RA	Dec	LS Per. [min]	Amp. [mmag]	g'	$U-g'$	$g'-r'$	J	J−H	H−K	μ_α, μ_δ [mas y^{-1}]	Notes
1	3-11-2-3507	18:02:50.6	+00:43:52.8	34.1	41.6	18.67	0.64	0.46					δ Sct / SX Phe [1,3]
2	3-11-4-9303	18:04:15.8	+00:41:00.6	60.7	95.5	19.20	0.74	0.63					δ Sct / SX Phe
3	3-11-4-19198	18:03:44.5	+00:45:53.9	62.0	104.1	19.31	0.60	0.63					δ Sct / SX Phe
4	3-14-1-13507	18:00:35.3	+00:25:35.5	6.0	121.5	20.73	0.06	0.38					Pulsating WD?
5	3-28-3-4339	20:31:33.6	+27:34:32.6	46.6	95.6	20.09	−0.71	0.38					Pulsating WD
6	4-4-3-3953	02:52:37.1	+50:51:25.5	100.9	320.1	20.40	−0.62	−0.04					β Cep?
7	4-5-4-21796	21:00:55.5	+44:27:22.3	39.3	89.4	20.09	−0.48	1.69	15.76	0.56	0.47		
8	4-6-3-12509	23:47:20.9	+56:34:13.8	97.7	~ 600	18.37	0.49	0.44					P=195.5? [4]
9	4-6-4-2813	23:49:06.9	+56:24:40.2	22.6	41.1	18.03	0.55	0.49	16.64	0.26	0.67		δ Sct / SX Phe [1,3]
10	4-6-4-11525	23:47:46.8	+56:28:52.2	31.2	103.6	21.18	−0.38	0.25					Pulsating WD [3]
11	4-9-2-26107	20:57:32.0	+45:19:24.5	90.6	138.1	20.64		0.78					no U mag, δ Scu?
12	4-9-2-26146	20:57:26.5	+45:19:23.0	55.8	230.1	20.89		0.05					no U mag, P=111.6? [4]
13	4-9-4-14918	20:59:03.0	+45:37:36.1	15.3	77.0	18.43	−0.15	0.19					ZZ Ceti [3]
14	4-13-1-9769	21:08:19.4	+44:02:31.8	69.9	64.0	19.91	−0.13	1.27	15.26	0.57	0.46		
15	4-16-4-20312	21:05:18.8	+46:17:08.1	61.2	26.0	19.31	0.35	1.57	16.36	0.63	−0.14		
16	4-21-1-15898	23:56:21.7	+56:00:07.5	71.5	44.5	18.78	−0.72	0.89					
17	4-22-1-9937	01:41:31.0	+53:49:42.3	12.1	99.2	20.54	0.17	0.13					Pulsating WD?
18	5-5-3-3836	23:40:02.6	+57:09:02.5	81.3	93.7	17.42	0.89	0.55	15.69	0.02	−0.01		δ Sct / SX Phe
19	5-5-3-3970	23:40:00.1	+57:18:17.2	69.3	56.7	18.88	−1.68	0.94	16.41	0.71	0.19		
20	5-6-3-4828	04:32:10.4	+40:33:34.0	8.4	220.0	20.50	−0.20	0.24					Pulsating WD [2,3]
21	5-7-1-7259	06:55:15.7	+10:22:56.9	13.7	302.0	21.95	−1.84	0.79					
22	6-2-2-600654	00:01:34.9	+51:06:04.5	11.8	40.8	19.16	−0.38	0.00					ZZ Ceti
23	6-5-2-500125	20:08:21.3	+50:14:15.9	52.2	16.1	17.01	0.74	0.41	15.81	0.48	0.14		δ Sct / SX Phe
24	6-5-3-100238	20:10:34.9	+50:29:43.1	33.2	25.6	15.91	0.70	0.26	15.01	0.12	0.15	$-1.1, 1.4$	δ Sct
25	6-10-3-100564	20:07:59.4	+49:50:03.7	76.6	144.4	17.68		0.33					no U mag, δ Scu? / GW Vir?
26	7-1-4-800677	23:59:59.5	+55:58:54.2	77.8	72.3	20.36	−0.39	0.75					
27	7-5-3-600162	23:15:55.9	+54:41:00.9	31.8	8.2	16.95	0.51	0.47	15.52	0.04	−1.31	$4.1, -12.0$	δ Sct
28	7-8-2-800088	07:29:08.8	+04:45:11.9	18.3	9.1	16.38	0.21	0.19	15.72	0.27	−0.05	$0.2, -9.9$	roAp?
29	8-1-3-100467	18:43:51.4	+30:50:22.8	93.5	264.1	17.95	0.38	0.28	16.77	−0.97	1.15		δ Sct / SX Phe
30	8-5-3-501006	19:58:23.9	+44:37:52.2	38.6	13.0	18.05	0.67	0.54	16.54	0.32	0.21		δ Sct / SX Phe
31	8-11-1-700980	19:49:50.4	+44:16:57.6	73.4	43.7	15.81	0.43	0.35	14.58	0.17	0.11	$-1.8, 0.6$	δ Sct

[1] A-type star spectrum, [2] Low signal-to-noise spectrum—no obvious emission lines, [3] Barclay (2010) and Barclay et al. (2011)
[4] Long period δ Scu or Contact Binary?

5.3 Revealing the nature of blue variables

In this section I present further details about the blue variable objects identified in §5.2. I determine their nature based on their distribution in the $(g' - r')$ *vs* $(U - g')$ plane (Figure 5.3), and the information extracted from their light curves (*i.e.* periods and amplitudes).

In Figure 5.3 blue variables (except 3 objects that do not have U magnitude) are shown together with the non-variable blue objects, overplotted with unreddened main sequence and white dwarf cooling tracks. One can see that they can be divided into three groups — objects coinciding on the δ Scuti instability strip on the main-sequence between A- and F-type stars; compact object candidates close to white dwarf cooling tracks which are most probably pulsating WDs; and "*purple*" objects (blue in $(U - g')$ and red in $(g' - r')$) that can most likely be reddened compact objects (*e.g.* single or binary WDs, CVs, AM CVns, *etc.*), WD+dM systems, pulsating sdBs or QSOs. These three groups of objects and the ones without U mag are discussed in details, and their light curves and spectra (if available) are shown in the following subsections.

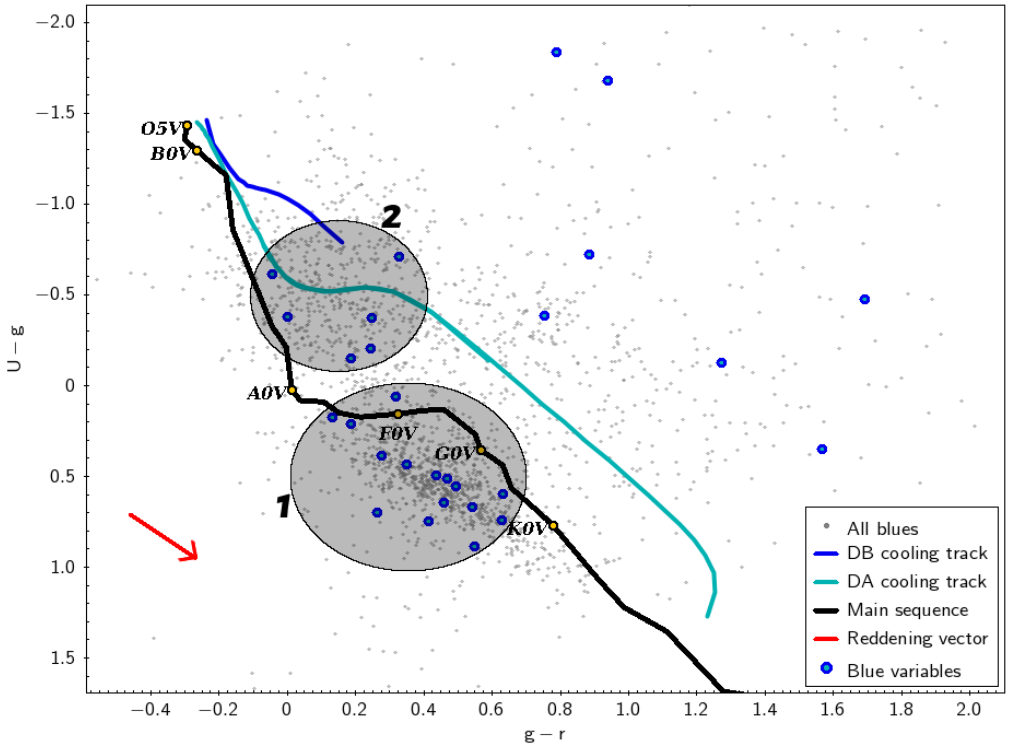

Figure 5.3: The blue variables are shown in the $(g' - r')$, $(U - g')$ colour-colour plane along with all the non-variable blue objects. The tracks are for $E(B-V) = 0$, and represent He-rich (dark blue) and H-rich WD (Cyan) cooling tracks, and main-sequence (black). The red arrow points the reddening direction and its size represents $E(B-V) = 0.2$. Considering their position on the plane, blue variables are divided into three groups — δ Sct candidates (area #1); compact object candidates (area #2); and the others.

5.3.1 δ Scuti region

Region 1 in the $(g' - r')$ *vs* $(U - g')$ plane (Figure 5.3) harbours δ Scuti and –their cousins– SX Phe pulsators, γ Dor pulsators, and rapidly oscillating chemically peculiar A (roAp) stars (see Breger (2000) for δ Scuti stars and Eyer and Mowlavi (2008) for variable stars across the HR diagram). Given that γ Dor stars have pulsation periods longer than a few hours, it is unlikely that any of these 15 blue variables (Table 5.2) are γ Dor stars. However, their periods are consistent with δ Sct, SX Phe or roAp pulsators. The period, amplitude and magnitude distributions are given in Figure 5.4, and light curves are plotted with best sinusoidal fits in Figure 5.5. The fits to the light curves are found using `LS` periods as the starting point for the iterative process, and the peak-to-peak amplitudes are determined from the fits.

Table 5.2: δ Sct star candidates selected based on their position in the $(g' - r')$ *vs* $(U - g')$ plane (region 1 in Figure 5.3). The catalogue names (Run-Field-Chip-ID); Right Ascension; Declination; Lomb-Scargle periods; Amplitudes; g' magnitudes; $U - g'$ and $g' - r'$ colours from RATS; and proper motions (Zacharias et al., 2013) of the candidates are presented.

#	Cat. name	RA	Dec	LS Per. [min]	Amp. [mmag]	g	U−g	g−r	μ_α, μ_δ [mas y^{-1}]	Notes
1	3-14-1-13507	18:00:35.3	+00:25:35.5	6.0	121.5	20.73	0.06	0.38		WD?
2	4-22-1-9937	01:41:31.0	+53:49:42.3	12.1	99.2	20.54	0.17	0.13		WD?
3[1]	7-8-2-800088	07:29:08.8	+04:45:11.9	18.3	9.1	16.38	0.21	0.19	0.2, −9.9	roAp?
4[1,3]	4-6-4-2813	23:49:06.9	+56:24:40.2	22.6	41.1	18.03	0.55	0.49		[2] / δ Sct / SX Phe
5[1]	7-5-3-600162	23:15:55.9	+54:41:00.9	31.8	8.2	16.95	0.51	0.47	4.1, −12.0	δ Sct
6[1]	6-5-3-100238	20:10:34.9	+50:29:43.1	33.2	25.6	15.91	0.70	0.26	−1.1, 1.4	δ Sct
7[3]	3-11-2-3507	18:02:50.6	+00:43:52.8	34.1	41.6	18.67	0.64	0.46		[2] / δ Sct / SX Phe
8[1]	8-5-3-501006	19:58:23.9	+44:37:52.2	38.6	13.0	18.05	0.67	0.54		δ Sct / SX Phe
9[1]	6-5-2-500125	20:08:21.3	+50:14:15.9	52.2	16.1	17.01	0.74	0.41		δ Sct / SX Phe
10	3-11-4-9303	18:04:15.8	+00:41:00.6	60.7	95.5	19.20	0.74	0.63		δ Sct / SX Phe
11	3-11-4-19198	18:03:44.5	+00:45:53.9	62.0	104.1	19.31	0.60	0.63		δ Sct / SX Phe
12[1]	8-11-1-700980	19:49:50.4	+44:16:57.6	73.4	43.7	15.81	0.43	0.35	−1.8, 0.6	δ Sct
13[1]	5-5-3-3836	23:40:02.6	+57:09:02.5	81.3	93.7	17.42	0.89	0.55		δ Sct / SX Phe
14[1]	8-1-3-100467	18:43:51.4	+30:50:22.8	93.5	264.1	17.95	0.38	0.28		SX Phe?
15	4-6-3-12509	23:47:20.9	+56:34:13.8	97.7	∼ 600	18.37	0.49	0.44		P=195.5?[4]

[1] Have 2MASS counterpart, [2] A-type star spectrum, [3] Barclay (2010); Barclay et al. (2011)
[4] Long period δ Sct or Contact Binary?

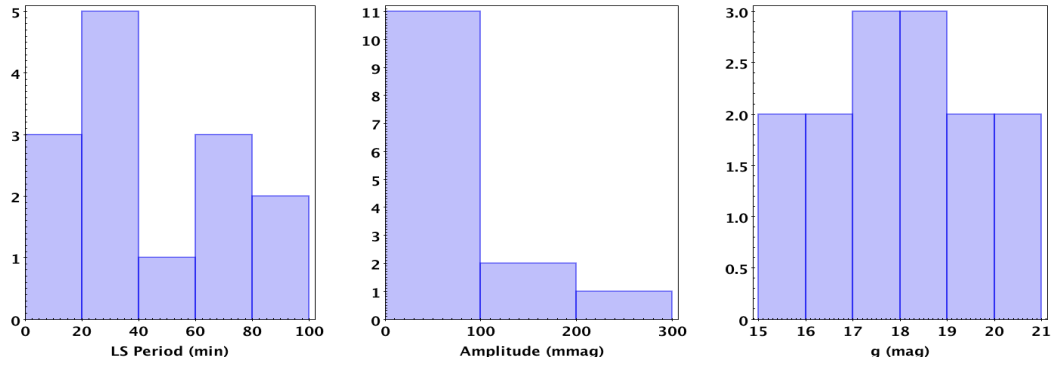

Figure 5.4: Lomb-Scargle period, amplitude and magnitude distributions of the δ Sct candidates.

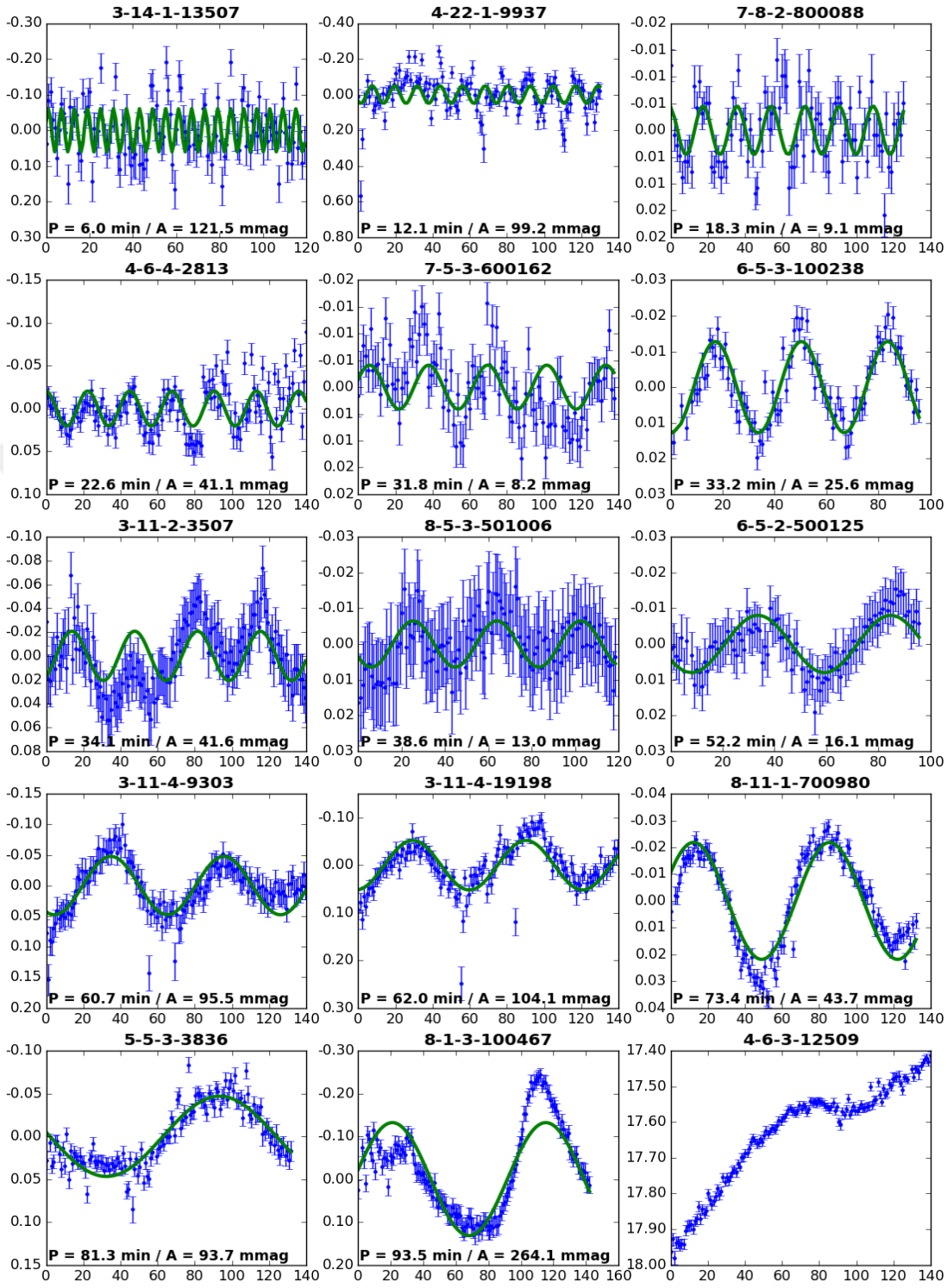

Figure 5.5: Light curves of the 15 short period blue variable objects in the region 1 (δ Sct-like) in Figure 5.3. Overplotted are best sinusoidal fits with the LS periods as starting period of the iterative fitting procedure. The given amplitudes are peak-to-peak amplitudes of the fits.

The δ Scuti stars are pulsating variables that are core or shell hydrogen burning, therefore on the main-sequence or immediate post-main-sequence stage of evolution. With spectral types from A0 to F5, they are situated in the region where the main sequence meets the higher surface gravity ($\log g$) tip of the Cepheid instability strip on the H-R diagram. Their pulsations are, in general, driven by the opacity (κ) mechanism in the He II ionization zone (pressure modes), although gravity modes (longer periods) may also be present. As they generally pulsate with more than one simultaneously excited radial and non-radial modes, they are considered as well-suited for asteroseismological studies (Breger, 2007). The typical values for pulsation periods are between 0.02 and 0.25 days (0.5 and 6 hours), however GCVS (General Catalogue of Variable Stars (Samus et al., 2009)) gives the lower limit as 0.01 days (14.4 min). Photometric amplitudes of the dominant modes are between 0.003 and 0.9 magnitude in Johnson V. They are mostly found in the Galactic disc (Samus et al., 2009). An extensive review about these objects is given by Breger (2000).

SX Phe stars show very similar characteristics to δ Sct stars with their spectral types, typical periods and amplitudes being consistent with limits for δ Sct stars (*i.e.* A2-F5, 1.5-3.25 hours and up to 0.7 magnitude in Johnson V (Samus et al., 2009)), although different period ranges can be found in the literature. For example, the shortest period object in the *SX Phe stars in globular clusters catalogue* of Rodriguez and López-González (2000) has a period of 0.0301 days (43.3 min) and 120 out of 149 objects in the catalogue have periods shorter than given in GCVS (1.5h).

Traditionally, SX Phe stars are defined as sub-solar metallicity subdwarf (not hot subdwarfs) cousins of solar metallicity dwarf δ Scuti stars. But there are *metal-rich* SX Phe stars recently discovered in the *Kepler* field (Nemec et al., 2015), and lower metallicity HADSs (high amplitude δ Scuti) in the Large Magellanic Cloud which are main-sequence dwarfs in the same evolutionary stage as normal δ Sct stars (Garg et al., 2010). Therefore, it is better to define SX Phe stars based on evolutionary state instead of metallicity —old, Population II stars, which are usually found in globular cluster in the Galaxy or neighbour galaxies.

Chemically peculiar (Ap) stars are magnetic main-sequence stars with A-type spectra which show abnormally strong lines of certain elements (*i.e.* Si, Cr, Sr and Eu). Noteworthy variations in their line strengths, light or magnetic field with periods ranging from a few days to many years are common. The rapidly oscillating chemically peculiar A stars (roAp) are a sub-group of these objects that pulsate rapidly with periods in the range of 5.7-23.6 minutes. Because of the multi-periodic and non-radial nature of their pulsations, the roAp stars are also considered well-suited for asteroseismology. Typical pulsational amplitudes are between 0.8-15 mmag in Johnson B (Sachkov, 2014). Currently $\sim$ 60 roAp stars are known (Holdsworth and Smalley, 2013) and they have very similar photometric, kinematic, chemical abundance and magnetic field properties with non-pulsating Ap stars (Hubrig et al., 2000).

Of the 15 blue variables lying in Region 1 in the $(g'-r')$ *vs* $(U-g')$ colour-colour plane, one object (`RAT J1843+3050`) has an amplitude (0.26 mag) that is close to the lower limit for high-amplitude δ Scuti stars (HADS), which is 0.3 mag, and the rest have very typical δ Scuti values between 8 and 122 mmag. Its period of 93.5 minute is also consistent with known HADS. Unlike low amplitude δ Scuti stars which may have radial or non-radial pulsations, the light-curves of HADSs are dominated by radial pulsations, therefore they have a semi-empirical period-luminosity relationship similar to classic Cepheids which allows one to determine their distances through the *distance modulus*. Thus, we can calculate the distance of `RAT J1843+3050` using Equation 5a and 5b of McNamara (2011), which is for HADS and SX Phe stars with periods between 45.5 and 181.3 min, and accounts for metallicity as well:

$$\langle M_v \rangle = (-2.90 \pm 0.05) logP - (0.19 \pm 0.015)[Fe/H] - (1.27 \pm 0.05) \quad for\ [Fe/H] > -2.0 \tag{5.1a}$$

$$\langle M_v \rangle = (-2.90 \pm 0.05) logP - (0.89 \pm 0.05) \quad for\ [Fe/H] \leqslant -2.0 \tag{5.1b}$$

where M_v is in magnitudes and P is in days.

As we do not know its metallicity, let us assume a solar ([Fe/H]$= 0$, `case1`) and a sub-solar ([Fe/H]$= -1$, `case2`) value for (5.1a), and a lower than -2 *dex* (`case3`) value for (5.1b) which gives mean absolute visual magnitude $\langle M_v \rangle$ as 2.174 ± 0.078, 2.364 ± 0.079 and 2.554 ± 0.078, for three cases respectively. Converting our g' magnitude to V using the relation

$$V = g' - 0.59 \times (g' - r') - 0.01 \tag{5.2}$$

taken from Jester et al. (2005), which gives $V = 17.78$, and taking extinction at the edge of the Galaxy $A_v = 1.674$ into account that is calculated via

$$N_H = (2.21 \pm 0.09) \times 10^{21} A_V \tag{5.3}$$

given by Guver and Ozel (2009) where $N_H = 3.7 \times 10^{21}\ cm^{-2}$ (Kalberla et al., 2005) and is the total average neutral hydrogen column density of the RATS fields close to the Galactic plane, which gives corrected visual magnitude $V_{corr} = 16.10$, allows us to calculate distance, d, via distance modulus

$$M_v - V_{corr} = -5logd + 5 \tag{5.4}$$

as 6.10 ± 0.22, 5.59 ± 0.20 and 5.12 ± 0.18 kpc for three cases. These distances give our object's height above the Galactic plane, z, as 1.58 ± 0.06, 1.45 ± 0.05 and 1.33 ± 0.05 kpc,

which are calculated simply as $z = d \times sinb$, where d is the distance and the b is the Galactic latitude of the object, which is 15 deg. In all cases, the object is located well above the thin disc, and in the thick disc. Additionally, its galactic longitude, $l = 60.3$, places it at ~ 6.5 kpc from the galactic center. Its place in the Galaxy suggests an advanced evolutionary status. Thus it is more likely to be a SX Phe star than a δ Sct star.

RAT J1800+0025 (6.0 min), RAT J0141+5349 (12.1 min), RAT J0729+0445 (18.3 min) and RAT J2349+5624 (22.6 min) have periods shorter than half an hour, a widely accepted lower limit for δ Scuti stars. This raises the possibility of their roAp nature, as roAp stars have periods in the range of 5.7–23.6 minutes. But with their relatively higher amplitude than the upper limit of 15 mmag, RAT J1800+0025 (122 mmag), RAT J0141+5349 (99 mmag) and RAT J2349+5624 (41 mmag) are most probably not roAp stars. This leaves us with one object, RAT J0729+0445, with a period and amplitude (9 mmag) consistent with known roAp stars, but without confirming its chemical abundance via spectral analysis, we cannot differentiate between δ Scuti and roAp nature, thus the question mark next to type (roAp?) in the Table 5.2.

Although the periods of typical δ Scuti-type pulsators are in the range of 0.5-6h, a number of shorter period objects are found in the last decades, such as the pre-main sequence star HD 34282 with 18.12 min (Amado et al., 2004). Therefore RAT J2349+5624 with 22.6 minute period certainly could be a δ Scuti star. Additionally, it happens to be one of two δ Sct star candidates of which we have the spectrum at our disposal (Barclay, 2010). With $T_{\rm eff} = 8320 \pm 50$K and $\log g = 4$ as the fitting suggests, it is certainly an A-type dwarf (Figure 5.6). The second object with a spectrum is RAT J1802+0043, and with $T_{\rm eff} = 8150 \pm 100$K and $\log g = 4$, it is also an A-type dwarf. Furthermore, it has 34.12 min period and 42 mmag amplitude. Hence, it is clearly a δ Scuti star. Both spectra can be seen in Figure 5.6, with the best fits to the Balmer lines.

The spectra were fitted[1] with the FITSB2 routine (Napiwotzki et al., 2004) using a grid of local thermodynamic equilibrium models calculated with the ATLAS9 code (Kurucz, 1992) with convective overshooting switched off. The effective temperatures were estimated from the hydrogen Balmer lines, and since no gravity sensitive features are accessible in our low resolution spectra, gravity was fixed at $\log g = 4.0$, which is a typical value (*e.g.*. McNamara (1997)).

The two shortest period objects in the region, RAT J1800+0025 and RAT J0141+5349, with their 6.0 and 12.1 min periods, are very likely not δ Scuti-type pulsators. Also their amplitudes are high for roAp stars. Considering the regions on the two colour diagram are determined very roughly and these two objects are very close to the compact objects region (# 2 in Figure 5.3), they very well might be pulsating white dwarfs as their periods and amplitudes

[1] Spectral fitting is done by my supervisor Dr. Gavin Ramsay.

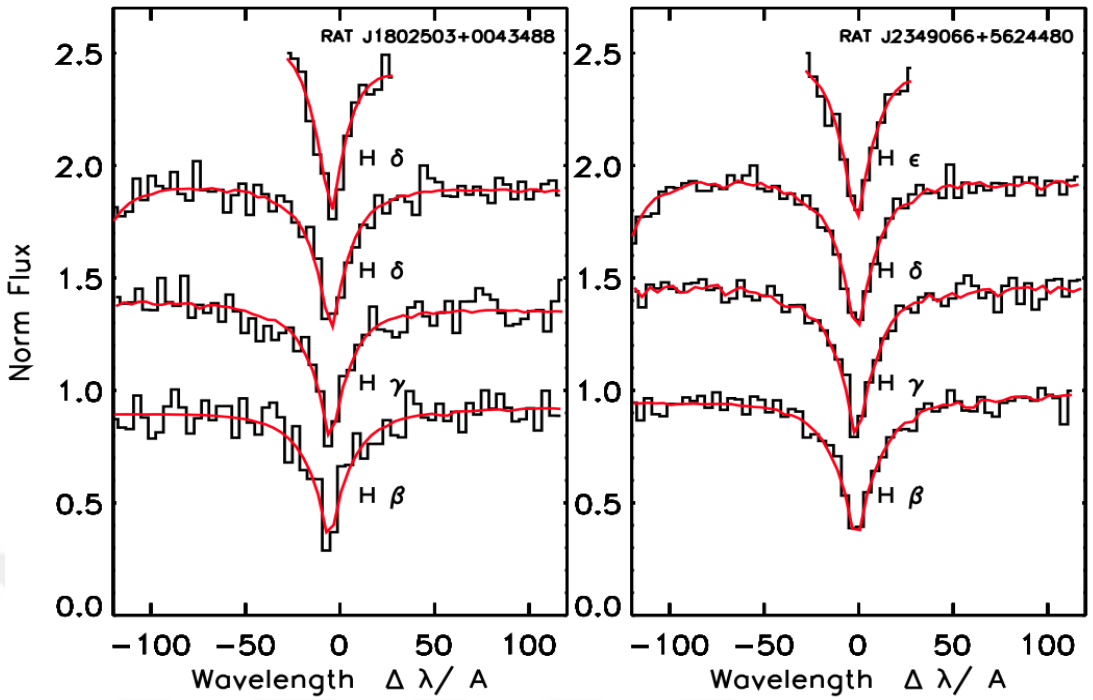

Figure 5.6: Spectral fits to two δ Sct star candidates, `RAT J1802+0043` and `RAT J2349+5644`, of which spectra were available to us (Barclay, 2010). Details about the fits are given in the text (page 112).

consistent with compact pulsators (see Table 5.3). Spectra with higher spectral resolution are required to discriminate between these alternatives.

Additionally, it is not possible to distinguish between δ Sct and SX Phe stars by amplitude and periods or even by metallicity as recent studies suggest (see Balona and Nemec (2012) and references therein). Only determining their evolutionary status would allow us to make this distinction, but this is very difficult for field stars. In addition to a detailed spectral analysis which may allow age determination, kinematics also could be useful to differentiate field stars, which may belong to the thick disc or halo, depending on their proper motions, and therefore, may be considered to be in an advanced stage of evolution. Thus, δ Scuti type pulsators with high spatial velocities may be classified as SX Phe stars. In this context, I found proper motions of 4 objects in the Fourth US Naval Observatory CCD Astrograph Catalog (Zacharias et al., 2013), of which one is a roAp star candidate. Balona and Nemec (2012) selected SX Phe candidates amongst δ Sct stars in the *Kepler* field based on their proper motion to be higher than 30 $mas\ y^{-1}$ in at least one of the RA and Dec, and tangential velocities to be higher than 60 $km\ s^{-1}$, which definitely place them out of the disc. The proper motions of our blue variables are significantly lower than this limit. Therefore it is likely that they are part of the disc population, thus δ Sct stars.

Although the colour of RAT J2347+5634 placed it in this group, its light curve differs from the others. This might be because it is a longer period δ Scuti star, or a contact binary (ie W UMa variable). Also the period (97.7 min) given by the LS test is obviously wrong. We know that in some cases it may give the half of the period, thus the period might be 195 min. For the other 6 candidates, although all the information we have suggest a δ Scuti type pulsator nature, without any information about their kinematics, we are not able to differentiate between δ Sct and SX Phe nature.

5.3.2 Compact pulsators region

The region 2 in Figure 5.3 is populated by compact pulsators (*e.g.* pulsating WDs and sdBs). These objects could be one of the three distinct groups of isolated pulsating white dwarfs — He/C/O-atmosphere GW Vir stars with $T_{\rm eff} \approx$ 120000K, He-atmosphere V777 Her stars with $T_{\rm eff} \approx$ 25000K, and H-atmosphere ZZ Ceti stars with $T_{\rm eff} \approx$ 12000K — which all show multi-periodic luminosity variations caused by low-order and low-degree g-mode instabilities, or two groups of pulsating subdwarfs — short period EG14026 objects with periods between 80 sec and 8 min, and long period 'Betsy' stars (PG 1716) with periods of 30 to 150 min. Typical period and amplitude values for the blue compact pulsators, and typical examples of light curves of them are given in Table 5.3 and Figure 5.7.

Table 5.3: Typical period and amplitude values of compact blue pulsators taken from Table 1 of Eyer and Mowlavi (2008).

	Type	Period [min]	Ampiltude [mmag]
White Dwarfs	GW Vir	$5-80$	<200
	V777 Her (DBV)	$2-16$	<200
	ZZ Ceti (DAV)	$0.5-25$	<200
Subdwarfs	Betsy (PG 1716)	$30-150$	$\lesssim 10$
	EG 14026	$1.3-8$	$\lesssim 30$

We have six objects in this region of the colour-colour diagram that I assigned as compact pulsator candidates (Table 5.4). Although their colours and periods are in agreement with known compact pulsators, their amplitudes are too high to be subdwarfs, as the one with the smallest amplitude, RAT 0001, has an amplitude of 40.8 mmag and pulsating subdwarfs have amplitudes less than 30 mmag. Therefore, none of them should be subdwarfs. On the other hand, one object, namely RAT 0252, has a period and an amplitude greater than usual values for pulsating WDs with 100.9 min and 320.1 mmag while the longest periods seen are of GW Vir pulsators with 80 min and greatest amplitudes are around 200 mmag for all three types, which suggests that this object might not be a compact pulsator but more likely a B-type pulsator (*e.g.* β Cep). The light curves of these 6 objects from which their periods and amplitudes derived

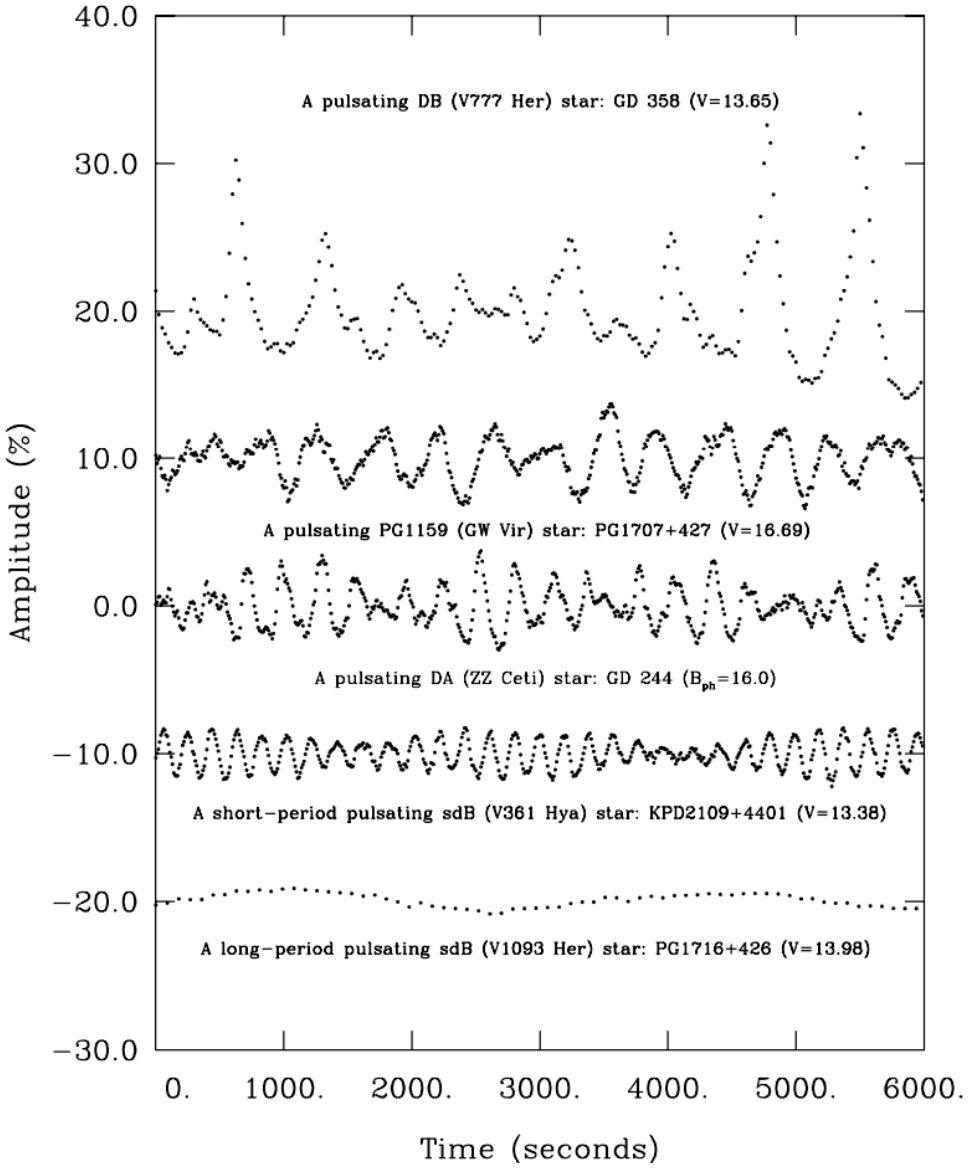

Figure 5.7: Examples of typical optical light curves for compact pulsators. The figure is taken from Fontaine and Brassard (2008).

can be seen in Figure 5.8 with the best sinusoidal fits.

Amongst the 6 compact pulsator candidates, there are only 2 objects, `RAT J0001` and `RAT J2059`, that we have follow-up spectral observations (Barclay, 2010). In Figure 5.9 I show spectra of these objects with the best fit overplotted.

`RAT J2059`, the variable with the bluest $(U - g')$ colour on the colour-colour diagram, is indeed a pulsating WD with H-atmosphere (*i.e.* DAV or ZZ Ceti), as classified by Barclay (2010), but "*it may have an unusual nature*" states Barclay based on the spectra (Figure 5.9, left panel) and further photometric observations in several regions of the electromagnetic spectrum

Table 5.4: Compact pulsator candidates selected based on their position in the $(g'-r')$ *vs* $(U-g')$ plane (region 2 in Figure 5.3). LS periods, amplitudes determined from the fits to the light curves (Figure 5.11), and RATS colours are presented.

#	Cat. name	RA	Dec	LS Per. [min]	Amp. [mmag]	g	U−g	g−r	Notes
1	5-6-3-4828	04:32:10.4	+40:33:34.0	8.4	220.0	20.50	−0.20	0.24	Pul.WD
2	6-2-2-600654	00:01:34.9	+51:06:04.5	11.8	40.8	19.16	−0.38	0.00	ZZ Ceti[1,2]
3	4-9-4-14918	20:59:03.0	+45:37:36.1	15.3	77.0	18.43	−0.15	0.19	ZZ Ceti[2]
4	4-6-4-11525	23:47:46.8	+56:28:52.2	31.2	103.6	21.18	−0.38	0.25	Pul.WD[2]
5	3-28-3-4339	20:31:33.6	+27:34:32.6	46.6	95.6	20.09	−0.71	0.38	Pul.WD
6	4-4-3-3953	02:52:37.1	+50:51:25.5	100.9	320.1	20.40	−0.62	−0.04	β Cep?

[1] Low signal-to-noise spectrum, no obvious emission lines
[2] Barclay (2010) and Barclay et al. (2011)

he obtained which are put under scrutiny in §6.2 of his thesis. Taking all the observations into account, Barclay (2010) suggests that RAT J2059 may be a binary system comprising a variable cool DA component (*i.e.* DAV) and a hot WD component, which would make this

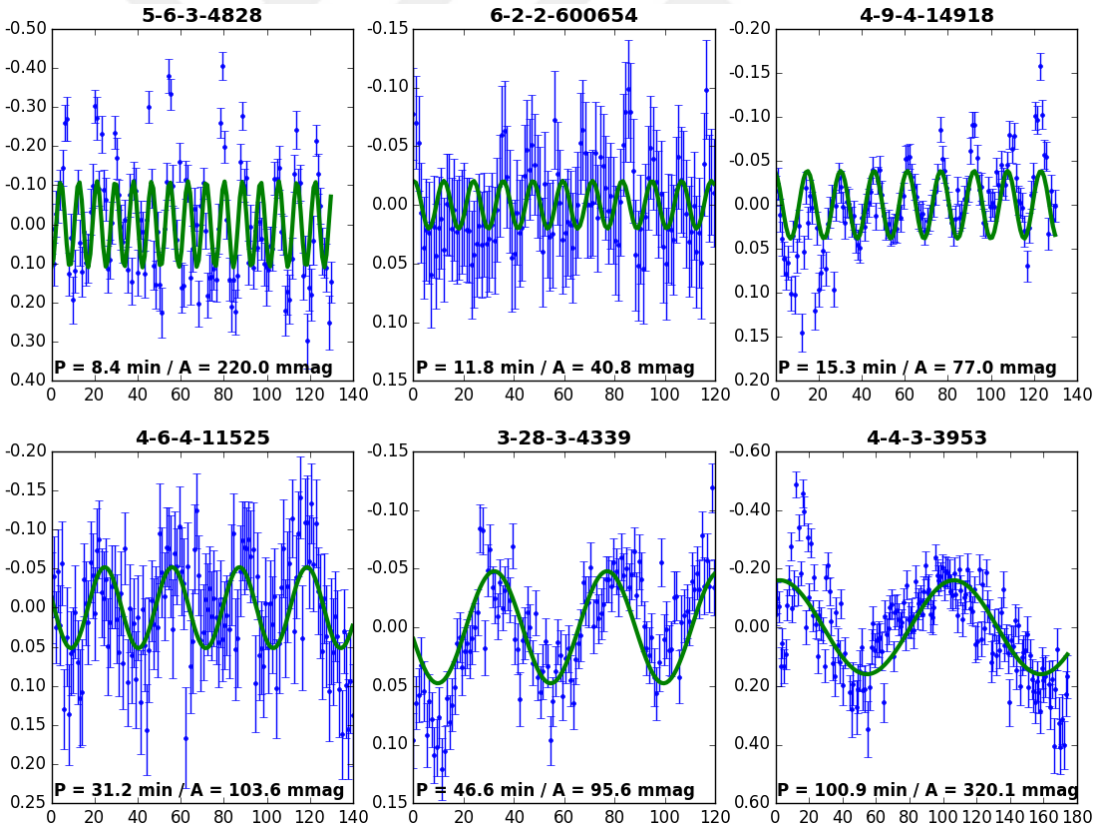

Figure 5.8: Light curves of the 6 short period blue variable objects in the region 2 (Compact pulsators) in Figure 5.3, with the best sinusoidal fits over plotted in a similar manner as in Figure 5.5.

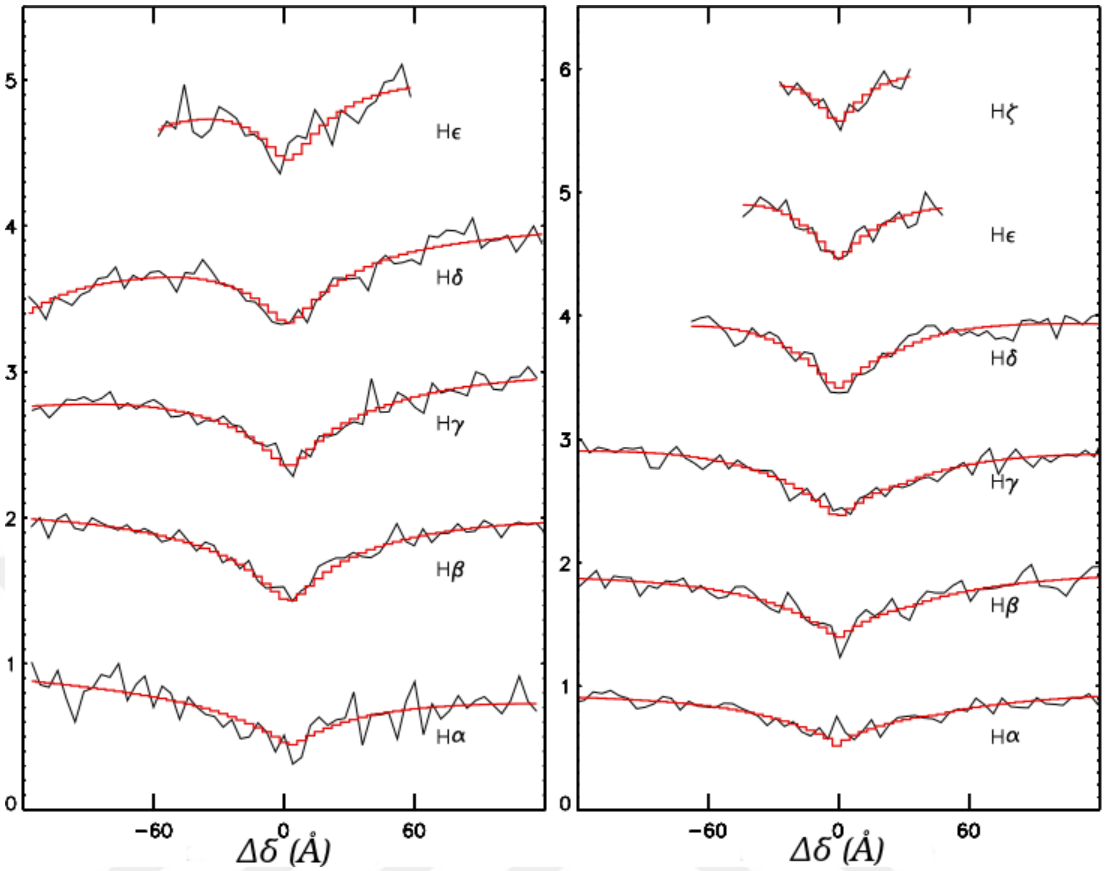

Figure 5.9: The Balmer lines of RAT J2059 (left panel) and RAT J0001 (right panel) over-plotted with our best-fitting DA white dwarf model. Each line has been normalised to 1.0 and every line after H_α has been shifted up by 1.0 flux unit. The spectra were obtained during the RATS follow-up program (Barclay, 2010).

system "*the first close binary consisting of a DAV and a companion*" as he puts it. However, he could not find any evidence to confidently declare the system as a binary and notes that the $T_{\rm eff}$ and $\log g$ values derived from two-component model are not well constrained.

The one other object with an optical spectrum, `RAT J0001`, is also a DAV, as the $T_{\rm eff} = 11590 \pm 760$K and $\log g = 8.3 \pm 0.2$ derived from the fit to its spectrum (Figure 5.9, right panel) places it amongst the variable DAs (variability strip) on the $T_{\rm eff}$-$\log g$ plane (Figure 5.10). This supports the DAV nature in addition to the period and amplitude of the object which are in agreement with typical DAV values. We have spectra of `RAT J0432` also, but no useful information could be extracted from them as the signal-to-noise ratio was very poor. Only it can be said that there are no obvious emission lines.

The other objects in the sample were cross matched with other catalogues (e.g. 2MASS, SDSS *etc*.) but no further information was obtained. Therefore, we cannot determine their nature other than the possibility that they are likely compact blue variables.

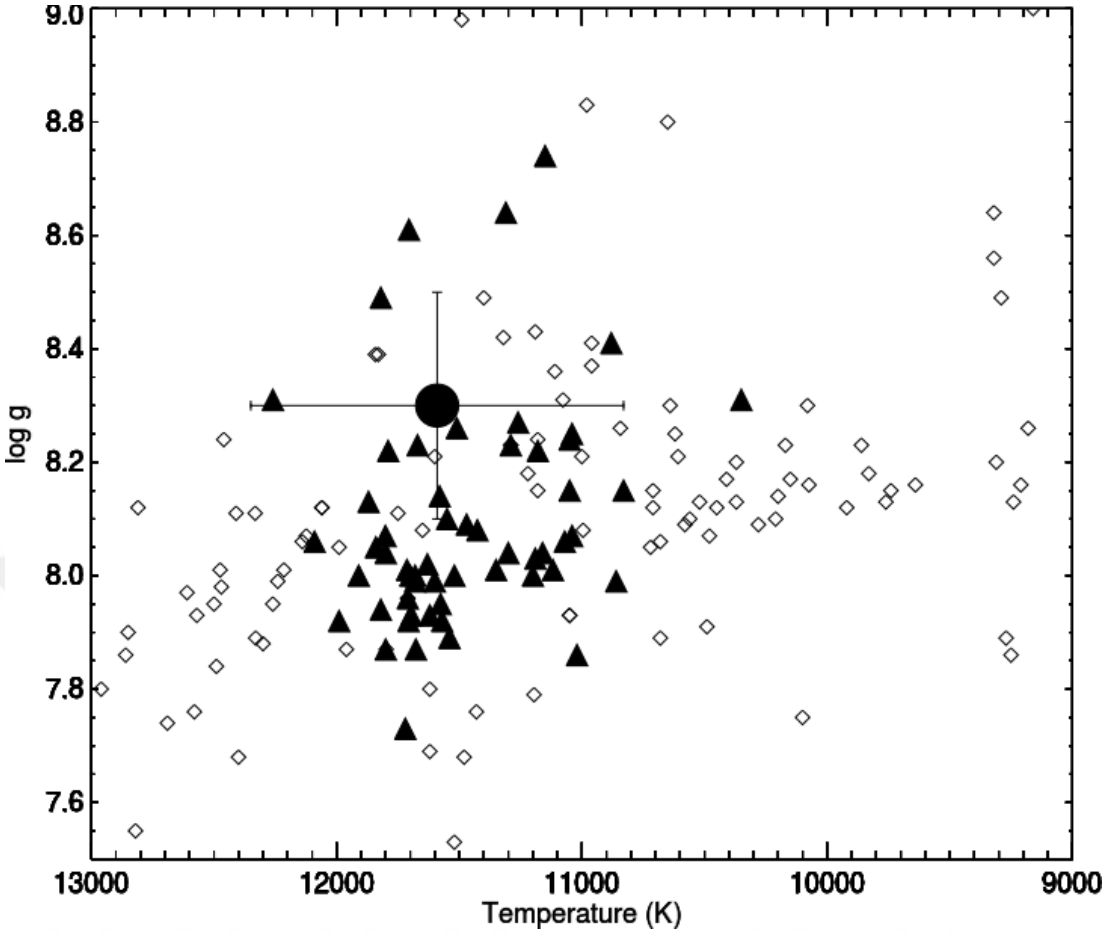

Figure 5.10: The location of RAT J0001 in the $T_{\rm eff}$ –$\log g$ plane together with non-variable (unfilled dimonds) and variable (filled triangles) DA white dwarfs from literature (Mukadam et al., 2004; Gianninas et al., 2005; Mullally et al., 2005; Castanheira et al., 2010).

5.3.3 Purple objects

There are 7 objects that have blue $(U-g')$ colour, but a red $(g'-r')$ colour, and are scattered in the top-right part of Figure 5.3. These objects could most likely be reddened pulsating compact objects (*e.g.* single or binary WDs, CVs, AM CVns, subdwarfs etc.), WD+dM binary systems, or QSOs. Follow-up spectral observations are needed to determine their nature conclusively. Here I show their light curves in Figure 5.11 and the details including their LS periods, and amplitudes extracted from these light curves in Table 5.5.

Table 5.5: Details of 7 objects scattered over the top-right part of two colour diagram in Figure 5.3. LS periods, amplitudes determined from the fits to the light curves (Figure 5.11), RATS and 2MASS colours are presented.

#	Cat. name	RA	Dec	LS Per. [min]	Amp. [mmag]	g	U−g	g−r	J	J−H	H−K
1	4-5-4-21796	21:00:55.5	+44:27:22.3	39.3	89.4	20.09	−0.48	1.69	15.76	0.56	0.47
2	4-13-1-9769	21:08:19.4	+44:02:31.8	69.9	64.0	19.91	−0.13	1.27	15.26	0.57	0.46
3	4-16-4-20312	21:05:18.8	+46:17:08.1	61.2	26.0	19.31	0.35	1.57	16.36	0.63	-0.14
4	4-21-1-15898	23:56:21.7	+56:00:07.5	71.5	44.5	18.78	−0.72	0.89			
5	5-5-3-3970	23:40:00.1	+57:18:17.2	69.3	56.7	18.88	−1.68	0.94	16.41	0.71	0.19
6	5-7-1-7259	06:55:15.7	+10:22:56.9	13.7	302.0	21.95	−1.84	0.79			
7	7-1-4-800677	23:59:59.5	+55:58:54.2	77.8	72.3	20.36	−0.39	0.75			

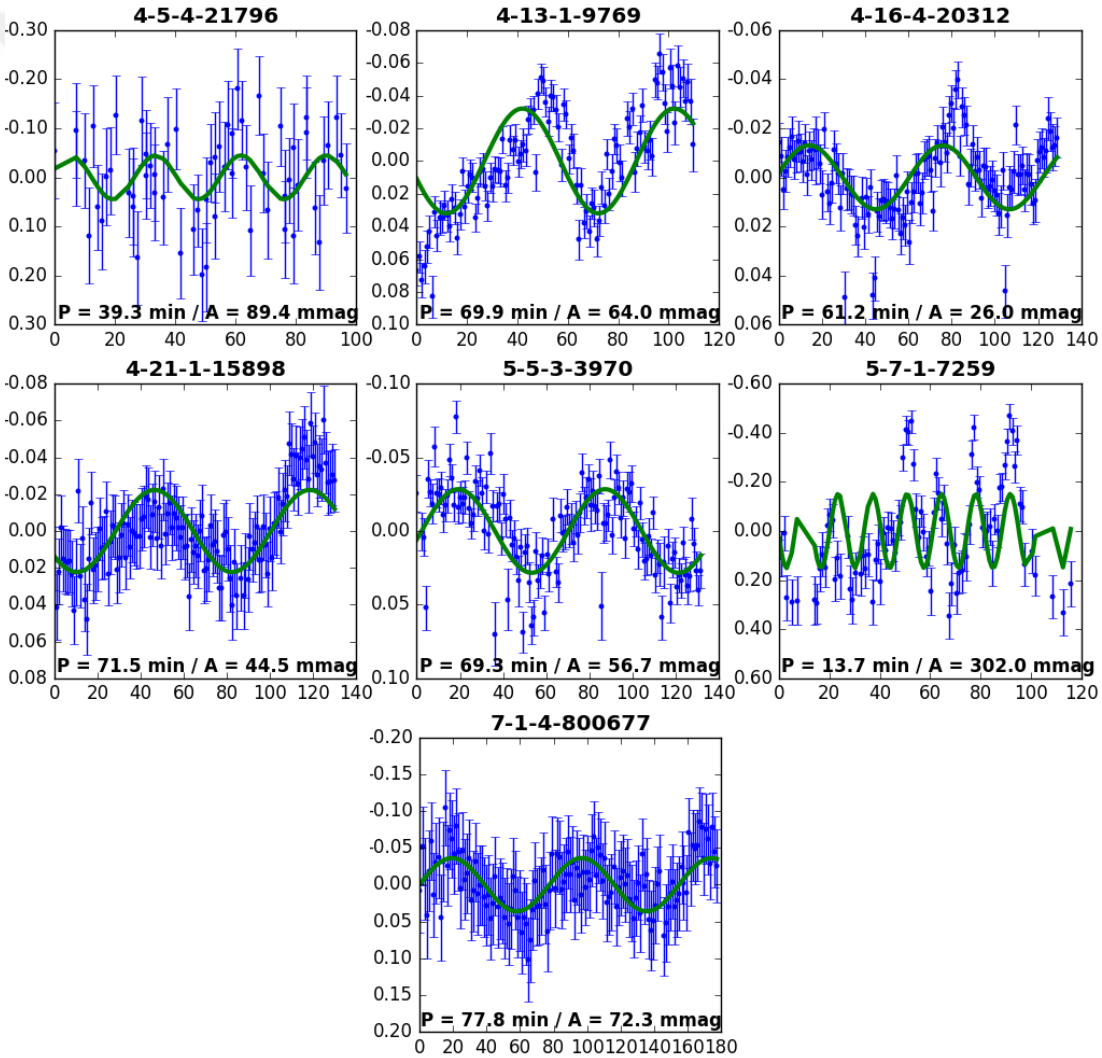

Figure 5.11: Light curves of the 7 short period blue variable objects that are scattered over the top-right part of Figure 5.3, with the best sinusoidal fits overplotted as in Figure 5.5.

5.3.4 *Blue variables with no U magnitude*

Amongst the blue variables, there are 3 objects for which we do not have U filter observation. Therefore they are not shown in the $(g'-r', U-g')$ colour-colour diagram. Their light curves are shown in Figure 5.12 and the details including their LS periods, and amplitudes determined from these fits are shown in in Table 5.6.

The LS test gives a 55.8 min period for RAT J205726.5+451923.0 but as it can be seen in Figure 5.12, a period twice this value can give a much better fit to its light curve. As for RAT J234720.9+563413.8, the case might be that this is the half of the real period and this object is a longer period δ Scuti or a contact binary. The other two objects might be δ Scuti stars, and RAT J200759.4+495003.7 could be a GW Vir pulsator as its period and amplitude is consistent with known GW Vir stars. Spectra with moderate resolution are needed to establish the nature of these objects.

Table 5.6: Details of 3 objects with no U magnitudes. LS periods, amplitudes determined from the fits to the light curves (Figure 5.11), g' magnitudes and $(g'-r')$ colours are presented.

#	Cat. name	RA	Dec	LS Per. [min]	Amp. [mmag]	g	g−r	Notes
1	4-9-2-26146	20:57:26.5	+45:19:23.0	55.8[1]	495.1	20.89	0.05	δ Scu? / CB?
2	6-10-3-100564	20:07:59.4	+49:50:03.7	76.6	144.4	17.68	0.33	δ Scu? / GW Vir?
3	4-9-2-26107	20:57:32.0	+45:19:24.5	90.6	138.1	20.64	0.78	δ Scu?

[1] Is LS period half of the real period?

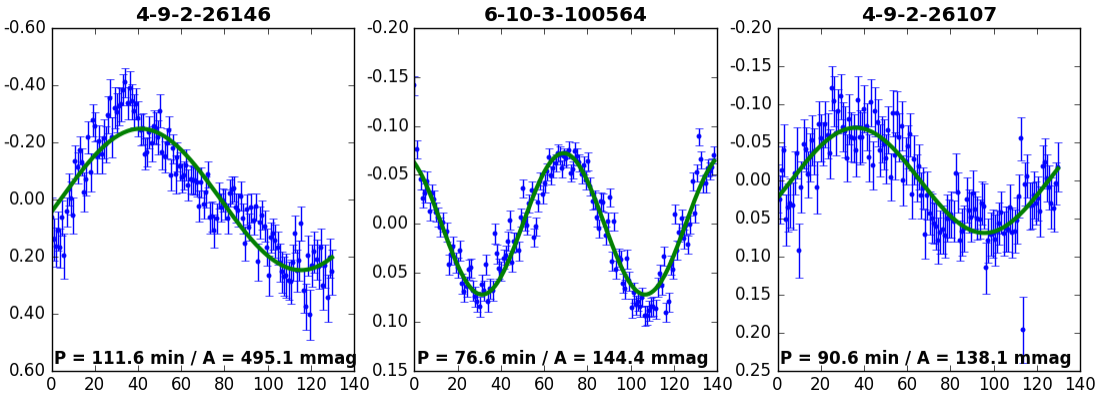

Figure 5.12: Light curves of the 3 short period blue variable objects of which we do not have U magnitude, with the best sinusoidal fits same as in Figure 5.5, except the left panel where twice of the LS period is used for the fit.

5.4 Summary

In this chapter, I have presented blue variables found in the RATS archive by cross-matching the variables selected by Barclay (2010) and Barclay et al. (2011), and the blue objects that I have outlined in §2. This cross-match has yielded 31 blue variables (§5.2). Using the colours, light curves, and optical spectra, I have revealed the nature of some of these blue variables, and have speculated most likely determinations for the rest (§5.3).

To summarise, I have identified 3 δ Sct stars, 8 δ Sct or SX Phe stars, 1 roAp candidate, 2 long period δ Scu or contact binary candidate, 2 Pulsating WD candidate, 2 ZZ Ceti, 3 pulsating WDs, 1 β Cep candidate, 1 δ Sct or GW Vir candidate and 7 purple objects which are blue in $(U-g')$ and while red in $(g'-r')$ and could be reddened compact objects (*e.g.* single or binary WDs, CVs, AM CVns, *etc.*), WD+dM systems, pulsating sdBs or QSOs.

Chapter 6

Conclusion and Outlook

This study was initiated to exploit the RATS archive, which has light-curves and colour information of more than 3 million stars. Although the main motivation of the RATS project was to discover AM CVn systems, many kinds of objects with a wide range of characteristics can be found in the dataset, and I have focused my search on a wider family of objects that also includes AM CVns, which are ultra compact binaries.

The light-curves in the archive was analysed before I started on the project by Barclay (2010), and he used the colour information as an additional diagnostic. I, on the other hand, used the colour information as my main diagnostic with variability information providing additional information. I have developed a selection method to identify the most astrophysically interesting systems to us —a method that selects candidate UCBs through their colours.

Since RATS data mainly come from galactic latitude $-15^o < |b| < 15^o$ (with a smaller number of fields at higher latitude), there is a big difference between individual fields' line of sight extinction (see in Fig. 2.1). Therefore, my method is a field-by-field colour selection method, which selects objects according to their relative position in the colour-magnitude or colour-colour space for every field (§2). This search has yielded 2826 blue objects (Table 2.3 on page 46), containing 384 UCB (Ultra Compact Binary) candidates (Table 2.4 on page 46), which have been selected since their colours are similar to known AM CVn systems.

For 17 of these objects, I obtained low resolution, low S/N spectra through a poor weather programme using OSIRIS instrument attached to 10.4 metre GTC (Grand Telescopio Canarias), and the spectral identification resulted in 3 He-rich O-type subdwarfs (He-sdO), 3 B-type subdwarfs (sdB) and 2 B-type (sub)dwarfs, 2 sdOs, 2 H-atmosphere (DA) white dwarfs, 2 QSOs and 3 possible subdwarf and cool dwarf binary systems (Table 3.1 on page 57). The detailed discussion about this spectral follow-up effort is presented in § 3.3 on page 78.

For the two of the He-sdOs identified through the spectral follow-up, which are as rare (*i.e.* only 51 known, Table3.3) and important as AM CVns, I led a successful bid for ESO time to observe these two new helium rich stars using the high resolution UVES echelle spectrograph attached to VLT (Very Large Telescope) in Chile (§4). The spectral analysis of the UVES spectra confirmed their nature and allowed me to determine their main physical parameters $T_{\rm eff}$ and $\log g$.

Finally, I have identified blue variables found in the RATS archive by cross-matching the variables selected by Barclay (2010) and Barclay et al. (2011), and the blue objects that I have outlined in §2, which yielded 31 blue variables. I have revealed their nature using their colours, light-curves and spectra (§5)—3 δ Sct stars, 8 δ Sct or SX Phe stars, 1 roAp candidate, 2 long period δ Scu or contact binary candidate, 2 Pulsating WD candidate, 2 ZZ Ceti, 3 pulsating WDs, 1 β Cep candidate, 1 δ Sct or GW Vir candidate and 7 "*purple*" objects which are blue in $(U-g')$ and while red in $(g'-r')$ and could be reddened compact objects (*e.g.* single or binary WDs, CVs, AM CVns, etc.), WD+dM systems, pulsating sdBs or QSOs.

In this chapter, I also had the opportunity to compare my results to Barclay (2010)'s results of blue variable object selection in the RATS database. I have found 31 variable blue objects, while Barclay has found 66 variable objects with similar colours to known AM CVn systems, and only 5 object are in both lists. A detailed distribution of these numbers are presented in Figure 5.2 on page 105 in the form of a Venn-diagram.

There are a number of reasons for this discrepancy. The first and the obvious reason is that 10 objects from his list are observed in the first two observation run of which data I have not used. Similarly for ten objects from my list is from INT6, INT7 and INT8 runs of which data he did not used. When these differences in the samples are accounted for, I have identified 21 blue objects against his 56 blue objects.

The main difference is caused by the colour selection methods: most of his blue variables (48) are not selected as blue objects by my method, which is not surprising as his color selection method was in comparison somewhat crude since it did not account for varying extinction from field to field.

The other difference is in the variable selection. 33 of his blue variables were not picked by the improved variable selection method. This is expected as the improved method is more conservative than the initial version, and therefore might leave some genuine variables out while results in a sample which has a lower number of false positives.

Finally, Barclay was searching for variable objects in general and only examined blue stars within these variable stars, while I was searching for blue objects in general and used already available variable list to learn more about my blue objects. These two approaches are not competitive but complementary in my opinion. In other words, if one is searching for variable

blue objects, should not choose one over other and use both, as both are computationally very cheap methods which can easily be handled by an ordinary laptop.

6.1 Future Work

The colour selection has compiled a list of blue objects, and the use of additional information gathered form the literature fine tuned our list to the objects that we are most interested in—UCBs. Unfortunately, only a small fraction of these UCB candidates have been spectroscopically studied.

If time permitted, I would have done a detailed chemical analysis of the high resolution UVES spectra of two extremely helium rich sdOs, as here I have just scratched the surface by determining the atmospheric parameters only. Also, there is a third extreme He-sdO of which high resolution spectra is yet to be acquired.

My next step would be to spectroscopically observe the rest of the objects, all of them, therefore we can identify their nature, and test our selection method fairly. Being rational about the observation time required, I would priortise my targets so that first ones would be `RAT J0432+4033`,`RAT J2347+5628` and `RAT J2031+2734`, which I identified as pulsating white dwarfs with 8.4^{min}, 31.2^{min} and 46.6^{min} periods, respectively (Table 5.4 on page 116), based on the information at hand. `RAT J0432+4033` and `RAT J2347+5628` also have the possibility to be AM CVn systems, as their periods shorter than 40^{min} (see 1.4.5 on page 17) and amplitudes are similar to known AM CVns as well as their colours.

6.2 The Next Generation High Cadence Photometric Surveys

6.2.1 OmegaWhite Survey

The immediate successor to RATS project is OmegaWhite (OW) survey, which is a wide-field high-cadence g-band synoptic survey (Macfarlane et al., 2015). It ultimately aims to cover $400 deg^2$ along the Galactic plane ($|b| < 5$ deg) and Galactic bulge ($|l|, |b| < 10$ deg) reaching a depth of $g = 21.5$ mag (10σ), using OmegaCam on the VLT Survey Telescope (VST) with a very similar observing strategy to RATS. It is design to unveil the Galactic population of short-period variable stars with periods $< 80^{min}$, including UCBs and stellar pulsators. The survey indeed led to discovery of samples of several classes of short period variables, including an UCB, a DQ white dwarf, a compact object with evidence of a 100 min rotation period, three CVs, one eclipsing binary with an 85^{min} period, a symbiotic binary which shows evidence of a 31^{min} photometric period, and a large sample of candidate δ Sct type stars including one with

a 9.3^{min} period (Toma et al., 2016).

The UCB discovered in the OW survey, `OWJ074106.0294811.0`, which shows a period of 22.6^{min} in the OW light curve, is one of the bluest variable star in their sample. Macfarlane et al. (2015) present an optical spectrum of this star obtained using SALT, which shows H_α as a very weak absorption line, while H_β and H_γ as stronger absorption lines. Further observations of this star showed that it has an orbital period of 44^{min}. It appears to be a very rare UCB that it is composed of an sdO/sdB star plus an unseen companion (Kupfer et al., in preparation).

6.2.2 Zwicky Transient Facility

The Zwicky Transient Facility[1] (ZTF) is a future time-domain survey that will have first light at Palomar Observatory in 2017, which is the successor of the Palomar Transient Factory (PTF). With a 47 square degree field of view camera will provide ZTF with an extremely wide field and with fast readout electronics, which will enable a survey to scan more than 3750 square degrees an hour to a depth of 20.5-21 mag.

With this speed, ZTF will be able to discover a young supernova less than 24 hours after its explosion each night and search for rare and exotic transients. Repeated imaging of the Northern sky (including the Galactic Plane) will produce a photometric variability catalog with nearly 300 observations each year, ideal for studies of variable stars, binaries, AGN, and asteroids.

6.2.3 Gravitational wave Optical Transient Observatory (GOTO)

GOTO project[2] is developed to follow-up the early phases of gravitational wave (GW) events' electro-magnetic (EM) counterparts in optical light. For these events, sky localisation will be the poor. Also the large and complex error boxes need to be searched over quickly for rapidly evolving transients. The earliest (and likely brightest) phases are the best for rapid localization of viable candidates.

The synoptic survey mode will work when not pursuing an event trigger. It will ensure that very recent reference images are available across the visible sky, which is critical for identifying false-positives and will offer a broad array of time-domain/transient science.

The hardware is designad to imnimize cost. It is scalable, adaptable and upgradable, using "*off-the-shelf*" components. In order to achieve a large instantaneous field of view and to keep the cost low, the systems is based on an array of 40 cm diameter astrographs (f/2.5), an robotic

[1] `http://www.ptf.caltech.edu/ztf`
[2] `http://www.goto-observatory.org/`

mount which can 8 astrographs within a clamshell enclosure, and large format, lower grade detectors.

Bibliography

Ahmad, A. and Jeffery, C. S.: 2003, *Astron. Astrophys.* **402(1)**, 335

Amado, P. J., Moya, A., Suárez, J. C., Martín-Ruiz, S., Garrido, R., Rodríguez, E., Catala, C., and Goupil, M. J.: 2004, *Mon. Not. R. Astron. Soc.* **352(2)**, L11

Anderson, S. F., Becker, A. C., Haggard, D., Prieto, J. L., Knapp, G. R., Sako, M., Halford, K. E., Jha, S., Martin, B., Holtzman, J., Frieman, J. A., Garnavich, P. M., Hayward, S., Ivezić, Ž., Mukadam, A. S., Sesar, B., Szkody, P., Malanushenko, V., Richmond, M. W., Schneider, D. P., and York, D. G.: 2008, *Astron. J.* **135(6)**, 2108

Anderson, S. F., Haggard, D., Homer, L., Joshi, N. R., Margon, B., Silvestri, N. M., Szkody, P., Wolfe, M. A., Agol, E., Becker, A. C., Henden, A., Hall, P. B., Knapp, G. R., Richmond, M. W., Schneider, D. P., Stinson, G., Barentine, J. C., Brewington, H. J., Brinkmann, J., Harvanek, M., Kleinman, S. J., Krzesinski, J., Long, D., Neilsen, J., Nitta, A., and Snedden, S. A.: 2005, *Astron. J.* **130(5)**, 2230

Augusteijin, T., van der Hooft, F., de Jong, J., and van Paradijs, J.: 1996, *Astron. Astrophys.* **311**, 889

Balona, L. A. and Nemec, J. M.: 2012, *Mon. Not. R. Astron. Soc.* **426(3)**, 2413

Barclay, T.: 2010, Ph.d., University College London

Barclay, T., Ramsay, G., Hakala, P., Napiwotzki, R., Nelemans, G., Potter, S., and Todd, I.: 2011, *Mon. Not. R. Astron. Soc.* **413(4)**, 2696

Becker, A. C., Wittman, D. M., Boeshaar, P. C., Clocchiatti, A., Dell'Antonio, I. P., Frail, D. A., Halpern, J., Margoniner, V. E., Norman, D., Tyson, J. A., and Schommer, R. A.: 2004, *Astrophys. J.* **611(1)**, 418

Beers, T. C., Doinidis, S. P., Griffin, K. E., Preston, G. W., and Shectman, S. A.: 1992, *Astron. J.* **103**, 267

Behara, N. T. and Jeffery, C. S.: 2006, *Astron. Astrophys.* **451(2)**, 643

Benvenuto, O. G. and De Vito, M. A.: 2005, *Mon. Not. R. Astron. Soc.* **362(3)**, 891

Bergeron, P., Fontaine, G., Billeres, M., Boudreault, S., and Green, E. M.: 2003, *Astrophys. J.* **600(1)**, 404

Borucki, W. J., Koch, D., Basri, G., Batalha, N., Brown, T., Caldwell, D., Caldwell, J., Christensen-Dalsgaard, J., Cochran, W. D., DeVore, E., Dunham, E. W., Dupree, A. K., Gautier, T. N., Geary, J. C., Gilliland, R., Gould, A., Howell, S. B., Jenkins, J. M., Kondo, Y., Latham, D. W., Marcy, G. W., Meibom, S., Kjeldsen, H., Lissauer, J. J., Monet, D. G., Morrison, D., Sasselov, D., Tarter, J., Boss, A., Brownlee, D., Owen, T., Buzasi, D., Charbonneau, D., Doyle, L., Fortney, J., Ford, E. B., Holman, M. J., Seager, S., Steffen, J. H., Welsh, W. F., Rowe, J., Anderson, H., Buchhave, L., Ciardi, D., Walkowicz, L., Sherry, W., Horch, E., Isaacson, H., Everett, M. E., Fischer, D., Torres, G., Johnson, J. A., Endl, M., MacQueen, P., Bryson, S. T., Dotson, J., Haas, M., Kolodziejczak, J., Van Cleve, J., Chandrasekaran, H., Twicken, J. D., Quintana, E. V., Clarke, B. D., Allen, C., Li, J., Wu, H., Tenenbaum, P., Verner, E., Bruhweiler, F., Barnes, J., and Prsa, A.: 2010, *Science (80-.).* **327(5968)**, 977

Breedt, E., Gänsicke, B. T., Drake, A. J., Rodríguez-Gil, P., Parsons, S. G., Marsh, T. R., Szkody, P., Schreiber, M. R., and Djorgovski, S. G.: 2014, *Mon. Not. R. Astron. Soc.* **443(4)**, 3174

Breger, M.: 2000, in M. Breger and M. Montgomery (eds.), *Delta Scuti and Related Stars*, Vol. 210 of *Astronomical Society of the Pacific Conference Series*, p. 3, Vienna, Austria

Breger, M.: 2007, *Commun. Asteroseismol.* **150**, 25

Burbidge, G., Burbidge, M., and Hoyle, F.: 1967, *Astrophys. J.* **147**, 1219

Campbell, H. C., Marsh, T. R., Fraser, M., Hodgkin, S. T., de Miguel, E., Gänsicke, B. T., Steeghs, D., Hourihane, A., Breedt, E., Littlefair, S. P., Koposov, S. E., Wyrzykowski, L., Altavilla, G., Blagorodnova, N., Clementini, G., Damljanovic, G., Delgado, A., Dennefeld, M., Drake, A. J., Fernández-Hernández, J., Gilmore, G., Gualandi, R., Hamanowicz, A., Handzlik, B., Hardy, L. K., Harrison, D. L., Ilkiewicz, K., Jonker, P. G., Kochanek, C. S., Kolaczkowski, Z., Kostrzewa-Rutkowska, Z., Kotak, R., van Leeuwen, G., Leto, G., Ochner, P., Pawlak, M., Palaversa, L., Rixon, G., Rybicki, K., Shappee, B. J., Smartt, S. J., Torres, M. A. P., Tomasella, L., Turatto, M., Ulaczyk, K., van Velzen, S., Vince, O., Walton, N. A., Wielgórski, P., Wevers, T., Whitelock, P., Yoldas, A., De Angeli, F., Burgess, P., Busso, G., Busuttil, R., Butterley, T., Chambers, K. C., Copperwheat, C., Danilet, A. B., Dhillon, V. S., Evans, D. W., Eyer, L., Froebrich, D., Gomboc, A., Holland, G., Holoien, T. W. S., Jarvis, J. F., Kaiser, N., Kann, D. A., Koester, D., Kolb, U., Komossa, S., Magnier, E. A., Mahabal, A., Polshaw, J., Prieto, J. L., Prusti, T., Riello, M., Scholz, A., Simonian, G., Stanek, K. Z., Szabados, L., Waters, C., and Wilson, R. W.: 2015, *Mon. Not. R. Astron. Soc.* **452(1)**, 1060

Carter, P. J., Gansicke, B. T., Steeghs, D., Marsh, T. R., Breedt, E., Kupfer, T., Gentile Fusillo, N. P., Groot, P. J., and Nelemans, G. A.: 2014, *Mon. Not. R. Astron. Soc.* **439(3)**, 2848

Carter, P. J., Marsh, T. R., Steeghs, D., Groot, P. J., Nelemans, G., Levitan, D., Rau, A., Copperwheat, C. M., Kupfer, T., and Roelofs, G. H. A.: 2013, *Mon. Not. R. Astron. Soc.* **429(3)**, 2143

Castanheira, B. G., Kepler, S. O., Kleinman, S. J., Nitta, A., and Fraga, L.: 2010, *Mon. Not. R. Astron. Soc.* **405(4)**, 2561

Chornock, R. and Filippenko, A. V.: 2003, *IAU Circ., 8084, 3*

Copperwheat, C. M., Marsh, T. R., Dhillon, V. S., Littlefair, S. P., Woudt, P. A., Warner, B., Patterson, J., Steeghs, D., Kemp, J., Armstrong, E., and Rea, R.: 2011, *Mon. Not. R. Astron. Soc.* **413(4)**, 3068

Cox, J. P.: 1980, *Theory of stellar pulsation*, Princeton University Press

Daou, D., Wesemael, F., Fontaine, G., Bergeron, P., and Holberg, J. B.: 1990, *Astrophys. J.* **364**, 242

Devor, J.: 2005, *Astrophys. J.* **628(1)**, 411

Dreizler, S., Heber, U., Werner, K., Moehler, S., and de Boer, K. S.: 1990, *Astron. Astrophys.* **235**, 234

Drilling, J. S.: 1996, in C. S. Jeffery and U. Heber (eds.), *Hydrogen Deficient Stars*, Vol. 96 of *Astronomical Society of the Pacific Conference Series*, p. 461

Drilling, J. S., Jeffery, C. S., Heber, U., Moehler, S., and Napiwotzki, R.: 2013, *Astron. Astrophys.* **551**, A31

Edelmann, H., Heber, U., Hagen, H.-J., Lemke, M., Dreizler, S., Napiwotzki, R., and Engels, D.: 2003, *Astron. Astrophys.* **400(3)**, 939

Eisenstein, D. J., Liebert, J., Harris, H. C., Kleinman, S. J., Nitta, A., Silvestri, N., Anderson, S. A., Barentine, J. C., Brewington, H. J., Brinkmann, J., Harvanek, M., Krzesiński, J., Neilsen, Jr., E. H., Long, D., Schneider, D. P., and Snedden, S. A.: 2006, *Astrophys. J. Suppl. Ser.* **167(1)**, 40

Espaillat, C., Patterson, J., Warner, B., and Woudt, P.: 2005, *Publ. Astron. Soc. Pacific* **117(828)**, 189

Eyer, L. and Mowlavi, N.: 2008, *J. Phys. Conf. Ser.* **118**, 012010

Farmer, A. J. and Phinney, E. S.: 2003, *Mon. Not. R. Astron. Soc.* **346(4)**, 1197

Fitzpatrick, E. L.: 1999, *Publ. Astron. Soc. Pacific* **111(755)**, 63

Fontaine, G. and Brassard, P.: 2008, *Publ. Astron. Soc. Pacific* **120(872)**, 1043

Fontaine, G., Brassard, P., and Bergeron, P.: 2001, *Publ. Astron. Soc. Pacific* **113(782)**, 409

Fontaine, G., McGraw, J. T., Dearborn, D. S. P., Gustafson, J., and Lacombe, P.: 1982, *Astrophys. J.* **258**, 651

Gänsicke, B. T., Dillon, M., Southworth, J., Thorstensen, J. R., Rodríguez-Gil, P., Aungwerojwit, A., Marsh, T. R., Szkody, P., Barros, S. C. C., Casares, J., de Martino, D., Groot, P. J., Hakala, P., Kolb, U., Littlefair, S. P., Martínez-Pais, I. G., Nelemans, G., and Schreiber, M. R.: 2009, *Mon. Not. R. Astron. Soc.* **397(4)**, 2170

Garg, A., Cook, K. H., Nikolaev, S., Huber, M. E., Rest, A., Becker, A. C., Challis, P., Clocchiatti, A., Miknaitis, G., Minniti, D., Morelli, L., Olsen, K., Prieto, J. L., Suntzeff, N. B., Welch, D. L., and Wood-Vasey, W. M.: 2010, *Astron. J.* **140(2)**, 328

Gianninas, A., Bergeron, P., and Fontaine, G.: 2005, *Astrophys. J.* **631(2)**, 1100

Gianninas, A., Bergeron, P., and Fontaine, G.: 2006, *Astron. J.* **132(2)**, 831

Giovannini, O., Kepler, S. O., Kanaan, A., Wood, A., Claver, C. F., and Koester, D.: 1998, *Balt. Astron.* 7

Girven, J., Steeghs, D., Heber, U., Gänsicke, B. T., Marsh, T. R., Breedt, E., Copperwheat, C. M., Pyrzas, S., and Longa-Peña, P.: 2012, *Mon. Not. R. Astron. Soc.* **425(2)**, 1013

Graham, M. J., Drake, A. J., Djorgovski, S. G., Mahabal, A. A., Donalek, C., Duan, V., and Maker, A.: 2013, *Mon. Not. R. Astron. Soc.* **434(4)**, 3423

Green, R. F., Schmidt, M., and Liebert, J.: 1986, *Astrophys. J. Suppl. Ser.* **61**, 305

Greenstein, J. L.: 1982, *Astrophys. J.* **258**, 661

Greenstein, J. L. and Matthews, M. S.: 1957, *Astrophys. J.* **126**, 14

Groot, P. J., Nelemans, G., Steeghs, D., and Marsh, T. R.: 2001, *Astrophys. J.* **558(2)**, L123

Groot, P. J., Verbeek, K., Greimel, R., Irwin, M., González-Solares, E., Gänsicke, B. T., de Groot, E., Drew, J., Augusteijn, T., Aungwerojwit, A., Barlow, M., Barros, S., van den Besselaar, E. J. M., Casares, J., Corradi, R., Corral-Santana, J. M., Deacon, N., van Ham, W., Hu, H., Heber, U., Jonker, P. G., King, R., Knigge, C., Mampaso, A., Marsh, T. R., Morales-Rueda, L., Napiwotzki, R., Naylor, T., Nelemans, G. A., Oosting, T., Pyrzas, S., Pretorius, M., Rodríguez-Gil, P., Roelofs, G. H. A., Sale, S., Schellart, P., Steeghs, D., Szyszka, C., Unruh, Y., Walton, N. A., Weston, S., Witham, A., Woudt, P., and Zijlstra, A.: 2009, *Mon. Not. R. Astron. Soc.* **399(1)**, 323

Groot, P. J., Vreeswijk, P. M., Huber, M. E., Everett, M. E., Howell, S. B., Nelemans, G., Van Paradijs, J., Van Den Heuvel, E. P. J., Augusteijn, T., Kuulkers, E., Rutten, R. G. M., and Storm, J.: 2003, *Mon. Not. R. Astron. Soc.* **339(2)**, 427

Guver, T. and Ozel, F.: 2009, *Mon. Not. R. Astron. Soc.* **400(4)**, 2050

Hagen, H.-J., Groote, D., Engels, D., and Reimers, D.: 1995, *Astron. Astrophys. Suppl. Ser.* **111**, 195

Hartman, J. D., Gaudi, B. S., Holman, M. J., McLeod, B. A., Stanek, K. Z., Barranco, J. A., Pinsonneault, M. H., and Kalirai, J. S.: 2008, *Astrophys. J.* **675(2)**, 1254

Haussler, K., Berthold, T., and Kroll, P.: 2006, *Information Bulletin on Variable Stars* 5732

Heber, U.: 1986, *Astron. Astrophys.* **155**, 33

Heber, U.: 2009, *Annu. Rev. Astron. Astrophys.* **47(1)**, 211

Heber, U., Dreizler, S., Werner, K., Engels, D., and Hagen, H.-J.: 1996, in C. Jeffery and U. Heber (eds.), *Hydrog. Defic. Stars*, Vol. 96 of *Astronomical Society of the Pacific Conference Series*, p. 241

Holdsworth, D. L. and Smalley, B.: 2013, *Putt. A Stars into Context Evol. Environ. Relat. Stars. Proc. Int. Conf. held June 3-7, 2013 Moscow M.V. Lomonosov State Univ. Moscow, Russ. Eds. G. Mathys, E. Griffin, O. Kochukhov, R. Monier,*

Hubrig, S., Kharchenko, N., Mathys, G., and North, P.: 2000, *Astron. Astrophys.* **355**, 1031

Humason, M. L. and Zwicky, F.: 1947, *Astrophys. J.* **105**, 85

Jeffery, C. S.: 1998, *Mon. Not. R. Astron. Soc.* **294(3)**, 391

Jeffery, C. S. and Heber, U.: 1992, *Astron. Astrophys.* **260**, 133

Jeffery, C. S., Woolf, V. M., and Pollacco, D. L.: 2001, *Astron. Astrophys.* **376(2)**, 497

Jester, S., Schneider, D. P., Richards, G. T., Green, R. F., Schmidt, M., Hall, P. B., Strauss, M. A., Vanden Berk, D. E., Stoughton, C., Gunn, J. E., Brinkmann, J., Kent, S. M., Smith, J. A., Tucker, D. L., and Yanny, B.: 2005, *Astron. J.* **130(3)**, 873

Justham, S., Podsiadlowski, P., Han, Z., and Wolf, C.: 2010, *Astrophys. Space Sci.* **329(1-2)**, 3

Kalberla, P. M. W., Burton, W. B., Hartmann, D., Arnal, E. M., Bajaja, E., Morras, R., and Pöppel, W. G. L.: 2005, *Astron. Astrophys.* **440(2)**, 775

Kato, T., Hambsch, F. J., and Monard, B.: 2015, *Publ. Astron. Soc. Japan* **67(2)**, L21

Kato, T., Hambsch, F.-J., Monard, B., Vanmunster, T., Maeda, Y., Miller, I., Itoh, H., Kiyota, S., Isogai, K., Kimura, M., Imada, A., Tordai, T., Akazawa, H., Tanabe, K., Otani, N., Ogi, M., Ando, K., Takigawa, N., Dubovsky, P. A., Kudzej, I., Shugarov, S. Y., Katysheva, N., Golysheva, P., Gladilina, N., Chochol, D., Starr, P., Kasai, K., Pickard, R. D., de Miguel, E., Kojiguchi, N., Sugiura, Y., Fukushima, D., Yamada, E., Uto, Y., Kamibetsunawa, T., Tatsumi, T., Takeda, N., Matsumoto, K., Cook, L. M., Pavlenko, E. P., Babina, J. V., Pit, N. V., Antonyuk, O. I., Antonyuk, K. A., Sosnovskij, A. A., Baklanov, A. V., Kafka, S., Stein, W., Voloshina, I. B., Ruiz, J., Sabo, R., Dvorak, S., Stone, G., Andreev, M. V., Antipin, S. V., Zubareva, A. M., Zaostrojnykh, A. M., Richmond, M., Shears, J., Dubois, F., Logie, L., Rau, S., Vanaverbeke, S., Simon, A., Oksanen, A., Goff, W. N., Bolt, G., Dębski, B., Kochanek, C. S., Shappee, B., Stanek, K. Z., Prieto, J. L., Stubbings, R., Muyllaert, E., Hiraga, M., Horie, T., Schmeer, P., and Hirosawa, K.: 2016, *Publ. Astron. Soc. Japan* **68(4)**, 65

Kato, T., Nogami, D., Baba, H., Hanson, G., and Poyner, G.: 2000, *Mon. Not. R. Astron. Soc.* **315**, 140

Kawaler, S. and Dahlstrom, M.: 2000, *Am. Sci.* **88(6)**, 498

Kepler, S. O., Pelisoli, I., Koester, D., Ourique, G., Kleinman, S. J., Romero, A. D., Nitta, A., Eisenstein, D. J., Costa, J. E. S., Kulebi, B., Jordan, S., Dufour, P., Giommi, P., and Rebassa-Mansergas, A.: 2015, *Mon. Not. R. Astron. Soc.* **446(4)**, 4078

Kolesnikova, D. M., Sat, L. A., Sokolovsky, K. V., Antipin, S. V., and Samus, N. N.: 2008, *Acta Astronomica* **58**, 279

Kraft, R. P., Mathews, J., and Greenstein, J. L.: 1962, *Astrophys. J.* **136**, 312

Kukarkin, B. V., Efremov, Y. N., Frolov, M. S., Medvedeva, G. I., Kholopov, P. N., Kurochkin, N. E., Kukarkina, N. P., Perova, N. B., and Fedorovich, V. P.: 1968, *Inf. Bull. Var. Stars. 311, 1.*

Kupfer, T., Geier, S., Heber, U., Østensen, R. H., Barlow, B. N., Maxted, P. F. L., Heuser, C., Schaffenroth, V., and Gansicke, B. T.: 2015, *Astron. Astrophys.* **576**, A44

Kupfer, T., Groot, P. J., Levitan, D., Steeghs, D., Marsh, T. R., Rutten, R. G. M., and Nelemans, G.: 2013, *Mon. Not. R. Astron. Soc.* **432(3)**, 2048

Kurucz, R. L.: 1992, *Rev. Mex. Astron. y Astrofis. Vol. 23, p. 181-186*

Lanning, H. and Lépine, S.: 2006, *Publ. Astron. Soc. Pacific* **118(850)**, 1639

Levitan, D., Fulton, B. J., Groot, P. J., Kulkarni, S. R., Ofek, E. O., Prince, T. A., Shporer, A., Bloom, J. S., Cenko, S. B., Kasliwal, M. M., Law, N. M., Nugent, P. E., Poznanski, D., Quimby, R. M., Horesh, A., Sesar, B., and Sternberg, A.: 2011, *ApJ* **739**, 68

Levitan, D., Kupfer, T., Groot, P. J., Kulkarni, S. R., Prince, T. A., Simonian, G. V., Arcavi, I., Bloom, J. S., Laher, R., Nugent, P. E., Ofek, E. O., Sesar, B., and Surace, J.: 2013, *Mon. Not. R. Astron. Soc.* **430(2)**, 996

Levitan, D., Kupfer, T., Groot, P. J., Margon, B., Prince, T. A., Kulkarni, S. R., Hallinan, G., Harding, L. K., Kyne, G., Laher, R., Ofek, E. O., Rutten, R. G. M., Sesar, B., and Surace, J.: 2014, *Astrophys. J.* **785(2)**, 114

Lisker, T., Heber, U., Napiwotzki, R., Christlieb, N., Reimers, D., and Homeier, D.: 2004, *Astrophys. Space Sci.* **291(3)**, 351

Littlefield, C., Garnavich, P., Applegate, A., Magno, K., Pogge, R., Irwin, J., Marion, G. H., Vinkó, J., and Kirshner, R.: 2013, *Astron. J.* **145(6)**, 145

Lomb, N. R.: 1976, *Astrophys. Space Sci.* **39(2)**, 447

Macfarlane, S. A., Toma, R., Ramsay, G., Groot, P. J., Woudt, P. A., Drew, J. E., Barentsen, G., and Eislöffel, J.: 2015, *Mon. Not. R. Astron. Soc.* **454(1)**, 507

Malmquist, K. G.: 1936, *Stock. Obs. Ann. vol. 12, pp.7.1-7.130*

Marsh, T. R.: 1998, *Mon. Not. R. Astron. Soc.* **304(2)**, 443

Maxted, P., Heber, U., Marsh, T., and North, R.: 2001, *Mon. Not. R. Astron. Soc.* **326(4)**, 1391

McNamara, D.: 1997, *Publ. Astron. Soc. Pacific* **109**, 1221

McNamara, D. H.: 2011, *Astron. J.* **142(4)**, 110

Miller Bertolami, M. M., Althaus, L. G., Unglaub, K., and Weiss, A.: 2008, *Astron. Astrophys.* **491(1)**, 253

Moehler, S., Heber, U., and Durell, P. R.: 1997, *Astron. Astrophys.* **317**, 83

Moehler, S., Richtler, T., de Boer, K. S., Dettmar, R. J., and Heber, U.: 1990, *Astron. Astrophys. Suppl. Ser. (ISSN 0365-0138)* **86**, 53

Moro, D. and Munari, U.: 2000, *Astron. Astrophys. Suppl. Ser.* **147(3)**, 361

Motsoaledi, M.: 2015, p. 70

Mukadam, A. S., Winget, D. E., von Hippel, T., Montgomery, M. H., Kepler, S. O., and Costa, A. F. M.: 2004, *Astrophys. J.* **612(2)**, 14

Mullally, F., Thompson, S. E., Castanheira, B. G., Winget, D. E., Kepler, S. O., Eisenstein, D. J., Kleinman, S. J., and Nitta, A.: 2005, *Astrophys. J.* **625(2)**, 966

Napiwotzki, R., Yungelson, L., Nelemans, G., Marsh, T. R., Leibundgut, B., Renzini, R., Homeier, D., Koester, D., Moehler, S., Christlieb, N., Reimers, D., Drechsel, H., Heber, U., Karl, C., and Pauli, E.-M.: 2004, in R. W. Hilditch, H. Hensberge, and K. Pavlovski (eds.), *Spectroscopically and Spatially Resolving the Components of the Close Binary Stars*, Vol. 318 of *Astronomical Society of the Pacific Conference Series*, pp 402–410

Naslim, N., Jeffery, C. S., Ahmad, A., Behara, N. T., and Şahin, T.: 2010, *Mon. Not. R. Astron. Soc.* **409(2)**, 582

Nather, R. E., Robinson, E. L., and Stover, R. J.: 1981, *Astrophys. J.* **244**, 269

Nelemans, G. and Tauris, T.: 1998, *Astron. Astrophys.* **335**, 85

Nelemans, G. A., Portegies Zwart, S. F., Verbunt, F., and Yungelson, L. R.: 2001a, *Astron. Astrophys.* **368(3)**, 939

Nelemans, G. A., Yungelson, L. R., and Portegies Zwart, S. F.: 2004, *Mon. Not. R. Astron. Soc.* **349(1)**, 181

Nelemans, G. A., Yungelson, L. R., Portegies Zwart, S. F., and Verbunt, F.: 2001b, *Astron. Astrophys.* **365(3)**, 491

Nemec, J. M., Balona, L. A., Kinemuchi, K., Murphy, S. J., Jeon, Y.-B., Kurtz, D. W., and Pigulski, A.: 2015, *EPJ Web Conf.* **101**, 06049

Paczyński, B.: 1967, *Acta Astron. Vol. 17, p.287*

Paczynski, B. and Sienkiewicz, R.: 1981, *Astrophys. J.* **248**, L27

Patterson, J., Kemp, J., Shambrook, A., Thomas, E., Halpern, J. P., Skillmand, D. R., Harvey, D. A., Vanmunster, T., Retter, A., Fried, R., Buckley, D., Nogami, D., Kato, T., and Baba, H.: 1997, *Publ. Astron. Soc. Pacific* **109**, 1100

Patterson, J., Walker, S., Kemp, J., O'Donoghue, D., Bos, M., and Stubbings, R.: 2000, *Publ. Astron. Soc. Pacific* **112(771)**, 625

Podsiadlowski, P., Han, Z., Lynas-Gray, A. E., and Brown, D.: 2008, *Hot Subdwarf Stars Relat. Objects ASP Conf. Ser.* 392

Pollacco, D., Skillen, I., Cameron, A., Christian, D., Irwin, J., Lister, T., Street, R., West, R., Clarkson, W., Evans, N., Fitzsimmons, A., Haswell, C., Hellier, C., Hodgkin, S., Horne, K., Jones, B., Kane, S., Keenan, F., Norton, A., Osborne, J., Ryans, R., and Wheatley, P.: 2006, in *Astrophys. Space Sci.*, Vol. 304, pp 253–255

Press, W. H., Rybicki, G. B., and Hewitt, J. N.: 1992, *Astrophys. J.* **385**, 404

Prialnik, D.: 2010, *An Introduction to the Theory of Stellar Structure and Evolution*, Cambridge University Press

Prieto, J. L., Morrell, N., Grupe, D., Stanek, K. Z., Kochanek, C. S., Holoien, T. W. S., Davis, A. B., Basu, U., Beacom, J. F., Bersier, D., Shappee, B. J., Brimacombe, J., Szczygiel, D., and Pojmanski, G.: 2014, *Astron. Telegr.* 6475

Ramsay, G., Brooks, A., Hakala, P., Barclay, T., Garcia-Alvarez, D., Antoci, V., Greiss, S., Still, M., Steeghs, D., Gansicke, B., and Reynolds, M.: 2014, *Mon. Not. R. Astron. Soc.* **437(1)**, 132

Ramsay, G. and Hakala, P.: 2005, *Mon. Not. R. Astron. Soc.* **360(1)**, 314

Ramsay, G., Hakala, P., Barclay, T., Wheatley, P., Marshall, G., Lehto, H., Napiwotzki, R., Nelemans, G., Potter, S., and Todd, I.: 2009, *Mon. Not. R. Astron. Soc.* **398(3)**, 1333

Ramsay, G., Napiwotzki, R., Barclay, T., Hakala, P., Potter, S., and Cropper, M.: 2011, *Mon. Not. R. Astron. Soc.* **417(1)**, 400

Ramsay, G., Napiwotzki, R., Hakala, P., and Lehto, H.: 2006, *Mon. Not. R. Astron. Soc.* **371(2)**, 957

Rau, A., Roelofs, G. H. A., Groot, P. J., Marsh, T. R., Nelemans, G., Steeghs, D., Salvato, M., and Kasliwal, M. M.: 2010, *Astrophys. J.* **708(1)**, 456

Reimers, D.: 1990, *The Messenger* **60**, 13

Rodriguez, E. and López-González, M. J.: 2000, *Delta Scuti Star Newsletter* **14**, 33

Roelofs, G. H. A., Groot, P. J., Benedict, G. F., McArthur, B. E., Steeghs, D., Morales-Rueda, L., Marsh, T. R., and Nelemans, G. A.: 2007a, *Astrophys. J.* **666(2)**, 1174

Roelofs, G. H. A., Groot, P. J., Marsh, T. R., Steeghs, D., Barros, S. C. C., and Nelemans, G.: 2005, *Mon. Not. R. Astron. Soc.* **361(2)**, 487

Roelofs, G. H. A., Groot, P. J., Nelemans, G., Marsh, T. R., and Steeghs, D.: 2006, *Mon. Not. R. Astron. Soc.* **371(3)**, 1231

Roelofs, G. H. A., Groot, P. J., Nelemans, G., Marsh, T. R., and Steeghs, D.: 2007b, *Mon. Not. R. Astron. Soc.* **379(1)**, 176

Roelofs, G. H. A., Groot, P. J., Steeghs, D., and Nelemans, G.: 2004, in G. Tovmassian and E. Sion (eds.), *Revista Mexicana de Astronomia y Astrofisica Conference Series*, Vol. 20 of *Revista Mexicana de Astronomia y Astrofisica Conference Series*, pp 254–254

Roelofs, G. H. A., Groot, P. J., Steeghs, D., Rau, A., De Groot, E., Marsh, T. R., Nelemans, G., Liebert, J., and Woudt, P.: 2009, *Mon. Not. R. Astron. Soc.* **394(1)**, 367

Roelofs, G. H. A., Nelemans, G., and Groot, P. J.: 2007c, *Mon. Not. R. Astron. Soc.* **382(2)**, 685

Roelofs, G. H. A., Rau, A., Marsh, T. R., Steeghs, D., Groot, P. J., and Nelemans, G.: 2010, *Astrophys. J.* **711(2)**, L138

Ruiz, M. T., Rojo, P. M., Garay, G., and Maza, J.: 2001, *Astrophys. J.* **552(2)**, 679

Sachkov, M.: 2014, in G. Mathys, E. R. Griffin, O. Kochukhov, R. Monier, and G. M. Wahlgren (eds.), *Putting A Stars into Context: Evolution, Environment, and Related Stars*, pp 315–322

Saffer, R. A., Bergeron, P., Koester, D., and Liebert, J.: 1994, *Astrophys. J.* **432**, 351

Samus, N., Durlevich, O., and Et Al.: 2009, *VizieR Online Data Cat.* **1**, 2025

Scargle, J. D.: 1982, *Astrophys. J.* **263**, 835

Schwartz, M.: 1998, *IAU Circ., 6982, 1 (1998). Ed. by Green, D. W. E.*

Schwarzenberg-Czerny, A.: 1989, *Mon. Not. R. Astron. Soc.* **241(2)**, 153

Schwarzenberg-Czerny, A.: 1996, *ApJ* **460**, L107

Sion, E. M., Greenstein, J. L., Landstreet, J. D., Liebert, J., Shipman, H. L., and Wegner, G. A.: 1983, *Astrophys. J.* **269**, 253

Smak, J.: 1967, *Acta Astron. 17, 255*

Solheim, J.-E.: 2010, *Publ. Astron. Soc. Pacific* **122(896)**, 1133

Steeghs, D., Marsh, T. R., Barros, S. C. C., Nelemans, G., Groot, P. J., Roelofs, G. H. A., Ramsay, G., and Cropper, M.: 2006, *Astrophys. J.* **649(1)**, 382

Stroeer, A., Heber, U., and Lisker, T.: 2007, *Astron. Astrophys. Astrophys.* **462**, 269

Tamuz, O., Mazeh, T., and North, P.: 2006, *Mon. Not. R. Astron. Soc.* **367(4)**, 1521

Tassoul, M., Fontaine, G., and Winget, D. E.: 1990, *Astrophys. J. Suppl. Ser.* **72**, 335

Toma, R., Ramsay, G., Macfarlane, S., Groot, P. J., Woudt, P. A., Dhillon, V., Jeffery, C. S., Marsh, T., Nelemans, G., and Steeghs, D.: 2016, *Mon. Not. R. Astron. Soc.* **463(1)**, 1099

Vanden Berk, D. E., Richards, G. T., Bauer, A., Strauss, M. A., Schneider, D. P., Heckman, T. M., York, D. G., Hall, P. B., Fan, X., Knapp, G. R., Anderson, S. F., Annis, J., Bahcall, N. A., Bernardi, M., Briggs, J. W., Brinkmann, J., Brunner, R., Burles, S., Carey, L., Castander, F. J., Connolly, A. J., Crocker, J. H., Csabai, I., Doi, M., Finkbeiner, D., Friedman, S., Frieman, J. A., Fukugita, M., Gunn, J. E., Hennessy, G. S., Ivezić, Ž., Kent, S., Kunszt, P. Z., Lamb, D. Q., Leger, R. F., Long, D. C., Loveday, J., Lupton, R. H., Meiksin, A., Merelli, A., Munn, J. A., Newberg, H. J., Newcomb, M., Nichol, R. C., Owen, R., Pier, J. R., Pope, A., Rockosi, C. M., Schlegel, D. J., Siegmund, W. A., Smee, S., Snir, Y., Stoughton, C., Stubbs, C., SubbaRao, M., Szalay, A. S., Szokoly, G. P., Tremonti, C., Uomoto, A., Waddell, P., Yanny, B., and Zheng, W.: 2001, *Astron. J.* **122(2)**, 549

Vennes, S., Kawka, A., and Németh, P.: 2011, *Mon. Not. R. Astron. Soc.* **410(3)**, 2095

Verbeek, K., de Groot, E., Groot, P. J., Roelofs, G. H. A., Drew, J., Greimel, R., Irwin, M., González-Solares, E., Gänsicke, B. T., Casares, J., Corral-Santana, J. M., Deacon, N., and Steeghs, D.: 2012, *Mon. Not. R. Astron. Soc.* **420(2)**, 1115

Viton, M., Deleuil, M., Tobin, W., Prevot, L., and Bouchet, P.: 1991, *A&A* **242**, 175

Wade, R. A., Stark, M. A., Green, R. F., and Durrell, P. R.: 2009, *Astron. J.* **138(2)**, 606

Wagner, R. M., Kaur, A., Porter, A., Wilber, A., Woodward, C. E., Starrfield, S. G., Hartmann, D. H., Davis, A. B., Holoien, T. W. S., Simonian, G., Stanek, K. Z., Kochanek, C. S., Shappee, B. J., and Prieto, J. L.: 2014, *Astron. Telegr.* 6669

Warner, B.: 2003, *Cataclysmic Variable Stars*

Wesemael, F., Greenstein, J. L., Liebert, J., Lamontagne, R., Fontaine, G., Bergeron, P., and Glaspey, J. W.: 1993, *Publ. Astron. Soc. Pacific* **105**, 761

Wevers, T., Torres, M. A. P., Jonker, P. G., Wetuski, J. D., Nelemans, G., Steeghs, D., Maccarone, T. J., Heinke, C., Hynes, R. I., Udalski, A., Kostrzewa-Rutkowska, Z., Groot, P. J., Gazer, R., Szymanski, M. K., Britt, C. T., Wyrzykowski, L., and Poleski, R.: 2016, *MNRAS* **462**, 106

Winget, D. E. and Fontaine, G.: 1982, in J. P. Cox and C. J. Hansen (eds.), *Pulsations in Classical and Cataclysmic Variable Stars*, p. 46

Wood, M. A., Casey, M. J., Garnavich, P. M., and Haag, B.: 2002, *Mon. Not. R. Astron. Soc.* **334(1)**, 87

Wood-Vasey, W. M., Aldering, G., Nugent, P., and Li, K.: 2003, *IAU Circ., 8077, 1 (2003). Ed. by Green, D. W. E.*

Woudt, P. A. and Warner, B.: 2003, *Mon. Not. R. Astron. Soc.* **345(4)**, 1266

Woudt, P. A., Warner, B., and Motsoaledi, M.: 2013, *Astron. Telegr.* 4726

Woudt, P. A., Warner, B., and Rykoff, E.: 2005, *Int. Astron. Union Circ.* 8531

Zacharias, N., Finch, C. T., Girard, T. M., Henden, A., Bartlett, J. L., Monet, D. G., and Zacharias, M. I.: 2013, *Astron. J.* **145(2)**, 44

Zhang, X. and Jeffery, C. S.: 2012, *Mon. Not. R. Astron. Soc.* **419(1)**, 452

Appendices

Appendix A

The Computer Scripts

Here I present a selection of the scripts I have wirtten and used during this study, which I think it would be very usefull if I have read in someone elses thesis. In this mentallity, I want to share no matter how basic some of them are.

A.1 Colour Selection

There are two main piece of codes that constitute the foundation of this theses—colour selection codes which are written in Python scripting language as shown in here.

A.1.1 Blue Object Selection on Colour-Magnitude plane

```
from pylab import *  # import everything in the module
import numpy as np   # import the module and use a shorter namespace
import pyfits        # to be able to handle fits files
import csv           # to be able to handle csv files
import math
import collections
import os
import time
import matplotlib.pyplot as plt


from matplotlib import rc
rc('text', usetex=True)
```

```
#================================================================
# SECTION 1: Creating variables, files and folders will be needed
#================================================================

#data to use. You must give the full path!
fits_file = '/home/osa/Dropbox/PhD/Work/201305-New_colours/int3-8eso2.fits'

system = sys.argv[1]
colour = sys.argv[2]
binning= sys.argv[3]

#colour = raw_input('colour?              : ')
#system = raw_input('AB or Vega?          : ')
#binning = raw_input('binning1 or binning2?  : ')

# Magnitude names must be identical to column name in the fits file
if system == 'AB':
    if colour == 'uming':
        plane = 'g-uming_ab' # just for naming folder and files
        colour = 'uming_ab'
        mag_1 = 'gab' #must be same with mag in the "plane"
        mag_2 = 'uab' #the other magnitude
        err_1 = 'gaberr'
        err_2 = 'uaberr'

    elif colour == 'gminr':
        plane = 'g-gminr_ab' # just for naming folder and files
        colour = 'gminr_ab'
        mag_1 = 'gab' #must be same with mag in the "plane"
        mag_2 = 'rab' #the other magnitude
        err_1 = 'gaberr'
        err_2 = 'raberr'

    else:
        sys.exit('Wrong color!!!!')

elif system == 'Vega':
    if colour == 'Uming':
```

```
        plane = 'g-Uming' # just for naming folder and files
        colour = 'Uming'
        mag_1 = 'g' #must be same with mag in the "plane"
        mag_2 = 'U' #the other magnitude
        err_1 = 'gerr'
        err_2 = 'Uerr'

    elif colour == 'gminr':
        plane = 'g-gminr' # just for naming folder and files
        colour = 'gminr'
        mag_1 = 'g' #must be same with mag in the "plane"
        mag_2 = 'r' #the other magnitude
        err_1 = 'gerr'
        err_2 = 'rerr'

    else:
        sys.exit('Wrong color!!!!')
else:
    sys.exit("type exactly 'AB' or 'Vega' (without quotes, of course)!")


n_bins = 15 #total number of bins in a field


## These are just strings!!!!
# If you're going to use these as string, then no problem.
# If you would like to use them as variables, IT IS A PROBLEM!!!!
# You need to call them from variable name space by using
# "vars()" function.
#
# Example:
# let say gmag = 15
# mag_1 give 'gmag'
# but vars()[mag_1]) gives 15.
# vars()[mag_1] ==> vars()['gmag'] ==> 15

# let say f_gmag = 16
# vars()['f_%s'%mag_1] ==> vars()['f_gmag'] ==> 16
```

```
#to see what's going on
print """
Main ingredients are:
    fits_file   =  %s
    plane       =  %s
    colour      =  %s
    mag_1       =  %s
    mag_2       =  %s
    err_1       =  %s
    err_2       =  %s
    binning     =  %s
""" % (fits_file, plane, colour, mag_1, mag_2, err_1, err_2, binning)

#sort the fits file according to mag_1 before using it.
#make a copy, use it (and at the end delete it)
# stilts, command line version of TOPCAT should be installed
if not os.path.exists('sorted-%s-%s.fits' %(plane,binning)):
    os.system("stilts tpipe cmd='sort %s' %s out=sorted-%s-%s.fits"
        %(mag_1,fits_file,plane,binning))

## Read the data and columns
fitspointer = pyfits.open('sorted-%s-%s.fits' %(plane,binning))
data = fitspointer[1].data

#to see what's going on
print "number of run=%s" % len(data.field('RUN'))
print "number of %s=%s" % (mag_1,len(data.field(mag_1)))

print "="*15 #cosmetic
print " "    #empty line

#create a folder to put the output files
os.system("mkdir -p ./%s" %(plane))
os.system("mkdir -p ./%s/%s" %(plane,binning))

path_folder = "./%s/%s" %(plane,binning)

#to see what's going on
print "%s has been created" % path_folder
```

```
print " "    #empty line
print "="*15 #cosmetic
print " "    #empty line

####_____________________________________________________
# Create a csv file to write the name of the files that are empty
# which means there is no blue object in that particular field.
# To be able to write a row from any field in any run to
# this file, I need to create the file before the run loop.

#define your file and give details of it:
#name and path
name_empty = '0_noblue_fields_%s.csv' %plane
path_empty = '%s/%s' %(path_folder,name_empty)

#open your file
empty_files = open(path_empty,'wb')

#name your writer
empty_writer = csv.writer(empty_files)

#write a row which is the header
empty_writer.writerow(['RUN','FIELD','Reason','Plane','Mag_sys','Binning'])

#flush the file to write the changes to disk.
empty_files.flush()

#to see what's going on
print "%s has been created in %s" %(name_empty,path_folder)
print " "    #empty line
print "="*15 #cosmetic
print " "    #empty line
####_____________________________________________________

#### Create a csv file to write all the data of blue ones.

#define your file and give details of it:
#name and path
name_all = '0_all_blues_%s.csv' %plane
```

```
path_all = '%s/%s' %(path_folder,name_all)

#open your file
all_blues = open(path_all,'wb')

#name your writer
blue_writer = csv.writer(all_blues)

#write a row which is the header
blue_header = []
for t in fitspointer[1].columns.names:
    blue_header.append(t)
blue_header.extend(['Plane','Mag_sys','Binning','bin_no','median','sigma'])
blue_writer.writerow(blue_header)

#flush it babe!
all_blues.flush()

#to see what's going on
print "%s has been created in %s" %(name_all,path_folder)
print " "    #empty line
print "="*15 #cosmetic
print " "    #empty line
####_____________________________________________________

if binning == 'binning1':
    name_skipped = '0_skipped_bins_%s.csv' %plane
    path_skipped = '%s/%s' %(path_folder,name_skipped)

    #open your file
    skipped_bins = open(path_skipped,'wb')

    #name your writer
    writer_skipped = csv.writer(skipped_bins)

    #write a row which is the header
    writer_skipped.writerow(['RUN','FIELD','bin','bin_bright',\
                             'bin_faint','n_stars', 'Plane',\
                             'Mag_sys','Binning'])
```

```
    #flush the file to write the changes to disk.
    skipped_bins.flush()

    #to see what's going on
    print "%s has been created in %s" %(name_skipped,path_folder)
    print " "    #empty line
    print "="*15 #cosmetic
    print " "    #empty line

#                  The End of SECTION 1
#==============================================================

#==============================================================
# SECTION 2: Preparing the data to selection process

## Remove objects has no magnitude or colour information.
## Just keep the ones that have both.

full = logical_and( logical_not(isnan(data.field(colour))),
                    logical_not(isnan(data.field(mag_1))))
# notice mag_1 and colour are both string

# there are some cells that are not empty but not usefull either.
# for example umag = -50.0  :s
# we need to remove those as well

# notice mag_1 and mag_2 are both string
good = full & (data.field(mag_1) > 10)
            & (data.field(mag_1) < 25)
            & (data.field(mag_2) > 10)
            & (data.field(mag_2) < 25)
            & (data.field(colour) > -3)
            & (data.field(colour) < 4)
# this number (10) should be
# as greater as possible to remove all nonsense datapoint.
# 10 is good enough. There is no star brighter than ~14 magnitude in
# our data, so we don't exclude any object.
```

```
#to see what's going on
print "="*15 #cosmetic
print " "    #empty
print "Does 'good' has False?"
print list(set(good))
print " "


good_data = data.field('RUN')[good]
print "%s out of %s star has colour and magnitude."
    % (len(good_data),len(data.field('RUN')))
print " "

###select data points that satisfies the condition e.g. "good" ones
g_data = data[good]

#to see what's going on
print "="*15 #cosmetic
print " "    #empty line
print "number of good_run = %s" % len(g_data.field('RUN'))
print "number of good_field = %s" % len(g_data.field('FIELD'))
print " "


#============================================================
#                  SECTION 3: Selection process.

# Apply the selection to all runs,
## one-by-one, separately, not all at once...
## you: OK, I got it!!
## me : Oh, sorry :)
##=========================================

run_list = list(set(data.field('RUN')))
        # set() shows the unique values in a list,
        # and list() writes them in a list.
run_list.sort()
# Example:
# >>> a = [1,1,2,2,2,3,4,5,5,6,6,7]
```

```
# >>> set(a)
# set([1, 2, 3, 4, 5, 6, 7])
# >>> list(set(a))
# [1, 2, 3, 4, 5, 6, 7]

#to see what's going on
print "="*15 #cosmetic
print " "    #empty line
print "There are %s runs in this FITS file." % len(run_list)
print "which are:"
print run_list

#In run_list we have field numbers. So, to apply selection
#method to each run, we only need a for loop.
for r in run_list:

    #to see what's going on
    print " "
    print "="*50
    print " "
    print "This is run %s." % r # r is the run number
    print " "
    print "lenght of run_list = %s" % len(run_list)
    print run_list

    #condition for being in this run
    run_to_use = (g_data.field('RUN') == r)

    #to see what's going on
    print "number of run_to_use=%s" % len(run_to_use)
    count_of_false = collections.Counter(run_to_use)
    print count_of_false

    #select data points that satisfies the condition,
    #that is observed in this run, and rename them.
    # !!!rename is necessary!!!
    r_data = g_data[run_to_use]

    # If there is no data
```

```
    if len(r_data) == 0:
        print "There is NO data in this run :("
        print " "
        print "="*50
        print " "
        empty_writer.writerow([r, 'ALL','No good data',
                               plane,system,binning])
        empty_files.flush()

        continue #skip this run and go to the next one

    #to see what's going on
    print "="*50
    print " "
    print r_data.field('RUN')
    print "number of r_run=%s" % (len(r_data.field('RUN')))

    if len(list(set(r_data.field('RUN')))) == 1:
        print "all r_runs equal to %s"
            % (list(set(r_data.field('RUN'))))[0]
    else:
        print """there is at least one different run here,
                 which is a problem.
                 see below:
              """
        forbidden_runs = list(set(r_data.field('RUN')))
        sys.exit("\n\n\n\n\n\n\n###################### \
            \n\n\n\n\n\n\n\n\n\n there is at least one different run here,\
             which is a problem.\n see below: \
             \n %s\n\n\n\n\n\n\n\n\n ######################"
             %(forbidden_runs))
    print "number of r_%s=%s" % (mag_1,len(r_data.field(mag_1)))
    print "number of r_field=%s" % len(r_data.field('FIELD'))
    print "="*50
    print " "

    ##============================================================
    ## Apply the selection to all fields,
    ## one-by-one, separately, not all at once
```

```
## you: I said, I got it!!
## me : Oh, sorry, again:)
##=======================================

field_list = list(set(r_data.field('FIELD')))

#to see what's going on
print "There are %s fields in this run." % len(field_list)
print "which are:"
print field_list

# In field_list we have field numbers
# So, to apply selection method to each field,
# we just need a for loop, yahooo :)
for f in field_list:
    print " "
    print "="*50
    print " "
    print "This is run%s field%s." % (r,f) # r is the run number
                                          # f is the field number
    print " "

    #to see what's going on
    print "number of field_list = %s" % len(field_list)
    print field_list


    #condition for being in this run
    field_to_use = (r_data.field('FIELD') == f)

    #to see what's going on
    print "number of field_to_use=%s" % len(field_to_use)
    count_of_false = collections.Counter(field_to_use)
    print count_of_false

    #select data points that satisfies the condition,
    #that is observed in this field, and rename them.
    # !!!rename is necessary!!!
    f_data = r_data[field_to_use]
```

```
if len(f_data) < 20*n_bins:
    print '''There are only
                    %s
                  data-points
                  in this field!!!
          ''' %len(f_data)
    empty_writer.writerow([r,f,'too less data in the field',\
                           plane, system, binning])
    empty_files.flush()
    continue

#to see what's going on
print "="*50
print " "
print "f_run is:"
print "="*15
print " "
print f_data.field('RUN')
print "number of f_run=%s" % (len(f_data.field('RUN')))
print "all f_runs equal to %s" % (list(set(f_data.field('RUN'))))[0]
print "number of f_%s=%s" % (mag_1,len(f_data.field(mag_1)))
print "number of f_field=%s" % len(f_data.field('FIELD'))
print "="*50
print " "


#========Create a ".csv" file to write "blue" ones==========
# In order to write data coming from all bins in a particular
# field into one single file, we need to create this file
# outside of(before) the binning loop and in the field loop.


#define your file and give details of it:
#_____________________________________________________________
#Funny thing below (if and elif chain) is just for fun:
#To have filenames like 'r01f03.csv' instead of 'r1f3.csv'
#Those zeros are important for me, I love them :)
#If you don't need those zeros, you can use only the last
```

```
#'field_file = open(...)...' part by deleting between "from here"
#and "till here"!
#Best regards :)
#-------------------------------------------------------------

# "from here"
if (f_data.field('RUN')[0] < 10)
    & (f_data.field('FIELD')[0] < 10):
    name_field_file = 'r0%s_f0%s' %(r,f)

elif (f_data.field('RUN')[0] >= 10)
    & (f_data.field('FIELD')[0] < 10):
    name_field_file = 'r%s_f0%s' %(r,f)

elif (f_data.field('RUN')[0] < 10)
    & (f_data.field('FIELD')[0] >= 10):
    name_field_file = 'r0%s_f%s' %(r,f)

elif (f_data.field('RUN')[0] >= 10)
    & (f_data.field('FIELD')[0] >= 10):
# "till here"
# and of course you need to de-indent part below if you delete above.
    name_field_file = 'r%s_f%s' %(r,f)

path_field_file = '%s/%s.csv' %(path_folder,name_field_file)
field_file = open(path_field_file,'wb')

#name your writer
fbyf_writer = csv.writer(field_file)

#write headers(column names) to the file
fbyf_header = []
for h in fitspointer[1].columns.names:
    fbyf_header.append(h)
fbyf_header.extend(['Plane','Mag_sys',\
                    'Binning',"bin_no",\
                    'median','sigma'])
fbyf_writer.writerow(fbyf_header)
field_file.flush()
```

```
#============================================================
#================== Gotta Bin'em all!!! ====================
#============================================================
given_labels = [] #workaround for multiple legends of the plots
plt.plot(f_data.field(colour), f_data.field(mag_1),\
         'ro', markersize=5, label='r%sf%s goods'%(r,f))
given_labels.append('r%sf%s goods'%(r,f))

if binning == 'binning1':
    #defining some variables

    # magnitude of dimmest star in the field
    faintest_mag = max(f_data.field(mag_1))
    # magnitude of brightest star in the field
    brightest_mag = min(f_data.field(mag_1))

    #In order not to exclude faintest star in the binning process,
    faintest_mag = faintest_mag + 0.1
    #I'm stretching the border outwards.

    # I think no need to say
    # "The brighter the magnitude, the smaller the number"
    #               :)

    #to see what's going on
    print "faintest_mag = %.20f" % faintest_mag
    print "brightest_mag= %.20f" % brightest_mag

    #width of any bin
    w_bin  = (faintest_mag - brightest_mag)/n_bins

    #to see what's going on
    print "w_bin     =  %.10f" % w_bin
    print "="*15
    print " "

    #============ Actual binning part! ============
    for i in range(n_bins):
```

```
print "="*15
print " "

#borders of a bin
bin_bright = brightest_mag + i*w_bin    #bright border
bin_faint = brightest_mag + (i+1)*w_bin #faint border

#for last bin:
# I want that star at the end :p
# I don't want to lose it because of rounding.
if i == n_bins - 1:
    bin_faint = faintest_mag
    print " "
    print "="*15
    print "This is bin15"
    print "="*15
    print " "

bin_no = i+1 #bin number

#to see what's going on
print "bin_no    = %.0f" % bin_no
print "bin_bright= %.2f" % bin_bright
print "bin_faint = %.2f" % bin_faint
print "w_bin     =  %.2f" % w_bin
print " "

the_bin = ((f_data.field(mag_1)) >= bin_bright)
        & ((f_data.field(mag_1)) < bin_faint)
# Stretching the border makes sense now, doesn't it? :)
# Check out the second part of the condition.

#select data points that satisfies the condition,
#that is being in this bin, and rename them.
# !!!rename is necessary!!!
bin_data = f_data[the_bin]

#info about bin
```

```
print "There are %s stars in this bin" % len(bin_data)
print " "

# If there are too less star in a bin, just skip it!
if len(bin_data) < 20:
    print """

    There are too less object in this bin.

             So just skipping it...

    ======================================
    """
    writer_skipped.writerow([r, f, bin_no, bin_bright,
                             bin_faint, len(bin_data),
                             plane, system, binning])

    skipped_bins.flush()

    if 'skipped bin' in given_labels:
        plt.plot(bin_data.field(colour),
                 bin_data.field(mag_1),
                 'o', color='0.5', markersize=5)
    else:
        plt.plot(bin_data.field(colour),
                 bin_data.field(mag_1),
                 'o', color='0.5', markersize=5,
                 label='skipped bin')
        given_labels.append('skipped bin')

    continue

#=====================================================
# ============ Actual Selection Part!!! =============
#=====================================================

#find the median in colour axis
med = median(bin_data.field(colour))
print "Median =%f" % med
```

```
print " "

#condition for being on left(blue)-side of the median
left = bin_data.field(colour) < med

#values of blue-siders:
#select data points that satisfies the condition,
#that is being on blue-side, and rename them.
# !!!rename is necessary!!!
left_data = bin_data[left]

#information
print "There are %s stars on the blue side of median"
    %len(left_data)
print " "

#sigma calculation
residuals = left_data.field(colour) - med
sigma = sqrt(sum(residuals**2)/len(residuals))

print "Sigma =%f" % sigma
print " "

#3sigma-cutting
sigma_cut = med - 3*sigma

#condition for being blue!
#Distance To Sigma Cut
distance = abs(left_data.field(colour) - sigma_cut)

blue = (left_data.field(colour) < sigma_cut)
     & ((left_data.field(err_1)*3) < distance)
     & ((left_data.field(err_2)*3) < distance)

#select data points that satisfies the condition,
#that is being blue, and rename them.
# !!!rename is necessary!!!
blue_data = left_data[blue]
```

```
#If there is no blue one:
if len(blue_data) == 0:
    print """There is NO "blue" object in this bin:("""
    print " "
    print "="*50
    print " "

    if 'no blue' in given_labels:
        plt.plot(bin_data.field(colour),
                 bin_data.field(mag_1),
                 'yo', markersize=5)
    else:
        plt.plot(bin_data.field(colour),
                 bin_data.field(mag_1),
                 'yo', markersize=5, label='no blue')
        given_labels.append('no blue')

    if 'median' in given_labels:
        plt.plot([med,med],
                 [min(bin_data.field(mag_1)),
                  max(bin_data.field(mag_1))],
                 'g-', linewidth=2.0)
    else:
        plt.plot([med,med],
                 [min(bin_data.field(mag_1)),
                  max(bin_data.field(mag_1))],
                 'g-', linewidth=2.0, label='median')
        given_labels.append('median')

    if '3sigma' in given_labels:
        plt.plot([sigma_cut,sigma_cut],
                 [min(bin_data.field(mag_1)),
                  max(bin_data.field(mag_1))],
                 'k-', linewidth=2.0)
    else:
        plt.plot([sigma_cut,sigma_cut],
                 [min(bin_data.field(mag_1)),
                  max(bin_data.field(mag_1))],
                 'k-', linewidth=2.0, label='3sigma')
```

```
                given_labels.append('3sigma')

        continue
        #going to the next bin
        #if this is the last bin in this field, moving forward.

    #If there are some:
    print """There are %s "blue" stars in this bin."""
         % len(blue_data)
    print " "

    #============================================================
    # ============ Write the blue objects to the file ============
    #============================================================

    print '''
    Writing data to both files,
    field-specific csv file and the big file...

    '''

    #write data: mind the order of headers!!!
    for i in blue_data:
        satir = list(i)
        satir.extend([plane,system,binning,bin_no,med,sigma])

        fbyf_writer.writerow(satir)
        blue_writer.writerow(satir)

    print '''
    Data of blue objects from Bin %s has been added
    to the both files.
    ''' % bin_no
    print "="*30
    print " "
    field_file.flush()
    all_blues.flush()

    if 'blue ones' in given_labels:
```

```
                plt.plot(blue_data.field(colour),
                         blue_data.field(mag_1),
                         'bo', markersize=5)
            else:
                plt.plot(blue_data.field(colour),
                         blue_data.field(mag_1),
                         'bo', markersize=5, label='blue ones')
                given_labels.append('blue ones')

            if 'median' in given_labels:
                plt.plot([med,med],
                         [min(bin_data.field(mag_1)),
                          max(bin_data.field(mag_1))],
                         'g-', linewidth=2.0)
            else:
                plt.plot([med,med],
                         [min(bin_data.field(mag_1)),
                          max(bin_data.field(mag_1))],
                         'g-', linewidth=2.0, label='median')
                given_labels.append('median')

            if '3sigma' in given_labels:
                plt.plot([sigma_cut,sigma_cut],
                         [min(bin_data.field(mag_1)),
                          max(bin_data.field(mag_1))],
                         'k-', linewidth=2.0)
            else:
                plt.plot([sigma_cut,sigma_cut],
                         [min(bin_data.field(mag_1)),
                          max(bin_data.field(mag_1))],
                         'k-', linewidth=2.0, label='3sigma')
                given_labels.append('3sigma')

            #going back to do the same thing for next bin
            #if this is the last bin in this field, moving forward.

    elif binning == 'binning2':
        #defining some variables
```

```
#n_bins, number of bins, is defined at the beginning

N_star=len(f_data) #total number of stars in the field

n_star=N_star/n_bins #number of stars in every bin

print "There are %s bins in every field" %n_bins
print "There are %s stars in this field" % N_star
print "There should be %s stars in every bin" %n_star
print "="*15
print " "

#============ Actual binning part! ============

for i in range(n_bins):
    bin_no = i+1
    print "This is Bin %s" % bin_no

    #define new arrays that contains data only for this bin
    # !!!rename is necessary!!!
    if i < n_bins-1:
        bin_data = f_data[n_star*i:n_star*(i+1)]


    elif i == n_bins-1:
        bin_data = f_data[n_star*i:]

    else:
        print """
        Yok artik Ali Sami!!!
        """

    #info about bin
    print "There are %s stars in this bin" % len(bin_data)
    print " "

    #=================================================
    # ============ Actual Selection Part!!! =============
    #=================================================
```

```
#find the median in colour axis
med = median(bin_data.field(colour))
print "Median =%f" % med
print " "

#condition for being on left(blue)-side of the median
left = bin_data.field(colour) < med

#values of blue-siders:
#select data points that satisfies the condition,
#that is being on blue-side, and rename them.
# !!!rename is necessary!!!
left_data = bin_data[left]

#information
print "There are %s stars on the blue side of median"
    %len(left_data.field('RUN'))
print " "

#sigma calculation
residuals = left_data.field(colour) - med
sigma = sqrt(sum(residuals**2)/len(residuals))

print "Sigma =%f" % sigma
print " "

#3sigma-cutting
sigma_cut = med - 3*sigma

#condition for being blue!
 #Distance To Sigma Cut
distance = abs(left_data.field(colour) - sigma_cut)

blue    = (left_data.field(colour) < sigma_cut)
        & ((left_data.field(err_1)*3) < distance)
        & ((left_data.field(err_2)*3) < distance)

#select data points that satisfies the condition,
```

```
#that is being blue, and rename them.
# !!!rename is necessary!!!
blue_data = left_data[blue]

#If there is no blue one:
if len(blue_data) == 0:
    print """There is NO "blue" object in this bin:("""
    print " "
    print "="*50
    print " "

    if 'no blue' in given_labels:
        plt.plot(bin_data.field(colour),
                 bin_data.field(mag_1),
                 'yo', markersize=5)
    else:
        plt.plot(bin_data.field(colour), b
                 in_data.field(mag_1),
                 'yo', markersize=5, label='no blue')
        given_labels.append('no blue')

    if 'median' in given_labels:
        plt.plot([med,med],
                 [min(bin_data.field(mag_1)),
                  max(bin_data.field(mag_1))],
                 'g-', linewidth=2.0)
    else:
        plt.plot([med,med],
                 [min(bin_data.field(mag_1)),
                  max(bin_data.field(mag_1))],
                 'g-', linewidth=2.0, label='median')
        given_labels.append('median')

    if '3sigma' in given_labels:
        plt.plot([sigma_cut,sigma_cut],
                 [min(bin_data.field(mag_1)),
                  max(bin_data.field(mag_1))],
                 'k-', linewidth=2.0)
    else:
```

```
            plt.plot([sigma_cut,sigma_cut],
                     [min(bin_data.field(mag_1)),
                      max(bin_data.field(mag_1))],
                     'k-', linewidth=2.0, label='3sigma')
            given_labels.append('3sigma')

        continue

    #If there are some:
    print """There are %s "blue" stars in this bin.

    """ % len(blue_data)

    #=================================================
    # ============ Write the blue objects to the file ===
    #=================================================

    print '''
    Writing data to both files, field-specific csv file
    and the big file...
    '''
    #write data: mind the order of headers!!!
    for i in range(len(blue_data)):
        satir = list(blue_data[i])
        satir.extend([plane,system,binning,bin_no,med,sigma])

        fbyf_writer.writerow(satir)
        blue_writer.writerow(satir)

    print '''
    Data of blue objects from Bin %s has been added
    to the both files.
    ''' % bin_no
    print "="*30
    print " "
    field_file.flush()
    all_blues.flush()

    xerrp = [max(left_data.field(err_1)[i],
```

```
                left_data.field(err_2)[i])
            for i in range(len(left_data.field(err_1)))]
xerrn = zeros(len(left_data.field(err_1)))
yerrp = zeros(len(left_data.field(err_1)))
yerrn = zeros(len(left_data.field(err_1)))

if 'blue ones' in given_labels:
    plt.plot(blue_data.field(colour),
             blue_data.field(mag_1),
             'bo', markersize=5)
else:
    plt.plot(blue_data.field(colour),
             blue_data.field(mag_1),
             'bo', markersize=5, label='blue ones')
    given_labels.append('blue ones')

if 'median' in given_labels:
    plt.plot([med,med],
             [min(bin_data.field(mag_1)),
              max(bin_data.field(mag_1))],
             'g-', linewidth=2.0)
else:
    plt.plot([med,med],
             [min(bin_data.field(mag_1)),
              max(bin_data.field(mag_1))],
             'g-', linewidth=2.0, label='median')
    given_labels.append('median')

if '3sigma' in given_labels:
    plt.plot([sigma_cut,sigma_cut],
             [min(bin_data.field(mag_1)),
              max(bin_data.field(mag_1))],
             'k-', linewidth=2.0)
else:
    plt.plot([sigma_cut,sigma_cut],
             [min(bin_data.field(mag_1)),
              max(bin_data.field(mag_1))],
             'k-', linewidth=2.0, label='3sigma')
    given_labels.append('3sigma')
```

```
        #going back to do the same thing for next bin
        #if this is the last bin in this field, moving forward.

    else:
        sys.exit("Type exactly 'binning1' or 'binning2'\
                 (without quotes, of course)")

    #close the file
    field_file.close()

    #If there is no blue in this field and csv file consists of only
    # headers, I would like to delete it.

    # read the file in...
    read_to_count = csv.reader(open(path_field_file, 'rb'))

    #count the rows!
    row_count = sum(1 for row in read_to_count)
    print '''
    there are %s blue objects in the run %s field %s'''
    %(row_count-1,r,f)

    # delete it if it is empty
    if row_count == 1:  #1 row means only header
        print "There is NO 'blue' object in this field :("
        print "So, deleting the empty csv file..."
        print " "
        print " "

        #Before removing it, I would like to note its name.
        empty_writer.writerow([r, f, 'no blue',plane,system,binning])
        print "Name of empty file has been added to the list."
        empty_files.flush()

        #remove it
        os.system("rm %s" %(path_field_file))
        print " "
```

```
            print "="*50

            plt.close() # otherwise, you'll see refugee plots from this field
                        # on the next field's plot
            continue

        #get rid of 'nan's
        os.system("sed 's/nan//g' %s > tmp && mv tmp %s"
                %(path_field_file,path_field_file))

        #last touches to the graph and then save it.
        plt.xlabel(colour)
        plt.ylabel(mag_1)

        plt.legend(prop={'size':10}, fancybox=True)

        plt.title('Run %s Field %s \n --- Blue Ones ---' %(r,f))
        plt.axis([-3,4,26,12])
        plt.savefig('%s/%s_blues.png' %(path_folder,name_field_file))
        print '%s/%s_blues.png has been saved! Yayy! :)'
            %(path_folder,name_field_file)
        plt.close()

        #going to do the same thing for next field.
        #if this is last field in this run, moving forward.

    #going to do the same thing for next run.
    #if this is last run, moving forward to end process.

empty_files.close()
print "empty_files is closed"

all_blues.close()
print "all_blues is closed"

#delete the sorted fits file
os.system('rm sorted-%s-%s.fits' %(plane,binning))

#get rid of 'nan's
```

```
os.system("sed 's/nan//g' %s > tmp && mv tmp %s" %(path_all,path_all))

print " "
print "All png files are being combined into a pdf file..."
os.system("/usr/bin/convert %s/*.png %s/all_fields.pdf"
    %(path_folder,path_folder))
print " "
print "%s/all_fields.pdf is created!" %(path_folder)
print " "

print " ================THE END================ "
```

A.1.2 Blue Object Selection on Colour-Colour plane

```
#!/home/osa/Apps/Epd/bin/python

''' Blue selection from (U-g)-(g-r) plane
            using RATS data.

written by Onur SATIR from Armagh Observatory

                2013


Usage: ./osa019_col-col.py AB
       ./osa019_col-col.py Vega
'''

from pylab import *  # import everything in the module
import numpy as np   # import the module and use a shorter namespace
import pyfits        # to be able to handling fits files
import csv           # to be able to handling csv files
import math
import collections
import os
import time
import matplotlib.pyplot as plt
from matplotlib import rc
```

```
#rc('text', usetex=True)

def cosmetic():
    '''
    just for fun :p
    '''
    print " "    #empty line
    print "="*15 #15 equal signs
    print " "    #empty line

def track_sigma(data,colx,coly):
    '''
    calculates and returns
    sigma and 3sigma curve
    for a given curve
    '''
    x = data.field(colx)
    y = data.field(coly)

    # fit --> y = mx + c
    p = np.polyfit(x,y,1)
    # parameters --> p = [m, c]

    # distance from the fit for every data point
    d = abs(y - p[0]*x - p[1]) / (sqrt(p[0]**2 + 1))

    # sigma
    sigma = mean(d)

    # 3sigma curve
    threesig = np.array([x + 3*sigma,y - 3*sigma])

    return sigma, threesig


system = sys.argv[1]
if system == 'AB':
    plane    = 'Uming-gminr_ab'     # Names must be identical
    colour_x = 'gminr_ab'           # with the column names in
```

```
    colour_y = 'Uming_ab'           # the fits file!!!
    err_1    = 'Uerr'
    err_2    = 'gerr'
    err_3    = 'rerr'
    track_x  = 'gminr0ab'
    track_y  = 'Uming0ab'

elif system == 'Vega':
    plane    = 'Uming-gminr'
    colour_x = 'gminr'
    colour_y = 'Uming'
    err_1    = 'Uerr'
    err_2    = 'gerr'
    err_3    = 'rerr'
    track_x  = 'gminr0'
    track_y  = 'Uming0'

else:
    sys.exit("type exactly 'AB' or 'Vega' (without quotes, of course)!")

#data to use. You must give the full path!
fits_file      = '/home/osa/Dropbox/PhD/Work/201305-New_colours/int3-8eso2.fits'
mainsq_colours = '/home/osa/Dropbox/PhD/Work/Catalogues/UVEXcolours_anakol.fits'
WD_colours     = '/home/osa/Dropbox/PhD/Work/Catalogues/UVEXcolours_DA-DB.fits'
#to see what's going on
print """
Main ingredients are:
    fits_file      =  %s
    mainsq_colours =  %s
    WD_colours     =  %s
    plane          =  %s
    colour_x       =  %s
    colour_y       =  %s
    err_1          =  %s
    err_2          =  %s
    err_3          =  %s
    track_x        =  %s
    track_y        =  %s
```

```
""" % (fits_file, mainsq_colours, WD_colours, plane,
       colour_x, colour_y, err_1, err_2, err_3,
       track_x, track_y)

## Read data and columns
fitspointer = pyfits.open(fits_file)
data = fitspointer[1].data

maindata = pyfits.open(mainsq_colours)[1].data
main_bool = np.array([True if x.endswith('V') else False for x
            in maindata.field('SpType')])
f6v_bool = maindata.field('SpType') == 'F6V'
mainsq = maindata[main_bool]
f6v = maindata[f6v_bool]

WD_col = pyfits.open(WD_colours)[1].data
bda_bool = WD_col.field('SpT') == 'B-DA'
kda_bool = WD_col.field('SpT') == 'K-DA'
kdb_bool = WD_col.field('SpT') == 'K-DB'
bda = WD_col[bda_bool]
kda = WD_col[kda_bool]
kdb = WD_col[kdb_bool]

#to see what's going on
print "number of run=%s" % len(data.field('RUN'))
print "number of %s =%s" % (colour_x,len(data.field(colour_x)))
print "number of %s =%s" % (colour_y,len(data.field(colour_y)))
cosmetic()

## Remove objects has not both colours.
full = logical_and(logical_not(isnan(data.field(colour_x))),
                   logical_not(isnan(data.field(colour_y)))
                  )

# filter data according to colours
good = full & (data.field(colour_x) > -3)
            & (data.field(colour_x) < 3)
            & (data.field(colour_y) > -3)
            & (data.field(colour_y) < 3)
```

```
# these numbers are choosen by me depending on nothing :)

#to see what's going on
cosmetic()
print "Does 'good' has 'False' in it?"
print list(set(good))
print " "

### select data points that satisfies the condition e.g. "good" ones
### and rename it!
g_data = data[good]

print "%s out of %s star has both colours." % (len(g_data),len(data))
cosmetic()

# Create files and folders that will be needed

#crate folders to put output files
os.system("mkdir -p ./%s" %(plane))
path_folder = "./%s" %(plane)

#to see what's going on
print "%s has been created" % path_folder
cosmetic()

# Create a csv file to write the name of files that are empty
# means there is no blue object in that particular field.
# To be able to write a row from any field in any run to
# this file, I need to create the file before the run loop.

#define your file and give details of it:
#name and path
name_empty = '0_noblue_fields_%s.csv' %plane
path_empty = '%s/%s' %(path_folder,name_empty)

#open your file
empty_files = open(path_empty,'wb')

#name your writer
```

```
empty_writer = csv.writer(empty_files)

#write the header row
empty_writer.writerow(['run','field','reason',"Plane","Mag_sys","Binning"])

#flush the file to write the changes to the disk.
empty_files.flush()

#to see what's going on
print "%s has been created in %s" %(name_empty,path_folder)
cosmetic()

# Create a csv file to write all the data of blue ones.
#define your file and give details of it:
#name and path
name_all = '0_all_blues_%s.csv' %plane
path_all = '%s/%s' %(path_folder,name_all)

#open your file
all_blues = open(path_all,'wb')

#name your writer
blue_writer = csv.writer(all_blues)

#write the header row by taking column names from fits file,
blue_header = []
for h in fitspointer[1].columns.names:
    blue_header.append(h)
# and adding a couple of extra column names.
blue_header.extend(["Plane","Mag_sys","Binning","med_x","sigma_x",\
    "med_y","sigma_y"])
blue_writer.writerow(blue_header)

#flush it babe!
all_blues.flush()

#to see what's going on
print "%s has been created in %s" %(name_all,path_folder)
cosmetic()
```

```
#                              Selection process.
## Apply the selection to all runs,
## one-by-one, seperatly, not all at once...
## you: OK, I got it!!
## me : Oh, sorry :)

run_list = list(set(data.field('RUN')))
# set() shows and sorts the unique values in a list,
# and list() writes them in a list.

run_list.sort() #set() should sort but it doesn't somehow!
#to see what's going on
cosmetic()
print "There are %s runs in this FITS file." % len(run_list)
print "which are:"
print run_list

# In run_list we have run numbers. So, to apply selection
# method to each run, we only need a for loop, yahooo :)
for r in run_list:
    #to see what's going on
    cosmetic()
    print "This is run %s." % r # r is the run number
    print " "
    print "number of run_list = %s" % len(run_list)
    print run_list

    #condition for being in this run
    run_to_use = (g_data.field('RUN') == r)

    #to see what's going on
    print "number of run_to_use=%s" % len(run_to_use)
    count_false = collections.Counter(run_to_use)
    print count_false

    #select data points that satisfies the condition,
    #that is being observed in this run, and rename them.
    # !!!rename is necessary!!!
```

```
r_data = g_data[run_to_use]

# If there is no data
if len(r_data.field('RUN')) == 0:
    print "There is NO data in this run :("
    cosmetic()
    empty_writer.writerow([r, 'ALL', 'no data in this run',\
        plane, system, "No_binning"])
    empty_files.flush()
    continue

#to see what's going on
cosmetic()
print "number of r_run=%s" % (len(r_data.field('RUN')))

if len(list(set(r_data.field('RUN')))) != 1:
    print """there is at least one different run here, which is a problem.
             see below:
          """
    forbidden_runs = list(set(r_data.field('RUN')))
    sys.exit('''\n\n\n\n\n\n\n######################
                \n\n\n\n\n\n\n\n\n\n %s\n\n\n\n\n\n\n\n\n
                ######################''' %(forbidden_runs))

print "all r_runs equal to %s" %r_data.field('RUN')[0]
print "number of r_%s=%s" % (colour_x,len(r_data.field(colour_x)))
print "number of r_field=%s" % len(r_data.field('FIELD'))
cosmetic()
##============================================================
## Apply the selection to all fields,
## one-by-one, seperatly, not all at once...
## you: I said, I got it!!
## me : Oh, sorry again:)
##========================================
field_list = list(set(r_data.field('FIELD')))

#to see what's going on
print "There are %s fields in this run." % len(field_list)
print "which are:"
```

```
print field_list

# In field_list we have field numbers
# So, to apply selection method to each field,
# we just need a for loop, yahooo :)
for f in field_list:
    #to see what's going on
    cosmetic()
    print "This is run%s field%s." % (r,f) # r is the run number
                                          # f is the field number
    #condition for being in this run
    field_to_use = (r_data.field('FIELD') == f)

    #to see what's going on
    print "length of field_to_use = %s" % len(field_to_use)
    count_false = collections.Counter(field_to_use)
    print count_false

    #select data for this field
    # !!!rename is necessary!!!
    f_data = r_data[field_to_use]

    # min and max.s for the field to use later for plotting
    minx = min(f_data.field(colour_x))
    maxx = max(f_data.field(colour_x))
    miny = min(f_data.field(colour_y))
    maxy = max(f_data.field(colour_y))


    if len(f_data) < 20:
        print '''There are only

                        %s
                    data-points
                    in this field!!!
              ''' % len(f_data)
        empty_writer.writerow([r,f,'too less data in the field',\
            plane, system, "No_binning"])
        empty_files.flush()
```

```
        continue

    #to see what's going on
    cosmetic()
    print "number of f_run=%s" % (len(f_data.field('RUN')))
    print "set(f_run) = %s" % (set(f_data.field('RUN')))
    print "number of f_%s=%s" % (colour_x,len(f_data.field(colour_x)))
    print "number of f_field=%s" % len(f_data.field('FIELD'))
    cosmetic()

    #========Create a ".csv" file to write "blue" ones==========
    # In order to write data coming from all bins in a particular
    # field into one single file, we need to create this file
    # outside of the binning loop and in the field loop.

    #define your file and give details of it:
    field_file_name = 'r%02d_f%02d' %(r,f)
    path_field_file = '%s/%s.csv' %(path_folder,field_file_name)
    field_file = open(path_field_file, 'wb')

    #name your writer
    fbyf_writer = csv.writer(field_file)
    #fbyf -> field by field

    #write headers(column names) to the file
    fbyf_header = []
    for h in fitspointer[1].columns.names:
        fbyf_header.append(h)
    fbyf_header.extend(["Plane","Mag_sys","Binning","med_x",\
        "sigma_x","med_y","sigma_y"])
    fbyf_writer.writerow(fbyf_header)

    # ======== CCD of the field ========
    plt.plot(f_data.field(colour_x), f_data.field(colour_y),
        'ro', markersize=5)

    plt.xlabel('g\' - r\'')
    plt.ylabel('U - g\'')
```

```
#plt.title('Run %s Field %s' %(r,f))
plt.axis([minx-0.1,maxx+0.1,maxy+0.3,miny-0.2])
plt.savefig('%s/%s_0_all.png' %(path_folder,field_file_name))
print '%s/%s_0_all.png has been saved! Yayy! :)'
    %(path_folder,field_file_name)
plt.close()

# ============ Actual Selection Part!!! =============

#           Get rid off 'purple' objects!
# iteration to fit data a line (y = mx + c) properly.

fit_data = f_data
for k in range(100):
    x = fit_data.field(colour_x)
    y = fit_data.field(colour_y)

    # fit the data a line (y = mx + c)
    vars()['p%s'%k] = np.polyfit(x,y,1)
    # parameters --> pk = [m, c]

    # distance from the fit for every data point
    d = (abs(y - vars()['p%s'%k][0]*x - vars()['p%s'%k][1]))
        / (sqrt(vars()['p%s'%k][0]**2 + 1))

    # sigma
    sig = mean(d)

    # condition to be in 3sigma
    keep = d < 3*sig

    # data that satisfies this condition
    fit_data = fit_data[keep]

    if k == 0:
        continue # Don't do following and go to next step of the iteration

    # delta m(slope)
    dm = vars()['p%s'%k][0] - vars()['p%s'%(k-1)][0]
```

```
        plt.plot(f_data.field(colour_x), f_data.field(colour_y),
            'ro', markersize=5)
        plt.plot(x, y, 'go', markersize=5)
        plt.plot(x, (x*vars()['p%s'%k][0]+vars()['p%s'%k][1]),
            'b-', markersize=5)

        #plt.xlabel(colour_x)
        #plt.ylabel(colour_y)
        plt.xlabel('g\' - r\'')
        plt.ylabel('U - g\'')

        plt.title('Run %s Field %s'
            %(f_data.field('RUN')[0],f_data.field('FIELD')[0]))
        plt.axis([minx-0.1,maxx+0.1,maxy+0.3,miny-0.2])

        if dm > 0.01: #to keep the iteration going
            continue

        p = vars()['p%s'%k]

        print "%s iteration has been done and finally fit is good\
               enough :)" %k

        print " "

        plt.text(-2.2, -2.2 , r"%s iterations"%k)
        plt.savefig('%s/%s_1_fit.png'
            %(path_folder,field_file_name))
        print '%s/%s_1_fit.png has been saved! Yayy! :)'
            %(path_folder,field_file_name)

        plt.close()

        break

print '''
==------------------------==
        m = %s
```

```
        c = %s

      ''' %(p[0],p[1])

# the fit (p) has arrived :)

# calculate sigma of data (whole data) according to
# that fitted line

# distance
d   = abs(f_data.field(colour_y)
    - p[0]*f_data.field(colour_x)
    - p[1]) / sqrt(p[0]**2 + 1)
# sigma
sig = mean(d)
print '''
       sigma of fit = %s
==------------------------==
    '''  %(sig)
keep = d < 3*sig

new_data = f_data[keep]

# ======== CCD Plot of "de-purpled" data with best fit ==============
plt.plot(f_data.field(colour_x), f_data.field(colour_y),
        'ro', markersize=5)
plt.plot(new_data.field(colour_x), new_data.field(colour_y),
        'o', markerfacecolor='#F2FF00', markersize=5)
plt.plot(x, (x*p[0]+p[1]), 'b-', markersize=5)

#plt.xlabel(colour_x)
#plt.ylabel(colour_y)
plt.xlabel('g\' - r\'')
plt.ylabel('U - g\'')

plt.title('Run %s Field %s' %(r,f))
plt.axis([minx-0.1,maxx+0.1,maxy+0.3,miny-0.2])
plt.savefig('%s/%s_2_dep.png' %(path_folder,field_file_name))
print '%s/%s_2_dep.png has been saved! Yayy! :)'
```

```
    %(path_folder,field_file_name)
plt.close()

#-------------------------------------------------------
#                  Selection, finally!
#-------------------------------------------------------

# ================== # X-axis # ======================

#find the median in x-axis
med_x = median(new_data.field(colour_x))
print "Median =%f" % med_x
print " "

#condition for being on left(blue)-side of the median
left = new_data.field(colour_x) < med_x

#values of blue-siders:
#select data points that satisfies the condition,
#that is being on blue-side, and rename them.
# !!!rename is necessary!!!
left_data = new_data[left]

#information
print " ============    X-axis    ================= "
print "There are %s stars on the blue side of median"
    % len(left_data.field('RUN'))
print " "

#sigma calculation
residuals_x = left_data.field(colour_x) - med_x
sigma_x = sqrt(sum(residuals_x**2)/len(residuals_x))

print "Sigma =%f" % sigma_x
print " "

#3sigma-cutting
sigma_cut_x = med_x - 3*sigma_x
```

```
#condition for being blue in x-colour!
#Distance To Sigma Cut
distance_x = abs(f_data.field(colour_x) - sigma_cut_x)

err_x = f_data.field(err_2) + f_data.field(err_3)

if np.isnan(np.sum(err_x)):
    blue_x = (f_data.field(colour_x) < sigma_cut_x)
    no_err_x = True
else:
    blue_x  = (f_data.field(colour_x) < sigma_cut_x)
            & ((err_x*3) < distance_x)
    no_err_x = False

blue_x_data = f_data[blue_x]

if len(blue_x_data) == 0:
    print """There is NO "blue" object in %s:(""" %colour_x
    cosmetic()

    # CCD Plot of "de-purpled" data with med and sigma cuts
    plt.plot(f_data.field(colour_x),
             f_data.field(colour_y),
             'ro', markersize=5)
    plt.plot(new_data.field(colour_x),
             new_data.field(colour_y),
             'o', markerfacecolor='#F2FF00', markersize=5)
    plt.plot([med_x,med_x],
             [min(f_data.field(colour_y)),
                max(f_data.field(colour_y))],
             'g-', linewidth=2.0)
    plt.text((med_x-0.25), (max(f_data.field(colour_y)+0.25)),
             r'$Median_x$')
    plt.plot([sigma_cut_x,sigma_cut_x],
             [min(f_data.field(colour_y)),
             max(f_data.field(colour_y))], 'g-', linewidth=2.0)
    plt.text((sigma_cut_x-0.25),
            (max(f_data.field(colour_y)+0.25)), r'$3\sigma _x$')
```

```
            plt.text(2, -2, r'No $Median_y$')
            plt.text(2, -1.5, r'No $\sigma _y$')
            plt.text(-2, -2, r'NO BLUE object')
            if no_err_x:
                plt.text(-2, -1.5, r'No error data')

#             plt.xlabel(colour_x)
#             plt.ylabel(colour_y)
            plt.xlabel('g\' - r\'')
            plt.ylabel('U - g\'')

            plt.title('Run %s Field %s' %(r,f))
            plt.axis([minx-0.1,maxx+0.1,maxy+0.3,miny-0.2])
            plt.savefig('%s/%s_3_blue.png'
                %(path_folder,field_file_name))
            print '%s/%s_3_blue.png has been saved! Yayy! :)'
                %(path_folder,field_file_name)
            plt.close()

            empty_writer.writerow([r, f, 'no blue in colour_x',
                                   plane, system, "No_binning"])
            print "Name of empty file has been added to the list."
            empty_files.flush()

            continue
        # ================== # Y-axis # ==================

        #find the median in y-axis
        med_y = median(new_data.field(colour_y))
        print "Median =%f" % med_y
        print " "

        #condition for being on up(blue)-side of the median
        up = new_data.field(colour_y) < med_y

        #values of blue-siders:
        #select data points that satisfies the condition,
        #that is being on blue-side, and rename them.
        # !!!rename is necessary!!!
```

```
up_data = new_data[up]

#information
print " ============    Y-axis    ================= "
print "There are %s stars on the blue side of median"
    % len(up_data.field('RUN'))
print " "

#sigma calculation
residuals_y = up_data.field(colour_y) - med_y
sigma_y = sqrt(sum(residuals_y**2)/len(residuals_y))

print "Sigma_y =%f" % sigma_y
print " "

#3sigma-cutting
sigma_cut_y = med_y - 3*sigma_y

#condition for being blue in y-colour!
#Distance To Sigma Cut
distance_y = abs(blue_x_data.field(colour_y) - sigma_cut_y)

err_y = blue_x_data.field(err_1) + blue_x_data.field(err_2)

# the ones that in blue_X_data at the same time
# at the upper side of sigma_cut_Y are the ones
# we are looking for!

if np.isnan(np.sum(err_y)):
    blue_y = (blue_x_data.field(colour_y) < sigma_cut_y)
    no_err_y = True
else:
    blue_y  = (blue_x_data.field(colour_y) < sigma_cut_y)
            & ((err_y*3) < distance_y)
    no_err_y = False

blue_data = blue_x_data[blue_y]

#If there is no blue one:
```

```
if len(blue_data) == 0:
    print """There is NO "blue" object in this field:("""
    cosmetic()

    # CCD Plot of "de-purpled" data with med and sigma cuts
    plt.plot(f_data.field(colour_x),
             f_data.field(colour_y),
             'ro',
             markersize=5)
    plt.plot(new_data.field(colour_x),
             new_data.field(colour_y),
             'o',
             markerfacecolor='#F2FF00',
             markersize=5)

    plt.plot([med_x,med_x],
            [min(f_data.field(colour_y)),
               max(f_data.field(colour_y))],
            'g-', linewidth=2.0)
    plt.text((med_x-0.25), (max(f_data.field(colour_y)+0.25)),
     r'$Median_x$')

    plt.plot([sigma_cut_x,sigma_cut_x],
             [min(f_data.field(colour_y)),
               max(f_data.field(colour_y))],
             'g-', linewidth=2.0)
    plt.text((sigma_cut_x-0.25),
      (max(f_data.field(colour_y)+0.25)), r'$3\sigma _x$')

    plt.plot([min(f_data.field(colour_x)),
              max(f_data.field(colour_x))],
             [med_y,med_y], 'k-', linewidth=2.0)
    plt.text((min(f_data.field(colour_x))-0.15),
             (med_y-0.1), r'$Median_y$')
    plt.plot([min(f_data.field(colour_x)),
              max(f_data.field(colour_x))],
             [sigma_cut_y,sigma_cut_y], 'k-', linewidth=2.0)
    plt.text((min(f_data.field(colour_x))-0.15),
             (sigma_cut_y-0.1), r'$3\sigma _y$')
```

```
        plt.text(-2, -2, r'NO BLUE object')
        if no_err_y:
            plt.text(-2, -1.5, r'No error data')

        #plt.xlabel(colour_x)
        #plt.ylabel(colour_y)
        plt.xlabel('g\' - r\'')
        plt.ylabel('U - g\'')

        plt.title('Run %s Field %s' %(r,f))
        plt.axis([minx-0.1,maxx+0.1,maxy+0.3,miny-0.2])
        plt.savefig('%s/%s_3_blue.png'
            %(path_folder,field_file_name))
        print '%s/%s_3_blue.png has been saved! Yayy! :)'
            %(path_folder,field_file_name)
        plt.close()

        empty_writer.writerow([r, f, 'no blue', plane, system,
            "No_binning"])
        print "Name of empty file has been added to the list."
        empty_files.flush()

        continue

    print """There are %s "blue" stars in this field."""
        % len(blue_data)
    print " "

    # ======== CCD Plot of "de-purpled" data with blue ones ==============
    plt.plot(f_data.field(colour_x), f_data.field(colour_y),
             'ro', markersize=5, label='all data')
    plt.plot(new_data.field(colour_x), new_data.field(colour_y),
             'o', color='#F2FF00', markersize=5,
             label='data used for median and sigma')


    upleft  = (f_data.field(colour_x) < sigma_cut_x)
            & (f_data.field(colour_y) < sigma_cut_y)
    upleft_data = f_data[upleft]
```

```
upleft_xcol = upleft_data.field(colour_x)
upleft_xerr = upleft_data.field(err_2)
            + upleft_data.field(err_3)
upleft_ycol = upleft_data.field(colour_y)
upleft_yerr = upleft_data.field(err_1)
            + upleft_data.field(err_2)

plt.errorbar( upleft_xcol,
              upleft_ycol,
              xerr=[zeros(len(upleft_xerr)),upleft_xerr*3],
              yerr=[zeros(len(upleft_yerr)),upleft_yerr*3],
              marker='o',
              color='r',
              ecolor='r',
              markerfacecolor='r',
              capsize=5,
              linestyle='None',
              label='not selected due to big error')


blue_errx = blue_data.field(err_2) + blue_data.field(err_3)
blue_erry = blue_data.field(err_1) + blue_data.field(err_2)

plt.errorbar( blue_data.field(colour_x),
              blue_data.field(colour_y),
              xerr=[zeros(len(blue_errx)),blue_errx*3],
              yerr=[zeros(len(blue_erry)),blue_erry*3],
              marker='o',
              color='b',
              ecolor='b',
              markerfacecolor='b',
              capsize=5,
              linestyle='None',
              label='blue ones')


plt.plot( [med_x,med_x], [miny,maxy], 'k-',
        linewidth=2.0)
```

```
plt.text((med_x-0.15), (maxy+0.2), r'$Median_x$')

plt.plot( [sigma_cut_x,sigma_cut_x], [miny,maxy], 'k-',
        linewidth=2.0)
plt.text((sigma_cut_x-0.05), (maxy+0.2), r'$3\sigma _x$')

plt.plot( [minx,maxx], [med_y,med_y], 'k-',
        linewidth=2.0)
plt.text(minx, (med_y-0.07), r'$Median_y$')

plt.plot( [minx,maxx], [sigma_cut_y,sigma_cut_y], 'k-',
        linewidth=2.0)
plt.text(minx, (sigma_cut_y-0.07), r'$3\sigma _y$')

# 3sigma_y in case no de-purpling
purmed_y = median(f_data.field(colour_y))
purres_y = f_data.field(colour_y) - purmed_y
pur3sig_y = sqrt(sum(purres_y**2)/len(purres_y))

plt.plot( [minx,maxx], [pur3sig_y,pur3sig_y], '-',
        color='#6600FF', linewidth=2.5)
plt.text(minx, (pur3sig_y-0.07), r'$3\sigma _y~with~purples$')


if no_err_y:
    plt.text(-2, -1.5, r'No error data')

#plt.xlabel(colour_x)
#plt.ylabel(colour_y)
plt.xlabel('g\' - r\'')
plt.ylabel('U - g\'')

plt.title('Run %s Field %s' %(r,f))

plt.legend(prop={'size':9}, fancybox=True, loc='best')

plt.axis([minx-0.1,maxx+0.1,maxy+0.3,miny-0.2])
plt.savefig('%s/%s_3_blue.png' %(path_folder,field_file_name))
print '%s/%s_3_blue.png has been saved! Yayy! :)'
```

```
    %(path_folder,field_file_name)
plt.close()

# ======== CCD Plot of "de-purpled" data with blue ones
#           overlayed with main sequance and WD tracks  ==============
plt.plot(f_data.field(colour_x), f_data.field(colour_y),
        'ro', markersize=5)
plt.plot(new_data.field(colour_x), new_data.field(colour_y),
        'o', markerfacecolor='#F2FF00', markersize=5)
plt.plot(blue_data.field(colour_x), blue_data.field(colour_y),
        'bo', linewidth=2.0)

# shift the tracks according to F6V colour and sigma cuts
difx = f6v.field(track_x)[0]-(sigma_cut_x+0.16)
dify = f6v.field(track_y)[0]-(sigma_cut_y+0.21)
plt.text(-3, -2.9, r'$difx = %.2f$'%difx)
plt.text(-3, -2.6, r'$dify = %.2f$'%dify)
#main sequence
plt.plot(mainsq.field(track_x)-difx,mainsq.field(track_y)-dify,
        'k-', linewidth=1.5)

#B-DA track
plt.plot(bda.field(track_x)-difx,bda.field(track_y)-dify,
        'k-', linewidth=1.5)

#K-DA track
plt.plot(kda.field(track_x)-difx,kda.field(track_y)-dify,
        'k-', linewidth=1.5)

#K-DB track
plt.plot(kdb.field(track_x)-difx,kdb.field(track_y)-dify,
        'k-', linewidth=1.5)


if no_err_y:
    plt.text(-2, -1.5, r'No error data')

plt.xlabel('g\' - r\'')
plt.ylabel('U - g\'')
```

```
plt.title('Run %s Field %s' %(r,f))
plt.axis([minx-0.1,maxx+0.1,maxy+0.3,miny-0.2])
plt.savefig('%s/%s_4_blue_tracks.png'
            %(path_folder,field_file_name))
print '%s/%s_4_blue_tracks.png has been saved! Yayy! :)'
    %(path_folder,field_file_name)
plt.close()

#=============================================================
#      ======= Write the blue objects to the file ======
#=============================================================
print "Writing data to field-specific csv file..."
print " "

#write data: mind the order of headers!!!
for k in blue_data:
    blue_satir = list(k)
    blue_satir.extend([plane,system,"No_binning"\
        ,med_x,sigma_x,med_y,sigma_y])
    fbyf_writer.writerow(blue_satir)
    blue_writer.writerow(blue_satir)

print "Data of blue objects from Run %s Field %s has been \
    added to the both file, field-specific and the big one..."
    % (r,f)
print "="*30
print " "
field_file.flush()
all_blues.flush()

#In order to complete to write your file to disk, you need to
#close it. Otherwise it will be just on memory, which means
#you can lose it!!!
#If you will use your file again, you need to use ".flush()"
#instead of ".close()"
field_file.close()

#If there is no blue in this field and csv file consists of only
```

```
        # headers, I would like to delete it.

        #count the rows!
        csv_file = csv.reader(open(path_field_file))
        row_count = sum(1 for row in csv_file)
        print "there are %s blue objects in the run %s field %s"
            %(row_count-1,r,f)

        # delete it if it is empty
        if row_count == 1:  #1 row means only header
            print "There is NO 'blue' object in this field :("
            print "So, deleting the empty csv file..."
            print " "
            print " "

            #remove it
            os.system("rm %s" %path_field_file)
            print " "
            print "="*50

            continue

        #get rid of 'nan's
        os.system("sed 's/nan//g' %s > tmp && mv tmp %s"
                %(path_field_file,path_field_file))

        #going to do the same thing for next field.
        #if this is last field in this run, moving forward.

    #going to do the same thing for next run.
    #if this is last run, moving forward to end process.


print " "
empty_files.close()
print "empty_files is closed"
print " "
all_blues.close()
print "all_blues is closed"
```

```
print " "

#get rid of 'nan's
os.system("sed 's/nan//g' %s > tmp && mv tmp %s" %(path_all,path_all))

print "All png files are being combined into a pdf file..."
os.system("/usr/bin/convert %s/*.png %s/all_fit_dep_blue_tracks.pdf"
        %(path_folder,path_folder))
print " "
print "%s/all_fit_dep_blue.pdf is created!" %(path_folder)
print " "

print " ================THE END================ "
```

A.2 Image Bringer

This script is written to speed up manual inspection of the numerous raw images in the RATS database to identify false colours caused by the effects explained in § 2.2 on page 37.

```
#!/usr/bin/env python

###############################################################
## Usage:   - Paste the action code into the TOPCAT
##          - click on a row in a table or a point
##            on a plot
##          Then script opens a DS9 window with images tiled,
##          zoomed and panned according to xy, with a green
##          circles around the object.
##
##  Notice that ALL image files have to be in the same folder
##  with a tidy naming scheme :)
##
##                          OR
##
##  You need to edit the script according to your need.
###############################################################

#### Example Action Code ######################################
```

```
#### you know that you need to edit this part :)
#### delete slashes (\) and make it one line
# exec("/home/osa/Dropbox/PhD/Work/Scripts/bring_image_coor.py"\
#  ,concat(toString(£1)," ",concat(toString(£2)," ",toString(£3)))\
#  ,concat(toString(£6)," ",toString(£7)),concat(toString(£8)," "\
#  ,\toString(£9)))

import os
import subprocess as s
import sys

print sys.argv[1]
print sys.argv[2]
print sys.argv[3]

run    = sys.argv[1].split(" ")[0]
field  = sys.argv[1].split(" ")[1]
chip   = sys.argv[1].split(" ")[2]
x      = sys.argv[2].split(" ")[0]
y      = sys.argv[2].split(" ")[1]
ra     = sys.argv[3].split(" ")[0] # should be in HMS format
dec    = sys.argv[3].split(" ")[1] # should be in DMS format

# run '3' --> '03'
# No worries, these are strings :)
if len(run)==1:
    run='0'+run

# field '7' --> '07'
if len(field)==1:
    field='0'+field

img_list = s.check_output(['ls -r \
        /home/osa/Work/wcs-images/r%sfield%s-*_%s-wcs.fits' \
        %(run,field,chip)], shell=True).splitlines()

ds9_cmd = 'ds9 -geometry 780x960 -tile -scale linear \
        -scale mode zscale -colorbar no'
```

```
opts = '-pan to %s %s -regions command \
            "circle %s %s 25 # color=green width=15"' %(x,y,ra,dec)

for img in img_list:
    ds9_cmd = ds9_cmd + ' ' + img + ' ' + opts

print '''

+++%s

=====================================================
''' %ds9_cmd

os.system('%s &' %ds9_cmd) #using & gives you the freedom keep going
                           #without closing ds9 window, compare two
                           #(or how many you want) star for example.
                           #This way it doesn't block TOPCAT.
```

A.3 Radial Velocity Measurments

Radial velocity measurements are done in two steps —first cross-correlation functions are created, and then these CCFs are fitted a spline.

A.3.1 Cross-correlation

The first step is done in DIPSO environment.

```
del 1 - 99
alasrd ../cn_obj1a_1_477_rmean2.dat, push
alasrd ../cn_obj1a_2_314_rmean2.dat, push
alasrd ../cn_obj1a_3_889_rmean2.dat, push
alasrd ../cn_obj1b_1_320_rmean2.dat, push
alasrd ../cn_obj1b_2_044_rmean2.dat, push
alasrd ../cn_obj1b_3_899_rmean2.dat, push
alasrd ../cn_obj2a_1_654_rmean2.dat, push
alasrd ../cn_obj2a_2_498_rmean2.dat, push
alasrd ../cn_obj2a_3_464_rmean2.dat, push
```

```
alasrd ../cn_obj2b_1_851_rmean2.dat, push
alasrd ../cn_obj2b_2_384_rmean2.dat, push
alasrd ../cn_obj2b_3_989_rmean2.dat, push

sl

pop 1, bin 3770 0.1, rxr 4050 4300, logx, ysub 1, push, del 1
pop 1, bin 3770 0.1, rxr 4050 4300, logx, ysub 1, push, del 1
pop 1, bin 3770 0.1, rxr 4050 4300, logx, ysub 1, push, del 1
pop 1, bin 3770 0.1, rxr 4050 4300, logx, ysub 1, push, del 1
pop 1, bin 3770 0.1, rxr 4050 4300, logx, ysub 1, push, del 1
pop 1, bin 3770 0.1, rxr 4050 4300, logx, ysub 1, push, del 1
pop 1, bin 3770 0.1, rxr 4050 4300, logx, ysub 1, push, del 1
pop 1, bin 3770 0.1, rxr 4050 4300, logx, ysub 1, push, del 1
pop 1, bin 3770 0.1, rxr 4050 4300, logx, ysub 1, push, del 1
pop 1, bin 3770 0.1, rxr 4050 4300, logx, ysub 1, push, del 1
pop 1, bin 3770 0.1, rxr 4050 4300, logx, ysub 1, push, del 1
pop 1, bin 3770 0.1, rxr 4050 4300, logx, ysub 1, push, del 1


xcorr 1 1
pop 15, tenx, xsub 1, xmult 3.e5, alaswr o1n1s1_o1n1s1.dat, \
        pdgpeak, del 13 - 15
xcorr 1 2
pop 15, tenx, xsub 1, xmult 3.e5, alaswr o1n1s1_o1n1s2.dat, \
        pdgpeak, del 13 - 15
xcorr 1 3
pop 15, tenx, xsub 1, xmult 3.e5, alaswr o1n1s1_o1n1s3.dat, \
        pdgpeak, del 13 - 15

xcorr 2 1
pop 15, tenx, xsub 1, xmult 3.e5, alaswr o1n1s2_o1n1s1.dat, \
        pdgpeak, del 13 - 15
xcorr 2 2
pop 15, tenx, xsub 1, xmult 3.e5, alaswr o1n1s2_o1n1s2.dat, \
        pdgpeak, del 13 - 15
xcorr 2 3
pop 15, tenx, xsub 1, xmult 3.e5, alaswr o1n1s2_o1n1s3.dat, \
        pdgpeak, del 13 - 15
```

```
xcorr 3 1
pop 15, tenx, xsub 1, xmult 3.e5, alaswr o1n1s3_o1n1s1.dat, \
        pdgpeak, del 13 - 15
xcorr 3 2
pop 15, tenx, xsub 1, xmult 3.e5, alaswr o1n1s3_o1n1s2.dat, \
        pdgpeak, del 13 - 15
xcorr 3 3
pop 15, tenx, xsub 1, xmult 3.e5, alaswr o1n1s3_o1n1s3.dat, \
        pdgpeak, del 13 - 15


xcorr 4 4
pop 15, tenx, xsub 1, xmult 3.e5, alaswr o1n2s1_o1n2s1.dat, \
        pdgpeak, del 13 - 15
xcorr 4 5
pop 15, tenx, xsub 1, xmult 3.e5, alaswr o1n2s1_o1n2s2.dat, \
        pdgpeak, del 13 - 15
xcorr 4 6
pop 15, tenx, xsub 1, xmult 3.e5, alaswr o1n2s1_o1n2s3.dat, \
        pdgpeak, del 13 - 15

xcorr 5 4
pop 15, tenx, xsub 1, xmult 3.e5, alaswr o1n2s2_o1n2s1.dat, \
        pdgpeak, del 13 - 15
xcorr 5 5
pop 15, tenx, xsub 1, xmult 3.e5, alaswr o1n2s2_o1n2s2.dat, \
        pdgpeak, del 13 - 15
xcorr 5 6
pop 15, tenx, xsub 1, xmult 3.e5, alaswr o1n2s2_o1n2s3.dat, \
        pdgpeak, del 13 - 15

xcorr 6 4
pop 15, tenx, xsub 1, xmult 3.e5, alaswr o1n2s3_o1n2s1.dat, \
        pdgpeak, del 13 - 15
xcorr 6 5
pop 15, tenx, xsub 1, xmult 3.e5, alaswr o1n2s3_o1n2s2.dat, \
        pdgpeak, del 13 - 15
xcorr 6 6
```

```
pop 15, tenx, xsub 1, xmult 3.e5, alaswr o1n2s3_o1n2s3.dat, \
        pdgpeak, del 13 - 15


xcorr 7 7
pop 15, tenx, xsub 1, xmult 3.e5, alaswr o2n1s1_o2n1s1.dat, \
        pdgpeak, del 13 - 15
xcorr 7 8
pop 15, tenx, xsub 1, xmult 3.e5, alaswr o2n1s1_o2n1s2.dat, \
        pdgpeak, del 13 - 15
xcorr 7 9
pop 15, tenx, xsub 1, xmult 3.e5, alaswr o2n1s1_o2n1s3.dat, \
        pdgpeak, del 13 - 15

xcorr 8 7
pop 15, tenx, xsub 1, xmult 3.e5, alaswr o2n1s2_o2n1s1.dat, \
        pdgpeak, del 13 - 15
xcorr 8 8
pop 15, tenx, xsub 1, xmult 3.e5, alaswr o2n1s2_o2n1s2.dat, \
        pdgpeak, del 13 - 15
xcorr 8 9
pop 15, tenx, xsub 1, xmult 3.e5, alaswr o2n1s2_o2n1s3.dat, \
        pdgpeak, del 13 - 15

xcorr 9 7
pop 15, tenx, xsub 1, xmult 3.e5, alaswr o2n1s3_o2n1s1.dat, \
        pdgpeak, del 13 - 15
xcorr 9 8
pop 15, tenx, xsub 1, xmult 3.e5, alaswr o2n1s3_o2n1s2.dat, \
        pdgpeak, del 13 - 15
xcorr 9 9
pop 15, tenx, xsub 1, xmult 3.e5, alaswr o2n1s3_o2n1s3.dat, \
        pdgpeak, del 13 - 15


xcorr 10 10
pop 15, tenx, xsub 1, xmult 3.e5, alaswr o2n2s1_o2n2s1.dat, \
        pdgpeak, del 13 - 15
xcorr 10 11
```

```
pop 15, tenx, xsub 1, xmult 3.e5, alaswr o2n2s1_o2n2s2.dat, \
        pdgpeak, del 13 - 15
xcorr 10 12
pop 15, tenx, xsub 1, xmult 3.e5, alaswr o2n2s1_o2n2s3.dat, \
        pdgpeak, del 13 - 15

xcorr 11 10
pop 15, tenx, xsub 1, xmult 3.e5, alaswr o2n2s2_o2n2s1.dat, \
        pdgpeak, del 13 - 15
xcorr 11 11
pop 15, tenx, xsub 1, xmult 3.e5, alaswr o2n2s2_o2n2s2.dat, \
        pdgpeak, del 13 - 15
xcorr 11 12
pop 15, tenx, xsub 1, xmult 3.e5, alaswr o2n2s2_o2n2s3.dat, \
        pdgpeak, del 13 - 15

xcorr 12 10
pop 15, tenx, xsub 1, xmult 3.e5, alaswr o2n2s3_o2n2s1.dat, \
        pdgpeak, del 13 - 15
xcorr 12 11
pop 15, tenx, xsub 1, xmult 3.e5, alaswr o2n2s3_o2n2s2.dat, \
        pdgpeak, del 13 - 15
xcorr 12 12
pop 15, tenx, xsub 1, xmult 3.e5, alaswr o2n2s3_o2n2s3.dat, \
        pdgpeak, del 13 - 15
```

A.3.2 Spline to CCF

The second part is handled by a python script.

```
import scipy.interpolate as inter
import numpy as np
import matplotlib.pyplot as plt
import sys

#### Read the ccf ####
datafile = sys.argv[1]
name = datafile[:-4] #get rid of extension
```

```
ccf_all = np.loadtxt(sys.argv[1])

x_all = ccf_all.transpose()[0]
y_all = ccf_all.transpose()[1]


ymax_index = ccf_all.argmax(axis=0)[1]

dx = int(sys.argv[2]) # x limit around zero for plot

# x limits around the peak for the fit
xlow = ccf_all[ymax_index][0] - dx
xhi  = ccf_all[ymax_index][0] + dx

ccf = ccf_all[ccf_all[:, 0] > xlow]
ccf = ccf[ccf[:,0] < xhi]

ccf = ccf.transpose()

x = ccf[0]
y = ccf[1]

baseline = (y.max()+y.min())/2.0
y_shifted = y - baseline

xx = np.arange(x.min(),x.max(),1)

s1 = inter.InterpolatedUnivariateSpline (x, y_shifted)
# Use a smallish value for s
s2 = inter.UnivariateSpline (x, y_shifted, s=0.005)

r1, r2 = s2.roots() # find the roots
fwhm = r2 - r1
sigma = fwhm / 2.355
std_err = sigma / np.sqrt(len(x))

fit_rv = xx[s2(xx).argmax()]
ccf_rv = x[y.argmax()]
```

```
print """
Name    = %s
FWHM    = %6.2f
sigma   = %6.2f
std_err= %6.2f
Fit RV = %6.2f
CCF RV = %6.2f
==============
""" %(name,fwhm,sigma,std_err,fit_rv,ccf_rv)


plt.plot(x_all, y_all, 'bo-', ms=2, label='Data')
# plt.plot(xx, s1(xx) + baseline, 'k-', label='Spline')
plt.plot(xx, s2(xx) + baseline, 'r-', lw=3, label='Spline, fit')

plt.minorticks_on()

plt.xlabel('RV km/s')
plt.ylabel('CCF Probability')

plt.text(x_all.min(),y_all.max()-0.05,'Fit RV = %6.1f' \
        %(fit_rv), family='monospace')
plt.text(x_all.min(),y_all.max()-0.10,'CCF RV = %6.1f' \
        %(ccf_rv), family='monospace')
plt.text(x_all.min(),y_all.max()-0.15,'FWHM   = %6.1f' \
        %(fwhm), family='monospace')
plt.text(x_all.min(),y_all.max()-0.20,r'$\sigma$      = %6.1f' \
        %(sigma), family='monospace')
plt.text(x_all.min(),y_all.max()-0.25,r'$\sigma_{\overline{x}}$     \
        = %6.1f' %(std_err), family='monospace')

plt.ylim([0,y_all.max()+0.1])

plt.show()
plt.savefig('%s_rv.png'%name)
```